UNIVERSITY OF SOUTHAMPTON
FACULTY OF PHYSICAL SCIENCES AND ENGINEERING
SCHOOL OF ELECTRONICS AND COMPUTER SCIENCE

Quality of Service Aware Cross-Layer Network Lifetime Maximization in Battery-Constrained Wireless Sensor Networks

by

Halil Yetgin
BEng, MSc

A thesis for the degree of
Doctor of Philosophy
at the University of Southampton

October 2015

Supervisor: *Professor Lajos Hanzo*
FREng, FIEEE, FIET, FEURASIP
Chair in Telecommunications
and
Second Supervisor: *Dr. Mohammed El-Hajjar*
BEng, MSc, PhD, MIEEE
Southampton Wireless Group
School of Electronics and Computer Science
University of Southampton
Southampton, SO17 1BJ
United Kingdom

Dedicated to my family.

UNIVERSITY OF SOUTHAMPTON

ABSTRACT

FACULTY OF PHYSICAL SCIENCES AND ENGINEERING
School of Electronics and Computer Science

Doctor of Philosophy

QUALITY OF SERVICE AWARE CROSS-LAYER NETWORK LIFETIME MAXIMIZATION IN BATTERY-CONSTRAINED WIRELESS SENSOR NETWORKS

by Halil Yetgin

In wireless sensor networks (WSNs), network lifetime (NL) maximization plays a significant role in striking a compelling compromise between maximizing the overall throughput and minimizing the energy dissipation, while extending the duration of adequate communications without battery-replacement, when the sensor nodes rely on limited energy supply. Hence, this thesis focuses on the NL maximization of battery-constrained WSNs, which is vitally important in industrial applications, where thousands of sensors may be deployed within a specific target area and the energy dissipation of each sensor node has to be minimized in order to reduce the overall cost of the applications to the industry. However, maintaining stringent quality of service (QoS) requirements under the above-mentioned NL constraints can be challenging and requires careful consideration of several conflicting design trade-offs. Naturally, the above-mentioned energy dissipation characteristics are dependent on the entire seven-layer OSI protocol stack, where each layer contributes to the dissipated energy. Therefore, NL maximization necessitates a cross-layer operation across all these layers, where each layer has to minimize its energy dissipation without deteriorating the QoS. Hence, our objective is to maximize the NL using cross-layer design techniques in the interest of maintaining certain QoS requirements and to provide the system designer with well-informed decisions prior to embarking on hardware implementations. Hence, our approach is to investigate and to model progressively more realistic WSNs.

We commence with a broad overview of the WSNs, of the design objectives and of the NL maximization techniques that have been investigated in the literature. We then provide a concise introduction to convexity, convex optimization, to the Lagrangian dual problem and to the Karush-Kuhn-Tucker (KKT) optimality conditions, which will be extensively used in our studies. Having presented the fundamentals, we formulate an initial study of the NL maximization problem based on a simple string topology in order to form a basic framework for the NL maximization of more realistic large scale networks. In this particular study, we maximize the NL in an interference-limited WSN considering a beneficial rate and power allocation scheme under both additive white Gaussian noise (AWGN) and fading

channel characteristics, where we employ the KKT optimality conditions for obtaining the optimal solution to the NL maximization problem using closed-form expressions. Therefore, we were able to derive analytical expressions of the globally optimal NL for a string network operating in an interference-limited scenario, while communicating either over an AWGN or over fading channels for a given link schedule. Furthermore, the maximum NL, the energy dissipation per node, the average transmission power per link and the lifetime of all nodes in the network are obtained. We quantify how the maximum NL is reduced as a function of the fading statistics due to the poor channel conditions. Furthermore, we demonstrate that given a certain network-sum-rate, the simultaneous scheduling of weakly interfering links benefits from the associated spatial reuse by allowing each node to transmit at a lower rate, which requires a reduced transmission power and hence results in an increased NL. We also conclude that the choice of the particular scheduling scheme depends on the application, since a lower source rate favors infrequent transmissions requiring a low transmit power, while avoiding the detrimental effects of interference, when aiming for extending the NL. However, we observe that for higher source rates, a higher NL can be achieved by aggressive spatial reuse. An interesting observation is that increasing the distance between the consecutive nodes substantially reduces the NL, especially for lower source rates. However, quite surprisingly, increasing the distance between the consecutive nodes results in an improved NL for higher source rates. This is due to the reduced impact of the interferers located at a higher distance. More explicitly, even though the transmit power required has to be increased to satisfy the rate constraint, at the same time the interferers are moved a bit further away. In this particular study, the NL and source rate are considered as the QoS measure as a function of both the transmit rate and the power, where an adaptive scheme is assumed. Finally, our proposed algorithm achieved reduced complexity NL maximization compared to other techniques found in the literature.

We then extend our NL maximization problem to a realistic scenario, where the parameters are selected from the practical data sheet of a *National Instruments* device, which is based on the *IEEE 802.15.4 Standard* and the energy dissipation of the signal processing operations, i.e. the energy dissipation of the transceiver circuits, is considered. Since achieving a reasonable NL at the cost of a tolerable end-to-end bit error rate (BER) for a fixed-rate system using various modulation and coding schemes (MCSs) is an important objective for the system designer considering the QoS, we strike a trade-off between the BER and the NL, which is crucial for network designers at an early design stage. Therefore, we aim for maximizing the NL for a predetermined set of target signal-to-interference-plus-noise ratio (SINR) values, which guarantees maintaining the predefined QoS of each link operating over either an AWGN channel or a Rayleigh block-fading channel, while considering or disregarding the signal processing power (SPP). We observed that especially for low target SINRs, the SPP has a dominant impact on the NL. However, for higher target SINRs the achievable NL only considering the transmit power whilst disregarding the SPP forms

a benchmark for the achievable NL of the particular scenario, when the SPP is jointly considered along with the transmit power.

As a further advance, a more realistic network is considered, where the same *National Instruments* device, which is based on the *IEEE 802.15.4 Standard* is used as a reference. For this realistic network, we also had to reconsider our NL definition, where we maximize the NL of a WSN relying on randomly and uniformly distributed fully connected nodes. This fully connected WSN imposes an exponentially increasing routing complexity upon increasing the number of nodes. More particularly, we focus our attention on the cross-layer optimization of the power allocation, scheduling and routing operations for the sake of NL maximization for predetermined per-link target SINR values. We use the so-called exhaustive search algorithm (ESA) as our benchmarker and conceive a near-optimal single-objective genetic algorithm (SOGA) imposing a substantially reduced complexity in fully connected WSNs. We show that our NL maximization approach is powerful in terms of prolonging the NL, while striking a trade-off between the NL and the QoS requirements.

Finally, we consider a multiobjective NL maximization problem, where the end-to-end delay and the energy dissipation are considered as our conflicting design objectives. More explicitly, we proposed a novel NL optimization design in order to reflect the effect of the end-to-end delay on the NL along with the aggregate energy dissipation of the same route. The distinctive aspect of this study is the simultaneous optimization of both the aggregate energy dissipation and of the end-to-end delay as a multi-objective optimization problem in order to provide the system designer with a trade-off between Pareto-optimal energy- and delay-solutions. We employ multi-objective evolutionary algorithms (MOEAs), namely the so-called non-dominated sorting based genetic algorithm-II (NSGA-II) and the multi-objective differential evolution (MODE) algorithm for obtaining the set of Pareto optimal NL-aware routes striking a trade-off between the aggregate energy dissipation and the end-to-end delay. Moreover, we characterize both the complexity and the convergence of both algorithms compared to the ESA.

Declaration of Authorship

I, **Halil Yetgin**, declare that the thesis entitled

Quality of Service Aware Cross-Layer Network Lifetime Maximization in Battery-Constrained Wireless Sensor Networks

and the work presented in it are my own and have been generated by me as the result of my own original research. I confirm that:

1. This work was done wholly or mainly while in candidature for a research degree at this University;
2. Where any part of this thesis has previously been submitted for a degree or any other qualification at this University or any other institution, this has been clearly stated;
3. Where I have consulted the published work of others, this is always clearly attributed;
4. Where I have quoted from the work of others, the source is always given. With the exception of such quotations, this thesis is entirely my own work;
5. I have acknowledged all main sources of help;
6. Where the thesis is based on work done by myself jointly with others, I have made clear exactly what was done by others and what I have contributed myself;
7. Parts of this work have been published, as seen in the list of publications.

Signed: Halil Yetgin

Date: 21 October 2015

Acknowledgements

I wish to express my heartfelt gratitude to my supervisor Professor Lajos Hanzo for his supervision and support throughout my research. I have greatly benefited from his excellent guidance, support and friendly discussions. His patience, enthusiasm, encouragement and wisdom have been highly supportive to me in my work.

I would also like to thank my friend and supervisor Dr. Mohammed El-Hajjar for his guidance, support and great patience during his supervision throughout my research. His knowledge and attention inspired me to always work harder.

I am deeply grateful to Dr. Kent Tsz Kan Cheung. His presence has helped me endure the ups and downs of being a researcher. Our discussions played an important role in the direction of my research.

The support and kindness of the many friends and colleagues whom I have made throughout these past few years have been invaluable to me. Although there are too many names to mention, I would like to express my gratitude to all those, who have been at least once with Southampton wireless, both past and present. I want to particularly thank Professor Lie-Liang Yang, Dr. Soon Xin Ng, Dr. Rob Maunder, Dr. Rong Zhang, Dr. Chen Dong, Dr. Jing Zuo, Dr. Shaoshi Yang, Dr. Chao Xu, Abdulah Jeza Aljohani, Dr. Shi Jia, Dr. Liang Wei, Dr. Yongkai Huo, Dr. Jie Hu, Xin Zuo, Dr. Li Li, Talha Rahman, Dimitrios Alanis, and all other colleagues and staff, too numerous to mention here explicitly.

Without the support, patience and guidance of the following people, this study would not have been completed. It is to them I owe my deepest gratitude.

- My dear friends and ex-housemates; Dr. Daniel Fernández Comesãna, Dr. Paúl Rodriguez, Dr. Eduardo Latorre Iglesias, Dr. Hessam Alavi.
- Football team; Wali Sayeed, Ruben Porras, Dr. Recep Kahraman, Giorgos Ragousis, Mansu Tarafdar, Dr. Amir Rmaile. Thank you for the championships in a row and cups we won. It has been an unforgettable team.
- Ali Bakkaloğlu, Okan Öztürkmenoğlu, Adem Çolak, Ahmet Yavuz Metinoğlu, Adil Alper Dalkıran, Gülşen Özkan, Alper Yıldırım, Mehmet Küçükgürses, far away from where I am, but have always been the source of my liveliness.

- Southampton has always been better with them; Dr. Elif Kara, Bünyamin Yıldız, Engin Hasan Çopur, Mehmet Emin Erendor, Mustafa Çağrı Kutlu, Aziz owner of Unikebab.
- Their support made me who I am now, my cousins Ali Işıl, Hasan Işıl, Ali Yetgin and my uncle Dr. Zeki Yetgin.
- Most of all, I am deeply grateful to Dr. Kaya Kuru and his family, who have been the source of inspiration for me during their stay in Southampton.

The financial support of Republic of Turkey Ministry of National Education is also gratefully acknowledged.

I would also like to express my appreciation to my parents, Ahmet Yetgin and Ayşe Yetgin, to my lovely sister Fatma Yetgin and to her husband Mustafa Uyar and to my brother Ali Yetgin, as well as to my beloved wife, Ayşe Saliha Sunar and her family, for their love, support and care for me.

List of First-Author Publications

Journal Paper

1. **H. Yetgin**, K. Tsz Kan Cheung, M. El-Hajjar and L. Hanzo, "Cross-layer Network Lifetime Maximization in Interference-Limited WSNs", *IEEE Transactions on Vehicular Technology*, vol.64, no.8, pp.3795-3803, August 2015.
2. **H. Yetgin**, K. Tsz Kan Cheung, M. El-Hajjar and L. Hanzo, "Cross-layer Network Lifetime Optimization Considering Transmit and Signal Processing Power in WSNs", *IET Wireless Sensor Systems (Special Issue on Intelligent Wireless Sensor Networks and Applications)*, vol. 4, no. 4, pp. 176-182, December 2014.
3. **H. Yetgin**, K. Tsz Kan Cheung, M. El-Hajjar and L. Hanzo, "Network-Lifetime Maximization of Wireless Sensor Networks", *IEEE Access*, Accepted.

Conference Paper

1. **H. Yetgin**, K. Tsz Kan Cheung and L. Hanzo, Multi-objective routing optimization using evolutionary algorithms, *IEEE Wireless Communications and Networking Conference (WCNC'12)*, Paris, France, April 2012.

List of Symbols

General notation

a_{ij}	the element of the matrix $\mathbf{A}$ at row i, column j.
$\mathbf{x}$	boldface lowercase letters denote column vectors.
x	standard lowercase letters denote scalars.
x_i	the ith element of the vector $\mathbf{x}$.
$\mathbf{A}^T$	transpose of the matrix $\mathbf{A}$.
$\mathbb{R}$	the field of real numbers.
$\mathbb{C}$	the field of complex numbers
$\mathbb{Z}$	the set of all integers.
$\mathbb{R}_+$	the set of all nonnegative real numbers.
$\mathbb{R}_{++}$	the set of all positive real numbers.
$\mathbb{R}_-$	the set of all nonpositive real numbers.
$\mathbb{R}_{--}$	the set of all negative real numbers.
$\mathbb{R}^n$	the n-dimensional vector of real numbers.
$\mathbb{R}^{m\times n}$	the $m \times n$-dimensional matrix of real numbers.
$\min(\cdot)$	minimum operator.
$\max(\cdot)$	maximum operator.
$\inf(\cdot)$	infimum operator.
$\sup(\cdot)$	supremum operator.
$\log(\cdot)$	natural logarithm operator.
$\log_2(\cdot)$	base 2 logarithm operator.
dom f	domain of function f.
$[a, b]$	closed set of real numbers between a and b.
(a, b)	open set of real numbers between a and b.
$\mathbf{A} \succeq 0$	$\mathbf{A}$ is a positive semidefinite matrix.
$\mathbf{x} \succeq a$	vector $\mathbf{x}$ is elementwise greater than a.
f'	first order derivative of function f.
f''	second order derivative of function f.
$[\cdot]^+$	projection onto the nonnegative field of real numbers.

Special symbols

d	distance between sensors.
V	number of sensors.
$\mathbf{A}$	network topology incidence matrix.
T	spatially periodic time sharing parameter.
n	slot indicator.
$l_{i,j}, n$	link l spanning from sensor node i to node j, scheduled for time slot n.
N	total number of slots in time-division multiple access time frame per link.
Act	desired communication.
Int	interfering communication.
m	path loss exponent.
$G_{i,j}$	channel gain of a link between the transmitter i and receiver j.
$P_{l_{i,j},n}$	transmit power of link l spanning from node i to node j in time slot n.
$(P_i)_{max}$	maximum affordable transmit power assigned to sensor node i.
Γ_l	signal-to-interference-plus-noise ratio (SINR) of link l.
N_0	noise power at the receiver.
γ	target SINR value.
$\mathcal{L}_n$	set of links in time slot n.
$BER_{l_{i,j}}$	bit error rate of link $l_{i,j}$.
T_i	lifetime of node i.
T_R	route lifetime.
$\mathcal{E}_i$	initial battery capacity of node i.
$f_{ED}(x)$	energy dissipation function.
u_i	a specific sensor operation imposing energy dissipation on sensor node i.
P_{sp}	signal processing power.
R_V	total number of distinct and non-looping routes for given V.
$(h+1)=\widehat{h}$	number of hops.
δ	number of packets.
τ	number of trials per network lifetime computation.
α	efficiency of the power amplifier.
$\aleph_{gen}$	number of generations.
$\aleph_{ind}$	number of individuals.
Pr_c	probability of crossover.
Pr_m	probability of mutation.
z	reciprocal of network lifetime.
$r_{l,n}$	transmission rate of link l in time slot n.
$Q_{l,n}$	logarithm of $P_{l,n}$ for link l in time slot n.
$H_{i,j} = \lvert h_{i,j} \rvert^2$	fading gain of the link between transmitter i and receiver j.

Special symbols (Cont.)

$\boldsymbol{\Omega}$	a set of dual variables for energy conservation constraint.
$\boldsymbol{\Psi}$	a set of dual variables for transmission rate constraint.
$\boldsymbol{\vartheta}$	a set of dual variables for transmit power constraint.
$\boldsymbol{\mu}$	a set of dual variables for flow constraint.
ϵ	convergence tolerance of the iterative algorithms.
$l \in \mathcal{O}(\upsilon)$	emerging link of node υ.
$l \in \mathcal{I}(\upsilon)$	incoming link of node υ.

Table of Contents

Chapter 1

Introduction

1.1 Introduction

Sensors are everywhere. They make our daily life easier, supporting the operation of our vehicles, our smart phones, our homes, so on. Additionally, wireless sensor networks (WSNs) are being extensively used in mission-critical applications, ranging from smart environments relying on the automation of control systems, smart homes, smart cities to health monitoring and military systems. This is because the recent advances in wireless sensor technology enable the industry to focus on the optimization and on the development of the product- and service-oriented applications of WSNs. From an industrial point of view, these applications have to rely on low-power and low-cost nodes without any significant reduction in their quality of service (QoS). However, during the design of these applications, WSNs face design challenges, such as maintaining a high network lifetime for battery-constrained sensor devices, guaranteeing reliability, connectivity and robustness in harsh environments and so on. Therefore, while designing our lifetime maximization framework for WSNs, we aim for answering the following questions in the thesis.

1. How and in what ways a cross-layer design approach can assist us in maximizing the network lifetime (NL)? For example, how the methods including the balancing of the energy dissipation of sensors, mitigating the interference with the aid of scheduling methods, increasing the spatial reuse, exploiting multihop routing affect the NL?
2. What is the impact of the hostile channel characteristics on the NL?
3. What is the trade-off between the source rate and the distance, while maximizing the NL in an interference-limited WSN?
4. How scheduling affects the NL?
5. What are the impact of the signal processing power (SPP) and the transmit power on the NL. How dominant is the SPP over transmit power?

6. How the bit error rate (BER) requirement at the physical layer affects both the NL (BER versus NL trade-off) and the network performance?
7. How the choice of the application-dependent NL definitions affect the NL?
8. How the network topology and the network size affect both the NL and the routing complexity?
9. Do the routing decisions affect the NL, when the objective function is constituted by the maximization of the NL?
10. How the energy-delay trade-off affects the achievable NL?

To answer these questions, first of all we have to develop a deep understanding of the WSNs, of theirs applications and design objectives. Hence, we commence with the history of the WSNs.

The research on WSNs started back in the 1980s by investigating the family of the distributed sensor networks (DSNs) at the defense advanced research projects agency (DARPA) [1]. The availability of inexpensive, low-power and miniature components, such as sensors, radios, processors, signal processing units and memory devices that are commonly accommodated on a single chip made it possible to attract industrial attention [1–3]. The ensuing research effort invested in WSNs improved numerous facets of the WSNs. Then the concept of WSNs was developed further to the concept of the Internet of Things (IoT) conceived by Kevin Ashton in 1999 [4], where he refers to the communication of any uniquely identifiable objects over an Internet-like architecture. Indeed, many other definitions of the IoT has been disseminated in the literature [5]. For example, a definition is provided in [6] as a global network of uniquely addressable interconnected objects relying on a predetermined communication protocol. By definition, attaining a unique sensor address will make it possible for any object to dynamically connect with the existing network and efficiently collaborate, cooperate and accomplish various tasks.

Whilst IoT does not assume any specific communication protocol, the trending IoT communication protocol is the Internet protocol (IP), which is capable of supporting smooth connectivity between objects [6–8]. Although, the applications of WSNs can be supported by the IP, several important problems still have to be addressed, such as security, QoS, configuration and data privacy [9–12]. For example, innovative security mechanisms have to be implemented, since WSNs are vulnerable to common attacks using the Internet [11, 12]. The device heterogeneity within the WSN will require the support of an unbalanced resource utilization [9]. The workload may be partitioned based on the knowledge of the amount of resources available. Nonetheless, the usual QoS based resource-allocation approaches of the Internet may not be applicable to WSNs, since the availability of resources is limited by the channel. Hence adaptive reconfiguration of the WSN topology may be required [9, 10]. Additionally, novel network management and configuration mechanisms may be required for supporting self-organizing networks [10]. Upon addressing these specific problems, WSNs

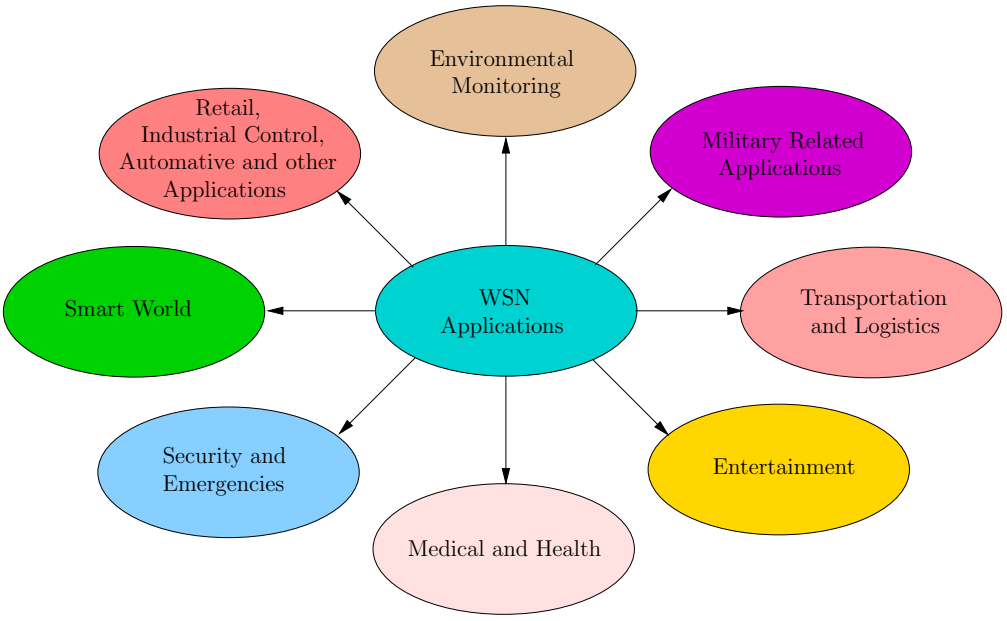

FIGURE 1.1: The taxonomy of the WSN applications.

may be expected to be capable of the IoT at a low cost and low power, whilst relying on miniature sensor devices. Hence understanding WSNs and the Internet plays a significant role in powering the IoT and its sophisticated applications. Here, we focus our attention on WSNs, their applications and on their specific design objectives, with an emphasis on their network lifetime.

A WSN is composed of spatially-distributed autonomous devices communicating wirelessly and utilizing sensors in order to gather information or to detect certain events of significance in the physical and environmental conditions. These sensor devices are capable of simultaneously sensing, processing and communicating, which offers a vast number of compelling applications [1–3, 13–16], as illustrated in Fig. 1.1. For example, one of the oldest application areas of WSNs is found in environmental monitoring, ranging from tracking herds of animals to monitoring hard-to-reach areas [1, 2, 13]. Military battlefields also constitute a potential application of WSNs, especially in inaccessible or hostile territory, where WSNs may be indispensable for the detection of snipers, intruders and for tracking their activity [1]. Additionally, the deployment of WSNs can be very useful for improving logistics, where tackling the challenges in managing goods that are being transported can preserve their quality by monitoring the temperature of containers, etc. As another example, WSNs can be used for improving the gaming experience by enhancing the interactions between the physical world and virtual world using wearable and implantable camera sensors. Medical and health applications form another important set of WSN applications enabling carers to monitor the conditions of patients either in hospital or in elder people's home. Radiation level control, explosive gas level and leakage detection, as well as restricted area control also form part of the potential security and emergency applications.

In the new IoT era, many smart applications using WSNs are proposed by a company called "libelium[1]" [17], which provides sensor devices for diverse applications in smart cities, smart environments, for smart metering, smart water provision, for efficient and smart agriculture, for smart farming and so on [5]. Many other sophisticated WSN applications have been proposed in the literature for improving the quality of human life, such as supply-chain control for retail purposes, remote control of home appliances, industrial factory automation, automotive-, rail-, and air-traffic control as well as disaster control [1–3, 13–15].

The above-mentioned applications have been designed for accomplishing a specific objective or a desired task. Therefore, as illustrated in Fig. 1.2, there are several design criteria that necessitate the careful consideration of the WSN deployment depending on the application requirements and on the objectives to be achieved [2, 3, 13, 15]. Observe in Fig. 1.2 that the particular choice of the communication medium affects the design of the communication protocols, because different radio spectral bands require different communication configurations, including the transmit power, the effective transmission distance, the presence or absence of line-of-sight propagation, the interference levels encountered, and so on. Similarly, once the carrier frequency has been determined, the related channel characteristics [18–20] play a significant role in predetermining the attainable performance of the application considered. Additionally, as illustrated in Fig. 1.2, the cost of each sensor device is also an important design factor in terms of determining the total cost of the WSN, since the application considered may require the scattering of thousands of sensor devices in a specific field [21, 22]. Hence, indepth studies have been dedicated to minimizing the total cost of the WSN, while providing the maximum grade of connectivity and coverage quality [23, 24]. Fig. 1.2 captures the main design objectives of WSNs at a glance, demonstrating that the battery capacity, computing and storage capabilities constitute precious limited resources, which the design of WSNs hinges on. Furthermore, from a physical layer point of view, maximizing the throughput whilst concurrently reducing the BER may be feasible, but only at an increased implementational complexity and at a commensurately increased energy dissipation (ED) necessitated by sophisticated signal processing [25], again, as illustrated in Fig. 1.2.

Fig. 1.2 also suggests that the network topology [26–29] is another crucial aspect influencing the design of WSNs, since it is often conceived for a particular application, which indeed affects all the salient network characteristics, such as the delay, the capacity, the routing complexity, the energy consumption and so on. Additionally, it is crucial to maintain a high grade of connectivity and coverage quality, which is facilitated by the appropriate density of nodes. To elaborate a little further, an excessive node-density generates excessive traffic conveying correlated data, whilst an insufficient density degrades the coverage quality. Observe in Fig. 1.2 that the provision of sophisticated interference management or alignment techniques [30, 31] plays a significant role in reducing the ED, while provid-

[1] http://www.libelium.com

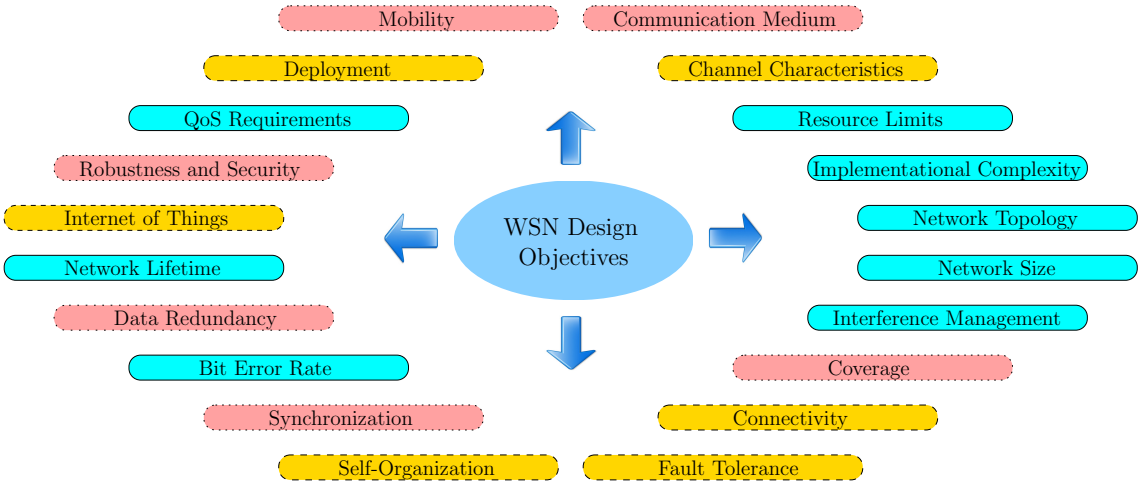

FIGURE 1.2: The design objectives of the WSNs.

ing an increased network capacity. Coverage quality has been extensively studied in the context of WSNs [23, 24, 32], which is crucial for the sake of maintaining seamless connectivity. Explicitly, the coverage quality and the grade of connectivity influences the choice of data gathering methods and routing algorithms designed for achieving the desired QoS requirements, as indicated in Fig. 1.2.

Moreover, the data gleaned from a particular sensor node may be corrupted by the hostile, error-prone wireless channel, hence it is important to verify and if necessary, to correct the information relayed to the sink node for increasing the attainable reliability [20, 33–36]. Additionally, maintaining fault tolerance is also of high significance, as indicated in Fig. 1.2. Specifically, in large-scale WSN deployments, self-organization and self-configuration assist the network in replacing the failing sensor nodes without perturbing the entire application [37], as illustrated in Fig. 1.2. Time synchronization [38] is often provided by the global positioning system (GPS), but the light-weight sensor node batteries may be unable to satisfy the energy requirement of high-power GPS receivers. Therefore, as observed in Fig. 1.2, the conception of low-power yet efficient localization and time synchronization techniques [38] is crucial for the longevity of WSNs. The attainable capacity of a wireless link strictly depends on the signal power, on the noise and on the interference levels at the receiver [30, 31]. Since the channel conditions are time-variant, maintaining the required BER can be a challenging task in a low-power WSN [39], as indicated in Fig. 1.2.

In densely populated WSNs, the data observed by the adjacent sensors may be correlated [40], which may result in an inefficient exploitation of the resources. The *lifetime* of a WSN represents the total amount of time, over which the network remains operational and hence supports the application considered [31, 39]. Therefore, observe in Fig. 1.2 that the network's lifetime is one of the most important design factors in WSNs, since all the above-mentioned design objectives can only be met, if the network is operational. The inte-

gration of WSNs with the Internet and other networks is important in terms of supporting the emerging vision of the IoT. More explicitly, there are billions of networked devices on the market, but their compatibility is not guaranteed. Therefore, cross-platform considerations, device addressing and the interoperability of applications are critical for the realization of the IoT combined with WSNs in order to conceive smart applications [5].

In the event of node failure, the network still has to remain operational and robust [41], as indicated in Fig. 1.2. It also has to be resilient against denial-of-service (DoS) attacks and must be resistant to eavesdropping [13, 15]. Additionally, application-specific QoS requirements, such as the latency, ED, lifetime, BER and throughput have to be taken into account during the deployment of the WSN in order to guarantee the seamless operation of the application considered [39, 42], as illustrated in Fig. 1.2. The specific deployment strategies of WSNs [21, 22] substantially affect the characteristics of the network, such as the sensor node density, the specific sensor locations and the anticipated degree of network dynamics. Similarly, the grade and the nature of mobility also has a significant impact on the degree of network dynamics, which affect the design of both the routing protocols and of the associated distributed algorithms [13, 15, 43–45]. Explicitly, the above-mentioned design factors crucially depend on the mobility characteristics, as presented in Fig. 1.2. Therefore, the design factors of self-configuration, self-organization, robustness, reliability and fault tolerance play a significant role in constructing an adaptive and scalable WSN [41]. We note that in Fig. 1.2 the box printed using solid line with rounded corners (in turquoise color) represents the particular design objectives we focused our attention on in our own WSN deployment, while the dashed-lined box with rounded corners (in gold-yellow color) illustrates the design objectives relevant to ours, but not specifically addressed. Finally, the dotted-lined box with rounded corners (in pink color) shows the objectives that are beyond our current scope. Explicitly, in this treatise we specifically focused our attention on the NL as our design objective and characterized the trade-off between the NL and the BER, with the BER being our salient QoS requirement. Furthermore, we considered the effect of different network sizes in the context of a specific network topology in order to illustrate the implementational complexity of a battery-constrained interference-limited WSN deployment.

Sensor nodes usually rely on a limited energy supply in WSNs. Therefore, the energy dissipation of each sensor has to be carefully considered in such networks, since the failure of a node may lead to wasting of the network's resources. Due to the impact of the OSI layers on the energy dissipation, exploiting interactions between layers, such as the physical layer, MAC layer, network layer and transport layer may lead to a more energy-efficient use of the limited resources. For example, power control in the physical layer will affect the network connectivity and thus the overall network topology. Therefore, in order to minimize the energy dissipation caused by the interference and potential retransmissions, scheduling and channel assignment carried out in the MAC layer will have to be dynami-

cally adapted due to the instantaneous network connectivity adjustment encountered in the physical layer. Furthermore, the adaptation of scheduling and channel assignment in the MAC layer will influence the routing decisions and flow distributions in the network layer. For example, if a sensor is scheduled to switch to its sleep mode, routing adjustments have to be made accordingly. More explicitly, one of the two options are more beneficial for the sake of energy-efficiency and of NL maximization, which is to enforce the waking up of the sleeping sensor and use it for forwarding data, where the network layer over-rules the MAC. Alternatively, the sensor may remain in its sleep mode, where the MAC layer over-rules the network layer. Explicitly, exploiting the adaptive interactions amongst the various layers can be beneficial for NL maximization. Additionally, when considering the design objectives described in Fig. 1.2, guaranteeing the QoS required may be a challenging task. However, maintaining an adequate QoS is crucial for applications and networks providing sophisticated real-time services, such as audio, voice over IP (VoIP) and video surveillance. Nonetheless, all the above-mentioned design objectives may be related to one or more of these layers. For example, maintaining a target BER is the duty of the physical layer, while the MAC layer is responsible for scheduling operations. By contrast, routing decisions are made at the network layer. A WSN considering these layers independently may perform poorly, since a decision made at the physical layer may affect the performance of both the MAC layer and of the network layer as mentioned before, especially when the resources are limited. In order to circumvent the potential design conflicts mentioned in Fig. 1.2 and to maintain the desired QoS requirements, various solutions have been proposed in the literature relying on the information gleaned from the independent layers [46]. However, this conventional approach of using independent layers was essentially conceived for wired networks [46]. On the other hand, rather than having an independent layered design, WSNs benefit from the information exchange between different layers, when aiming for enhancing the overall network performance operating in a dynamic environment, relying on an ad hoc infrastructure and time-varying channel conditions. Therefore, the QoS requirements can only be maintained by exploiting the interactions between the various layers, which leads us to the so-called cross-layer design philosophy.

A review of the cross-layer design conceived for maintaining the desired QoS in wireless networks has been presented in the context of scheduling in [47], in delay- and reliability-aware applications in [48] and in the context of multihop wireless networks in [46]. For example, minimizing the energy dissipation and maximizing the network lifetime is crucial in battery-constrained WSNs, where coupling various layers is beneficial for cooperatively minimizing the energy dissipation of each layer, which is expressed in [49–53]. It is shown in [46] that due to the inherent interdependence of the layers, cross-layer optimization techniques can be exploited in order to improve the energy-efficiency using adaptive transmission, power and resource allocation schemes, while maintaining certain service requirements and tackling the environmental dynamics and channel characteristics. For example, Johansson *et al.* [54]

jointly optimized the end-to-end rates, routing, power allocation and scheduling. The authors of [54] specifically focused their attention on the optimization of the resource allocation that maintains fair end-to-end rates, where a solution was proposed based on the so-called nonlinear column generation technique, which converges to the optimal solution. Similarly, Cui *et al.* in [55] jointly optimized the physical, MAC and routing layers, where the circuit energy consumption was also considered. The cross-layer problem considered in [55] was relaxed to a convex optimization problem formulated as a powerful low-complexity solution algorithm, which provided substantial energy savings. *In this treatise, we focus our attention on the NL as our salient QoS requirement, where we use cross-layer design in order to minimize the energy dissipation of each layer and to maximize the NL by exploiting the interactions of various layers.*

The NL can be defined as the total amount of time during which the network is capable of maintaining its full functionality and/or of achieving particular objectives during its operation, as exemplified in [56] and [57]. Moreover, the NL is a crucial metric of enabling the network designer to make informed decisions for the sake of maintaining the desired network performance and QoS in WSNs, which usually relies on the limited battery capacity of the sensor nodes within the WSN. In realistic applications, such as for example in case of sensors embedded into glaciers for measuring climate changes [58], replenishing the battery energy of the sensors and/or replacing the sensors is usually impractical and/or costly. Therefore, the NL is constrained by the battery of the individual sensors in the WSN considered [2,3]. However, the NL definition may vary depending on the specific application, on the objective function and on the network topology considered. Specifically, the authors of [59], [60] and [61] defined the expiration of the NL as the time instant at which a certain number of nodes in the network depleted their batteries. As a further example, the NL was defined in [62] as the lifetime of the specific sensor node associated with the highest energy consumption rate, whereas the authors of [63], [64] and [65] considered the lifetime of the network to be expired at the particular instant, when the first node's battery was depleted. The NL in [64] was also defined as the instant, when the first data collection failure occurred. Note that there are various alternative NL definitions, which were discussed in [13, 29, 39, 56, 63, 64, 66]. In summary, the NL models considered in the literature are as follows:

1. The earliest time instant at which any of the sensor nodes in the network fully depletes its battery energy [30, 31, 63–65].
2. The time instant, when a certain fraction of operational nodes exists in the network [59–61].
3. The time, at which the first cluster head fully discharges its battery energy [67].
4. The time, when all the sensor nodes in the network fully deplete their battery energy [68].
5. The duration, when the target area is covered by at least k number of nodes, which was termed as the k-coverage [69].

6. The time, until a specific target area [70] or whole area [71, 72] is covered by at least a single sensor node.
7. The time duration, in which a certain fraction of a region is covered by at least one node [73].
8. The time duration, in which the coverage falls below a predefined threshold [74].
9. The total amount of time, until either the coverage or the packet delivery ratio falls below a certain threshold [75].
10. The time, when a certain amount of information is transmitted [76].
11. The instant, when the first data collection failure occurred [64].
12. The cumulative active time, when the first loss of coverage occurs [71].
13. The time, when a percentage of sensors in the network maintains a specific path to the base station [75].
14. The time, when either the connectivity or the coverage is lost [32].
15. The duration, when the network becomes incapable of maintaining a reasonable event detection ratio [68].
16. The duration, when the concurrent analysis of connectivity probability and k-coverage stays above a predefined threshold [69].
17. In [56], a parameterized NL definition, including the above common definitions, such as node availability, coverage, connectivity, service disruption tolerance and so on, is provided. This NL definition can be used for most of the applications, since the required objective can be incorporated into or discarded from the formulation of the NL definition.
18. The estimation task cycles achieved before the network becomes nonoperational [77].
19. The time, when the last report is delivered to the sink [43]. More explicitly, the time, when the sink node is no longer able to receive data and is disconnected from sensors.
20. The number of data collections, when the number of depleted sensor nodes reaches a certain threshold [18].
21. The longest time, when the QoS constraint, such as the signal-to-noise ratio (SNR) requirement is satisfied [78].

Up to this stage, we have covered the topics on the history of WSNs and IoT, on WSNs and IoT integration, on the classification of WSN applications, on the design objectives of WSNs, on their QoS requirements, on their cross layer design and its importance in WSNs as well as on the NL definition, used in the literature. In the next section we provide a comprehensive survey of NL maximization techniques.

1.1.1 Network Lifetime Maximization Techniques

There are several NL maximization techniques in the literature, as classified in Fig. 1.3. Each of them may consider a different NL definition and a different objective function, where the NL definition may also vary depending on the application, on the particular objective and on

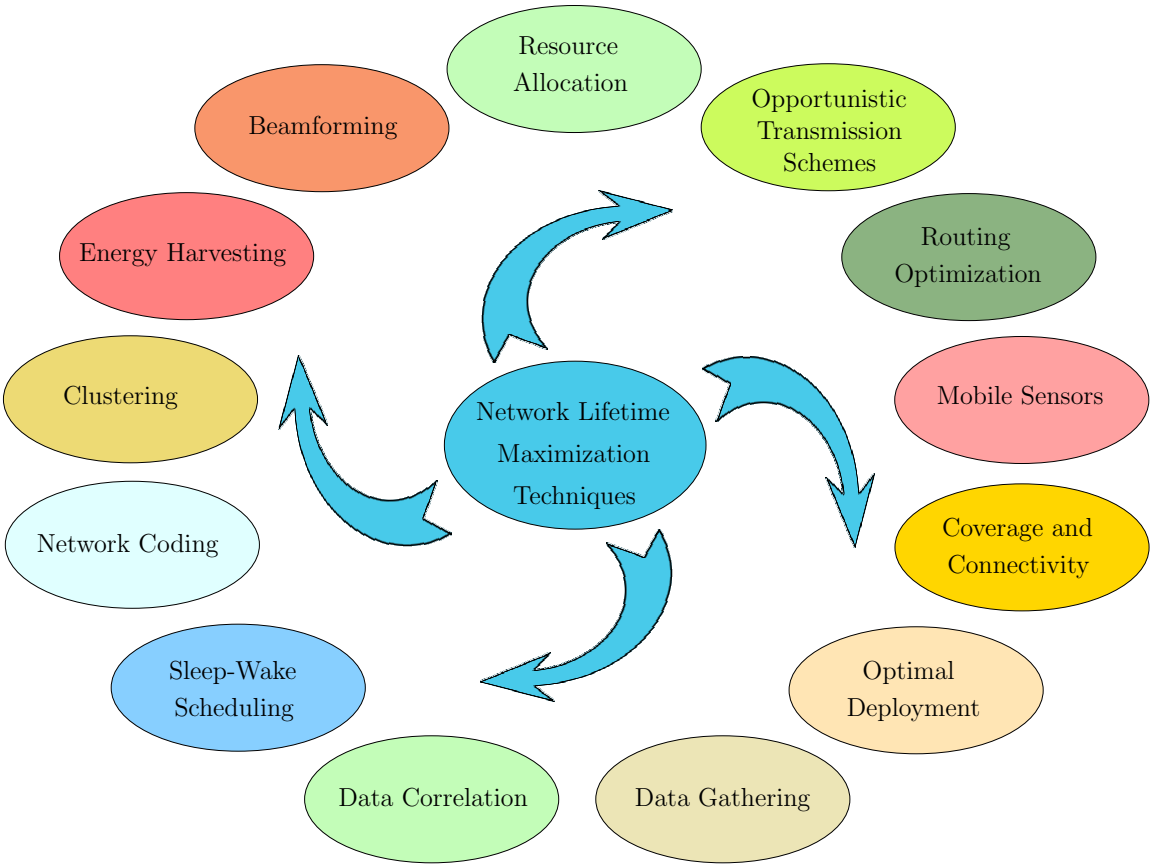

FIGURE 1.3: The classification of the NL maximization techniques.

the network topology considered. Observe in Fig. 1.3 that resource allocation, opportunistic transmission schemes, routing optimization, mobile sensors, coverage and connectivity, optimal deployment, data gathering, temporal-spatial data correlation (data aggregation), sleep-wake scheduling, network coding, clustering, energy harvesting and beamforming are the techniques we highlight in this part of the chapter. Therefore, we classify these techniques, as illustrated in Fig. 1.3, where the NL was maximized using a particular technique from the literature. In the following, we discuss each NL maximization technique in detail based on Fig. 1.3.

1.1.1.1 Resource Allocation

Resource allocation is one of the most important and perhaps the most frequently investigated NL maximization techniques in the literature [20, 28, 30, 31, 35, 79], which essentially relies on the cross-layer optimization of various cross-layer design objectives, including the transmission reliability, routing, power control, scheduling, optimal deployment, throughput maximization, estimation quality and rate adaptation, which indeed form part of the design objectives in WSNs, as presented in Fig. 1.2. For example, Hoesel *et al.* [80] proposed a cross-layer approach for jointly optimizing the MAC and routing layer in order to maximize

the NL, where the MAC layer sets the sensors to either their active- or inactive-mode and the routing layer aims for finding energy-efficient routes in the face of a dynamic topology. In [35], Kwon *et al.* investigated the NL maximization problem of WSNs, which jointly considers the physical layer, the MAC layer and the routing layer in conjunction with the end-to-end transmission success probability constraint. The authors of [35] demonstrated that the joint optimization of power control, retransmission control and routing optimization is capable of significantly improving the NL compared to suboptimal algorithms. Another resource allocation approach was proposed for NL maximization by Xu *et al.* [20], examining the conflicting design objectives, including the transmit rate, delivery reliability and NL using an optimization framework imposing time-varying channel capacity, reliability and energy constraints and demonstrated that the selection of the suitable weights for each of these objectives is crucial for the sake of meeting the desired application performance.

Additionally, the authors of [30] considered the joint optimal design of the transmit rate, power and link scheduling for the sake of NL maximization in an interference-limited WSN communicating over an AWGN channel and demonstrated the benefit of multi-hop routing, traffic-load balancing, interference management and spatial reuse in extending the NL. Similarly, in [82] the cross-layer operation of the link layer, MAC layer and routing was invoked for maximizing the NL considering the transmitter's circuit energy dissipation in a WSN communicating over an AWGN channel. Another cross-layer optimization technique was employed in [81] for illustrating the trade-off between NL maximization and application performance. As a further advance, the authors of [83] investigated the trade-off between the energy consumption and application-layer performance exploiting the interplay between network lifetime maximization and rate allocation problems with the aid of cross-layer operation in WSNs. Additionally, Wang *et al.* [28, 79] advocated a cross-layer approach in order to minimize the energy dissipation and to maximize the NL of a WSN composed of multiple sources and a single sink, where power allocation, link scheduling and routing problems were jointly optimized. A similar study was performed in [84], formulating the network lifetime maximization problem as a joint power, rate and scheduling problem subjected to rate distortion constraints, capacity constraints of the links, energy constraint of the sensor batteries and delay constraint of the encoded data arriving at the sink node. Another cross-layer approach conceived for maximizing the NL was proposed in [86], where MAC-aware routing optimization schemes were designed for WSNs that are capable of multichannel access. A different approach to NL maximization was introduced in [91], where both the contention probability and the sleep control probability of the sensor nodes was utilized for formulating the NL maximization problem, while maintaining both the throughput and the SINR requirements.

An optimal control approach was invoked for maximizing the NL with the aid of a carefully selected routing probability [65], where all the sensors were configured to deplete their energy exactly at the same time. Additionally, Phan *et al.* [21] presented a two-stage cross-

TABLE 1.1: Milestones of resource allocation techniques that maximize the lifetime of WSNs. (Part-I)

Year	Author(s)	Contribution
2004	Hoesel *et al.* [80]	proposed a cross-layer approach for jointly optimizing the MAC and routing layer in order to maximize the NL, where the MAC layer sets the sensors to either their active- or inactive-mode and the routing layer is involved in finding energy-efficient routes, despite of the dynamics of the topology.
2006	Kwon *et al.* [35]	investigated the NL maximization problem of WSNs, which jointly considers the physical layer, the MAC layer and the routing layer in conjunction with the end-to-end transmission success probability constraint.
	Madan *et al.* [30]	considered the joint optimal design of the transmit rate, power and link scheduling for the sake of NL maximization in an interference-limited WSN communicating over an AWGN channel.
	Nama *et al.* [81]	performed a cross-layer optimization approach illustrating the trade-off between NL maximization and application performance.
2007	Madan *et al.* [82]	cross-layer operation of the link layer, MAC layer and routing was invoked for maximizing the NL considering the transmitter's circuit energy dissipation in a WSN communicating over an AWGN channel.
	Zhu *et al.* [83]	investigated the trade-off between the energy consumption and application-layer performance exploiting the interplay between network lifetime maximization and rate allocation problems with the aid of cross-layer optimization of WSNs.
2008	Li *et al.* [84]	formulated the network lifetime maximization problem as a joint power, rate and scheduling problem based on rate distortion constraints, capacity constraints of the links, energy constraint of the sensor batteries and delay constraint for the encoded data arriving at the sink node.
2009	Phan *et al.* [21]	presented a two-stage cross-layer optimization problem, where the first stage involves maximizing the number of sensor nodes deployed the for existing WSN and the second stage includes the power allocation and scheduling operations in order to maximize the NL.
2011	Luo *et al.* [85]	studied the trade-off between conflicting throughput and NL objectives with the aid of a cross-layer power allocation scheme and demonstrated that an optimal choice of transmit power is essential in the interest of achieving a high throughput and a high NL.
2012	Ehsan *et al.* [86]	cross-layer MAC-aware routing optimization schemes were designed for WSNs that are capable of multichannel access for the sake of NL maximization.

TABLE 1.2: Objective function(s) (OF), constraint(s) and optimization algorithm(s) of Table 1.1 in the context of resource allocation techniques that maximize the lifetime of WSNs.

Year	Author(s)	OF(s)	Constraint Function(s)	Optimization tool(s)
2004	Hoesel *et al.* [80]	NL	TDMA-based MAC protocol, sleep scheduling, routing, dynamic topology	An on-demand source routing algorithm [87] using OMNeT++
2006	Kwon *et al.* [35]	NL	Power control, retransmission control, energy efficient routing, end-to-end transmission success probability	Greedy power allocation, cost-based routing, greedy retry limit allocation, cost-based routing and power control algorithms [35]
	Madan *et al.* [30]	NL	Flow conservation, rate constraints, energy conservation, power limits, link scheduling	An iterative algorithm solving a series of convex optimization problems
	Nama *et al.* [81]	NL, application performance	Source rate control, resource allocation, flow control energy dissipation constraint	An iterative algorithm based on subgradient method [88]
2007	Madan *et al.* [82]	NL	Rate and power allocation, flow and energy conservation, scheduling	An iterative algorithm for finding the optimal transmission scheme
	Zhu *et al.* [83]	NL, fair rate allocation	Flow constraints, power control, energy constraints, MAC contention	A fully distributed algorithm considering network utility maximization framework
2008	Li *et al.* [84]	NL	Rate and power allocation, capacity limits, scheduling, energy dissipation, rate distortion, delay constraint	Successive convex approximation algorithm [89]
2009	Phan *et al.* [21]	NL	Sensor node admission and deployment, power allocation, link scheduling	Cross-layer optimization framework based on mixed integer linear programming using CPLEX library [90]
2011	Luo *et al.* [85]	NL, throughput	Power allocation, flow conservation, capacity limit, scheduling constraint, energy dissipation constraint	Algorithms for max-min NL with max-min throughput, for maximizing the throughput under NL constraint, for maximizing the NL under throughput constraint
2012	Ehsan *et al.* [86]	NL	MAC contention control, rate requirement, energy dissipation constraint, flow balance constraint	Routing schemes based on linear programming models and mixed integer programming model using CPLEX [90] and Matlab

TABLE 1.3: Milestones of resource allocation techniques that maximize the lifetime of WSNs. (Part-II)

Year	Author(s)	Contribution
2013	Jeon *et al.* [91]	both the contention probability and the sleep control probability of the sensor nodes was utilized for formulating the NL maximization problem, while maintaining both the throughput and SINR requirement.
2014	Xu *et al.* [20]	examined the conflicting design objectives including transmit rate, delivery reliability and NL through an optimization framework with time-varying channel capacity, reliability and energy constraints in an energy-constrained WSN and demonstrated that the selection of the suitable weights for each objective is crucial for the desired application performance.

TABLE 1.4: OF(s), constraint(s) and optimization algorithm(s) of Table 1.3 in the context of resource allocation techniques that maximize the lifetime of WSNs.

Year	Author(s)	OF(s)	Constraint function(s)	Optimization tool
2013	Jeon *et al.* [91]	NL	Contention and sleep control probability, throughput and SINR requirements, energy constraints	An algorithm based on subgradient method [88] for finding the optimal Lagrange multipliers
2014	Xu *et al.* [20]	NL, transmit rate, delivery reliability	Capacity limits, reliability and energy dissipation constraints	Stochastic subgradient algorithm [92, 93]

layer optimization problem, where the first stage involves maximizing the number of sensor nodes deployed for the existing WSN and the second stage includes the power allocation and scheduling operations in order to maximize the NL. A similar cross-layer design approach was proposed in [94] by adopting the constraints of the joint routing and MAC layers in order to maximize the NL. The authors of [85] studied the trade-off between conflicting throughput and NL objectives with the aid of a cross-layer power allocation scheme and demonstrated that an optimal choice of transmit power is essential in the interest of achieving a high throughput and a high NL. The authors of [95] investigated the impact of the transmit rate on the NL for both single-hop and multi-hop transmission scenarios by exploiting the interplay between the estimation accuracy of the channel as well as the data transmitted and energy-efficiency, since increasing the transmit rate degrades the NL, but on the other hand improves the estimation quality of the data transmitted. The major contributions on resource allocation techniques conceived for maximizing the lifetime of WSNs

TABLE 1.5: Milestones of opportunistic transmission techniques that maximize the lifetime of WSNs.

Year	Author(s)	Contribution
2005	Chen *et al.* [64]	advocated an efficient MAC protocol, which relies both on the channel state information and on the MAC's knowledge of the residual energy in order to maximize the NL.
2007	Chen *et al.* [96]	focused their attention on the transmission scheduling of specific access points communicating over a fading channel relying both on the opportunistic channel state information and on the remaining battery charge information for the sake of NL maximization.
	Chen *et al.* [18]	considered the cross-layer design of an opportunistic transmission protocol by jointly considering both the channel state information and the residual battery charge.
2010	Phan *et al.* [97]	proposed an energy-efficient transmission scheme based on the prevalent channel conditions in order to maximize the NL.
	Hung *et al.* [98]	developed a routing protocol exploiting the advantages of opportunistic routing in order to maximize the NL.
2011	Wu *et al.* [99]	proposed a coalition formation game-theory method in the interest of selecting the best possible transmission scheme for maximizing the NL.

are summarized in Tables 1.1 and 1.3, where their OFs, constraints and their optimization algorithms are surveyed in Table 1.2 and 1.4, respectively.

1.1.1.2 Opportunistic Transmission Schemes

Once the information has been gathered by the sensors, its transmission to the sink node can be initiated. However, it has to be carefully considered, which specific group of sensors should relay the sensed data to the destination node, at which instant in time, especially when communicating over fading channels. Plausible logic dictates that transmission using those particular sensors, which momentarily experience better channels conserves considerable amount of energy, provided that the network is 'young'. However, when the network is 'old', balancing the residual battery energy plays a significant role in extending the NL. Explicitly, in [18,19] the authors considered the cross-layer design of an opportunistic transmission protocol by jointly considering both the channel state information and the residual battery charge, each of which may dramatically affect the achievable NL. It was demonstrated that the trade-off between the channel state information and the residual battery charge had to take into account the specific age of the WSN. More explicitly, if the network is young, it will be beneficial to prioritize the sensor nodes having the benefit of better channels, since reducing the energy consumption is of high priority for young WSNs. On the other hand, when the network is old, relying on the sensors with more residual battery

TABLE 1.6: OF(s), constraint(s) and optimization algorithm(s) of Table 1.5 in the context of opportunistic transmission techniques that maximize the lifetime of WSNs.

Year	Author(s)	OF(s)	Constraint function(s)	Optimization tool
2005	Chen *et al.* [64]	NL	Channel state information (CSI), residual energy information (REI)	A greedy max-min algorithm [100] in order to maximize the NL by exploiting CSI and REI
2007	Chen *et al.* [96]	NL	Transmission scheduling, CSI, REI, optimal scheduling	Formulated as a stochastic shortest path Markov decision process [101] and solved using a dynamic protocol for lifetime maximization
	Chen *et al.* [18]	NL	CSI, REI	The performance of the greedy max-min algorithm is compared to a dynamic protocol for lifetime maximization
2010	Phan *et al.* [97]	NL	Instantaneous channel conditions, energy efficient transmission scheme, throughput end-to-end delay	An algorithm based on binary decision aided transmission with channel aware back-off adjustment
	Hung *et al.* [98]	NL	Opportunistic routing, path diversity, reliability, delay	A distributed routing scheme, namely the so-called energy-efficient opportunistic routing technology [102]
2011	Wu *et al.* [99]	NL	Transmission scheme selection, transmission distance, outage probability, power allocation	A coalition formation game [103] using non-transferable utility game theory model

charge is beneficial in order to balance the overall energy dissipation of the network and to maximize the NL. Similarly, Matamoros *et al.* [104] proposed opportunistic power allocation and sensor selection schemes for parameter estimation, where only the specific sensors enjoying favorable channel conditions were involved in the estimation of the data transmitted via adapting their transmit power relying on both the channel state information and the residual battery charge information in order to enhance the NL. Furthermore, Chen and Zhao [64] advocated an efficient MAC protocol, which relies both on the channel state information and on the MAC's knowledge of the residual energy in order to maximize the NL. In [96] the authors focused their attention on the transmission scheduling of specific access points communicating over a fading channel relying both on the opportunistic channel state information and on the remaining battery charge information for the sake of NL maximization. Phan *et al.* [97] proposed an energy-efficient transmission scheme based on the prevalent

channel conditions in order to maximize the NL. More explicitly, transmissions were only activated, when the channel quality was above a predefined threshold, while communicating over fading channels. Moreover, a routing protocol exploiting the advantages of opportunistic routing in order to maximize the NL was presented in [98], where both the end-to-end transmission cost as well as the residual battery charge of each sensor and the transmission success probability of each relay node was jointly considered. As a further development, Wu *et al.* [99] proposed a coalition formation game-theory framework in the interest of selecting the best possible transmission scheme for maximizing the NL. The major contributions of the opportunistic transmission techniques conceived in the interest of maximizing the NL are summarized in Table 1.5, where their OFs, constraints and their optimization algorithms are surveyed in Table 1.6.

1.1.1.3 Routing Optimization

Routing decisions play a significant role in determining the achievable NL. Specifically, constructing lifetime-aware routes is crucial for the sake of NL maximization, since a dynamic route created by the sensors having the maximum residual battery charge can be beneficially exploited, each time when a transmission from the source node to destination node is initiated, which assists the network in balancing the overall energy dissipation and ultimately in extending its lifetime. In order to maximize the NL, in [105] the routing of the tele-traffic had to be balanced across the WSN considered, since repeatedly using the same route depletes the battery of the corresponding sensors more rapidly than that of the rest of the sensors and thus degrades the NL. However, exploiting the battery energy of the remaining active sensors has the potential of extending the NL. Therefore, optimizing the routes directly affects the NL. For instance, Liu *et al.* [109] considered a joint routing and sleep-mode scheduling algorithm for balancing the traffic load across the entire network and for reducing the energy dissipation by allowing the idle sensors to switch to their sleep mode. The joint optimization based algorithm proposed in [109] extended the NL by 29% compared to either the pure routing optimized scheme or to a pure sleep-mode scheduling scheme operating without their joint optimization. Furthermore, a dramatic NL improvement of about 284% was observed compared to the conventional optimal routing schemes relying on a fixed sleep-mode scheduling. Similarly, Hsu *et al.* [113] proposed the appropriate organization of sensors for jointly optimizing both their sleep-mode for energy-efficiency and their opportunistic routing for the sake of balancing their traffic load distribution and for improving the attainable transmission reliability across the network for the sake of NL maximization. On the other hand, the joint optimization of the data aggregation[2] and maximum-lifetime-

[2]Data aggregation is an information processing technique, which incorporates data arriving from various sensor nodes in order to cope with the spatial and temporal data correlation by eliminating the redundant information, while minimizing the number of transmissions with the aid of aggregators located at specific sensor nodes.

TABLE 1.7: Milestones on the routing optimization techniques that maximize the lifetime of WSNs.

Year	Author(s)	Contribution
2000	Chang *et al.* [105]	advocated that the routing of the tele-traffic had to be balanced across the WSN considered in order to maximize the NL.
2004	Chang *et al.* [106]	formulated the maximum-NL routing challenge as a linear programming problem, which was used as the bench marker of the near-optimal NL acquired by their proposed routing algorithm.
2008	Hua *et al.* [107]	considered the joint optimization of the data aggregation and maximum lifetime routing.
2009	Cheng *et al.* [27]	another cross-layer approach was conceived for maximum NL routing,where the energy- and bandwidth-requirements were jointly optimized by carefully selecting the routing and rate allocation.
	Li *et al.* [77]	proposed three components for the NL optimization problem including optimizing the source coding, the source throughput of each sensor node and the multihop routing.
	He *et al.* [108]	distributed algorithms were developed by exploiting the so-called Lagrangian duality in order to find optimal solution to the lifetime maximization problem, which was formulated based on the joint optimization of the source rates, the encoder's power dissipation and the routing scheme.
2010	Liu *et al.* [109]	considered a joint routing and sleep-mode scheduling algorithm for balancing the traffic load across the entire network and for reducing the energy dissipation by allowing the idle sensors to switch to their sleep mode.
2011	Amiri *et al.* [110]	studied the joint optimization of traffic routing and camera selection strategy for the sake of NL maximization.
2012	Al-Shawi *et al.* [111]	developed a routing algorithm for WSNs for extending the NL, where the aim is to find an optimal route from the SN to the sink node with the aid of the highest remaining battery charge, the minimum number of hops and the minimum traffic load.
2013	Peng *et al.* [112]	invoked intra-route coordination for allowing the nodes along the same route to balance their node lifetime durations, which was combined with inter-route coordination for additionally balancing the lifetime durations of the sensors on different routes in order to collaboratively maximize the NL.
2014	Cassandras *et al.* [65]	an optimal routing scheme was proposed with the objective of maximizing the NL, where the authors considered realistic nonideal batteries by modeling the nonlinear energy dissipation behavior of the typical batteries.
	Hsu *et al.* [113]	proposed the appropriate organization of sensors for jointly optimizing both their sleep-mode for energy-efficiency and their opportunistic routing for the sake of balancing their traffic load distribution and for improving the transmission reliability across the network for the sake of NL maximization.

TABLE 1.8: OF(s), constraint(s) and optimization algorithm(s) of Table 1.7 in the context of routing optimization techniques that maximize the lifetime of WSNs.

Year	Author(s)	OF(s)	Constraint function(s)	Optimization tool
2000	Chang *et al.* [105]	NL	Balancing energy dissipation rates amongst nodes, flow routing	Flow augmentation algorithm [114], flow redirection algorithm [115]
2004	Chang *et al.* [106]	NL	Flow conservation, routing control packets, energy dissipation rate, residual energy levels	Flow augmentation algorithm based on the shortest path routing strategy using the link cost quantified by the communication energy dissipation and residual energy levels
2008	Hua *et al.* [107]	NL	Traffic reduction, traffic balancing, data aggregation	Maximum lifetime routing algorithm using routing adaptation and the classic gradient method
2009	Cheng *et al.* [27]	NL	Energy and bandwidth constraints, link rate allocation, routing	Algorithms for scalable rate allocation along the shortest paths and optimizing the lifetime subject to a band-width constraint
	Li *et al.* [77]	NL	Source coding, source throughput, multihop routing	An algorithm using character-based routing [77], which relays data only over nodes having higher importance
	He *et al.* [108]	NL	Source rate, encoding power, routing scheme	A distributed algorithm using subgradient method [88, 116]
2010	Liu *et al.* [109]	NL	Balanced traffic routing, sleep scheduling	An iterative geometric programming algorithm [89] based on signomial programming [117]
2011	Amiri *et al.* [110]	NL	Traffic routing, camera selection strategy, node collaboration	Collaborative routing and camera selection algorithm, heuristic routing and camera selection algorithm
2012	Al-Shawi *et al.* [111]	NL	Optimal route, residual battery charge, number of hops, traffic load	An algorithm based on the joint design of a fuzzy approach [118] and an A-star algorithm [119]
2013	Peng *et al.* [112]	NL	Balancing node lifetime, delivery delay constraint, power dissipation	A holistic lifetime balancing technique, namely the so-called intra-route and inter-route coordination method
2014	Cassandras *et al.* [65]	NL	Optimal routing scheme, nonlinear battery discharging, balancing energy dissipation	An algorithm solving a set of non-linear programming problems based on kinetic battery model [120]
	Hsu *et al.* [113]	NL	Sleep scheduling, traffic balance, route diversity, transmission reliability, opportunistic routing	Joint design of asynchronous sleep-wake-up scheduling and opportunistic routing technique

oriented routing was considered in [107], where the data aggregation reduces the traffic-load across the network by avoiding the transmission of the redundant data, which is identified with the aid of the temporal-spatial data correlation. Hence, the power dissipation of the sensor nodes that are adjacent to the sink node can be substantially reduced, while the maximum-lifetime routing policy balances the traffic for avoiding the overloading some of the sensors. Additionally, Amiri *et al.* [110] studied the joint optimization of traffic routing and camera selection strategy for the sake of NL maximization, where efficient sensor collaboration was required for data sensing and camera selection for the sake of extending the NL. This approach supports the collaboration of different sensors to avoid redundant sensing of various areas in the WSN and assists in the cooperative routing of the tele-traffic generated. In [111], Al-Shawi *et al.* developed a routing algorithm for WSNs for extending the NL, where the aim is to find an optimal route from the SN to the sink node with the aid of the highest remaining battery charge, the minimum number of hops and the minimum traffic load. Peng *et al.* [112] invoked intra-route coordination for allowing the nodes along the same route to balance their node lifetime durations, which was also combined with inter-route coordination for additionally balancing the lifetime durations of the sensors along different routes in order to collaboratively maximize the NL. This was carried out under a specific delivery delay constraint.

A cross-layer approach conceived for maximizing the NL was proposed in [86], where MAC-aware routing optimization schemes were designed for WSNs that are capable of multichannel access. Another cross-layer approach was conceived for maximum NL routing in [27], where the energy- and bandwidth-requirements were jointly optimized by carefully selecting the routing and rate allocation in a bandwidth- and energy-constrained WSN. Additionally, Chang *et al.* [106] formulated the maximum-NL routing challenge as a linear programming problem, which was used as the benchmarker of the near-optimal NL acquired by their proposed routing algorithm. However, the design goal in [106] was to simply find the specific flow that maximizes the NL relying on the flow conservation constraint[3]. Additionally, an optimal routing scheme was proposed in [65] with the objective of maximizing the NL, where the authors considered realistic nonideal batteries by modeling the nonlinear energy dissipation behavior of the typical batteries.

Li *et al.* [77] proposed three components for the NL optimization problem including optimizing the source coding, the source throughput of each sensor node and the multihop routing, where the bandwidth-efficient local quantization of the source-information and the employment of energy-conscious multihop routing are widely known to be essential for achieving

[3]For any sensor node, flow in is equivalent to flow out. If the source is generating b_j flows, in a directed graph with a set V nodes, we have $\sum f_{j,k} - \sum f_{i,j} = b_j$, where $f_{i,j}$ represents a flow from source node i to destination node j, for $i, j \in V$. Explicitly, if only a sensor node is generating source information for a destination node, then the intermediate node $k \in V$ can only have the additional amount of flow information that is generated at the source node, so that the flow generated at the source node is conserved for the destination node.

TABLE 1.9: Major contributions on mobility-aided techniques that extend the NL.

Year	Author(s)	Contribution
2008	Wang *et al.* [44]	the aim was to prolong the NL by moving the mobile sensors closer to those stationary sensors, which are heavily loaded by the network's tele-traffic.
	Hamida *et al.* [43]	advocated that the NL can be significantly improved via mobile sinks, where the relaying-overhead of sensor nodes that are close to the sink can be spread and the formation of undesired tele-traffic bottlenecks can be prevented.
2010	Luo *et al.* [45]	demonstrated that the mobile sink nodes are always more beneficial than the stationary sinks in terms of extending the NL.
2013	Yun *et al.* [121]	proposed a framework, where a sensor node transmits only on condition, if the location of the mobile sink is beneficial in terms of extending the NL, under the additional constraint that each sensor stores its data up to a predetermined delay tolerance threshold.
2014	Wang *et al.* [122]	a relocation scheme was proposed for the mobile sink for maximizing the NL, since the adjacent sensors of the sink node deplete their battery more rapidly than the rest of the nodes in WSNs.
2015	Tashtarian *et al.* [123]	studied the benefits of sink-mobility control in the context of event-driven applications in order to maximize the NL.

energy conservation. These three components were formulated as a linear programming problem for maximizing the NL. Similarly, distributed algorithms were developed by He *et al.* [108] by exploiting the so-called Lagrangian duality[4] in order to find the optimal solution to the lifetime maximization problem, which was formulated based on the joint optimization of the source rates, the encoder's power dissipation and the routing scheme. The major contributions on the routing optimization techniques designed for NL maximization are surveyed in Table 1.7, while their OFs, constraints and their optimization algorithms are summarized in Table 1.8.

1.1.1.4 Mobile Sensors

Data collection at the sink node often results in routing-congestion in the vicinity of sensors neighboring the sink node, since these sensors are frequently used for delivering the data to the destination node. This results in rapid battery depletion of these particular sensor nodes and leads to NL reduction due to the unbalanced traffic-load, thus imposing an unevenly

[4]A minimization problem can be referred to as a primal (original) problem, and there exists a dual maximization problem of that particular minimization primal problem, which can produce the same optimal solution as the primal one. The Lagrangian duality is preferred, since the dual optimization problem is always convex, which can be efficiently solved, even though the primal problem is a nonconvex one.

distributed energy dissipation across the WSN [124]. A beneficial method of circumventing this problem is to rely on a technique referred to as *controlled mobility*, which relies on *mobile sensors* or *mobile sinks*, where each mobile sensor cooperatively decides its direction of movement in order to prevent an uneven traffic burden distribution. As a benefit, the traffic-load becomes uniformly distributed across the network by taking advantage of the mobility. For instance, in [44] Wang *et al.* considered a WSN, which is constituted by several mobile relay sensor nodes and a large number of stationary nodes, where the resources of the mobile sensors are richer than those of the stationary sensors. The aim of the work presented in [44] was to prolong the NL by moving the mobile sensors closer to those stationary sensors, which are heavily loaded by the network's tele-traffic. Similarly, Hamida *et al.* [43] advocated that the NL can be significantly improved via mobile sinks, where the relaying-overhead of sensor nodes that are close to the sink can be spread and the formation of undesired tele-traffic bottlenecks can be prevented. On the other hand, Luo *et al.* [45] analyzed the effects of joint sink mobility and routing in order to maximize the NL, while constraining the position of the mobile sink to a limited number of locations. Interestingly, Luo *et al.* [45] demonstrated that the mobile sink nodes are always more beneficial than the stationary sinks in terms of extending the NL. A relocation scheme was proposed for the mobile sink by Wang *et al.* [122] for maximizing the NL, since the adjacent sensors of the sink node deplete their battery more rapidly than the rest of the nodes in WSNs. Their proposed scheme exploited the knowledge of the remaining battery charge information of the sensor nodes for adaptively adjusting the transmission distance of the sensor nodes and for the beneficial relocation of the sink node.

Additionally, similar studies were carried out in [121, 130], where a sensor node transmits only on condition, if the location of the mobile sink is beneficial in terms of extending the NL, under the additional constraint that each sensor stores its data up to a predetermined delay tolerance threshold. A different approach was proposed by Tashtarian *et al.* [123], who studied the benefits of sink-mobility control in the context of event-driven applications in order to maximize the NL. More explicitly, in the interest of maximizing the NL, an optimal single-hop link was relied upon in [123] without assuming any specific predetermined network structure, where the mobile sink node has to capture the occurrence of specific events gleaned from a group of sensors, until a certain deadline expired. The main contributions of the mobility-aided techniques that extend the NL are reviewed in Table 1.9, while their OFs, constraints and their optimization algorithms are characterized in Table 1.10.

1.1.1.5 Coverage and Connectivity

The term *coverage* is also referred to as sensing coverage, which indicates the observation quality of specific events within a target area, at a particular sensing point or within a barrier field covered by the sensors deployed. We note that the sensed information is processed

TABLE 1.10: OF(s), constraint(s) and optimization algorithm(s) of Table 1.9 in the context of mobility-aided techniques that maximize the lifetime of WSNs.

Year	Author(s)	OF(s)	Constraint function(s)	Optimization tool
2008	Wang *et al.* [44]	NL	Resource rich mobile relay sensors, assisting heavily burdened sensors, routing	Joint mobility of relay nodes and aggregation routing algorithm [125]
	Hamida *et al.* [43]	NL	Mobile sink nodes, overhead balancing, data dissemination	The geographic hash table [126], line based data dissemination [127], column-row location service [128]
2010	Luo *et al.* [45]	NL	Mobile sink nodes, routing flow conservation, rate and energy constraints	An efficient primal-dual algorithm [129] for a single mobile sink and extended duality theory based approximation algorithm for multiple sinks
2013	Yun *et al.* [121, 130]	NL	Mobile sink node, delay tolerance, optimal sink positioning, energy and flow conservation constraints	A subgradient algorithm based on delay tolerant mobile sink model [88,116] using GNU linear programming kit (GLPK) [131]
2014	Wang *et al.* [122]	NL	Mobile sink, sink relocation, residual battery energy, adaptive transmission range	Energy-aware sink relocation adopting energy-aware routing maximum capacity path
2015	Tashtarian *et al.* [123]	NL	Mobile sink, continuous and optimal trajectory (COT)	The COT is computed with the aid of convex optimization and a greedy heuristic algorithm

relying on a specific hardware component, which is distinct from the transceiver component of the particular sensor device [2, 3]. Naturally, a specific point within the target area may be concurrently sensed by several sensors. While this type of deployment can be beneficial in terms of improving the quality or reliability of the data observed, this also introduces data redundancy, which in turn results in wasted energy. Hence, it is beneficial to critically appraise, whether the data should or should not be transmitted to the base station. Explicitly, if insufficient sensors are deployed, the probability of adequate connectivity to the base station or to another sensor might become inadequately low. Crucially, ensuring high-quality connectivity of these sensors predetermines the ability of transmitting the sensed observations to the base station. As illustrated in Fig. 1.4, the sensing range R_s determines

TABLE 1.11: Major contributions on the coverage and connectivity improvement techniques designed for NL maximization.

Year	Author(s)	Contribution
2008	Zhao *et al.* [32]	proposed a scheduling approach necessitating for all the active sensors to maintain full-time coverage of a particular target area all the time and to send all the sensed information to the sink via subsets of sensors, which also requires full-time connectivity to the sink with the aid of multi-hop communication between these subsets.
2010	Hu *et al.* [132]	employed a genetic algorithm for solving the problem of finding the maximum number of disjoint subsets of sensors for maximizing the NL, while the disjoint subsets of sensors, where each sensor under a specific subset successively provides full coverage for the target area.
2012	Lin *et al.* [133]	proposed an ant colony optimization based approach that is capable of maximizing the lifetime of the heterogeneous WSNs, which each sensor can maintain both the coverage quality and reliable connectivity.
2013	Du *et al.* [61]	focused their attention on NL maximization subject to the barrier coverage constraints, where the sensors form continuous barriers, whose aim is to provide coverage to a certain location.
2015	Lu *et al.* [134]	investigated the sleep-mode scheduling problem in order to maximize the NL by only turning on a specific subset of sensors for monitoring the target spots and for exploiting the transmission of the sensed data over multiple hops, all the way to the base station.
	Deng *et al.* [135]	studied the issues of reliable coverage in the context of agricultural applications of WSNs, assuming that each node is equipped with sensors carrying out different tasks, where the aim was to schedule the activity of these heterogeneous sensors by ensuring that reliable coverage can be maintained, whilst the NL is maximized.
	Chen *et al.* [136]	developed a novel NL maximization algorithm, which allows the activation of the lowest possible number of sensor nodes with the aid of traffic balancing in order to provide reliable full coverage of a specific sensing field, while providing *any-time connectivity* to a base station.

TABLE 1.12: OF(s), constraint(s) and optimization algorithm(s) of Table 1.11 in the context of coverage and connectivity improvement techniques designed for maximizing the lifetime of WSNs.

Year	Author(s)	OF(s)	Constraint function(s)	Optimization tool
2008	Zhao *et al.* [32]	NL	Full-time coverage for a specific area, anytime connectivity to sink node via a multi-hop route	A heuristic algorithm based on an approximation algorithm called communication weighted greedy cover algorithm [32]
2010	Hu *et al.* [132]	NL	Maximum number of disjoint connected sensor subsets that maintain complete coverage, sleep scheduling	A hybrid genetic algorithm with schedule transition operations
2012	Lin *et al.* [133]	NL	Maximum number of disjoint connected sensor subsets that maintain sensing coverage and network connectivity	Ant colony optimization based approach for maximizing the number of connected sensor subsets
2013	Du *et al.* [61]	NL	Redeployment, sleep scheduling, k-discrete barrier coverage probability	Maximum-lifetime for k-discrete barrier coverage with limited-moving cost algorithm [61]
2015	Lu *et al.* [134]	NL	Sleep scheduling, target coverage, data collection multi-hop communication	Maximum lifetime coverage scheduling problem is solved using polynomial-time constant-factor approximation algorithm [137]
	Deng *et al.* [135]	NL	Confident information coverage, activity scheduling	Multi-modal confident information coverage problem solved via both a centralized and a distributed heuristic algorithm
	Chen *et al.* [136]	NL	Least number of sensor activation, traffic-balanced routing, full-time coverage, anytime connectivity	Maximum connected load-balancing cover tree algorithm based on heuristic coverage control and traffic balanced routing strategy [136]

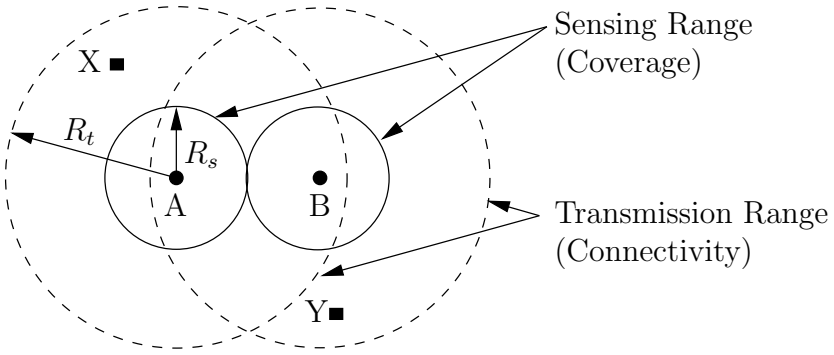

FIGURE 1.4: The relationship between the sensing and the connectivity ranges, when $R_t > R_s$.

the area within which adequate sensing is achieved, and the transmission range R_t defines the area of adequate transmission quality. More explicitly, an observation at points X and Y cannot be adequately recorded, since the sensing range of the given sensors is too restricted, even though the points lie within the adequate transmission range. Hence, other sensor nodes have to cover the X and Y points, but at the same time the sensors have to remain within the adequate transmission range of node-A and node-B, respectively, so that the observations can be adequately sensed and transmitted to the base station. Regarding this issue, Zhang *et al.* [138] formally proved that a complete coverage of a convex region implies having adequate connectivity amongst all the sensors deployed, provided that the transmission range is at least twice the sensing range, i.e. we have $R_t \geq 2R_s$. Further debates on the subjects of sensing range and transmission range can be found in [70, 138–141].

One of the most important objectives of the WSNs is to provide reliable full coverage of a particular sensing field at any moment in time and to relay all the sensed data to the sink node via a subset of the deployed sensors. Chen *et al.* [136] developed a novel NL maximization algorithm, which allows the activation of the lowest possible number of sensor nodes with the aid of traffic-balancing in order to provide reliable full coverage of a specific sensing field, while providing *any-time connectivity* to a base station. Similarly, Zhao *et al.* [32] proposed a scheduling approach necessitating for all the active sensors to maintain full-time coverage of a particular target area all the time and to send all the sensed information to the sink via subsets of sensors, which also requires full-time connectivity to the sink with the aid of multi-hop communication between these subsets. If the coverage of the target area and the anticipated connectivity within the subsets of sensors and the sink node cannot be maintained, then the authors of [32] assumed that the NL expires. Additionally, Deng *et al.* [135] studied the issues of reliable coverage in the context of agricultural applications of WSNs, assuming that each node is equipped with sensors carrying out different tasks, where the aim was to schedule the activity of these heterogeneous sensors by ensuring that reliable coverage can be maintained, whilst the NL is maximized. As an alternative solution, Lin *et al.* [133] proposed an ant colony optimization based approach that is capable of maximizing

the lifetime of heterogeneous WSNs, where a construction graph is used for determining the maximum number of disjoint connected coverage segments[5], where each sensor in this disjoint subset can individually maintain both the required coverage quality and reliable network connectivity, while the rest of the sensors of the same disjoint subset are in their sleep-mode. Du *et al.* [61] also focused their attention on NL maximization subject to the military barrier coverage constraints[6], where the sensors form continuous geographic area barriers with the goal of detecting the crossing of an area by the adversaries. Additionally, Lu *et al.* [134] investigated the sleep-mode scheduling problem in order to maximize the NL by only turning on a specific subset of sensors for monitoring the target spots and for exploiting the transmission of the sensed data over multiple hops, all the way to the base station. As another design alternative, Hu *et al.* [132] employed a genetic algorithm for solving the problem of finding the maximum number of disjoint subsets of sensors for maximizing the NL, where the disjoint subsets of sensors had the particular feature that each sensor of a specific subset provides full coverage of the target area. The major contributions on the subject of coverage and connectivity improvement techniques conceived for the sake of NL maximization are summarized in Table 1.11, while their OFs, constraints and their optimization algorithms are surveyed in Table 1.12.

1.1.1.6 Optimal Deployment

The sensors that are close to the sink node are often exposed to excessive tele-traffic, since these sensors have to relay data for a large number of sensors in the rest of the coverage area and hence they tend to drain their battery much more rapidly than the rest of the sensors. One way of alleviating this problem is to conceive an efficient node deployment that avoids the tele-traffic bottleneck. An optimal deployment must provide full coverage for the target area, while maintaining a reliable connectivity and best possible NL, for example by setting the redundant sensors to their sleep-mode within the same region. In the literature, there are various optimal deployment strategies that maximize the NL. A specific example of this can be found in [144], where Natalizio *et al.* analyzed the optimal placement of the sensor nodes within a particular sensing field in order to maximize the NL of the WSN considered. Liu *et al.* [22] focused their attention on identifying the tele-traffic bottlenecks and the *energy-hole* regions, thus further improving the node-deployment strategy, while achieving a balanced energy dissipation across the network was guaranteed for the sake of maximizing

[5] A specific sensor field is partitioned into smaller sensor subsets, where each subset may be composed of several sensors that are potentially closer to each other. The main idea of the disjoint subsets, also referred as the sensor covers, is to allow each sensor under the same subset to successively carry out all the tasks of that particular disjoint coverage area. More explicitly, the sensors within the same subset are not turned on at the same time. Instead, they are rather activated sequentially, after the previous sensor has run out of battery. This method assists in extending the NL.

[6] Barrier coverage is exploited especially in military applications, where an intruder crossing a particular region has to be detected. Therefore, a sensor barrier is usually formed by several connected sensors across the entire target region, which may feature a trip-wire-like structure to detect any potential crossings by intruders.

TABLE 1.13: Major contributions on the optimal deployment techniques conceived for NL maximization.

Year	Author(s)	Contribution
2006	Cristescu *et al.* [142]	investigated the power efficient data gathering problem subject to particular distortion constraints, while providing the optimal node placement solution by striking a trade-off between the total power dissipation and the NL.
2007	Wang *et al.* [23]	investigated the relay node placement problem under specific coverage, connectivity and NL constraints in heterogeneous WSNs.
	Himsoon *et al.* [143]	a deployment strategy was designed for maximizing the NL, which relied on the cooperation of sensor nodes.
2008	Natalizio *et al.* [144]	analyzed the optimal placement of the sensor nodes within a particular sensing field in order to maximize the NL of the WSN considered.
2009	Phan *et al.* [21]	presented a two-stage cross-layer optimization technique, where the first stage involved maximizing the number of sensor nodes deployed within the existing WSN, while the second stage considered both the power allocation and scheduling operations in order to maximize the NL.
2011	Zhang *et al.* [145]	An energy harvesting approach using a solar-powered relay node was conceived in support of the cluster head, where the optimal location of the cluster head was given by that maximizing the NL.
2013	Liu *et al.* [22]	focused their attention on identifying the tele-traffic bottlenecks and the *energy-hole* regions, thus further improving the node-deployment strategy, while achieving a balanced energy dissipation across the network was guaranteed for the sake of maximizing the NL.
2014	Najimi *et al.* [60]	proposed a node selection algorithm for balancing the energy dissipation of the sensors in order to maximize the NL, where the sensor nodes having the highest residual battery charges are chosen for spectrum sensing in wireless cognitive sensor networks.
	Mini *et al.* [146]	determined the optimal deployment locations of specific sensor nodes and developed a scheduling scheme for these optimally-located sensors so that the overall NL was maximized, while achieving the required target coverage level.
	Liu *et al.* [147]	an ant colony optimization based transmission scheme was designed for maximizing the NL, where each sensor was capable of adjusting its transmission range for data transmission using the best possible energy efficiency and the best possible energy balancing approaches.
2015	Wang *et al.* [41]	a robust traffic-flow-aware scale-free topology was developed, where the traffic-flow and hence also the energy dissipation across the network was balanced.

TABLE 1.14: OF(s), constraint(s) and optimization algorithm(s) of Table 1.13 in the context of optimal deployment techniques that maximize the lifetime of WSNs.

Year	Author(s)	OF(s)	Constraint function(s)	Optimization tool
2006	Cristescu *et al.* [142]	NL, total power dissipation	Optimal transmission scheme, optimal node placement, rate allocation, data gathering	An optimal placement algorithm and a lifetime optimization algorithm
2007	Wang *et al.* [23]	NL	Coverage quality, relay node placement, network connectivity	Local optimal approach for the placement of the first and second phase relay nodes
	Himsoon *et al.* [143]	NL	Cooperative diversity, BER constraint, node selection, power allocation, optimal deployment	A reduced complexity suboptimal algorithm
2008	Natalizio *et al.* [144]	NL	Optimal placement, power control, residual battery charge	Monte Carlo simulations
2009	Phan *et al.* [21]	NL	Node admission, deployment of maximum number of sensors, power allocation, link scheduling	Cross-layer optimization framework based on mixed integer linear programming using CPLEX library [90]
2011	Zhang *et al.* [145]	NL	Energy harvesting solar powered relay node, optimal location of cluster head, clustering	Single cluster algorithm for finding the best location of cluster head
2013	Liu *et al.* [22]	NL	Sensor deployment, adaptive transmission range, balanced energy dissipation, coverage quality, network connectivity, avoidance of energy hole regions, deployment strategy	An algorithm based on*first node die time* and *all nodes die time* NL definitions for finding the optimal transmission radius using OMNeT++
2014	Najimi *et al.* [60]	NL	Node selection for balanced energy dissipation, maximize minimum residual battery charge	An iterative algorithm using convex optimization based on Karush-Kuhn-Tucker optimality
	Mini *et al.* [146]	NL	Optimal deployment locations, sleep scheduling, require target coverage level	Artificial bee colony, particle swarm optimization and a heuristic method for sleep scheduling
	Liu et al. [147]	NL	Transmission range, maximum possible energy efficiency, maximum possible energy balancing	An algorithm for finding optimal transmission scheme based on ant colony optimization
2015	Wang *et al.* [41]	NL	Balanced energy dissipation and traffic flow, connectivity, robustness against node failure, energy-efficient topology	Flow-aware scale-free topology model analyzed using shortest path and low-energy adaptive clustering hierarchy [148] algorithms

the NL. Similarly, a robust traffic-flow-aware scale-free topology was developed by Wang *et al.* [41], where the traffic-flow and hence also the energy dissipation across the network was balanced.

An appealing node-deployment strategy was proposed by Magno *et al.* [149], where an ultra-low-power overlay network was *super-imposed* on a less energy-efficient WSN in order to extend the NL of the low-efficiency WSN designed for potentially power-hungry surveillance applications supported by the low-power overlay network relying on the most recent advances both in energy harvesting and wake-up radio technologies. Additionally, Mini *et al.* [146] determined the optimal deployment locations of specific sensor nodes and developed a scheduling scheme for these optimally-located sensors so that the overall NL was maximized, while achieving the required target coverage level. They also demonstrated [146] that in order to guarantee the target coverage level and to maximize the NL, only the minimum number of sensor nodes guaranteeing seamless connectivity was allowed to be scheduled, while the redundant sensors would only be used, when absolutely necessary for preventing any potential NL-expiry. More explicitly, turning on all the sensors together is energy-inefficient. Instead, turning off the sensors adjacent to the one currently operating and turning them on one-by-one, only when it is required, is capable of significantly increasing the NL, while maintaining the desired coverage probability. Similarly, Wang *et al.* [23] investigated the relay node placement problem under specific coverage, connectivity and NL constraints in heterogeneous WSNs. Phan *et al.* [21] presented a two-stage cross-layer optimization technique, where the first stage involved maximizing the number of sensor nodes deployed within the existing WSN, while the second stage considered both the power allocation and scheduling operations in order to maximize the NL. As a further beneficial solution, In [142], Cristescu *et al.* investigated the power efficient data gathering problem subject to particular distortion constraints, while providing the optimal node placement solution by striking a trade-off between the total power dissipation and the NL.

Najimi *et al.* [60] proposed a node selection algorithm for balancing the energy dissipation of the sensors in order to maximize the NL, where the sensor nodes having the highest residual battery charges are chosen for spectrum sensing in wireless cognitive sensor networks. Another deployment strategy designed for maximizing the NL was proposed in [143,150], which relied on the cooperation of sensor nodes. On the other hand, an ant colony optimization based transmission scheme was designed for maximizing the NL by *Liu et al.* [147], where each sensor was capable of adjusting its transmission range for data transmission using the best possible energy efficiency and the best possible energy balancing approaches. An energy harvesting approach using a solar-powered relay node was conceived in support of the cluster head by Zhang *et al.* [145], where the optimal location of the cluster head was given by that maximizing the NL. The major contributions to optimal deployment techniques designed for NL maximization are presented in Table 1.13, while their OFs, constraints and their optimization algorithms are surveyed in Table 1.14.

1.1.1.7 Data Gathering

One of the fundamental operations of the WSNs is to collect data from sensors and to convey it to the sink node. During the data collection stage, data aggregation can be employed to fuse data from different sensors in order to prevent redundant data transmission. More explicitly, He *et al.* [151] considered an energy-efficient cross-layer design for the gathering of spatially correlated sensory information, in order to minimize the energy-waste that would be assigned to redundant information and thus to maximize the NL. Similarly, Cristescu *et al.* [142] investigated power-efficient data gathering subject to certain distortion constraints, while providing the optimal node placement solution subject to striking a trade-off between the total power dissipation and the NL. Additionally, Bhardwaj *et al.* [71, 72] focused their attention on the fundamental constraints of the information gathering and transmission to a base station, while deriving the upper bounds of the achievable NL considering the impact of several parameters on the NL, including the base station location, path loss, initial battery charge, source location and so on. In [152], Liang *et al.* considered an energy-efficient data gathering method constructed for maximizing the NL, where the goal was to maximize the number of data gathering queries processed, until the first node failure occurs due to exhausted battery charge in the WSN considered. Additionally, another data gathering method was proposed in [153], where a data gathering tree was constructed for the transmission of the sensed data through each sensor all the way to the base station, while preventing the formation of tele-traffic bottlenecks in order to balance the traffic-load across the network and to extend the attainable NL.

1.1.1.8 Data Correlation

A salient characteristic of WSNs is that the data collected by the adjacent sensors may represent redundant information owing to the temporal-spatial data correlation characteristics of the neighboring sensors. Reducing the overall tele-traffic by removing the redundancy can be beneficial in terms of energy conservation and hence NL maximization. For example, He *et al.* [151] conceived an energy-efficient cross-layer design for the optimal data gathering from spatially correlated sensors in order to minimize the energy-wastage imposed by transmitting redundant information and thus to maximize the NL. Similarly, He *et al.* [40] proposed a method of predicting the data to be collected by a specific sensor based on the temporal-spatial correlations of its neighboring sensors, which may then lead to an extended NL, since these sensors whose data can be predicted may be turned off. Additionally, Heo *et al.* [154] introduced a prediction scheme for minimizing the traffic load across the WSN, which was further minimized by taking advantage of the spatial correlation of the various sensors in the interest of maximizing the NL. They demonstrated in [154] that the amount of data to be transmitted can be reduced by 20% using the proposed scheme by exploiting

both the context prediction and the spatial correlation amongst the sensors, which hence extended the NL.

The joint optimization of the data aggregation and maximum lifetime-based routing was considered in [107], where data aggregation reduces the traffic-load across the network by taking advantage of the temporal-spatial data correlation. As a benefit, the power dissipation of the sensor nodes that are adjacent to the sink node can be substantially reduced and then the ensuing maximum lifetime-based routing further balances the tele-traffic for the sake of avoiding any potential bottleneck formation.

1.1.1.9 Sleep-Wake Scheduling

The employment of sleep-wake mode based scheduling can be extremely beneficial in terms of an extended NL, especially in application scenarios, when the packets only arrive sporadically. Hence, Kim *et al.* [155] developed an optimal solution for controlling the sleep-wake mode scheduling of a so-called anycast packet-forwarding scheme[7] in order to maximize the NL subject to packet delay constraints. Another example of the sleep-wake mode scheduling can be found in [109], where Liu *et al.* advocated a joint routing and sleep scheduling algorithm for balancing the tele-traffic load across the entire network and for reducing the energy dissipation by allowing the idle sensors to become dormant. The algorithm proposed in [109] extended the NL by 29% compared to either an optimal routing scheme dispensing with sleep-wake scheduling or compared to a pure sleep scheduling scheme. As a benefit, a NL improvement of about 284% was observed compared to the conventional optimal routing schemes relying on a fixed sleep scheduling. Similarly, Hsu *et al.* [113] proposed the joint design of sleep-wake scheduling necessitating the appropriate organization of sensors to become dormant for the sake of improving the energy-efficiency and of opportunistic routing, which improved the routing diversity by spatially distributing the tele-traffic. This improved the reliability of transmission across the network, whilst additionally improving the NL.

An interesting sleep scheduling approach, namely the virtual backbone scheduling philosophy was employed in [158], where the traffic is only forwarded through the so-called backbone sensor nodes constituted by the non-correlated sensor nodes, while the rest of the sensors remain in sleeping-mode in the WSN considered. The sleep scheduling approach of Zhao *et al.* [158] provided a spatially balanced distribution of the energy dissipation and thus maximized the NL. Jeon *et al.* [91] suggested that the NL can be improved using joint contention and sleep-wake mode control, while guaranteeing both the throughput and the SINR requirements. Furthermore, Chamam *et al.* [157] focused their attention on finding the optimal sensor status in terms of their sleep-wake mode as well as their potential cluster head status for the sake of NL maximization subject to coverage, clustering and routing

[7] Each sensor node opportunistically transmits a packet to the closest neighboring sensor node that wakes up in the set of multiple sensor nodes.

TABLE 1.15: Major contributions of the sleep scheduling techniques that maximize the NL.

Year	Author(s)	Contribution
2004	Hoesel *et al.* [80]	proposed a cross-layer approach for jointly optimizing the MAC and routing layer in order to maximize the NL, where the MAC layer is in charge of setting the sensors to their active or inactive mode, while the routing layer identifies efficient routes in the face of a dynamic topology.
	Sichitiu *et al.* [156]	a sensor on-off mode scheduling scheme was proposed for awakening a specific sensor, if and only if necessary, so that more energy can be conserved for the sake of NL maximization.
2009	Chamam *et al.* [157]	focused their attention on finding the optimal sensor status in terms of their sleep-wake mode as well as their potential cluster head status for the sake of NL maximization subject to coverage, clustering and routing constraints.
2010	Kim *et al.* [155]	developed an optimal solution for controlling the sleep-wake mode scheduling of a so-called any-cast packet-forwarding scheme in order to maximize the NL subject to packet delay constraint.
	Liu *et al.* [109]	a joint routing and sleep scheduling algorithm was advocated for balancing the tele-traffic load across the entire network and for reducing the energy dissipation by allowing the idle sensors to become dormant.
2012	Zhao *et al.* [158]	the virtual backbone scheduling philosophy was employed, where the traffic is only forwarded through the so-called backbone sensor nodes constituted by the non-correlated sensor nodes, while the rest of the sensors remain in sleeping-mode in order to maximize the lifetime of the WSN considered.
2013	Jeon *et al.* [91]	suggested that the NL can be improved using joint contention and sleep-wake mode control, while guaranteeing both the throughput and the SINR requirements.
	Li *et al.* [159]	A joint data aggregation and MAC layer design was proposed, where both the network traffic was carefully adjusted with the aid of data aggregation and the power dissipation was reduced through sleep scheduling, which were jointly considered under the constraint of a specific packet delivery delay.
2014	Hsu *et al.* [113]	proposed the joint design of sleep-wake scheduling necessitating the appropriate organization of sensors to become dormant for the sake of improving the energy-efficiency and of opportunistic routing, which improved the routing diversity by spatially distributing the tele-traffic.

TABLE 1.16: OF(s), constraint(s) and optimization algorithm(s) of Table 1.15 in the context of sleep scheduling techniques that maximize the lifetime of WSNs.

Year	Author(s)	OF(s)	Constraint function(s)	Optimization tool
2004	Hoesel *et al.* [80]	NL	TDMA-based MAC protocol, sleep scheduling, routing, dynamic topology	An on-demand source routing algorithm [87] using OMNeT++
	Sichitiu *et al.* [156]	NL	Sleep scheduling, energy conservation	A distributed sleep-awake based scheduling algorithm relying on energy conservation scheme
2009	Chamam *et al.* [157]	NL	Coverage quality, clustering, routing, sleep scheduling	TABU search heuristic algorithm [160] based on integer linear programming model and solved using CPLEX library [90]
2010	Kim *et al.* [155]	NL	Sleep-wake scheduling, minimizing packet delay, any-cast forwarding	An optimal any-cast algorithm based on the value-iteration and local optimal algorithms
	Liu *et al.* [109]	NL	Balanced traffic routing, sleep scheduling	An iterative geometric programming algorithm [89] based on signomial programming [117] problem
2012	Zhao *et al.* [158]	NL	Sleep scheduling, energy-delay tradeoff, virtual backbone scheduling	Schedule transition graph, virtual scheduling graph algorithms, distributed iterative local replacement scheme
2013	Jeon *et al.* [91]	NL	Contention and sleep control probability, throughput and SINR requirements, energy constraints	An algorithm based on subgradient method [88] for finding the optimal Lagrange multipliers [129]
	Li *et al.* [159]	NL	Data aggregation, reduced network traffic, sleep scheduling, packet delivery delay	Joint aggregation and MAC solution using NS-2 simulations and testbed experiments
2014	Hsu *et al.* [113]	NL	Sleep scheduling, traffic balance, route diversity, transmission reliability, opportunistic routing	Joint design of asynchronous sleep-wake scheduling and opportunistic routing technology

constraints. A joint data aggregation and MAC layer design was proposed by Li *et al.* [159], where both the network traffic was carefully adjusted with the aid of data aggregation and the power dissipation was reduced through sleep scheduling, which were jointly considered under the constraint of a specific packet delivery delay.

Hoesel *et al.* [80] proposed a cross-layer approach for jointly optimizing the MAC and routing layer in order to maximize the NL, where the MAC layer is in charge of setting the sensors to their active or inactive mode, while the routing layer identifies efficient routes in the face of a dynamic node topology. Finally, an energy conservation method was designed by Sichitiu *et al.* [156] for the sake of NL maximization, where a sensor on-off mode scheduling scheme was proposed for awakening a specific sensor, if and only if necessary. The major contributions on the subject of sleep-wake-up mode scheduling techniques maximizing the NL are summarized in Table 1.15, while their OFs, constraints and their optimization algorithms are surveyed in Table 1.16.

1.1.1.10 Network Coding

Network coding was designed for enabling the intermediate nodes to compress their data packets that are received from their adjacent nodes [161]. Network coding has been shown to be able to enhance the energy-efficiency of wireless networks, hence improving their NL, as discussed in [162–164]. Further examples include [165], where Shah-Mansouri *et al.* analyzed the trade-off between NL maximization and minimizing the number of network coding operations, hence substantially reducing the required transmit power, albeit these signal processing operations dissipate additional power from the non-rechargeable battery. Decoding operations may also significantly reduce the NL. Similarly, Rout *et al.* [161] attempted to enhance the energy-efficiency of the frequently activated bottleneck nodes that are usually in the vicinity of the sink node by jointly considering sleep scheduling and network coding in order to maximize the NL.

1.1.1.11 Clustering

Long-haul communication with distant areas are costly in terms of energy dissipation in battery-powered WSNs. Hence, this scenario necessitates a multi-tier network architecture for relaying the data, while keeping the network operational for the longest possible period of time. An efficient method of increasing the lifetime of WSNs is to partition the network into several clusters under the control of a high-energy cluster head [166], which the network can rely on. Specifically, Gupta *et al.* [167] proposed an efficient fault-tolerant clustering scheme, where the sensors of a failed cluster may be incorporated into an operational cluster for the sake of network lifetime maximization. Similarly, the same authors developed an algorithm

in [168] for exploiting the gateways equipped with a high-energy battery in order to maximize the NL by avoiding spatially unbalanced energy dissipation across the network.

1.1.1.12 Energy Harvesting

Energy harvesting devices have been conceived for scavenging energy from the environment, hence they are often referred to as energy harvesting wireless sensor networks (EH-WSNs). Compared to conventional battery powered WSNs, EH-WSNs provide substantial benefits in terms of NL maximization. However, from a practical point of view, the entire WSNs cannot purely rely on nodes equipped with EH devices due to the high cost and owing to a range of other physical constraints of EH sensor devices. As an intermediate solution, a solar-powered node was used as the cluster head in [145], where the optimal location of the cluster head was determined using a specific cluster scheme conceived for lifetime optimization. De-Witt *et al.* [169] incorporated energy harvesting into the barrier coverage problem investigated in [61] and developed a certain solution to the problem of maximizing the lifetime of k-barrier coverage in EH-WSNs, while Martinez *et al.* [170] incorporated the energy harvesting capability and the energy storage capacity limits into the associated routing decisions.

1.1.1.13 Beamforming

Distributed or collaborative beamforming utilizes multiple single-antenna-aided transmitters, which form distributed antenna arrays, whose phase-coherently combined waves create angularly selective beams directed at the intended receiver, which significantly increases the transmission distance. Each transmitter can reduce its transmit power, since the energy dissipation is shared amongst several transmitters. However, consistently utilizing the same transmitters may completely drain the battery charge of these specific sensors. Therefore, the failing transmitters may lead to a coverage degradation in a particular area. A beneficial beamforming solution was provided by Feng *et al.* [171], where the authors explored the factors influencing the energy dissipation and the NL. Feng *et al.* [171] also proposed an algorithm providing a carefully balanced selection of the transmitters for maximizing the NL, where the NL is doubled compared to direct or multihop transmissions through a particular receiver that is located far-away from the sensing field. Similarly, Bejar-Haro *et al.* [78] designed an energy-efficient collaborative beamforming scheme for transmitting data to a far-away base station for the sake of NL maximization, while satisfying the target QoS requirement, such as the SNR requirement. Additionally, Han *et al.* [172] aimed for maximizing the NL by exploiting collaborative beamforming and cooperative transmission techniques that can be invoked by the closely located sensors in order to reduce the traffic-load and to prevent the relaying of data by the specific sensors having critical battery

charges. The NL can be improved by 10% to 90% using the transmission technique of [172] depending on the particular network topology considered.

1.1.2 Convex Optimization Preliminaries

Mathematical optimization is a method for finding the most desired element amongst several available alternatives based on some decision criterion. Mathematical optimization was conceived by Greek mathematicians back in 300 B.C., when they studied particular problems in geometry that required optimal solutions. For instance, Euclid studied the problem of minimum distance between a point and a line, which now constitutes a specific fundamental of classic geometry and it is used in many other fields. For a more complete discussion, the readers are referred to [129].

Convex optimization techniques are extensively utilized for the design and analysis of communication systems and signal processing applications. Specifically, convex optimization techniques play a significant role in solving engineering problems, since there is no risk of converging to a suboptimal solution, given that every locally optimal solution is also a globally optimal solution. Therefore, if an optimization problem is converted into a convex one, then it can be efficiently solved with powerful numerical algorithms and the structure of the optimal solution often provides further insights for a better understanding of the original design problem. In order to understand the convex optimization problems, we briefly introduce the basic concepts of convexity and the widely-used convex optimization models. More specifically, this section provides a concise introduction to convexity, convex optimization, Lagrangian relaxation, the Lagrangian dual problem and to the Karush-Kuhn-Tucker optimality conditions.

1.1.2.1 Basic Concepts

In this section, we provide a brief overview of the fundamental terminology of convex optimization by defining a *line, line segment, affine sets, convex sets and convex functions*, as follows:

Line and line segment: Assume that $x_1 \neq x_2$ are two points in $\mathbb{R}^n$ and $\theta \in \mathbb{R}$ indicates the *line* passing through x_1 and x_2 in $y = \theta x_1 + (1-\theta)x_2$ [129]. A value of θ between 0 and 1 forms the li*ne segment* between points x_1 and x_2, as illustrated in Fig. 1.5.

Affine sets: A set $S \subseteq \mathbb{R}^n$ is said to be *affine*, if the line through any specific two points in S lies in S, which can be formulated as $\theta x_1 + (1-\theta)x_2 \in S$ for any $x_1, x_2 \in S$ [129]. More explicitly, as long as the sum of the coefficients in the linear combination is equal to 1, S encompasses the linear combination of any two points in S, which can also be generalized for the *affine combination* of k points as follows:

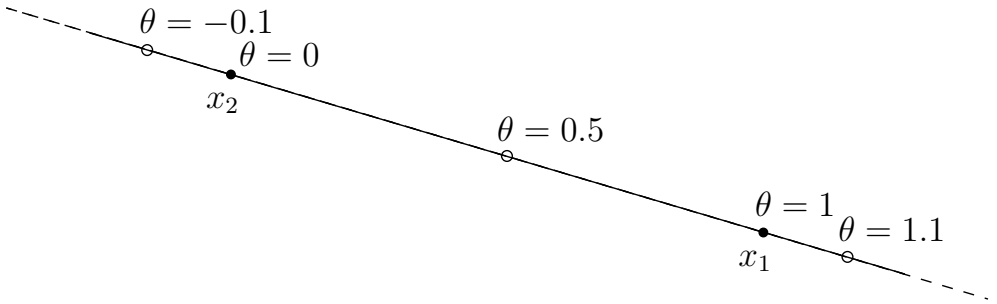

FIGURE 1.5: A line passing through the points x_1 and x_2 is defined by $\theta x_1 + (1 - \theta x_2)$, where θ oscillates in $\mathbb{R}$. The line segment constituted by x_1 and x_2 is illustrated by the chord between the filled circles, which is also represented by θ between 0 and 1.

$$\theta_1 x_1 + \theta_2 x_2 + \theta_3 x_3 + \cdots + \theta_k x_k, \tag{1.1}$$

which has to constitute the affine set, if $x_1, x_2, \cdots, x_k \in S$, $\theta_1 + \theta_2 + \theta_3 + \cdots + \theta_k = 1$ and $\theta_1, \theta_2, \theta_3, \cdots, \theta_k \in \mathbb{R}$. Hyperplanes form an affine set and their intersection also constitutes an affine set [129].

Convex sets: A set S is *convex,* if the line segment between any two points in S lies in S. More explicitly, a set S is convex, if $\forall x_1, x_2 \in S$ and $\theta \in [0, 1]$, so that

$$\theta x_1 + (1 - \theta) x_2 \in S \tag{1.2}$$

is satisfied [129]. Fig. 1.6 illustrates the convex and nonconvex sets, where the sets are shaded. As illustrated in Figs. 1.6(a)–1.6(c), a noncovex set is formed, since there exists a line segment that exits the set, e.g. the line segments between points A and B, C and D, G and H. However, Fig. 1.6(d) forms a convex set, since any line segment drawn remains within the set, e.g. the line segment between points E and F. Roughly speaking, a convex set does not contain any hole in the convex geometric region, as illustrated in Fig. 1.6(c) and always curves outward. Convex sets include ellipsoids, unit balls, polyhedral sets, hypercubes and so on. Another method often used for the analysis of convex sets is to check the exterior angle between any joined lines or line segments, which must be higher than or equal to 180° for convex sets. One of the most significant properties of the convex sets is that the intersection of convex sets also remains a convex set. Additionally, the intersection of convex sets and affine sets constitutes a convex set. On the other hand, the union of convex sets is usually nonconvex. Additionally, the image and inverse image of a convex set under affine functions, under perspective functions and under linear-fractional functions is convex.

Convex functions: A function f : $\mathbb{R}^n \to \mathbb{R}$ is said to be convex if its domain[8], denoted by

[8] *Domain* of a function is the set of input values for which the function is defined.

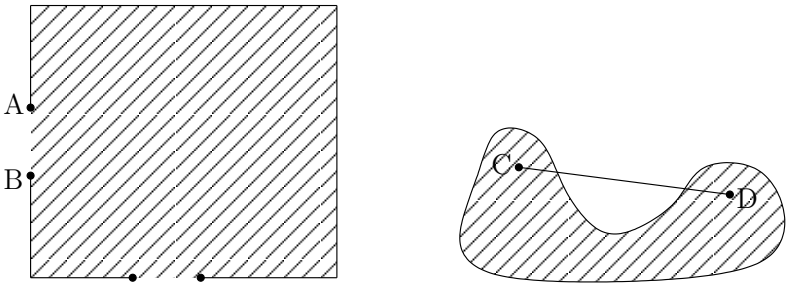

(a) A nonconvex set. (b) A nonconvex set.

(c) A nonconvex set. (d) A convex set.

FIGURE 1.6: Illustration of convex and nonconvex sets, where the sets are patterned.

dom f, is a convex set and if $\forall x_1, x_2 \in$ **dom** f and $\theta \in [0,1]$, then

$$f(\theta x_1 + (1-\theta)x_2) \leq \theta f(x_1) + (1-\theta) f(x_2) \tag{1.3}$$

is satisfied [129]. The geometric interpretation of the convex function definition is presented in Fig. 1.7. Observe in Fig. 1.7 that the line segment constituted by the points $[x_1, f(x_1)]$ and $[x_2, f(x_2)]$ lies *on* or *above* the curve constructed by $f(x)$. In fact, the line segment in Fig. 1.7 *always* remains above the curve. Hence, indeed $f(x)$ is strictly convex. Note that f is concave if $-f$ is convex. Hence, for concavity the line segment seen in Fig. 1.7 must lie below the function curve, which has a downwards-shaped (negative) curve. There is a large number of convex (and concave) functions, as exemplified by the most frequently encountered ones listed as follows [129].

1.1.2.1.1 Convex functions:

- Exponential function: $f(x) = e^{ax}$, for any $a \in \mathbb{R}$;
- Powers: $f(x) = x^a$ is convex for $a \leq 0$ and $a \geq 1$;
- Max function: $f(\mathbf{x}) = max\{x_1, \cdots, x_k\}$;
- Norm functions: $f(\mathbf{x}) = \|\mathbf{x}\|_p$, $p > 1$;
- Quadratic-over-linear function: $f(x,y) = \frac{x^2}{y}$, where $x \in \mathbb{R}$ and $y > 0$;
- Log-sum-exp: $f(\mathbf{x}) = \log(e^{x_1} + e^{x_2} + \cdots + e^{x_k})$, on $\mathbb{R}^k$.

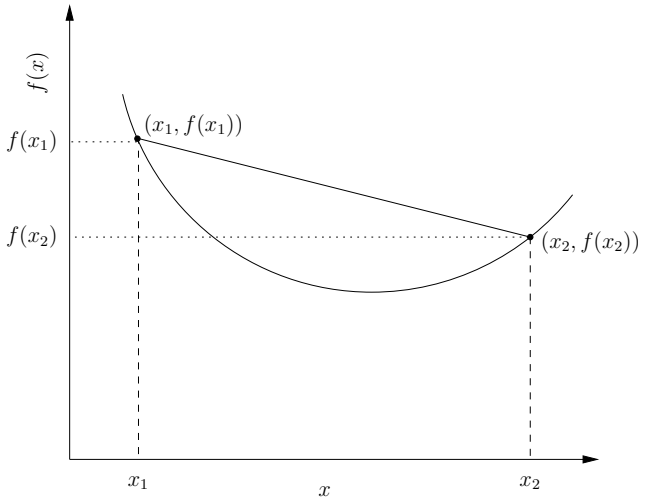

FIGURE 1.7: Geometric representation of the convex function definition.

1.1.2.1.2 Concave functions:

- Powers: $f(x) = x^a$ is concave, when $0 \leq a \leq 1$;
- Geometric mean: $f(\mathbf{x}) = (\prod_{i=1}^{k} x_i)^{\frac{1}{k}}$, where $\mathbf{dom}\, f = \mathbb{R}^k_{++}$;
- Logarithm function: $f(x) = \log(x)$, where $x \in \mathbb{R}_{++}$;
- Log-determinant: $f(\mathbf{X}) = \log\det \mathbf{X}$, on $\mathbf{dom}\, f = \mathbb{S}^k_{++}$.

Assuming that the function f is continuously differentiable, then the convexity of f is equivalent to

$$f(y) \geq f(x) + \nabla f(x)^{\mathrm{T}}(y - x), \tag{1.4}$$

where $\mathbf{dom}\, f$ is open and convex, while we have $x, y \in \mathbf{dom}\, f$. This is exemplified in Fig. 1.8, which indicates that the first-order Taylor series approximation of a convex function is a *global underestimator*[9] [129]. Conversely, if the first-order Taylor approximation of a function is always a global underestimator of the function, then the function is said to be convex. Equation (1.4) reveals the most important property of the convex functions, where a local information of the convex function, e.g. its value and its derivative, at a specific point is sufficient for deriving the particular global information, for example its global underestimator. Nevertheless, if the function f is twice differentiable, then the convexity of f becomes equal to its positive semidefinite Hessian ($\nabla^2 f(x) \succeq 0$, $\forall x \in \mathbb{R}^k$). Indeed, this property indicates that the function $f(x)$ has an upwards-shaped (positive) curve. Hence, all linear (affine) functions are convex (and concave) and it is a special case of convex functions, whereas the convexity of a quadratic function formulated as $x^{\mathrm{T}}Px + a^{\mathrm{T}}x + b$ strictly depends on the $P \succeq 0$ property. Note that a function may have both convex and concave segments (affine function) or can be neither convex nor concave. For example, as seen in Fig. 1.9

[9] Assume that we have $y \leq f(x)$, $\forall x \in \mathbf{dom}\, f$. Then, y is said to be a *global underestimator* of the function f.

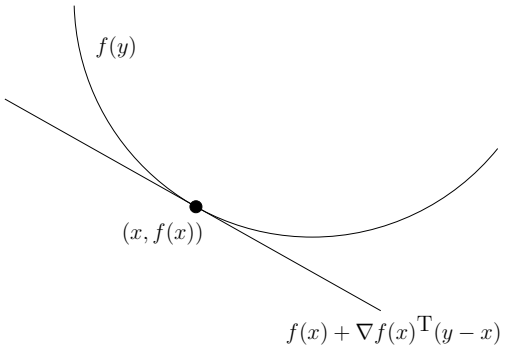

FIGURE 1.8: The first order conditions for convex functions.

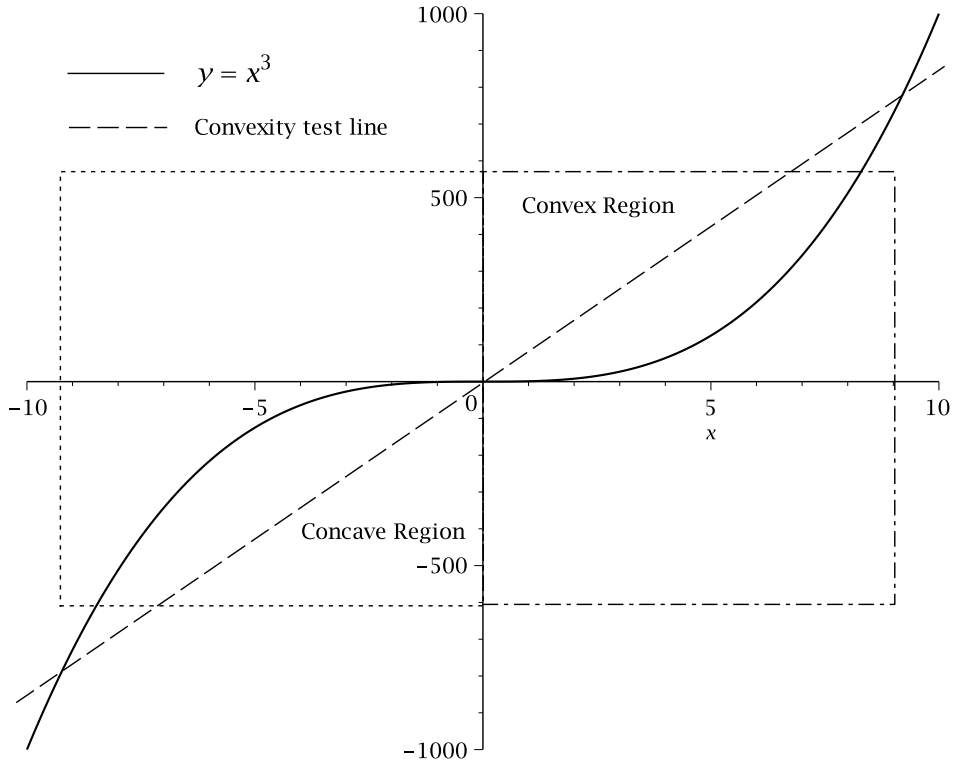

FIGURE 1.9: Function $y = x^3$ is convex in $[0, \infty)$, concave in $(-\infty, 0]$, but neither convex nor concave over $\mathbb{R}$, since convexity test line lies above the function curve at the convex region, but lies below $f(x)$ in the concave region, which cannot be defined neither for convexity or concavity over $\mathbb{R}$.

the function x^3 is convex in the region $[0, \infty)$ and concave in the region $(-\infty, 0]$. However, neither convex nor concave over $\mathbb{R}$.

1.1.2.2 Generic Optimization Problems

An optimization problem may have the following generic form [88, 129]

$$\underset{\mathbf{x}\in\mathcal{D}}{\text{minimize}} \quad f_0(\mathbf{x}) \tag{1.5}$$

$$\text{subject to} \quad f_i(\mathbf{x}) \leq 0,\ i = 1, \cdots, m \tag{1.6}$$

$$h_i(\mathbf{x}) = 0,\ i = 1, \cdots, p, \tag{1.7}$$

where $\mathbf{x} \in \mathbb{R}^n$ is the vector of *optimization variables* or *decision variables* that minimizes the objective or cost function $f_0(\mathbf{x}) : \mathbb{R}^n \to \mathbb{R}$, while satisfying m number of *inequality constraints* $f_i : \mathbb{R}^n \to \mathbb{R}$, $f_i(\mathbf{x}) \leq 0$, $i = 1, \cdots, m$, and p number of *equality constraints* $h_i : \mathbb{R}^n \to \mathbb{R}$, $h_i(\mathbf{x}) = 0$, $i = 1, \cdots, p$, respectively. Additionally, the domain $\mathcal{D}$ of the optimization problem in (1.5)–(1.7) is expressed as

$$\mathcal{D} = \left[\bigcap_{i=0}^{m} \mathbf{dom}\, f_i\right] \cap \left[\bigcap_{i=0}^{p} \mathbf{dom}\, h_i\right], \tag{1.8}$$

where any point $\mathbf{x} \in \mathcal{D}$ satisfying the constraints in (1.6)–(1.7) is referred to as a *feasible point*, whereas any other point is termed as *infeasible* [129]. All feasible points together form the feasible set. Similarly, the problem is said to be feasible, if there exists at least one feasible point, otherwise it is infeasible. As opposed to the *constrained optimization problem* of (1.5)–(1.7), an optimization problem without equality and inequality constraints is termed as an *unconstrained optimization problem*.

The *optimal value* of the optimization problem described in (1.5)–(1.7) is the minimum point (for the minimization problems) in the feasible set and it is denoted by p^*, which is obtained at an *optimal point* $\mathbf{x}^*$, as illustrated in Fig. 1.10 and defined as $f_0(\mathbf{x}^*) = p^*$. Explicitly, the *optimal value* of the optimization problem can be written as

$$p^* = \inf\left\{f_0(\mathbf{x}) \mid f_i(\mathbf{x}) \leq 0,\ i = 1, \cdots, m;\ h_i(\mathbf{x}) = 0,\ i = 1, \cdots, p\right\}. \tag{1.9}$$

More explicitly, the *optimal point* $\mathbf{x}^*$ minimizes[10] f_0 over the feasible set, which concurrently satisfies the constraints (1.6)–(1.7). Additionally, the *optimal point* $\mathbf{x}^*$ is referred to as a *globally optimal point*, if the problem is a convex optimization problem, since there is no risk of encountering a locally optimal point. As seen in Fig. 1.10, there is only one minimum, thus there is a single optimal point due to the convex property of $f(x)$.

Convex optimization problems rely on a convex objective function, on convex inequality constraint functions and on affine equality constraint functions. A convex objective function is minimized over a convex set in a convex optimization problem.

1.1.2.3 Convex Optimization Problems

The generic form of the optimization problem described in (1.5)–(1.7) is a *convex optimization problem*, if f_0 and f_i, $i = 1, \cdots, m$ are convex, while h_i, $i = 1, \cdots, p$ are affine. In

[10] An infimum (inf) is the greatest lower bound of a set [129]. Note that if a set has a minimum, which finite sets always have a minimum, then the minimum is also the infimum of the set. One distinction is that a minimum can be defined for a sequence, while an infimum of the set can be used to describe a lower bound.

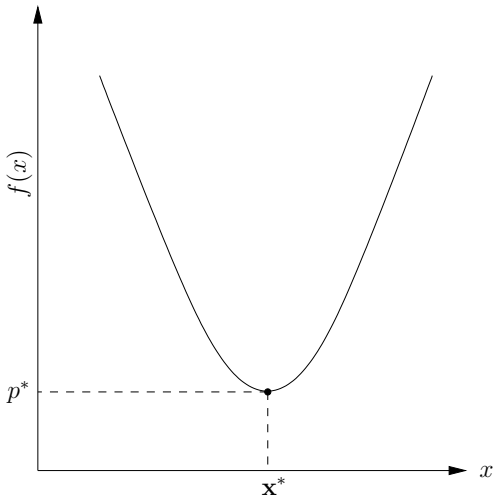

FIGURE 1.10: The *optimal value* of f_0 is achieved at $\mathbf{x}^*$, when $f_0(\mathbf{x}^*) = p^*$.

other words, a *convex optimization problem* is constituted by a convex objective function, by convex inequality constraint functions and by affine equality constraint functions. Strictly speaking, the feasible set of convex optimization problems constitutes a convex set, since the intersection of $(m+1)$ convex sets and p affine sets, e.g. hyperplanes forms a convex set, as we discussed in Section 1.1.2.1.

1.1.2.4 The Lagrangian Function and Duality

Initially, we rewrite the generic form of the optimization problem considered in (1.5)–(1.7) as a *Lagrangian function* by augmenting the objective function with a weighted sum of the constraint functions given by

$$\mathcal{L}(\mathbf{x}, \boldsymbol{\lambda}, \boldsymbol{\nu}) = f_0(\mathbf{x}) + \sum_{i=1}^{m} \lambda_i f_i(\mathbf{x}) + \sum_{i=1}^{p} \nu_i h_i(\mathbf{x}), \tag{1.10}$$

where both the inequality and equality constraints are weighted by the variables $\lambda_i \in \mathbb{R}_+, i = 1, \cdots, m$ and $\nu_i \in \mathbb{R}, i = 1, \cdots, p$, respectively, which are referred to as the *Lagrangian multipliers* or *dual variables* [129].

The Lagrange dual function is described as the minimum value of $\mathcal{L}(\mathbf{x}, \boldsymbol{\lambda}, \boldsymbol{\nu})$ for all values of $\mathbf{x}$ and it is written as

$$g(\boldsymbol{\lambda}, \boldsymbol{\nu}) = \inf_{\mathbf{x}}(\mathcal{L}(\mathbf{x}, \boldsymbol{\lambda}, \boldsymbol{\nu})) = \inf_{\mathbf{x}} \left(f_0(\mathbf{x}) + \sum_{i=1}^{m} \lambda_i f_i(\mathbf{x}) + \sum_{i=1}^{p} \nu_i h_i(\mathbf{x}) \right), \tag{1.11}$$

where the dual objective function $g(\boldsymbol{\lambda}, \boldsymbol{\nu})$ is always a concave function, since it is part of a family of affine functions in $(\boldsymbol{\lambda}, \boldsymbol{\nu})$, regardless whether it is a convex optimization problem [129]. Assuming that the optimal value of the *primal (original) problem* is denoted

by p^*, any *dual feasible* point of $(\boldsymbol{\lambda}, \boldsymbol{\nu})$ forms the lower bound of

$$g(\boldsymbol{\lambda}, \boldsymbol{\nu}) \leq p^*. \tag{1.12}$$

1.1.2.5 The Lagrange Dual Problem

The Lagrangian dual form of the optimization problem becomes

$$\begin{aligned} \text{maximize} \quad & g(\boldsymbol{\lambda}, \boldsymbol{\nu}) && (1.13) \\ \text{subject to} \quad & \boldsymbol{\lambda} \succeq 0, && (1.14) \end{aligned}$$

which may be conceived for finding the best possible *lower bound* to the primal optimization problem [129]. The pair $(\boldsymbol{\lambda}, \boldsymbol{\nu})$ represents the *dual feasible* solutions, while the optimal solution to the dual problem is denoted by $(\boldsymbol{\lambda}^*, \boldsymbol{\nu}^*)$, which is termed as *dual optimal* or *optimal Lagrangian multipliers*. Note that the Lagrange dual problem is a convex optimization problem, since the objective function is concave and the constraint is convex, regardless whether the primal optimization problem is a convex one.

1.1.2.6 Strong and Weak Duality

Let us assume that the dual optimal points $(\boldsymbol{\lambda}^*, \boldsymbol{\nu}^*)$ provide us with the dual optimal value, denoted by d^*, which is the maximum lower bound to the primal optimal value of the original optimization problem. Explicitly, *weak duality* is defined as

$$d^* \leq p^*, \tag{1.15}$$

regardless of the convex or nonconvex nature of the primal problem [129]. The discrepancy between the primal optimal value and the dual optimal value is termed as the *optimal duality gap* [129] and it is given by

$$p^* - d^* \geq 0. \tag{1.16}$$

Note that a dual feasible point assists us in finding a certain stopping criterion for solution algorithms, since the dual feasible point provides us with the lower bound to the optimal value of the optimization problem.

Nevertheless, *strong duality* holds under certain conditions [129], which is defined as

$$d^* = p^*. \tag{1.17}$$

More explicitly, the optimal duality gap is zero, which physically means that both the primal and the dual problems become equivalent optimization problems. For most convex

optimization problems, strong duality holds, but it is not limited to convex problems. The final decision depends upon the *constraint qualification tests*, which determine whether the optimization problem holds strong duality or not. For instance, *Slater's theorem* [129] indicates that if an optimization problem is convex and satisfies *Slater's condition* [129], then that particular convex optimization problem satisfies strong duality [129].

1.1.2.7 The Karush-Kuhn-Tucker Optimality Conditions

A major reason for using Lagrange relaxation and Karush-Kuhn-Tucker (KKT) optimality conditions is because the insights about the optimization variables and their dependencies can be readily observed, where we can characterize the system model with the aid of the closed form equations obtained from Lagrange relaxation and KKT analysis.

For the optimization problems showing strong duality with differentiable objective and constraint functions, the KKT conditions are well-suited for validating whether $\mathbf{x}$ and $(\boldsymbol{\lambda}, \boldsymbol{\nu})$ are primal and dual optimal points, respectively. In summary, the following KKT conditions are always sufficient and necessary under strong duality [129]:

$$f_i(\mathbf{x}^*) \leq 0, \ i = 1, \cdots, m \tag{1.18}$$

$$h_i(\mathbf{x}^*) = 0, \ i = 1, \cdots, p \tag{1.19}$$

$$\lambda_i^* \geq 0, \ i = 1, \cdots, m \tag{1.20}$$

$$\lambda_i^* f_i(\mathbf{x}^*) = 0, \ i = 1, \cdots, m \tag{1.21}$$

$$\nabla f_0(\mathbf{x}^*) + \sum_{i=1}^{m} \lambda_i^* \nabla f_i(\mathbf{x}^*) + \sum_{i=1}^{p} \nu_i^* \nabla h_i(\mathbf{x}^*) = 0. \tag{1.22}$$

Since the primal problem is convex, if the primal and dual variables represent arbitrary points that satisfy the KKT optimality conditions given by the primal feasibility in (1.18)–(1.19), the dual feasibility of (1.20), the complementary slackness in (1.21) and the first order optimality in (1.22), then the primal optimal and dual optimal points can be obtained with zero duality gap [129].

1.2 Organization and Novel Contributions of this Thesis

In Section 1.1 we have discussed the motivation of this thesis and provided some of the preliminaries, which will be relied upon in later chapters. In Section 1.1.1 a state-of-the-art literature review of NL maximization techniques used in WSNs has been performed. Let us now present the organization of this thesis and underline its novel contributions.

1.2.1 Organization of this Thesis

The characterization of our NL maximization problems is described in Table 1.17, where the evolution of our system model used in each of the chapters can be compared. Moreover, Fig. 1.11 presents an overview of the structure of this thesis, where the evolution and/or the relationship of each chapter can be captured. We can observe the specific evolution of rationale across the chapters in Fig. 1.11 using Table 1.17, where the characteristics of the chapters are referred to as "evolved" or "unchanged". For example, observe in Fig. 1.11 that the QoS metric is "evolved" during the transition from Chapter 2 to Chapter 3. To understand what has been evolved, the readers are referred to Table 1.17, where in this specific case the "QoS Metrics" are evolved from "NL, Source Rate" to "NL, SINR, BER". In the following, we elaborate on the characteristics of the system models considered in our specific NL maximization problems considered in each chapter.

- **Chapter 2**: Motivated by [30], we maximize the NL in an interference-limited WSN considering a rate and power allocation scheme under both AWGN and fading channel characteristics, since all the related contributions in the literature consider either a non-adaptive, i.e. fixed-mode system or non-fading channel characteristics. A generalized string network topology consisting of an arbitrary number of nodes is considered in our study, where we employ the KKT optimality conditions for obtaining the optimal solution to the NL maximization problem using closed-form expressions. Therefore, we are able to derive analytical expressions of the globally optimal NL for a string network operating in an interference-limited scenario, while communicating either over an AWGN or over fading channels for a given link schedule. Furthermore, the maximum NL, the energy dissipation per node, the average transmission power per link and the lifetime of all nodes in the network may be obtained. We quantify how the maximum NL is reduced as a function of the fading statistics due to the poor channel conditions. Furthermore, we demonstrate that given a certain network-sum-rate, the simultaneous scheduling of weakly interfering links benefits from the associated spatial reuse by allowing each node to transmit at a lower rate, which requires a reduced transmission power and hence results in a higher NL. We also conclude that the choice of the particular scheduling scheme depends on the application, since a lower source rate favors infrequent transmissions requiring a low transmit power, while avoiding the detrimental effects of interference, when aiming for extending the NL. However, we observe that for higher source rates, a higher NL can be achieved by aggressive spatial reuse.
- **Chapter 3**: In Chapter 2, both the NL and source rate are considered as the QoS measure as a function of the transmit rate and the power, where an adaptive scheme is assumed. Moreover, the energy dissipation of the signal processing operations, i.e. energy dissipation of the transceiver circuits, is neglected. However, system designers may want to predict the impact of the SPP on the NL. On the other hand, achieving a reasonable

NL at the cost of a tolerable end-to-end BER for a fixed-rate system using various MCSs is also a significant objective for the system designer considering the required QoS. More explicitly, the BER is the salient QoS metric of communication systems, but naturally, maintaining a longer NL for battery-limited devices is another important factor. Additionally, the choice of the physical layer parameters, such as the MCSs, and transmit power substantially affect the NL and these parameters also have a direct impact on the BER. Therefore, striking an attractive trade-off between the BER and the NL is crucial for network designers at an early design stage. In this chapter we aim for maximizing the NL for a predetermined set of target SINR values, which guarantees the predefined QoS of each link operating over either an AWGN channel or Rayleigh block-fading channel, while considering two scenarios operating either with or without SPP.

- **Chapter 4**: Our network obeys a string topology in Chapter 3, where the distances between consecutive nodes are fixed. However, in a more realistic network, there may be thousands of routes having diverse distances between consecutive sensor nodes. Moreover, in such a complex network we also have to reconsider our NL definition. Therefore, in this chapter we maximize the NL of a randomly and uniformly distributed fully connected WSN, where the fully connected WSN imposes an exponentially increasing routing complexity upon increasing the number of nodes. More particularly, this chapter is focused on the cross-layer optimization of the power allocation, scheduling and routing operations for the sake of NL maximization for predetermined per-link target SINR values. We use the so-called exhaustive search algorithm (ESA) as our benchmarker and conceive a near-optimal single objective genetic algorithm (SOGA) imposing a substantially reduced complexity in fully connected WSNs.
- **Chapter 5**: In Chapter 4 we consider a fully-connected WSN for NL maximization, where the NL is strictly dependent on the SN battery level, since we only transmit information generated at the SN, which is then directed towards the destination node (DN) via alternative routes depending on their route lifetime (RL) performance. Moreover, the NL is computed by the accumulation of the maximum RL values amongst these alternative routes, until the SN battery is fully depleted, where the RL is defined by the earliest time, at which a sensor node lying in the route fully drains its battery energy. Therefore, depending on the size of the network, the lifetime models used in our previous studies are based on a single-objective NL or RL maximization problem. However, several significant metrics, such as the end-to-end delay have not been considered for the sake of NL maximization, even though a high end-to-end delay may lead to a significant end-to-end throughput reduction during the lifetime of the network. Therefore, in this chapter we propose a novel NL optimization method in order to reflect the effect of the end-to-end delay on the NL along with the aggregate energy dissipation of the same route. The distinctive aspect of this study is the simultaneous optimization of both the aggregate energy dissipation and of the end-to-end delay as a multi-objective optimization problem in order to provide the system designer with a trade-off between

Pareto optimal energy and delay solutions. Therefore, we employ multi-objective evolutionary algorithms (MOEAs), namely the so-called non-dominated sorting based genetic algorithm-II (NSGA-II) and the multi-objective differential evolution (MODE) algorithm for obtaining the set of Pareto optimal NL-aware routes striking a trade-off between the aggregate energy dissipation and the end-to-end delay. Moreover, we characterize both the complexity and the convergence of both algorithms compared to the ESA.

In other words, in Chapter 2 we formulate an initial study of the NL maximization problem based on a string topology. To solve this optimization problem, the parameters have to be appropriately arranged, hence this particular system model does not consider the particular *IEEE Standards*. As a further advance, in Chapter 3 we extend our NL maximization problem to a realistic scenario, where the parameters are selected from the practical data sheet of a *National Instruments* device, namely that of the *wireless sensor network programmable analog input measurement nodes* [173], which is based on the *IEEE 802.15.4 Standard*. Note that apart from the transmit power, in Chapter 3 we also consider the impact of the signal processing power on the NL as a further practical improvement. Furthermore, Chapter 4 also considers the *IEEE 802.15.4 Standard* for the sake of constructing a practical scenario, where the string topology considered in Chapter 2 and Chapter 3 is also extended to a more complex network, namely the so-called fully connected network, which is considered for various scenarios supporting different number of nodes, with the objective of finding a near optimal solution at a reduced complexity. Finally, Chapter 5 focuses on the design of the multiobjective NL definition considering the trade-off between the end-to-end delay and the energy dissipation. The decision on the selection of a route that provides the best NL is made by the system designer. Again, the evolution structure of our system models from the conceptually simple towards the realistic can be observed from Fig. 1.11 and Table 1.17.

1.2.2 Contributions of this Thesis

The contributions of this thesis have been gradually developed considering several characteristics of the system models, as described in Table 1.17 and Fig. 1.11. The contributions focus on a range of novel transmission schemes and algorithms designed for the sake of NL maximization in WSNs. To elaborate:

- In Chapter 2, we formulate the NL maximization as a nonlinear optimization problem taking into account both the link scheduling, the transmission rates as well as transmit powers of all active time slots (TSs). The original nonlinear problem is converted into a convex optimization problem by employing an approximation of the SINR. We then derive the Lagrangian form of the convex optimization problem and employ the KKT optimality conditions [129] for deriving the analytical expressions of the globally optimal NL for an interference-limited string topology. In addition to the line-of-sight (LOS)

Characteristics	Chapter 2	Chapter 3	Chapter 4	Chapter 5
QoS Metrics	NL, Source Rate	NL, SINR, BER	NL, SINR, BER	(NL), Energy, Delay
Channel Model	AWGN, Block Fading	AWGN, Block Fading	AWGN	AWGN
Cross-layer Model	Phy, MAC, (Routing)	Phy, MAC	Phy, MAC, Routing	Phy, Routing
Network Topology	String Topology	String Topology	Fully-connected WSN	Fully-connected WSN
Objective Model	Single-objective	Single-objective	Single-objective	Multi-objective
BER Model	Fixed-BER	NL vs BER using MCSs	NL vs BER using MCSs	Error-free
Optimization Variables	NL, Rate, Power	NL, Power	NL, RL, Power	(NL), Energy, Delay
NL Model	Min. Node Lifetime	Min. Node Lifetime	SN Battery Level	Pareto Optimal Energy&Delay

TABLE 1.17: Characteristics of the system models considered.

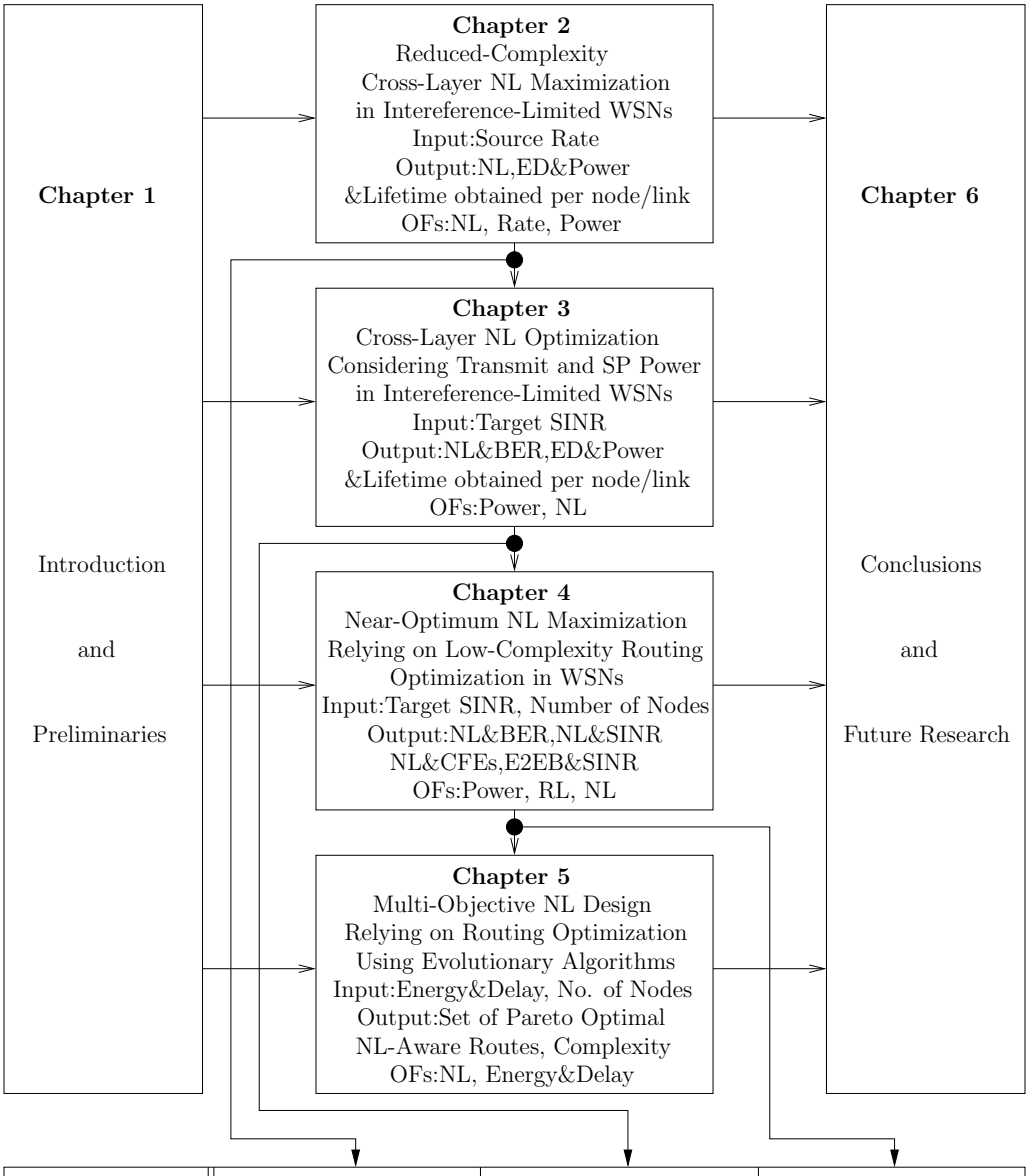

Characteristics	Chapter 2 → Chapter 3	Chapter 3 → Chapter 4	Chapter 4 → Chapter 5
QoS Metrics	Evolved	Unchanged	Evolved
Channel Model	Unchanged	Evolved	Unchanged
Cross-Layer	Unchanged	Evolved	Evolved
Network Topology	Unchanged	Evolved	Unchanged
Objective Model	Unchanged	Unchanged	Evolved
BER Model	Evolved	Unchanged	Evolved
Optim. Variables	Evolved	Evolved	Evolved
NL Model	Unchanged	Evolved	Evolved

FIGURE 1.11: Organization of the thesis, portraying, how the chapters evolve. "Evolved" and "Unchanged" are the terms used for the characteristics of the chapter transitions, which are evolved or remain unaltered. The specific chapter evolutions can be followed in Table 1.17.

AWGN channel model, the non-LOS Rayleigh block-fading[11] channel model is adopted for studying the effects of fading on the NL. Moreover, the maximum NL is evaluated along with the energy dissipation per node, the average transmission power per link and the lifetime of all nodes in the network for a given link schedule and source rate, again, in both LOS AWGN and non-LOS Rayleigh block-fading channels. The substantial effect of the distance amongst the consecutive nodes on the NL is also analyzed, when operating at source rates in a Rayleigh fading channel. Furthermore, the impact of the interferers is investigated in the context of higher source rates. When using the KKT optimality conditions, we have to evaluate $(2V + 4NL + 1)$ expressions, whereas the so-called interior-point method considered in [30] requires at least $(2V+4NL)^2$ operations to solve $(2V + 4NL)$ linear equations. Therefore, our proposed algorithm achieves reduced-complexity NL maximization.

- In Chapter 3, we built upon our previous work in Chapter 2 by incorporating a specific target QoS requirement defined by the target SINR of each link. As a result of this, we consider a fixed-rate system and quantify the effects of the physical layer parameters on the achievable NL, while considering an application-dependent target BER in both LOS AWGN and non-LOS Rayleigh block-fading channels in interference-limited string topology based WSNs. We analyze the impact of the SPP on the NL for both AWGN and fading channels. We demonstrate that the NL is substantially reduced due to the accumulated ED of SPP and the transmit power. Here, we charazterize the interplay between the transmit power and the SPP, where the NL of a high target SINR tends to converge to a certain constant NL, as observed in the SPP-related scenario. We examine both the ED of each node, as well as the required transmission power per link, the interference power imposed on each node and the lifetime of all nodes forming part of the string topology network, while considering different target SINR requirements, SPPs and channel characteristics. Furthermore, we consider two types of BER performances. The first one is the per-link BER requirement (PLBR), which defines the BER value attained by the weakest link. Hence, PLBR represents the worst BER that can be tolerated over the links. By contrast, the end-to-end BER (E2EB) is defined as the BER accumulated along the route spanning from the SN to the DN. We demonstrate that a similar NL performance is achieved, while a higher E2EB is maintained compared to PLBR. We show how the requirement of different target BER values at the physical layer affects both the NL and the network performance in the string topology considered. Considering our proposed system model, depending on the required QoS and network performance, the network designer can make well-informed decisions concerning the type of modulation schemes that should be used for different types of networks and/or applications.
- We further develop the system model studied in Chapter 3 for a more general network

[11] A channel is said to be block-fading channel if the fading process stays constant within the time-division multiple access (TDMA) frame and independently changes from one TDMA frame to another. The keyword "block" is referred to a TDMA frame per link, during which the fading coefficient remains constant.

topology, which in turn requires us to develop a novel NL definition. The proposed NL definition provides an extended NL due to exploiting alternative routes having the maximum RL for the end-to-end transmission in a fully connected WSN, where our aim is to carry the information generated at the SN to the DN, until the SN's battery is fully depleted. More explicitly, the accumulation of the maximum RL computed over alternative routes provides us with an extended NL, since the NL computation is composed of the summation of the several RL values, until the SN battery is fully depleted. Therefore, in this study the NL values are expected to be higher than that of Chapter 2 and Chapter 3. Moreover, we optimize the transmit power, the scheduling and the routing for the sake of NL maximization, where we propose the ESA and SOGA algorithms for random network topologies relying on fully connected nodes. Each SN-DN route is passed to an optimization function to find the optimal RL for the corresponding route. The ESA finds the best route and its RL by searching through all the possible solutions within the given number of nodes in the fully connected WSN. On the other hand, the SOGA finds the best solution, given a maximum affordable number of generations and individuals. We show that SOGA is capable of a near-optimal solution at a significantly reduced complexity compared to ESA, provided that the number of nodes is higher than 7. During the iterations of the ESA and SOGA algorithms, more than one maximum NL values may be returned. Therefore, the selection of the alternative most beneficial route is required, where the selection process determines the best SN-DN route for the end-to-end transmission. The selection process critically relies on the battery of the sensors, which has to be updated after each iteration for the forthcoming RL computation. Hence, we introduce various route selection schemes (RSSs), namely the route with the least total energy dissipation (LTED), the least number of hops (LNOH), the largest remaining SN battery (LRBAT) and random route selection (RANR). We assume that simply each hop introduces one unit of delay. Furthermore, we provide the E2EB as an upper bound of the BER of the interference-limited fully connected WSN using uncoded binary phase-shift keying (BPSK), 1/2-rate convolutional coded (CC) hard-decoded and soft-decoded quadrature phase-shift keying (QPSK) modulation and coding schemes (MCSs) for the proposed RSSs. The 1/2-rate CC soft-decoded QPSK MCS had a higher NL than the other MCSs in all scenarios of the ESA and the SOGA. We demonstrate that the RSS-LRBAT and RSS-LTED outperforms the other RSSs in terms of their NL, since they are the most NL aware RSSs. The E2EB of the RSS-LNOH is slightly better than the other RSSs, which is due to the lower bit error accumulation over the lower number of hops. Since we assume that the ED of any operation is negligible except that of the transmit power, introducing an additional sensor into the WSN extends the NL, since there will be more opportunities to relay information over the alternative routes. We observe that the NL gain due to incorporating an additional sensor into our current WSN, for example when a 5th sensor enters the WSN having 4 sensors provides an approximately 5500hrs NL improvement, when the WSN operates at 10dB over an AWGN channel. For seven

nodes, the computational complexity of the ESA and SOGA is similar, but it increases exponentially for the ESA, while much more modestly for the SOGA, albeit this is achieved at the cost of a small reduction in NL compared to the optimal NL for WSNs composed of $V > 7$ nodes.

- Considering the same fully connected WSN described in our previous study, we further evolve our NL definition by incorporating the aggregate energy dissipation and the end-to-end delay, as we suggested in Chapter 5. We consider a pair of MOEAs. The first is based on the NSGA-II, while the second one is the MODE algorithm [174, 175]. We invoke both algorithms for jointly optimizing the delay and energy dissipation of a fully connected network relying on randomly distributed nodes. We compare both algorithms in terms of the proximity of the solutions to the so-called Pareto front [176–178]. We evaluate their complexities and their rates of convergence, as the number of nodes in the network increases. We also demonstrate that at the same complexity, the MODE algorithm provides solutions approaching the true Pareto front more closely than the NSGA-II, and in general exhibits a higher convergence rate. Additionally, we demonstrate that both algorithms require substantially less cost-function evaluations for approximating the true Pareto front for networks of 10 or more nodes, when compared to an ESA. Furthermore, we propose a novel multi-objective NL definition, where the system designer can predict a trade-off between the aggregate energy dissipation and the end-to-end delay. Therefore, depending on the application and the target QoS required, the set of NL-aware routes lying on the Pareto front can be exploited as the Pareto optimal solutions in order to maximize the NL considering the interplay between the aggregate energy dissipation and the end-to-end delay.

Chapter 2

Reduced-Complexity Network Lifetime Maximization in Wireless Sensor Networks

2.1 Introduction

As described in Chapter 1, a wireless sensor network (WSN) is composed of a large number of nodes that monitor physical as well as environmental conditions and pass their accumulated data through the network to a sink node. There are numerous attractive applications for WSNs, including for example designing intelligent highways, controlling air pollution, providing remote health assistance for disabled or elderly people, monitoring river level variations, etc. As also indicated in Chapter 1, each of these applications may be composed of numerous sensor nodes each of which consumes a considerable amount of energy during their sensing, communication and data processing activities. Since each sensor node drains its limited energy supply as time elapses, the NL is a crucial metric in these applications and has a major impact on the achievable performance of WSNs. Hence, in this chapter we aim for analyzing and optimizing the NL of the WSNs under different channel conditions.

The NL defines the total amount of time during which the network is capable of maintaining its full functionality and/or achieves particular objectives during its operation, as exemplified in [56] and [57]. Specifically, the authors of [59], [60] and [61] defined the expiration of the NL as the time instant at which a certain number of nodes in the network depleted their batteries. As a further example, the NL was defined in [62] as the lifetime of the specific sensor node associated with the highest energy consumption rate, whereas the authors of [63], [64] and [65] considered the lifetime of the network to be expired at the particular instant, when the first node's battery was depleted. The NL in [64] was also defined as

the instant, when the first data collection failure occurred. In our contribution the NL is deemed to be expired, when at least one of the nodes fails due to its discharged battery. Therefore, extending the lifetime of a single node becomes an important and challenging task due to the battery-dependent characteristics of the wireless sensor nodes. This common NL definition is used in our contribution, since we consider a network of linearly connected sensor nodes, where a single node's failure may destroy the entire string topology of nodes and hence the information of the source cannot be relayed to the sink. When considering the energy dissipated at a sensor node, the battery life is predominantly related to the node's communication activity, where the transmission rate and power must be optimized, while taking into account the battery capacity, the efficiency of the power amplifiers, the receiver and transmitter circuit energy consumption and other physical layer parameters, including the modulation and coding schemes, the attainable coding gain, the path loss and so on.

It is widely recognized that transmission at a high transmission rate requires the use of a high transmit power, which potentially leads to strong interference amongst the transmission links [179]. Therefore the battery depletion of an individual sensor node may become inevitable and hence the NL may be reduced. However, in large networks spatial reuse may be adopted for improving the attainable transmission rates at the cost of imposing interference on the network [180]. In this case, link scheduling [30] and multiple access schemes [181] play a significant role in coordinating the resultant interference. More explicitly, we will demonstrate that scheduling weakly interfering links simultaneously allows the network to maintain a given sum-rate at a reduced per-node transmit power, which hence extends the battery-life of the nodes and hence extends the NL [179]. This is one of the methods routinely employed for taking advantage of spatial reuse in order to control the level of interference imposed on the network [180]. This method extends the NL, since mitigating the interference imposed implies that each transmission requires less power. Therefore, intelligent scheduling should carefully balance the number of simultaneous active links as well as their transmission durations for the sake of keeping the required transmit power at a minimum. Furthermore, multi-hop relaying [182] is capable of conserving the energy of the source node, since intermediate nodes may be employed for reducing the transmission power necessary for maintaining a given end-to-end rate. Hence, we consider the joint optimal design of the transmission rate, transmission power and scheduling in order to maximize the NL of energy-constrained WSNs.

There is a paucity of contributions in the literature on the issue of cross-layer NL optimization in the context of WSNs. Hoesel *et al.* [80] proposed a cross-layer approach for jointly optimizing the MAC and routing layer in order to maximize the NL. Chen and Zhao [64] proposed an efficient MAC protocol, which relies both on the channel state information and on the MAC's knowledge of the residual energy to maximize the NL. In [35], Kwon *et al.* investigated the NL maximization problem of WSNs, which jointly considers the physical layer, the MAC layer and the routing layer in conjunction with the transmission

success probability constraint. Additionally, the trade-off between NL maximization and application performance was studied in [81] by using cross-layer optimization. A similar study also investigated the trade-off between the energy consumption and application-layer performance with the aid of cross-layer optimization of WSNs [83]. Another cross-layer approach conceived for maximizing the NL was proposed in [86], where MAC-aware routing optimization schemes were designed for WSNs that are capable of multichannel access. In [183], the authors invoked random linear network coding for the lifetime maximization of wireless networks within a fixed-rate system for communicating over both AWGN and Rayleigh fading channels. A different approach to NL maximization was introduced in [91], where both contention and sleep control probabilities of the sensor nodes were utilized for formulating the NL maximization problem, while guaranteeing both the required throughput and the SINR requirements. Najimi *et al.* [60] proposed a node selection algorithm for balancing the energy usage of the sensors in a fixed-mode cognitive sensor network. A similar idea to that of the optimal control approach invoked for maximizing the NL with the aid of a carefully selected routing probability was exploited in [65], where all the sensors were configured to deplete their energy exactly at the same time for the sake of lifetime maximization. Another similar study advocating an effective transmission scheme was proposed in [147], where both the maximum possible energy efficiency and the best possible energy balancing was maintained with the aid of ant colony optimization.

2.1.1 Novel Contributions

However, all related work mentioned above considers either a non-adaptive, i.e. fixed-mode system or non-fading channel characteristics. An adaptive system conceived for the sake of NL maximization was studied by Wang *et al.* [28], who considered only an interference-free scenario for an AWGN channel by employing the Karush-Kuhn-Tucker (KKT) optimality conditions [129] to the optimal TDMA NL maximization problem of [30] in order to derive the analytical expressions of the optimal NL. Madan *et al.* [30] considered an interference-limited scenario relying on an adaptive system, operating in an AWGN channel, but the impact of the fading channel characteristics on the NL was not presented. The authors of [28] obtained a closed form solution for a specific network topology. By contrast, a generalized string network topology consisting of an arbitrary number of nodes is considered in our work, where we employ the KKT optimality conditions for obtaining the optimal solution to the NL maximization problem using closed-form expressions. Therefore, we are able to derive analytical expressions of the globally optimal NL for a string network operating in an interference-limited scenario, while communicating either over an AWGN or over fading channels for a given link schedule. Furthermore, the maximum NL, the energy dissipation per node, the average transmission power per link and the lifetime of all nodes in the network may be obtained. We quantify how the maximum NL decreases as a function of the fading statistics due to the poor channel conditions. Furthermore, it is demonstrated that

given a certain network-sum-rate, the simultaneous scheduling of weakly interfering links benefits from the associated spatial reuse by allowing each node to transmit at a lower rate, which requires a reduced transmission power and hence results in a higher NL. Against this background, the novel contributions of this chapter can be summarized as follows:

1. The KKT optimality conditions [129] are invoked for deriving the analytical expressions of the globally optimal NL for an interference-limited string topology.
2. In addition to the line-of-sight (LOS) AWGN channel model, the NLOS Rayleigh block-fading[1] channel model is adopted for studying the effects of fading on the NL.
3. The maximum NL is evaluated, as well as the energy dissipation per node, the average transmission power per link and the lifetime of all nodes in the network is quantified for a given link schedule and source rate in both LOS AWGN and NLOS Rayleigh block-fading channels.
4. The substantial effect of the distance amongst the consecutive nodes on the NL is also analyzed for lower source rates, when operating in a Rayleigh fading channel. The impact of the interferers is also investigated in the context of higher source rates.
5. Using the KKT optimality conditions, we have to evaluate $(2V + 4NL + 1)$ expressions, whereas the algorithm considered in [30] and relying on the so-called interior-point method requires at least $(2V + 4NL)^2$ operations to solve $(2V + 4NL)$ linear equations. Therefore, our proposed algorithm imposes a reduced complexity during the NL maximization.

2.1.2 Chapter Organization

The rest of this chapter is organized as follows. Section 2.2 describes our system model and the constraints of the optimization problem considered. Our problem formulation, KKT analysis and solution approach are presented in Sections 2.3, 2.3.8 and 2.3.9, respectively, while our numerical results are illustrated in Section 2.5. The limitations imposed on optimal scheduling are presented in Section 2.6. Finally, Section 2.7 summarizes the chapter and offers our conclusions.

2.2 System Model

In this section we first describe our centralized network model, which relies on a string topology, since in this simple scenario the effect of transmission variables on the NL can be explicitly exposed and analyzed. The string topology is also capable of providing insights

[1] A channel is said to be block-fading channel if the fading process stays constant within the TDMA frame and independently changes from one TDMA frame to another. The keyword "block" is referred to a TDMA frame per link, during which the fading coefficient remains constant.

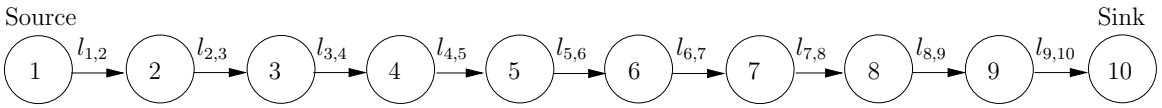

FIGURE 2.1: String topology with $V = 10$ nodes including one SN and one DN.

concerning a randomly distributed network relying on many nodes, since a specific set of nodes can be assumed to constitute a single route of the randomly distributed network. On the other hand, the calculation of both the transmit power and the rate of a specific node relies on the prior knowledge gleaned from other nodes, possibly from its interferers. Therefore, in our system model the sink node is a control center, which handles the variables of the optimization problem and passes the near-instantaneous values of the variables to each of the individual nodes. However, compared to a distributed scheme, this centralized solution will impose a delay on the system, since complex operations such as channel estimation are required at the initial stage. Moreover, the near-instantaneous transmission rate and power values computed by the control center constituted by the sink node should be forwarded to each individual node, and hence a non-negligible delay will be imposed on the network.

In the following we detail our transceiver model in Section 2.2.2, where we evaluate the NL for transmission over both AWGN and block-fading channels. Our transmission scheduling strategy is also described and exemplified at the end of Section 2.2.2. Finally, our NL discussions are provided in Section 2.2.3.

2.2.1 Network Model

We consider a string topology composed of V sensor nodes, where the SN and the sink or the DN are linearly connected by intermediate nodes. An example of this string-topology for $V = 10$ is shown in Fig. 2.1 and hence the number of links is $L = V - 1 = 9$.

Each link is unidirectional and the antenna of each node is omni-directional. The network can be modeled as a directed graph $\mathcal{G} = \{\mathcal{V}, \mathcal{L}\}$, where $\mathcal{V} = \{1, 2, 3, \cdots, V\}$ is the set of all sensor nodes and $\mathcal{L} = \{l_{1,2}, l_{2,3}, \cdots, l_{V-1,V}\}$ is the set of all directed links in the network. Here, $l_{i,j}$ represents the directed link spanning from the transmitter node i to receiver node j. Therefore, the topology can be modeled with the aid of an incidence matrix of the graph $\mathcal{G}$ given by $\mathbf{A} \in \mathbf{R}^{|\mathcal{V}|\times|\mathcal{L}|}$, as illustrated in Table 2.1. The entries $a_{i,l}$, of $\mathbf{A}$ are given by

$$a_{i,l} = \begin{cases} 1, & \text{if } i \text{ is the transmitter of link } l, \\ -1, & \text{if } i \text{ is the receiver of link } l, \\ 0, & \text{otherwise.} \end{cases} \tag{2.1}$$

Nodes/Links	$l_{1,2}$	$l_{2,3}$	$l_{3,4}$	$l_{4,5}$	$l_{5,6}$	$l_{6,7}$	$l_{7,8}$	$l_{8,9}$	$l_{9,10}$
1	1	0	0	0	0	0	0	0	0
2	−1	1	0	0	0	0	0	0	0
3	0	−1	1	0	0	0	0	0	0
4	0	0	−1	1	0	0	0	0	0
5	0	0	0	−1	1	0	0	0	0
6	0	0	0	0	−1	1	0	0	0
7	0	0	0	0	0	−1	1	0	0
8	0	0	0	0	0	0	−1	1	0
9	0	0	0	0	0	0	0	−1	1
10	0	0	0	0	0	0	0	0	−1

TABLE 2.1: Illustration of the incidence matrix of graph $\mathcal{G}$ for $V = 10$.

We may assume that only the SN generates information, for example the temperature information which has to be conveyed to the DN. Alternatively, we may assume that each sensor node in the directed string topology of Fig. 2.1 generates information of its own and transmits this information in addition to relaying the information arriving from other sensor nodes. Hence, the DN may seek the multiple commodities generated by the different sensor nodes forming part of our string topology, which hence has been referred to as a multi-commodity flow. Therefore, the so-called generalized flow-conservation constraint of a single SN that generates information is given by

$$\sum_{l\in\mathcal{O}(i)}\left(\sum_{n=1}^{N} r_{l,n}\right) - \sum_{l\in\mathcal{I}(i)}\left(\sum_{n=1}^{N} r_{l,n}\right) = s_{SN}, \tag{2.2}$$

for each node i, where s_{SN} is the source information generated by the SN, while N is the total number of TSs per TDMA frame and $r_{l,n}$ is the transmission rate of link l in TS n. More explicitly, node i has to transmit the data it received so that the flow-conservation criterion of each node is satisfied. Physically, this means that the information generated at the SN has to arrive at the DN, where $l \in \mathcal{O}(i)$ denotes an emerging link and $l \in \mathcal{I}(i)$ represents an incoming link of node i. Additionally, we assume that both the SN as well as the corresponding relay nodes always have packets to send in their buffer.

2.2.2 Channel Model and MAC Layer Scheme

In each TS n, each node can only act as a transmitter or a receiver. Each transmitter is only allowed to communicate with a single receiver, which cannot receive from other nodes

in the same TS. This is due to the half-duplex nature of the transceivers, where nodes communicate via the same shared wireless channel. The LOS AWGN channel is modeled by a certain propagation path-loss law and a fixed noise power at the receivers. The channel gain of the link between transmitter i and receiver j is given by

$$G_{i,j} = 1/\left(d_{i,j}\right)^m, \tag{2.3}$$

where $d_{i,j}$ is the distance between nodes i and j, whilst the path-loss exponent is m. These channel gains are arranged into the network's channel-gain matrix denoted by $\mathbf{G}$. Each node i is capable of transmitting at a power less than the maximum power of that node denoted by $(P_i)_{max}$. The total energy dissipation at a node cannot exceed the initial battery energy of that node. No node is allowed to simultaneously transmit multiple data packets and the link quality is defined in terms of the SINR. Based on the above assumptions, when node i transmits a packet $\mathbf{x}_i$, the observations received by node j can be expressed as

$$\mathbf{y}_j = \mathbf{x}_i + \mathbf{n}_j,\ i = \mathcal{O}^{-1}(l_{i,j}) \text{ and } j = \mathcal{I}^{-1}(l_{i,j}), \tag{2.4}$$

where $\mathbf{n}_j$ is the Gaussian noise added at the receiver node j, given the link l spanning from node i to node j, while $\mathcal{O}^{-1}(l_{i,j})$ denotes the node from which the link emerges and $\mathcal{I}^{-1}(l_{i,j})$ represents the node at which the link arrives. Given a specific link l, the SINR is denoted by Γ_l in the AWGN channel model. The maximum achievable rate per unit bandwidth is $r_l = \log(1 + K \cdot \Gamma_l)$ given in nats/s/Hz, where we have $K = -1.5/\log(5\text{BER})$ [184] and BER represents the target BER required by the system. Therefore, the SINR is given by [181]

$$\Gamma_{l_{i,j},n} = \frac{G_{i,j} P_{l_{i,j},n}}{\sum_{i' \neq i, l_{i',j'} \in \mathcal{L}_n} G_{i',j} P_{l_{i',j'},n} + N_0}, \tag{2.5}$$

where $P_{l_{i,j},n}$ is the transmission power of link l spanning from node i to node j in TS n. Furthermore, K is assumed to incorporate the coding gain and any other gain factors, which is a suitable model for M-ary quadrature amplitude modulation (M-QAM) associated with $M \geq 4$ [184]. The factor K is assumed to be absorbed into the gain matrix $\mathbf{G}$.

On the other hand, when the packet $\mathbf{x}_i$ transmitted from node i experiences fading, the observations received by node j can be expressed as

$$\mathbf{y}_j = h_{i,j}\mathbf{x}_i + \mathbf{n}_j,\ i = \mathcal{O}^{-1}(l_{i,j}) \text{ and } j = \mathcal{I}^{-1}(l_{i,j}), \tag{2.6}$$

where $h_{i,j}$ is the channel coefficient capturing the fading effects of the link between transmitter i and receiver j, while $\mathbf{n}_j$ is the Gaussian noise added at the receiving node j. Therefore, the channel of each link is modeled as a multiplicative Rayleigh fading channel contaminated by the noise added at the receivers. We consider block fading also referred to as quasi-static fading, where the fading gain is kept constant throughout the TDMA frame for the link

Links \ Slots	1	2	3	4	5	6	7	8	9	10	11	12	13	14	15	16	17	18
l_{1-2}	•+			•			•			•+			•			•		
l_{2-3}		•+			•			•			•+			•			•	
l_{3-4}			•+			•			•			•+			•			•
l_{4-5}	•			•+			•			•			•+			•		
l_{5-6}		•			•+			•			•			•+			•	
l_{6-7}			•			•+			•			•			•+			•
l_{7-8}	•			•			•+			•			•			•+		
l_{8-9}		•			•			•+			•			•			•+	
l_{9-10}			•			•			•+			•			•			•+

• : $T = 3$ SPTS + : $T = 9$ SPTS

FIGURE 2.2: Link scheduling with SPTS parameter $T = 3$ and $T = 9$, when $N = 18$ and $V = 10$.

and independently changes for the TDMA frame of the other links, which represents slowly fading channels, i.e. low-Doppler pedestrian speeds. This requires a modification of the SINR used in AWGN channels, which is formulated as [184]

$$\widetilde{\Gamma}_{l_{i,j},n} = \frac{H_{i,j} G_{i,j} P_{l_{i,j},n}}{\sum_{i' \neq i, l_{i',j'} \in \mathcal{L}_n} H_{i',j} G_{i',j} P_{l_{i',j'},n} + N_0}, \tag{2.7}$$

where $H_{i,j} = |h_{i,j}|^2$ is the fading gain of the link between transmitter i and receiver j, while $P_{l_{i',j'},n}$ denotes the transmit power of the interfering link l spanning from the interfering node i' to the receiving node j of the transmitter i.

We assume a link scheduling associated with spatially periodic time sharing (SPTS) [30], where we consider a distance T between the links that are transmitting in the same TS and the link is reactivated after every T TSs. Fig. 2.2 illustrates the link scheduling for the SPTS parameters of $T = 3$ and $T = 9$. For $T = 3$, at the first TS, links $l_{1,2}$, $l_{4,5}$, $l_{7,8}$ are simultaneously scheduled and each link is activated 6 times in total in TSs of 1, 4, 7, 10, 13, 16. On the other hand, for $T = 9$, each TS only has a single active transmission, which represents an interference-free scenario, and each link is activated twice, as shown in Fig. 2.2.

2.2.3 Network Lifetime Model

Various definitions of the NL can be found in [64], [30], [185], [186], [106]. For example, Madan *et al.* [30] and Chang *et al.* [106] assumed that the lifetime of node i is defined by

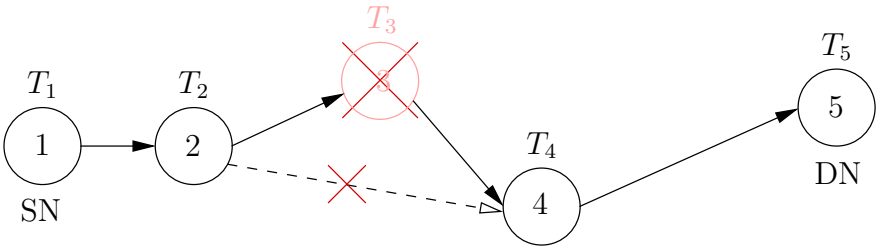

FIGURE 2.3: The SN cannot relay its data to DN due to a failure caused by the depleted battery of Node-3.

the specific time instant, when the node completely drains its initial battery energy which is denoted by T_i. The most commonly used assumption for the NL's definition is that the failure of a single node destroys the connectivity of the entire network. This assumption may seem too pessimistic, since a single node's failure may not have such a dramatic impact on the WSN considered. For example, since in a fully connected network each node has many alternative routes to transmit its data through in the direction of the DN, the failure of that node due to battery depletion may be negligible in the network. Hence, the above NL definition may indeed become too pessimistic for such scenarios. However, as shown in Fig. 2.3 for a string (linear) or congested-node topology, the failure of a single node may in fact lead to a disjoint network. Explicitly, Node-2 cannot transmit to Node-4 in Fig 2.3 due to the failure of Node-3. This assumption may still be used for characterizing the worst-case scenario. Cheng *et al.* [185] proposed a NL definition, which was determined by the time instant, when a certain fraction of sensor nodes in the network fails. By contrast, Verdone and Buratti [187] assumed the NL stretches to the time instant, when the connectivity and coverage targets are first violated. As another alternative, Dong [186] defines the NL in terms of the time instant, when the packet delivery ratio drops below a predetermined threshold. In this chapter, we consider a similar NL definition, as described in [30] and [106], which is the time instant at which the first sensor depletes its battery, i.e. we have $T_{net} = \min_{i \neq DN, i \in \mathcal{V}} T_i$, for the string topology considered in Fig. 2.1.

2.3 Problem Formulation

Given the assumptions and constraints discussed in Section 2.2, we commence by the formulation of the optimization problem. However, before we proceed with the details of the optimization problem, for the sake of clarity we would like to guide the reader through the following ten major steps of our problem formulation procedures, starting from the initial nonconvex problem formulation towards its solution algorithm, as portrayed in Fig. 2.4.

Broadly speaking, in our scenario we are aiming for finding an optimal transmission scheme that maximizes the NL, but minimizes the transmit power required, while satisfying the transmit rate constraint. This optimal transmission scheme can be constructed by solving

the optimization problem formulated in (2.8)–(2.12) during the N TSs of each link. To solve the nonconvex optimization problem formulated in (2.8)–(2.12), we have to proceed by following each step of Fig. 2.4, which also provides a summary of the procedures employed throughout this section. For convenience, we provide a concise summary of each step, where the following enumerated list corresponds to the step of Fig. 2.4, as follows:

1. Having discussed the system model in Section 2.2, in the *Nonconvex Problem Formulation* step, we formulate the general non-convex optimization problem of (2.8)–(2.12). However, there are three main reasons, why the above optimization problem is non-convex and hence cannot be readily solved using conventional convex optimization techniques.
2. The first reason illustrated in the second step of Fig. 2.4 is that T_{net} and P in (2.11) are in the form of a product. Since the product of the two optimization variables is in general non-convex [129], the change of variable method[2] of $z = \frac{1}{T_{net}}$ is applied both to (2.8) and (2.11), which results in the transformed optimization problem of (2.13)–(2.17).
3. In the third step of Fig. 2.4, we have to apply an approximation of the SINR to the rate constraint by simply transforming $\log(1 + \text{SINR})$ to $\log(\text{SINR})$. This is necessary, because utilizing the geometric programming method of [129] without this approximation still leads to a nonconvex optimization problem. Therefore, this approximation has to be applied to (2.10) in order to obtain a convex optimization problem with the aid of geometric programming, as described in the fourth step of Fig. 2.4.
4. However, the optimization problem in (2.13)–(2.17) still remains non-convex. More explicitly, the third reason is that (2.15) is a non-convex function of the optimization variables (z, $P_{l,n}$, $r_{l,n}$), since the rate constraint of each link in each TS cannot be readily rewritten as a convex function for the sake of minimizing the reciprocal of the NL, which is denoted by z. Using the geometric programming approach of [129] and employing the appropriate change of variables, as indicated in the fourth step of Fig. 2.4, we can rewrite the general optimization problem of (2.8)–(2.12) as the convex problem of (2.30)–(2.36).
5. After employing the second, third and fourth steps of Fig. 2.4, which are concerned with the convex transformations, we obtain the optimization problem in its convex form of (2.30)–(2.36), as portrayed in the fifth step of Fig. 2.4.
6. Then, the rate constraint (2.32) of the optimization problem is modified in order to derive the required transmit rate-related expressions after determining its first derivative, which is required for satisfying the KKT optimality conditions in the following sections for deriving the analytical expressions of the globally optimal transmission rates and powers. Otherwise, the first derivative of the expression $\log\left(\frac{N_0}{G_{i,j}} e^{r_{l_{i,j},n} - Q_{l_{i,j},n}} + \sum_{i' \neq i, l_{i',j'} \in \mathcal{L}_n} \frac{G_{i',j}}{G_{i,j}} e^{r_{l_{i,j},n} + Q_{l_{i',j'},n} - Q_{l_{i,j},n}}\right)$ fails to provide further insights about the attainable transmit rate, since its first derivative with respect to $r_{l_{i,j},n}$ is equal to 1.

[2] Assuming that T_{net} cannot be zero, since each sensor forming part of the string topology has an initial battery capacity, each node has to transmit at least for a certain minimum amount of time.

Therefore, (2.44) is converted to the non-logarithmic form of (2.45), where we rewrite the optimization problem of (2.30)–(2.36) in its convex and non-logarithmic form given by (2.46)–(2.52), as illustrated in the sixth step of Fig. 2.4.

7. The optimal solution of the constrained optimization problem described in (2.46)–(2.52) may often be found by using the so-called Lagrangian method of [129]. Therefore, observe in the seventh step of Fig. 2.4 that we can rewrite the optimization problem provided in (2.46)–(2.52) as a Lagrangian dual function by extending the objective function with the aid of a weighted sum of the constraint functions given by (2.59).
8. In the eighth step of Fig. 2.4, the KKT optimality conditions [129] are provided, which are the first order necessary conditions for a solution to be optimal. Therefore, we employ the KKT optimality conditions of (2.59) in order to derive the analytical expressions of (2.60)–(2.66) for finding the globally optimal transmission scheme. Further related details can be found in Section 2.3.8.
9. Using the globally optimal analytical expressions derived in the eighth step of Fig. 2.4, we can obtain the closed-form equations of the transmit powers and rates, as seen in the ninth step of Fig. 2.4. For example, in Section 2.3.9 we will substitute (2.80) into (2.81), since the closed-form equation of the power variable can be readily obtained, as given by (2.86). Similarly, rearranging the transmit rate equation of (2.80), we can derive the closed-form equation of the transmit rate, which is given by (2.88). Then, Equations (2.86) and (2.88) are generalized for any particular link and TS given by (2.89) and (2.90) using (2.74)–(2.79) and (2.68)–(2.73), respectively.
10. Finally, in the tenth step of Fig. 2.4 we apply our iterative solution algorithm, described in Section 2.4, to these globally optimal analytical expressions, as outlined in Fig. 2.5. The dual variables, the reciprocal of the NL as well as the transmit powers and rates are then randomly initialized and updated using the Gauss-Seidel algorithm and iteratively improved in the direction of the optimal solution relying on the gradient ascent algorithm using sufficiently small step sizes for each gradient function, which again allows the algorithm to iteratively approach the optimal solution.

2.3.1 Nonconvex Problem Formulation

Given the assumptions and constraints provided in Section 2.2, in the first step of Fig. 2.4 we formulate the general optimization problem of maximizing the NL, which may be formulated for an AWGN channel as:

$$\text{max.} \quad T_{net} \tag{2.8}$$

$$\text{s.t.} \quad \mathbf{A}(\mathbf{r}_1 + \mathbf{r}_2 + ... + \mathbf{r}_N) = \mathbf{s} \cdot N, \tag{2.9}$$

$$\log\left(1 + \frac{G_{i,j} P_{l_{i,j},n}}{\sum_{i' \neq i, l_{i',j'} \in \mathcal{L}_n} G_{i',j} P_{l_{i',j'},n} + N_0}\right) \geqslant r_{l_{i,j},n}, \tag{2.10}$$

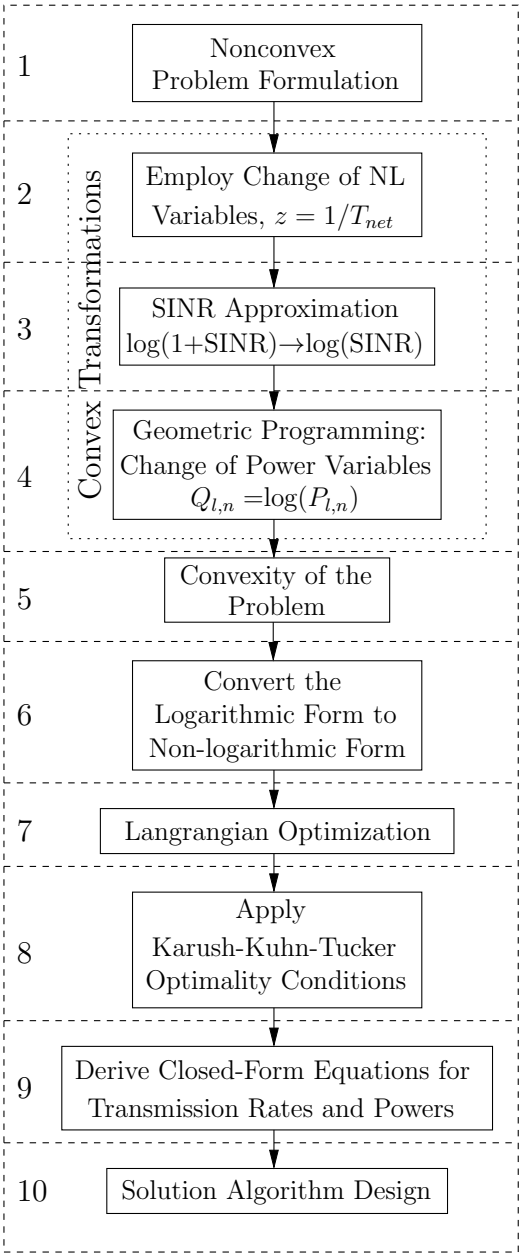

FIGURE 2.4: The steps for solving the nonconvex optimization problem formulated in (2.8)–(2.12) is outlined as a flow-chart.

$$\frac{T_{net}}{N}\sum_{n=1}^{N}\left((1+\alpha)\mathbf{A}^{+}P_n + P_{ct}\mathbf{1}_t(P_n) + P_{cr}\mathbf{1}_r(P_n)\right) \preceq \mathcal{E}, \tag{2.11}$$

$$\mathbf{r}_n \succeq 0, \quad 0 \preceq P_n \preceq (P_i)_{max}, \tag{2.12}$$

where T_{net}, $P_{l,n}$, $r_{l,n}$ are the variables to be optimized for each TS $n = \{1, ..., N\}$, and $l \in \mathcal{L}_n$, while $\mathbf{r}_n$ and P_n represent the transmit rate and power variables of all the links for each TSs, respectively. Assuming that the transmitter and receiver circuits do not dissipate energy, we can set $P_{ct} = 0$ and $P_{cr} = 0$, where P_{ct} and P_{cr} denote the power required by the transmitter and receiver circuits, respectively. The transmitters and receivers, as well

as their corresponding circuits are identified with the aid of the vectors $\mathbf{1}_t(P_n)$ and $\mathbf{1}_r(P_n)$. In (2.8), T_{net} is the NL to be maximized under the constraints of (2.9)–(2.12), where the flow-conservation constraint introduced in (2.9) ensures that the information generated at the SN is transmitted to DN using the relay nodes, while (2.10) describes the capacity constraint requiring that each link's capacity is higher than the throughput required. The constraint defined by (2.11) represents the energy dissipation constraint per node, namely that the sensors must not exceed their initial battery capacity. Finally, (2.12) defines the transmit rate and power limits for the system model considered, where the maximum affordable transmit power per node is bounded by $(P_i)_{max}$. We note that T_{net} and P in (2.11) are in the form of a product and the product of the two optimization variables is in general non-convex [129]. Later in this section we will elaborate on these constraints in (2.30)–(2.36).

2.3.2 Change of NL Variables

The change of NL variable $z = \frac{1}{T_{net}}$ is employed in the second step of Fig. 2.4, which results in the transformed optimization problem of

$$\text{min.} \quad z \tag{2.13}$$

$$\text{s.t.} \quad \mathbf{A}(\mathbf{r}_1 + \mathbf{r}_2 + ... + \mathbf{r}_N) = \mathbf{s} \cdot N, \tag{2.14}$$

$$\log\left(1 + \frac{G_{i,j}P_{l_{i,j},n}}{\sum_{i' \neq i, l_{i',j'} \in \mathcal{L}_n} G_{i',j}P_{l_{i',j'},n} + N_0}\right) \geqslant r_{l_{i,j},n}, \tag{2.15}$$

$$\sum_{n=1}^{N}\left((1+\alpha)\mathbf{A}^{+}P_n + P_{ct}\mathbf{1}_t(P_n) + P_{cr}\mathbf{1}_r(P_n)\right) \preceq z \cdot \mathcal{E} \cdot N, \tag{2.16}$$

$$\mathbf{r}_n \succeq 0, \quad 0 \preceq P_n \preceq (P_i)_{max}. \tag{2.17}$$

After applying the second step of Fig. 2.4, the optimization variables r and P in (2.15) are in the form of a product. Again, since the product of the two optimization variables is in general non-convex [129], the variables have to be modified or rearranged to preserve convexity. Hence, in the following we modify the rate constraint by employing an approximation to the SINR.

2.3.3 Approximation of SINR

We consider an interference-limited WSN scenario, where mutually interfering links are allowed to be scheduled simultaneously within the same TS with the aid of a fixed link scheduling strategy referred to as SPTS [30, 188, 189], which was described in Section 2.2.2 and illustrated in Fig. 2.2. Observe in the third step of Fig. 2.4 that for a fixed link schedule, the non-convex rate constraint of (2.15) can be relaxed for an AWGN channel by employing

an approximation to the function $\log(1+\Gamma_{l_{i,j},n})$ as follows,

$$r_{l_{i,j},n} \leq \log\left(\frac{G_{i,j}P_{l_{i,j},n}}{\sum_{i'\neq i, l_{i',j'}\in\mathcal{L}_n} G_{i',j}P_{l_{i',j'},n}+N_0}\right), \tag{2.18}$$

while the non-convex rate constraint of (2.15) can be approximated for a Rayleigh fading channel as follows,

$$r_{l_{i,j},n} \leq \log\left(\frac{H_{i,j}G_{i,j}P_{l_{i,j},n}}{\sum_{i'\neq i, l_{i',j'}\in\mathcal{L}_n} H_{i',j}G_{i',j}P_{l_{i',j'},n}+N_0}\right). \tag{2.19}$$

In (2.18), $\log(\Gamma_{l_{i,j},n})$ represents a lower bound imposed on the achievable rate, since the true or maximum value of the rate should have been as high as $\log(1+\Gamma_{l_{i,j},n})$. However, the transmit rate has to be satisfied for a given source rate formulated in (2.14) for the links activated within the same TS. Therefore, the transmit power has to be increased in order to satisfy the required transmit rate and to compensate for the rate-loss between (2.15) to (2.18), which in turn reduces the NL. Hence, the NL estimated on the basis of this approximation represents a lower bound of the optimal NL. This becomes a tight bound, when $\Gamma_{l_{i,j},n}$ is increased for the active link. More explicitly, the NL computed using this approximation is only an estimate of the actual NL achieved. Furthermore, this estimated NL becomes more accurate at higher SINR values, since the effect of the approximation invoked is reduced for SINR $>>$ 1. However, this approach may not be feasible for $\Gamma_{l_{i,j},n} \approx 1$. Let us for example consider a scenario associated with a single SN and a single DN, and one TS for the transmission link spanning from SN to DN. Then, the attainable rate becomes $r = \log(1+(P_{l_{SN,DN}}G_{SN,DN})/N_0)$, which is considered as a rate benchmark for the optimal NL and $r = \log\left[(P_{l_{SN,DN}}G_{SN,DN})/N_0\right]$ is utilized for the approximation method of the SINR, where $G_{SN,DN}$ is the power gain which is assumed to be 1, the noise power is given by $N_0 = 1$, and $(P_{l_{SN,DN}}G_{SN,DN})/N_0 = \text{SINR}$.

Let us now assume that $r = \{1, 3\}$ for two simple scenarios, where $r = 1$ corresponds to SINR $= 2.72$ for the approximated SINR scenario, while SINR $= 1.72$ for the benchmark result. Furthermore, $r = 3$ conforms to SINR $= 20.10$ for the approximated SINR case and SINR $= 19.10$ for the benchmark function. Hence, we have $P_{l_{SN,DN}} = \exp(r)/G_{SN,DN}$ for the approximated SINR method and $P_{l_{SN,DN}} = (\exp(r)-1)/G_{SN,DN}$ for the benchmark function. Considering that the SN battery capacity is 50 Joule, we arrive at the NL given by $T_{net} = 50/P_{l_{SN,DN}}$. Table 2.2 presents the NL results both for our low and high SINR values, given the approximated SINR method and the benchmark function. An important observation is that the NL obtained from the approximated SINR method given by $r = \log(\text{SINR})$ represents a lower bound of the optimal NL of the benchmark function given by $r = \log(1+\text{SINR})$. When considering the higher SINR value, the NL gap between the approximated SINR method and the benchmark function becomes insignificant, where the

r	SINR for $r = \log(1 + \text{SINR})$ [dB]	NL of $r = \log(1 + \text{SINR})$ [s]	NL of $r = \log(\text{SINR})$ [s]
1	1.72	29.10	18.39
3	19.10	2.62	2.49

TABLE 2.2: The NL computed using the SINR approximation constitutes a lower bound of the optimal NL.

NL gap with respect to the optimal is reduced from 10.71s to 0.13s upon increasing the SINR in the benchmark function from 1.72 to 19.10. We will further discuss the low- and high-SINR regimes from the point of optimal scheduling in Section 2.6.

2.3.4 Geometric Programming: Change of Power Variables

The fourth step of Fig. 2.4 considers the geometric programming method of [129] that assists in avoiding the product of two variables, since again, the product of two optimization variables is in general non-convex [129]. With the aid of the geometric programming method of [129] and using this time a change of power-related variables according to $Q_{l_{i,j},n} = \log(P_{l_{i,j},n})$, we can transform the non-convex rate constraint of (2.18) into a convex function of $Q_{l,n}$ and $r_{l,n}$ [30]. The derivation of the convex rate constraint from (2.18) for an AWGN channel is formulated as follows,

$$e^{r_{l_{i,j},n}} \leq \frac{G_{i,j} e^{Q_{l_{i,j},n}}}{\sum_{i' \neq i, l_{i',j'} \in \mathcal{L}_n} G_{i',j} e^{Q_{l_{i',j',n}}} + N_0}, \tag{2.20}$$

$$\Longrightarrow \quad \frac{e^{r_{l_{i,j},n} - Q_{l_{i,j},n}}}{G_{i,j}} \leq \frac{1}{\sum_{i' \neq i, l_{i',j'} \in \mathcal{L}_n} G_{i',j} e^{Q_{l_{i',j',n}}} + N_0}, \tag{2.21}$$

$$\Longrightarrow \quad \left(\frac{\sum_{i' \neq i, l_{i',j'} \in \mathcal{L}_n} G_{i',j} e^{Q_{l_{i',j',n}}} + N_0}{G_{i,j}} \right) \cdot e^{r_{l_{i,j},n} - Q_{l_{i,j},n}} \leq 1, \tag{2.22}$$

$$\Longrightarrow \quad \left(\frac{N_0}{G_{i,j}} e^{r_{l_{i,j},n} - Q_{l_{i,j},n}} + \sum_{i' \neq i, l_{i',j'} \in \mathcal{L}_n} \frac{G_{i',j}}{G_{i,j}} e^{r_{l_{i,j},n} + Q_{l_{i',j',n}} - Q_{l_{i,j},n}} \right) - 1 \leq 0, \tag{2.23}$$

$$\Longrightarrow \quad \log \left(\frac{N_0}{G_{i,j}} e^{r_{l_{i,j},n} - Q_{l_{i,j},n}} + \sum_{i' \neq i, l_{i',j'} \in \mathcal{L}_n} \frac{G_{i',j}}{G_{i,j}} e^{r_{l_{i,j},n} + Q_{l_{i',j',n}} - Q_{l_{i,j},n}} \right) \leq 0. \tag{2.24}$$

By contrast, for a Rayleigh block fading scenario, the convex rate constraint can be derived as follows:

$$e^{r_{l_{i,j},n}} \leq \frac{H_{i,j}G_{i,j}e^{Q_{l_{i,j},n}}}{\sum_{i'\neq i, l_{i',j'}\in\mathcal{L}_n} H_{i',j}G_{i',j}e^{Q_{l_{i',j'},n}} + N_0}, \tag{2.25}$$

$$\Longrightarrow \quad \frac{e^{r_{l_{i,j},n}-Q_{l_{i,j},n}}}{H_{i,j}G_{i,j}} \leq \frac{1}{\sum_{i'\neq i, l_{i',j'}\in\mathcal{L}_n} H_{i',j}G_{i',j}e^{Q_{l_{i',j'},n}} + N_0}, \tag{2.26}$$

$$\Longrightarrow \quad \left(\frac{\sum_{i'\neq i, l_{i',j'}\in\mathcal{L}_n} H_{i',j}G_{i',j}e^{Q_{l_{i',j'},n}} + N_0}{H_{i,j}G_{i,j}}\right)\cdot e^{r_{l_{i,j},n}-Q_{l_{i,j},n}} \leq 1, \tag{2.27}$$

$$\Longrightarrow \quad \left(\frac{N_0}{H_{i,j}G_{i,j}}e^{r_{l_{i,j},n}-Q_{l_{i,j},n}} + \sum_{i'\neq i, l_{i',j'}\in\mathcal{L}_n}\frac{H_{i',j}G_{i',j}}{H_{i,j}G_{i,j}}e^{r_{l_{i,j},n}+Q_{l_{i',j'},n}-Q_{l_{i,j},n}}\right) - 1 \leq 0, \tag{2.28}$$

$$\Longrightarrow \quad \log\left(\frac{N_0}{H_{i,j}G_{i,j}}e^{r_{l_{i,j},n}-Q_{l_{i,j},n}} + \sum_{i'\neq i, l_{i',j'}\in\mathcal{L}_n}\frac{H_{i',j}G_{i',j}}{H_{i,j}G_{i,j}}e^{r_{l_{i,j},n}+Q_{l_{i',j'},n}-Q_{l_{i,j},n}}\right) \leq 0. \tag{2.29}$$

2.3.5 Convexity of the Problem

Therefore, the second, third and fourth steps of Fig. 2.4 jointly transform the nonconvex optimization problem into a convex one in the fifth step of Fig. 2.4, where (2.24) can be used in the optimization problem[3] formulation given by (2.30)–(2.36), since it constitutes a strictly convex constraint. We can therefore formulate the NL maximization problem in its convex form for an AWGN channel as follows,

$$\text{min.} \quad z \tag{2.30}$$

$$\text{s.t.} \quad \mathbf{A}(\mathbf{r}_1 + \mathbf{r}_2 + ... + \mathbf{r}_N) = \mathbf{s}\cdot N, \tag{2.31}$$

$$\log\left(\frac{N_0}{G_{i,j}}e^{r_{l_{i,j},n}-Q_{l_{i,j},n}} + \sum_{i'\neq i, l_{i',j'}\in\mathcal{L}_n}\frac{G_{i',j}}{G_{i,j}}e^{r_{l_{i,j},n}+Q_{l_{i',j'},n}-Q_{l_{i,j},n}}\right) \leq 0, \forall n, l, l\in\mathcal{L}_n, \tag{2.32}$$

$$\sum_{n=1}^{N}\left(\sum_{l\in\mathcal{O}(i)\cap\mathcal{L}_n}\left((1+\alpha)\cdot e^{Q_{l_{i,j},n}} + P_{ct}\right) + \sum_{l\in\mathcal{I}(i)\cap\mathcal{L}_n} P_{cr}\right) \leq z\cdot\mathcal{E}_i\cdot N, \ \forall i, \tag{2.33}$$

$$Q_{l_{i,j},n} \leq \log\Big((P_i)_{max}\Big), \ l\in\mathcal{L}_n, \tag{2.34}$$

$$\mathbf{r}_n \geq 0, \forall n, \tag{2.35}$$

$$r_{l_{i,j},n} = 0, \ \forall l \notin \mathcal{L}_n. \tag{2.36}$$

[3]In this chapter we use natural logarithm instead of base 2 logarithm, because it ascertains that the rate constraint function in (2.24) can be readily transformed into the form of a convex function of $f(x) = \log\left(\sum_j^k c_j e^{x_j}\right)$. Then the rate constraint expressed in (2.24) is said to be convex in the variables $Q_{l,n}$ and $r_{l,n}$, with the aid of the vector composition rule, since it is a nondecreasing function of each argument of x_j [129]. Explicitly, using natural logarithm does not affect the optimal solution.

The corresponding convex problem formulation for a Rayleigh block fading channel becomes:

$$\text{min.} \quad z \tag{2.37}$$

$$\text{s.t.} \quad \mathbf{A}(\mathbf{r}_1 + \mathbf{r}_2 + ... + \mathbf{r}_N) = \mathbf{s} \cdot N, \tag{2.38}$$

$$\log\left(\frac{N_0}{H_{i,j}G_{i,j}} e^{r_{l_{i,j},n} - Q_{l_{i,j},n}} + \sum_{i' \neq i, l_{i',j'} \in \mathcal{L}_n} \frac{H_{i',j}G_{i',j}}{H_{i,j}G_{i,j}} e^{r_{l_{i,j},n} + Q_{l_{i',j'},n} - Q_{l_{i,j},n}}\right) \leq 0, \forall n, l,$$

$$l \in \mathcal{L}_n, \tag{2.39}$$

$$\sum_{n=1}^{N} \left(\sum_{l \in \mathcal{O}(i) \cap \mathcal{L}_n} \left((1+\alpha) \cdot e^{Q_{l_{i,j},n}} + P_{ct} \right) + \sum_{l \in \mathcal{I}(i) \cap \mathcal{L}_n} P_{cr} \right) \leq z \cdot \mathcal{E}_i \cdot N, \ \forall i, \tag{2.40}$$

$$Q_{l_{i,j},n} \leq \log\Big((P_i)_{max}\Big), \ l \in \mathcal{L}_n, \tag{2.41}$$

$$\mathbf{r}_n \geq 0, \forall n, \tag{2.42}$$

$$r_{l_{i,j},n} = 0, \ \forall l \notin \mathcal{L}_n, \tag{2.43}$$

where we only modify the rate constraint in (2.32) by taking into account the effect of the fading gain from (2.7) provided in (2.29) so that (2.39) is derived. The links that are active in TS n are denoted by the set $\mathcal{L}_n$, while $\mathbf{s} = \begin{bmatrix} s_1, 0, \cdots, 0, -s_1 \end{bmatrix}^T$ is the source rate vector, where the first and last elements are nonzero, but the remaining elements are set to zero, because the first node is the SN and the last node is the DN, while the other nodes act as relay nodes. The variables of the optimization problem are z, $Q_{l,n}$ and $r_{l,n}$ for $l \in \mathcal{L}_n$, $n = 1, \cdots, N$. The vector of rate variables associated with TS n is given by $\mathbf{r}_n = \begin{bmatrix} r_{l_{1,2},n}, r_{l_{2,3},n}, \cdots, r_{l_{V-1,V},n} \end{bmatrix}^T$. Furthermore, we denote the power amplifier's efficiency by $(1-\alpha)$ [190]. The objective function and the constraints of the optimization problem for an AWGN are as follows.

1. **Objective function - minimization of the reciprocal of the NL:** In (2.30), we minimize z so that the NL is maximized. We can rewrite (2.33) as $\sum_{n=1}^{N} \left(\sum_{l \in \mathcal{O}(i) \cap \mathcal{L}_n} \left((1+\alpha) \cdot e^{Q_{l_{i,j},n}} + P_{ct} \right) + \sum_{l \in \mathcal{I}(i) \cap \mathcal{L}_n} P_{cr} \right) \leq \frac{1}{T_{net}} \cdot \mathcal{E}_i \cdot N$ and we can multiply the left hand side of the inequality by T_{net}, but the multiplication of the two optimization variables is in general non-convex. Therefore, we use a change of variable and minimize $z = \frac{1}{T_{net}}$, which keeps the right hand side of the inequality linear and left hand side convex.
2. **Flow-conservation constraint:** Equation (2.31), using matrix $\mathbf{A}$ with entries given by (2.1) ensures flow-conservation, which physically implies that the information generated at the SN has to arrive at the DN.
3. **Transmission rate constraint:** We have to satisfy the rate constraint of our interference limited scenario for each link of the same TS in (2.32).
4. **Energy-conservation constraint:** Each sensor node can dissipate at most the initial

amount of battery energy, which we set to 5000J. Therefore, the energy conservation constraint is given in (2.33) for each node.

5. **Transmit power constraint:** (2.34) represents the transmission power at a node, which has to be less than the maximum affordable transmit power of that node.
6. **No transmission:** Finally, the transmission rate of nodes that are not scheduled for transmission is set to zero in (2.36).

The constraints described above also apply to the fading scenario characterized in (2.37)–(2.43). The optimization problem is solved for the sake of finding the optimal scheme for transmission over each link for a given link schedule, which is defined by the SPTS method discussed in Section 2.2.2.

2.3.5.1 Convexity Analysis

Let us now consider the convexity of our optimization problem provided in (2.30)–(2.36). Given the optimization variables z, $Q_{l,n}$ and $r_{l,n}$, we should check if the minimization problem is convex with respect to the optimization variables. The convexity conditions for a convex optimization problem are described in Section 1.1.2, which are composed of a convex objective function, convex inequality constraint functions and affine equality constraint functions. Therefore, we have to verify, whether the objective function $f_{obj}(x) = z$ is convex in (2.30). The reciprocal of the NL $f_{obj}(x) = z$ is a linear function with respect to the optimization variable z. Therefore, we can say that the objective function $f_{obj}(x) = z$ is a linear function of z, which is a special case of the convexity. We can also clearly see that the equality constraint of (2.31) is affine, since subtracting a constant $(\mathbf{s} \cdot N)$ from a linear function of the form $(\mathbf{r}_1 + \mathbf{r}_2 + ... + \mathbf{r}_N)$ results in an affine function [129]. Since the rate constraint function of (2.32) can be readily transformed into the convex function form of $f(x) = \log\left(\sum_j^k c_j e^{x_j}\right)$, the rate constraint of (2.32) is said to be convex in the variables $Q_{l,n}$ and $r_{l,n}$, with the aid of the vector composition rule, since it is a nondecreasing function of each argument of x_j [129]. The terms $(r_{l_{i,j},n} - Q_{l_{i,j},n})$ and $(r_{l_{i,j},n} + Q_{l_{i',j'},n} - Q_{l_{i,j},n})$ correspond to x_j in our problem formulation, which is linear and thus convex. The terms $\frac{N_0}{G_{i,j}}$ and $\frac{G_{i',j}}{G_{i,j}}$ also correspond to c_j, which are always higher than zero. Hence, the rate constraint in (2.32) satisfies the convexity conditions described in Section 1.1.2 for the variables $Q_{l,n}$ and $r_{l,n}$. In fact, (2.32) is strictly convex. As for the energy inequality constraint function of (2.33), we partition the formulation into smaller parts in order to check its convexity. We can readily say that e^x is convex in all $\mathbb{R}$ [129], which confirms the convexity of $e^{Q_{l,n}}$ in $Q_{l,n}$. Multiplication of a convex function with a positive constant, as exemplified by $(1+\alpha) \cdot e^{Q_{l,n}}$ is also convex [129]. Summation of a convex function with a constant, as given by $\left[(1+\alpha) \cdot e^{Q_{l,n}} + P_{ct}\right]$ is also convex. Finally, the summation of convex functions was also shown to be convex in [129], which confirms the convexity of $\sum_{l \in \mathcal{O}(i) \cap \mathcal{L}_n} \left[(1+\alpha) \cdot e^{Q_{l,n}} + P_{ct}\right]$. The terms $z \cdot \mathcal{E}_i \cdot N$ are linear and subtracting a linear function from a convex function preserves the convexity.

The entire summation in (2.33) satisfies the convexity conditions. Similarly, (2.35) is affine. Consequently, our optimization problem formulation preserves the convexity conditions for a general convex optimization problem. In fact, (2.30)–(2.36) define a strictly convex optimization problem that has a unique solution. Note that the same convexity analysis applies to the scenario of a Rayleigh block fading channel in (2.37)–(2.43). The reader is referred to Section 1.1.2 for further details on the operations that preserve convexity.

2.3.6 Convert the Logarithmic Form to Non-Logarithmic Form

The rate constraint (2.32) of the optimization problem is modified in order to derive transmit rate related expressions after determining its first derivative, which is required for the KKT optimality conditions in the following sections for deriving the analytical expressions of the globally optimal transmission rates and powers. Otherwise, the first derivative of the expression $\log\left(\frac{N_0}{G_{i,j}}e^{r_{l_{i,j},n}-Q_{l_{i,j},n}}+\sum_{i'\neq i,l_{i',j'}\in\mathcal{L}_n}\frac{G_{i',j}}{G_{i,j}}e^{r_{l_{i,j},n}+Q_{l_{i',j'},n}-Q_{l_{i,j},n}}\right)$ fails to provide further insights about the transmit rate, since its first derivative with respect to $r_{l_{i,j},n}$ is equal to 1. Therefore, in sixth step of Fig. 2.4, (2.32) is relaxed to a non-logarithmic form as follows,

$$\log\left(\frac{N_0}{G_{i,j}}e^{r_{l_{i,j},n}-Q_{l_{i,j},n}}+\sum_{i'\neq i,l_{i',j'}\in\mathcal{L}_n}\frac{G_{i',j}}{G_{i,j}}e^{r_{l_{i,j},n}+Q_{l_{i',j'},n}-Q_{l_{i,j},n}}\right)\leq 0, \quad (2.44)$$

$$\text{becomes}\quad 0<\left(\frac{N_0}{G_{i,j}}e^{r_{l_{i,j},n}-Q_{l_{i,j},n}}+\sum_{i'\neq i,l_{i',j'}\in\mathcal{L}_n}\frac{G_{i',j}}{G_{i,j}}e^{r_{l_{i,j},n}+Q_{l_{i',j'},n}-Q_{l_{i,j},n}}\right)\leq 1. \quad (2.45)$$

We know that $\left(\frac{N_0}{G_{i,j}}e^{r_{l_{i,j},n}-Q_{l_{i,j},n}}+\sum_{i'\neq i,l_{i',j'}\in\mathcal{L}_n}\frac{G_{i',j}}{G_{i,j}}e^{r_{l_{i,j},n}+Q_{l_{i',j'},n}-Q_{l_{i,j},n}}\right)$ is always higher than zero in (2.45), since the product of $\frac{N_0}{G_{i,j}}$ and the exponential function is always positive. Therefore, the left hand inequality $(0<\cdots)$ of (2.45) is trivially satisfied. Hence, we can concentrate on the right hand side inequality $(\cdots\leq 1)$ of (2.45), where the first derivative of (2.45) provides us with further insights considering the transmit rate. Having derived the non-logarithmic rate constraint of (2.45), we may now generalize the optimization problem formulation for the AWGN channel before converting it into its Lagrangian form as follows,

$$\text{min.} \quad z \quad (2.46)$$

$$\text{s.t.} \quad \mathbf{A}(\mathbf{r}_1+\mathbf{r}_2+\ldots+\mathbf{r}_N)=\mathbf{s}\cdot N, \quad (2.47)$$

$$\left(\frac{N_0}{G_{i,j}}e^{r_{l_{i,j},n}-Q_{l_{i,j},n}}+\sum_{i'\neq i,l_{i',j'}\in\mathcal{L}_n}\frac{G_{i',j}}{G_{i,j}}e^{r_{l_{i,j},n}+Q_{l_{i',j'},n}-Q_{l_{i,j},n}}\right)-1\leq 0, \forall n,l,l\in\mathcal{L}_n, \quad (2.48)$$

$$\sum_{n=1}^{N}\left(\sum_{l\in\mathcal{O}(i)\cap\mathcal{L}_n}\left((1+\alpha)\cdot e^{Q_{l_{i,j},n}}+P_{ct}\right)+\sum_{l\in\mathcal{I}(i)\cap\mathcal{L}_n}P_{cr}\right)\leq z\cdot\mathcal{E}_i\cdot N,\ \forall i, \quad (2.49)$$

$$Q_{l_{i,j},n} \leq \log\Big((P_i)_{max}\Big),\ l \in \mathcal{L}_n, \tag{2.50}$$

$$\mathbf{r}_n \geq 0, \forall n, \tag{2.51}$$

$$r_{l_{i,j},n} = 0,\ \forall l \notin \mathcal{L}_n. \tag{2.52}$$

Similarly, the optimization problem can also be generalized for our Rayleigh-distributed block-fading scenario by carrying out the modifications previously invoked for generating (2.48) from (2.37)–(2.43).

To solve the optimization problem formulated in (2.46)–(2.52), we transformed it to its Lagrangian form and then the KKT optimality conditions [129] are employed for deriving the globally optimal analytical expressions that can provide closed-form equations. Let us first familiarize ourselves with the Lagrangian function and the KKT optimality conditions.

The classic Lagrange multipliers based technique may be invoked for solving optimization problems subject to one or more equality constraints. If the constraints are constituted by a combination of both equality and inequality constraints, then the Lagrange multipliers method has to be extended to the KKT optimality conditions [129], which are the first order necessary conditions for a solution to be optimal. Above, we first described how and why a modification is applied to the optimization problem defined in (2.30)–(2.36) for an AWGN scenario and then this modification was also invoked for our Rayleigh fading scenario of (2.37)–(2.43). Therefore, above we modified the rate constraint of (2.32) in the AWGN scenario for the sake of a clear understanding of the rate variable. Moreover, we convert the modified equivalent optimization problem into its Lagrange form as a weighted combination of the objective function and of the constraint functions with the aid of the Lagrange multipliers in Section 2.3.7 and employ the KKT optimality conditions to derive analytical expressions of the globally optimal transmission scheme for the string topology of Fig. 2.1. In fact, the main reason for using the Lagrange relaxation and the KKT optimality conditions is because the intricate relationship of the optimization variables and of their dependencies can be readily observed, where we can characterize the system model with the aid of the closed-form equations obtained from Lagrange relaxation and KKT analysis. Another important reason is that the relaxed problem is generally easy to solve compared to the original problem, which is the case in our scenario. For example, using the KKT optimality conditions we have to evaluate on the order of $\mathcal{O}(2V + 4NL + 1)$ expressions for updating the primal and dual variables. In a few special cases, the optimization problems can even be readily solved with the aid of numerical analysis. However, an algorithm like the interior point method [129, 191] solves our optimization problem using at least on the order of $\mathcal{O}(2V + 4NL)^2$ operations. More explicitly, in the interior point algorithm at least $\mathcal{O}(2V + 4NL)^2$ operations are required to solve $(2V + 4NL)$ linear equations, which leads to a higher complexity. Considering the scenario of a Rayleigh block fading channel, using the interior point method further increases the complexity, since the NL has to be computed and averaged over several thousand trials, and therefore we opt for using the Lagrange

multipliers method and the KKT optimality approach.

2.3.7 Lagrangian Constrained Optimization

Let us now turn our attention to the seventh step of Fig. 2.4 considering the Lagrangian formulation of our constrained optimization problem described in (2.46)–(2.52) for the AWGN channel scenario. Note that from now on we will only provide the related formulations for the AWGN channel scenario, which can also be readily extended to the Rayleigh-distributed block-fading scenario using the fading gain matrices of (2.39). The optimal solution of a constrained optimization problem described in (2.46)–(2.52) may often be found by using the so-called Lagrangian method. Let us first define the sets of the optimization variables and of the Lagrangian multipliers as,

$$\boldsymbol{R} = \left\{ r_{l_{1,2},1}, ..., r_{l_{V-1,V},N} \right\}, \tag{2.53}$$

$$\boldsymbol{Q} = \left\{ Q_{l_{1,2},1}, ..., Q_{l_{V-1,V},N} \right\}, \tag{2.54}$$

$$\boldsymbol{\Omega} = \left\{ \omega_1, ..., \omega_{V-1} \right\}, \tag{2.55}$$

$$\boldsymbol{\Psi} = \left\{ \psi_{l_{1,2},1}, ..., \psi_{l_{V-1,V},N} \right\}, \tag{2.56}$$

$$\boldsymbol{\vartheta} = \left\{ \vartheta_{l_{1,2},1}, ..., \vartheta_{l_{V-1,V},N} \right\}, \tag{2.57}$$

$$\boldsymbol{\mu} = \left\{ \mu_1, ..., \mu_V \right\}. \tag{2.58}$$

Adopting the Lagrangian duality technique [129] described in Section 1.1.2, we can rewrite the optimization problem provided in (2.46)–(2.52) as a Lagrangian dual function by augmenting the objective function with a weighted sum of the constraint functions. Note that according to our assumptions the transmitter and the receiver circuits do not dissipate energy, hence we remove these parameters from the Lagrangian form. Thus, the Lagrangian of (2.46)–(2.52) is simplified to:

$$\mathcal{L}(z, \boldsymbol{R}, \boldsymbol{Q}, \boldsymbol{\Omega}, \boldsymbol{\Psi}, \boldsymbol{\vartheta}, \boldsymbol{\mu}) = z + \sum_{i=1}^{V-1} \omega_i \cdot \left[\sum_{n=1}^{N} \left(\sum_{l \in \mathcal{O}(i) \cap \mathcal{L}_n} \left((1+\alpha) \cdot e^{Q_{l_{i,j},n}} \right) \right) - z \cdot \mathcal{E}_i \cdot N \right]$$

$$+ \sum_{n=1}^{N} \sum_{l \in \mathcal{L}_n} \psi_{l_{i,j},n} \cdot \left[\left(\frac{N_0}{G_{i,j}} e^{r_{l_{i,j},n} - Q_{l_{i,j},n}} + \sum_{l_{i',j'} \in \mathcal{L}_n, i' \neq i} \frac{G_{i',j}}{G_{i,j}} e^{r_{l_{i,j},n} + Q_{l_{i',j'},n} - Q_{l_{i,j},n}} \right) - 1 \right]$$

$$+\sum_{n=1}^{N}\sum_{l\in\mathcal{L}_n}\vartheta_{l_{i,j},n}\cdot\left[Q_{l_{i,j},n}-\log\Big((P_i)_{max}\Big)\right]+\sum_{i=1}^{V}\mu_i\cdot\left[\sum_{l\in\mathcal{I}(i)}\left(\sum_{n=1}^{N}r_{l_{i,j},n}\right)\right.$$
$$\left.-\sum_{l\in\mathcal{O}(i)}\left(\sum_{n=1}^{N}r_{l_{i,j},n}\right)\right], \tag{2.59}$$

where z is the objective function, ω_i is the energy multiplier, $\psi_{l_{i,j},n}$ is the transmit rate multiplier, $\vartheta_{l_{i,j},n}$ is the transmit power multiplier and μ_i is the flow rate multiplier, which are the Lagrange multipliers associated with the inequality constraints of (2.49), (2.48), (2.50) and with the equality constraint of (2.47), respectively. Note that the constraints (2.51) and (2.52) are taken into account, when deriving the optimal primal variables. For the energy constraint ω_i, the DN (ω_V) is not taken into account, since we assume that the sink is plugged into mains power source and thus it is capable of receiving data all the time.

2.3.8 Applying the KKT Optimality Conditions

We employ the KKT optimality conditions for (2.59) in the eighth step of Fig. 2.4, which are given by

$$\frac{\partial\mathcal{L}}{\partial z} = 1-\sum_{i=1}^{V}\omega_i\Big(\mathcal{E}_i\cdot N\Big)=0, \tag{2.60}$$

$$\frac{\partial\mathcal{L}}{\partial r_{l_{i,j},n}} = \mu_{\mathcal{I}^{-1}(l)}-\mu_{\mathcal{O}^{-1}(l)}$$
$$+\psi_{l_{i,j},n}\left(\frac{N_0}{G_{i,j}}e^{r_{l_{i,j},n}-Q_{l_{i,j},n}}+\sum_{l_{i',j'}\in\mathcal{L}_n,i'\neq i}\frac{G_{i',j}}{G_{i,j}}e^{r_{l_{i,j},n}+Q_{l_{i',j'},n}-Q_{l_{i,j},n}}\right)=0,\forall l,n, \tag{2.61}$$

$$\frac{\partial\mathcal{L}}{\partial Q_{l_{i,j},n}} = \omega_{\mathcal{O}^{-1}(l)}\Big((1+\alpha)e^{Q_{l_{i,j},n}}\Big)+\vartheta_{l_{i,j},n}$$
$$-\psi_{l_{i,j},n}\left(\frac{N_0}{G_{i,j}}e^{r_{l_{i,j},n}-Q_{l_{i,j},n}}+\sum_{l_{i',j'}\in\mathcal{L}_n,i'\neq i}\frac{G_{i',j}}{G_{i,j}}e^{r_{l_{i,j},n}+Q_{l_{i',j'},n}-Q_{l_{i,j},n}}\right)=0,\forall l,n, \tag{2.62}$$

$$0 = \sum_{i=1}^{V-1}\omega_i\left[\sum_{n=1}^{N}\left(\sum_{l\in\mathcal{O}(i)\cap\mathcal{L}_n}\Big((1+\alpha)e^{Q_{l_{i,j},n}}\Big)\right)-z\cdot\mathcal{E}_i\cdot N\right], \tag{2.63}$$

$$0 = \psi_{l_{i,j},n}\left[\left(\frac{N_0}{G_{i,j}}e^{r_{l_{i,j},n}-Q_{l_{i,j},n}}+\sum_{l_{i',j'}\in\mathcal{L}_n,i'\neq i}\frac{G_{i',j}}{G_{i,j}}e^{r_{l_{i,j},n}+Q_{l_{i',j'},n}-Q_{l_{i,j},n}}\right)-1\right],\forall l,n, \tag{2.64}$$

$$0 = \vartheta_{l_{i,j},n}\left[Q_{l_{i,j},n}-\log\Big((P_i)_{max}\Big)\right],\forall l,n, \tag{2.65}$$

$$\omega_i \geq 0,\ \psi_{l_{i,j},n} \geq 0,\ \vartheta_{l_{i,j},n} \geq 0, \tag{2.66}$$

where $\mathcal{I}^{-1}(l)$ denotes the specific node associated with the incoming link l, while $\mathcal{O}^{-1}(l)$ represents the particular node associated with the outgoing link l. Since the primal problem [129] is convex, if z, $\boldsymbol{R}$, $\boldsymbol{Q}$, $\boldsymbol{\Omega}$, $\boldsymbol{\Psi}$, $\boldsymbol{\vartheta}$, $\boldsymbol{\mu}$ represent arbitrary points that satisfy the KKT optimality conditions given by the primal feasibility [129] in (2.47)–(2.50), the dual feasibility [129] of (2.66), the complementary slackness [129] in (2.63)–(2.65) and the first order optimality [129] in (2.60)–(2.62), then z, $\boldsymbol{R}$, $\boldsymbol{Q}$ are primal optimal and $\boldsymbol{\Omega}$, $\boldsymbol{\Psi}$, $\boldsymbol{\vartheta}$, $\boldsymbol{\mu}$ are dual optimal with a zero duality gap [129]. We note that the optimal solution of the primal (original) problem is expressed as the primal optimal, while the dual problem provides us with the dual optimal solution, which is a lower bound to the optimal value of the original optimization problem. Since the primal problem is a minimization problem, its dual problem has to be a maximization problem, where the search direction of the solution space is just the opposite of that of the primal problem. Let us imagine that the optimal solution lies on a vertical line. Then, the primal problem searches for the optimal solution from top to the bottom, whereas the dual problem searches from the bottom to the top. Additionally, the duality gap [129] is defined as the difference between the optimal primal and optimal dual solutions. If the duality gap is zero, then the primal and the dual optimal solutions are equal and strong duality holds. The reader is referred to Section 1.1.2 of Chapter 1 for more details.

2.3.8.1 KKT Analytical Expressions

Let us now employ the KKT optimality conditions for deriving analytical expressions of the globally optimal transmission rates and powers for the string topology considered in Fig. 2.1. As an example, we derive the KKT analytical expressions for $T = 3$ SPTS parameters. From (2.60), we can readily obtain the NL derivatives for the $T = 3$ link schedule. However, as indicated in

$$\text{1-}\mathcal{E}\cdot\text{N}(\omega_1+\omega_2+\omega_3+\omega_4+\omega_5+\omega_6+\omega_7+\omega_8+\omega_9) = 0, \tag{2.67}$$

the energy constraint does not depend on the link scheduling, it rather relies on the number of sensor nodes and on the initial battery capacity of each node. Equation (2.61) represents the first-order derivative of the transmission rate, which is computed for each TS and for each link scheduled according to the $T = 3$ SPTS as follows,

$$\psi_{l_{1,2},1}\left(\frac{N_0}{G_{1,2}}e^{r_{l_{1,2},1}-Q_{l_{1,2},1}}+\frac{G_{4,2}}{G_{1,2}}e^{r_{l_{1,2},1}+Q_{l_{4,5},1}-Q_{l_{1,2},1}}+\frac{G_{7,2}}{G_{1,2}}e^{r_{l_{1,2},1}+Q_{l_{7,8},1}-Q_{l_{1,2},1}}\right) - \mu_1+\mu_2 = 0, \tag{2.68}$$

$$\psi_{l_{4,5},1}\left(\frac{N_0}{G_{4,5}}e^{r_{l_{4,5},1}-Q_{l_{4,5},1}}+\frac{G_{1,5}}{G_{4,5}}e^{r_{l_{4,5},1}+Q_{l_{1,2},1}-Q_{l_{4,5},1}}+\frac{G_{7,5}}{G_{4,5}}e^{r_{l_{4,5},1}+Q_{l_{7,8},1}-Q_{l_{4,5},1}}\right)$$
$$-\mu_4+\mu_5=0, \quad (2.69)$$

$$\psi_{l_{7,8},1}\left(\frac{N_0}{G_{7,8}}e^{r_{l_{7,8},1}-Q_{l_{7,8},1}}+\frac{G_{1,8}}{G_{7,8}}e^{r_{l_{7,8},1}+Q_{l_{1,2},1}-Q_{l_{7,8},1}}+\frac{G_{4,8}}{G_{7,8}}e^{r_{l_{7,8},1}+Q_{l_{4,5},1}-Q_{l_{7,8},1}}\right)$$
$$-\mu_7+\mu_8=0, \quad (2.70)$$

$$\vdots \qquad \vdots \qquad \vdots$$

$$\psi_{l_{3,4},18}\left(\frac{N_0}{G_{3,4}}e^{r_{l_{3,4},18}-Q_{l_{3,4},18}}+\frac{G_{6,4}}{G_{3,4}}e^{r_{l_{3,4},18}+Q_{l_{6,7},18}-Q_{l_{3,4},18}}\right.$$
$$\left.+\frac{G_{9,4}}{G_{3,4}}e^{r_{l_{3,4},18}+Q_{l_{9,10},18}-Q_{l_{3,4},18}}\right)-\mu_3+\mu_4=0, \quad (2.71)$$

$$\psi_{l_{6,7},18}\left(\frac{N_0}{G_{6,7}}e^{r_{l_{6,7},18}-Q_{l_{6,7},18}}+\frac{G_{3,7}}{G_{6,7}}e^{r_{l_{6,7},18}+Q_{l_{3,4},18}-Q_{l_{6,7},18}}\right.$$
$$\left.+\frac{G_{9,7}}{G_{6,7}}e^{r_{l_{6,7},18}+Q_{l_{9,10},18}-Q_{l_{6,7},18}}\right)-\mu_6+\mu_7=0, \quad (2.72)$$

$$\psi_{l_{9,10},18}\left(\frac{N_0}{G_{9,10}}e^{r_{l_{9,10},18}-Q_{l_{9,10},18}}+\frac{G_{3,10}}{G_{9,10}}e^{r_{l_{9,10},18}+Q_{l_{3,4},18}-Q_{l_{9,10},18}}\right.$$
$$\left.+\frac{G_{6,10}}{G_{9,10}}e^{r_{l_{9,10},18}+Q_{l_{6,7},18}-Q_{l_{9,10},18}}\right)-\mu_9+\mu_{10}=0. \quad (2.73)$$

Moreover, Equation (2.62) represents the analytical expressions of the transmit power for each TS and for each link scheduled according to the $T=3$ SPTS as follows,

$$\omega_1\left((1+\alpha)e^{Q_{l_{1,2},1}}\right)+\psi_{l_{4,5},1}\left(\frac{G_{1,5}}{G_{4,5}}e^{r_{l_{4,5},1}+Q_{l_{1,2},1}-Q_{l_{4,5},1}}\right)$$
$$+\psi_{l_{7,8},1}\left(\frac{G_{1,8}}{G_{7,8}}e^{r_{l_{7,8},1}+Q_{l_{1,2},1}-Q_{l_{7,8},1}}\right)-\psi_{l_{1,2},1}\left(\frac{N_0}{G_{1,2}}e^{r_{l_{1,2},1}-Q_{l_{1,2},1}}\right.$$
$$\left.+\frac{G_{4,2}}{G_{1,2}}e^{r_{l_{1,2},1}+Q_{l_{4,5},1}-Q_{l_{1,2},1}}+\frac{G_{7,2}}{G_{1,2}}e^{r_{l_{1,2},1}+Q_{l_{7,8},1}-Q_{l_{1,2},1}}\right)+\vartheta_{l_{1,2},1}=0, \quad (2.74)$$

$$\omega_4\left((1+\alpha)e^{Q_{l_{4,5},1}}\right)+\psi_{l_{1,2},1}\left(\frac{G_{4,2}}{G_{1,2}}e^{r_{l_{1,2},1}+Q_{l_{4,5},1}-Q_{l_{1,2},1}}\right)$$
$$+\psi_{l_{7,8},1}\left(\frac{G_{4,8}}{G_{7,8}}e^{r_{l_{7,8},1}+Q_{l_{4,5},1}-Q_{l_{7,8},1}}\right)-\psi_{l_{4,5},1}\left(\frac{N_0}{G_{4,5}}e^{r_{l_{4,5},1}-Q_{l_{4,5},1}}\right.$$
$$\left.+\frac{G_{1,5}}{G_{4,5}}e^{r_{l_{4,5},1}+Q_{l_{1,2},1}-Q_{l_{4,5},1}}+\frac{G_{7,5}}{G_{4,5}}e^{r_{l_{4,5},1}+Q_{l_{7,8},1}-Q_{l_{4,5},1}}\right)+\vartheta_{l_{4,5},1}=0, \quad (2.75)$$

$$\omega_7\left((1+\alpha)e^{Q_{l_{7,8},1}}\right)+\psi_{l_{1,2},1}\left(\frac{G_{7,2}}{G_{1,2}}e^{r_{l_{1,2},1}+Q_{l_{7,8},1}-Q_{l_{1,2},1}}\right)$$

$$+\psi_{l_{4,5},1}\left(\frac{G_{7,5}}{G_{4,5}}e^{r_{l_{4,5},1}+Q_{l_{7,8},1}-Q_{l_{4,5},1}}\right)-\psi_{l_{7,8},1}\left(\frac{N_0}{G_{7,8}}e^{r_{l_{7,8},1}-Q_{l_{7,8},1}}\right.$$
$$\left.+\frac{G_{1,8}}{G_{7,8}}e^{r_{l_{7,8},1}+Q_{l_{1,2},1}-Q_{l_{7,8},1}}+\frac{G_{4,8}}{G_{7,8}}e^{r_{l_{7,8},1}+Q_{l_{4,5},1}-Q_{l_{7,8},1}}\right)+\vartheta_{l_{7,8},1}=0, \quad (2.76)$$

$$\vdots \qquad \vdots \qquad \vdots$$

$$\omega_3\Big((1+\alpha)e^{Q_{l_{3,4},18}}\Big)+\psi_{l_{6,7},18}\left(\frac{G_{3,7}}{G_{6,7}}e^{r_{l_{6,7},18}+Q_{l_{3,4},18}-Q_{l_{6,7},18}}\right)$$
$$+\psi_{l_{9,10},18}\left(\frac{G_{3,10}}{G_{9,10}}e^{r_{l_{9,10},18}+Q_{l_{3,4},18}-Q_{l_{9,10},18}}\right)-\psi_{l_{3,4},18}\left(\frac{N_0}{G_{3,4}}e^{r_{l_{3,4},18}-Q_{l_{3,4},18}}\right.$$
$$\left.+\frac{G_{6,4}}{G_{3,4}}e^{r_{l_{3,4},18}+Q_{l_{6,7},18}-Q_{l_{3,4},18}}+\frac{G_{9,4}}{G_{3,4}}e^{r_{l_{3,4},18}+Q_{l_{9,10},18}-Q_{l_{3,4},18}}\right)$$
$$+\vartheta_{l_{3,4},18}=0, \quad (2.77)$$

$$\omega_6\Big((1+\alpha)e^{Q_{l_{6,7},18}}\Big)+\psi_{l_{3,4},18}\left(\frac{G_{6,4}}{G_{3,4}}e^{r_{l_{3,4},18}+Q_{l_{6,7},18}-Q_{l_{3,4},18}}\right)$$
$$+\psi_{l_{9,10},18}\left(\frac{G_{6,10}}{G_{9,10}}e^{r_{l_{9,10},18}+Q_{l_{6,7},18}-Q_{l_{9,10},18}}\right)-\psi_{l_{6,7},18}\left(\frac{N_0}{G_{6,7}}e^{r_{l_{6,7},18}-Q_{l_{6,7},18}}\right.$$
$$\left.+\frac{G_{3,7}}{G_{6,7}}e^{r_{l_{6,7},18}+Q_{l_{3,4},18}-Q_{l_{6,7},18}}+\frac{G_{9,7}}{G_{6,7}}e^{r_{l_{6,7},18}+Q_{l_{9,10},18}-Q_{l_{6,7},18}}\right)$$
$$+\vartheta_{l_{6,7},18}=0, \quad (2.78)$$

$$\omega_9\Big((1+\alpha)e^{Q_{l_{9,10},18}}\Big)+\psi_{l_{9,10},18}\left(\frac{G_{9,4}}{G_{3,4}}e^{r_{l_{3,4},18}+Q_{l_{9,10},18}-Q_{l_{3,4},18}}\right)$$
$$+\psi_{l_{6,7},18}\left(\frac{G_{9,7}}{G_{6,7}}e^{r_{l_{6,7},18}+Q_{l_{9,10},18}-Q_{l_{6,7},18}}\right)-\psi_{l_{9,10},18}\left(\frac{N_0}{G_{9,10}}e^{r_{l_{9,10},18}-Q_{l_{9,10},18}}\right.$$
$$\left.+\frac{G_{3,10}}{G_{9,10}}e^{r_{l_{9,10},18}+Q_{l_{3,4},18}-Q_{l_{9,10},18}}+\frac{G_{6,10}}{G_{9,10}}e^{r_{l_{9,10},18}+Q_{l_{6,7},18}-Q_{l_{9,10},18}}\right)$$
$$+\vartheta_{l_{9,10},18}=0. \quad (2.79)$$

The above analytical expressions obtained from the KKT analysis can be utilized for solving the optimization problem by deriving the globally optimal transmission rates and powers as well as the NL, as we will detail in Section 2.3.9.

2.3.9 Derive Closed-Form Equations for Transmission Rates and Powers

Ultimately, based on the eighth step of Fig. 2.4, given the analytical expressions of Section 2.3.8.1, we can now obtain closed-form expressions of both the transmit rate and of the transmission power variables in the ninth step of Fig. 2.4. Therefore, we use the first derivatives of the KKT optimality conditions for generalizing the globally optimal closed-form equations by exploiting the relationship between the transmission rate and the transmit

power. Explicitly, this relationship can clearly provide us with the optimal transmit rate and power values, given the initial points for the dual variables of $\boldsymbol{\Omega}$, $\boldsymbol{\Psi}$, $\boldsymbol{\vartheta}$, $\boldsymbol{\mu}$ in (2.88) and (2.86), so that the original optimization problem can be solved using the flowchart of Fig. 2.5. For instance, we show that the first analytical expressions of the transmit rate and the power derived for the SPTS parameter of $T = 3$ in (2.68) and (2.74) are utilized for generalizing the closed-form equations of the transmit rate and the power, respectively, as follows,

$$\begin{aligned} r_{l_{1,2},1} \quad \Rightarrow \quad & \psi_{l_{1,2},1}\left(\frac{N_0}{G_{1,2}}e^{r_{l_{1,2},1}-Q_{l_{1,2},1}} + \frac{G_{4,2}}{G_{1,2}}e^{r_{l_{1,2},1}+Q_{l_{4,5},1}-Q_{l_{1,2},1}}\right. \\ & \left. + \frac{G_{7,2}}{G_{1,2}}e^{r_{l_{1,2},1}+Q_{l_{7,8},1}-Q_{l_{1,2},1}}\right) - \mu_1 + \mu_2 = 0, \end{aligned} \tag{2.80}$$

$$\begin{aligned} \text{and } Q_{l_{1,2},1} \quad \Rightarrow \quad & \omega_1\Big((1+\alpha)e^{Q_{l_{1,2},1}}\Big) + \psi_{l_{4,5},1}\left(\frac{G_{1,5}}{G_{4,5}}e^{r_{l_{4,5},1}+Q_{l_{1,2},1}-Q_{l_{4,5},1}}\right) \\ & + \psi_{l_{7,8},1}\left(\frac{G_{1,8}}{G_{7,8}}e^{r_{l_{7,8},1}+Q_{l_{1,2},1}-Q_{l_{7,8},1}}\right) - \psi_{l_{1,2},1}\left(\frac{N_0}{G_{1,2}}e^{r_{l_{1,2},1}-Q_{l_{1,2},1}}\right. \\ & \left. + \frac{G_{4,2}}{G_{1,2}}e^{r_{l_{1,2},1}+Q_{l_{4,5},1}-Q_{l_{1,2},1}} + \frac{G_{7,2}}{G_{1,2}}e^{r_{l_{1,2},1}+Q_{l_{7,8},1}-Q_{l_{1,2},1}}\right) \\ & + \vartheta_{l_{1,2},1} = 0. \end{aligned} \tag{2.81}$$

We substitute (2.80) into (2.81), since the closed-form formula of the power variable, for example the first-order derivative of $Q_{l_{1,2},1}$, can readily be obtained. Hence, we proceed from (2.80) by replacing

$$\psi_{l_{1,2},1}\left(\frac{N_0}{G_{1,2}}e^{r_{l_{1,2},1}-Q_{l_{1,2},1}} + \frac{G_{4,2}}{G_{1,2}}e^{r_{l_{1,2},1}+Q_{l_{4,5},1}-Q_{l_{1,2},1}} + \frac{G_{7,2}}{G_{1,2}}e^{r_{l_{1,2},1}+Q_{l_{7,8},1}-Q_{l_{1,2},1}}\right) \tag{2.82}$$

with $(\mu_1 - \mu_2)$ and substituting it into the first derivative of $Q_{l_{1,2},1}$, it becomes equivalent to

$$\begin{aligned} & \omega_1\Big((1+\alpha)e^{Q_{l_{1,2},1}}\Big) + \psi_{l_{4,5},1}\left(\frac{G_{1,5}}{G_{4,5}}e^{r_{l_{4,5},1}+Q_{l_{1,2},1}-Q_{l_{4,5},1}}\right) \\ & + \psi_{l_{7,8},1}\left(\frac{G_{1,8}}{G_{7,8}}e^{r_{l_{7,8},1}+Q_{l_{1,2},1}-Q_{l_{7,8},1}}\right) = \mu_1 - \mu_2 - \vartheta_{l_{1,2},1}. \end{aligned} \tag{2.83}$$

By substituting (2.83) into the bracket of $e^{Q_{l_{1,2},1}}$, the following equation can be obtained,

$$e^{Q_{l_{1,2},1}}\left(\omega_1(1+\alpha) + \psi_{l_{4,5},1}\left(\frac{G_{1,5}}{G_{4,5}} \cdot e^{r_{l_{4,5},1}-Q_{l_{4,5},1}}\right) + \psi_{l_{7,8},1}\left(\frac{G_{1,8}}{G_{7,8}} \cdot e^{r_{l_{7,8},1}-Q_{l_{7,8},1}}\right)\right) \tag{2.84}$$

$$= \mu_1 - \mu_2 - \vartheta_{l_{1,2},1}. \tag{2.85}$$

Finally, we can derive the closed-form equation of $Q_{l_{1,2},1}$, which is the transmit power for the first link during the first TS as follows,

$$Q_{l_{1,2},1} = \log\left[\frac{\mu_1 - \mu_2 - \vartheta_{l_{1,2},1}}{\left(\omega_1(1+\alpha) + \psi_{l_{4,5},1}\left(\frac{G_{1,5}}{G_{4,5}} \cdot e^{r_{l_{4,5},1} - Q_{l_{4,5},1}}\right) + \psi_{l_{7,8},1}\left(\frac{G_{1,8}}{G_{7,8}} \cdot e^{r_{l_{7,8},1} - Q_{l_{7,8},1}}\right)\right)}\right]. \tag{2.86}$$

Similarly, rearranging (2.80) by using the bracket of $e^{r_{l_{1,2},1} - Q_{l_{1,2},1}}$, we can obtain the following first-order derivative of $r_{l_{1,2},1}$

$$\psi_{l_{1,2},1} \cdot e^{r_{l_{1,2},1} - Q_{l_{1,2},1}}\left(\frac{N_0}{G_{1,2}} + \frac{G_{4,2}}{G_{1,2}} \cdot e^{Q_{l_{4,5},1}} + \frac{G_{7,2}}{G_{1,2}} \cdot e^{Q_{l_{7,8},1}}\right) = \mu_1 - \mu_2. \tag{2.87}$$

A closed-form equation of $r_{l_{1,2},1}$, which is the transmit rate for the first link and the first TS becomes equivalent to the following,

$$r_{l_{1,2},1} = \log\left[\frac{\mu_1 - \mu_2}{\psi_{l_{1,2},1} \cdot \left(\frac{N_0}{G_{1,2}} + \frac{G_{4,2}}{G_{1,2}} \cdot e^{Q_{l_{4,5},1}} + \frac{G_{7,2}}{G_{1,2}} \cdot e^{Q_{l_{7,8},1}}\right)}\right] + Q_{l_{1,2},1}. \tag{2.88}$$

In (2.86) and (2.88), we obtained the instantaneous transmit rate and the transmit power equations for the first link activated during the first TS. We can generalize these equations for our system model in order to find the optimal values of $\boldsymbol{Q}$ and $\boldsymbol{R}$ in iteration $(t+1)$ as follows,

$$Q^{t+1}_{l_{i,j},n} = \log\left[\left(\mu^t_i - \mu^t_j - \vartheta^t_{l_{i,j},n}\right) \cdot \left(\omega^t_i(1+\alpha) + \sum_{l_{i',j'} \in \mathcal{L}_n, l_{i',j'} \neq l_{i,j}, i' \geq i} \psi^t_{l_{i',j'},n}\left(\frac{G_{i,j'}}{G_{i',j'}} \cdot e^{r^t_{l_{i',j'},n} - Q^t_{l_{i',j'},n}}\right)\right.\right.$$
$$\left.\left. + \sum_{l_{i',j'} \in \mathcal{L}_n, l_{i',j'} \neq l_{i,j}, i' < i} \psi^t_{l_{i',j'},n}\left(\frac{G_{i,j'}}{G_{i',j'}} \cdot e^{r^t_{l_{i',j'},n} - Q^{t+1}_{l_{i',j'},n}}\right)\right)^{-1}\right], \forall l, n, \tag{2.89}$$

$$r^{t+1}_{l_{i,j},n} = \log\left[\frac{\mu^t_i - \mu^t_j}{\psi^t_{l_{i,j},n} \cdot \left(\frac{N_0}{G_{i,j}} + \sum_{l_{i',j'} \in \mathcal{L}_n, l_{i',j'} \neq l_{i,j}} \frac{G_{i',j}}{G_{i,j}} \cdot e^{Q^{t+1}_{l_{i',j'},n}}\right)}\right] + Q^{t+1}_{l_{i,j},n}, \forall l, n. \tag{2.90}$$

We note that the generalized Eqs. (2.89) and (2.90) can also be readily obtained for a fading scenario by simply introducing the appropriate fading gain matrices of (2.39). Additionally, we can readily observe the relationship of the variables of $\boldsymbol{Q}$ and $\boldsymbol{R}$, as well as the effect of a parameter on the system performance and on the NL using (2.89) and (2.90). For

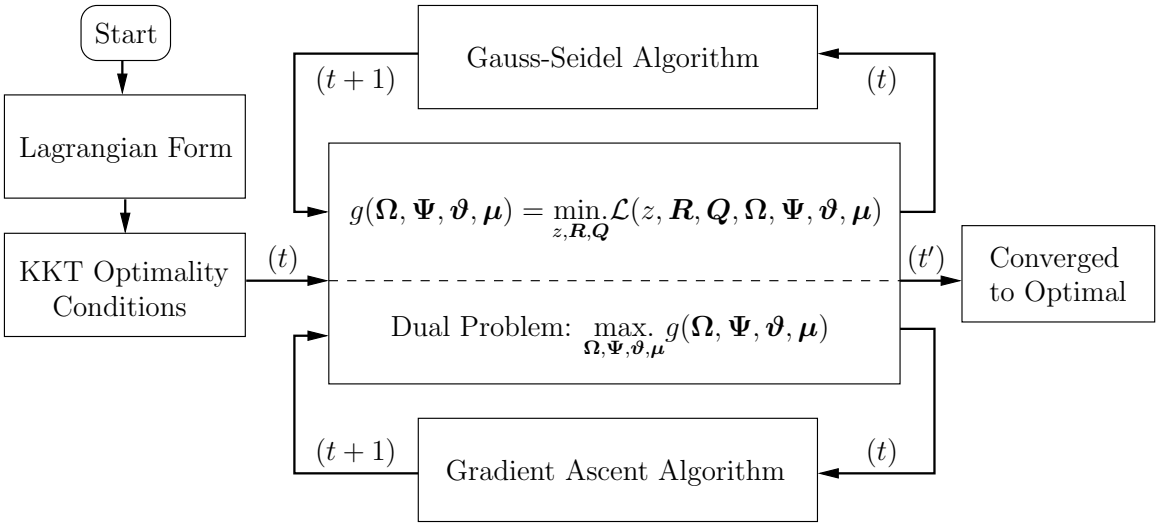

FIGURE 2.5: The schematic of the iterative solution algorithm of step nine in Fig. 2.4.

example, the instantaneous power is directly dependent on the energy multiplier $\boldsymbol{\Omega}$, on the power multiplier $\boldsymbol{\vartheta}$, on the transmit rate multiplier $\boldsymbol{\Psi}$, on the flow rate multiplier $\boldsymbol{\mu}$, on the power amplifier efficiency α and on the receiver's power gain $G_{i,j'}$. Similarly, the instantaneous transmit rate is directly proportional to the noise power N_0, $\boldsymbol{\mu}$, $\boldsymbol{\Psi}$, $\boldsymbol{Q}$ and to the transmitter's power gain $G_{i',j}$. For the sake of clarity, the receiver's power gain $G_{i,j'}$ and the transmitter's power gain $G_{i',j}$ are illustrated in Fig. 2.7. Let us now continue by outlining the design of the algorithm proposed for finding the globally optimal solutions to the optimization problem using (2.89) and (2.90).

2.4 Solution Algorithm Design

In this section, we describe the Gauss-Seidel algorithm of [88] utilized for updating the optimization variables. We also conceive the corresponding gradient ascent algorithm for updating the dual variables of the Lagrangian function of (2.59). Furthermore, the generalized structure of maximizing the NL is also provided in Algorithm 2.1, along with the iterative algorithm's schematic of Fig. 2.5. Broadly speaking, as previously discussed in the tenth step of Fig. 2.4, we apply our iterative solution algorithm to the globally optimal analytical expressions of (2.89) and (2.90), where the dual variables, the reciprocal of NL, the transmit powers and rates are randomly initialized and then they are iteratively updated using the Gauss-Seidel algorithm by gradually improving them towards the direction of the optimal solution relying on the gradient ascent algorithm. Naturally, a sufficiently small step size has to be used for each gradient function of (2.95)–(2.98), which again enables the algorithm to iteratively approach the optimal solution, as outlined in Fig. 2.5.

2.4.1 Gauss-Seidel Algorithm

Due to the interference terms in (2.61) and (2.62), each optimal variable in $\boldsymbol{Q}$ and $\boldsymbol{R}$ is dependent on the other variables of $\boldsymbol{Q}$ and $\boldsymbol{R}$, which implies that they are interdependent. More explicitly, the calculation of both the transmit power and of the rate of a specific node relies on the prior knowledge gleaned from other nodes, possibly from its interferers. Therefore, a control center is required, which handles the variables of the optimization problem and passes the near-instantaneous values of the variables to each of the individual nodes. However, compared to a distributed scheme, this centralized solution will impose a delay on the system, since high-complexity operations such as channel estimation are required at the initial stage. The near-instantaneous transmission rate and power values computed by the control center constituted by the sink node should be forwarded to each individual node. Therefore, a non-negligible delay will also be imposed on the reception of the sink node. As a solution method to the transmit power variables, the Gauss-Seidel algorithm [88] is utilized for iteratively updating the variables of (2.54) and (2.53) in an iterative fashion. For example, $Q_{l_{1,2},1}$ in (2.86) is dependent on the future values of the $\mathbf{Q}$ and $\boldsymbol{R}$ matrices, e.g. $Q_{l_{4,5},1}$, $r_{l_{4,5},1}$, $Q_{l_{7,8},1}$ and $r_{l_{7,8},1}$. Firstly, the $\mathbf{Q}$ and $\boldsymbol{R}$ matrices are randomly initialized with feasible initial values to compute the corresponding elements of the $\mathbf{Q}$ matrix. Similarly, the $\boldsymbol{R}$ matrix is also dependent on the previously calculated values of the $\mathbf{Q}$ matrix. This indicates that the $\boldsymbol{R}$ matrix is only dependent on the future values of $\mathbf{Q}$. The Gauss-Seidel algorithm recursively calculates the $\mathbf{Q}$ and $\boldsymbol{R}$ matrices in an iterative fashion until the convergence condition of the algorithm is satisfied. Formally, the variable dependencies may be expressed as:

$$Q_{l_{i,j},n}^{t+1} = f_1\left(\left\{Q_{l_{i',j'}\in\mathcal{L}_n,\, i'<i}^{t+1}\right\}, \left\{Q_{l_{i',j'}\in\mathcal{L}_n,\, i'\geq i}^{t}\right\}, R_{l_{i',j'}\in\mathcal{L}_n}^{t}\right), \tag{2.91}$$

$$R_{l_{i,j},n}^{t+1} = f_2\left(Q_{l_{i,j},n}^{t+1}\right), \tag{2.92}$$

where i denotes the current node, whose transmit power is being computed and i' represents the interfering nodes of node i in the same TS. Here, we have to know, if the instantaneous transmit power of the current node is dependent on the previously computed (future) power values or the current (previous) power values of the same TS. Therefore, we introduce the notation $i' < i$, which may also correspond to $\mathcal{O}^{-1}(l_{i',j'}) < \mathcal{O}^{-1}(l_{i,j})$, indicating that the power value of the current node i is dependent on the previously computed (iteration $(t+1)$) future power values of the interfering node(s) i', as shown in (2.91). Similarly, $i' \geq i$ may conform to $\mathcal{O}^{-1}(l_{i',j'}) \geq \mathcal{O}^{-1}(l_{i,j})$, where the transmit power computation of node i is dependent on the current (not computed or updated yet, iteration t) transmit power value of the interfering node(s) i' during the same TS, as indicated in (2.91). The

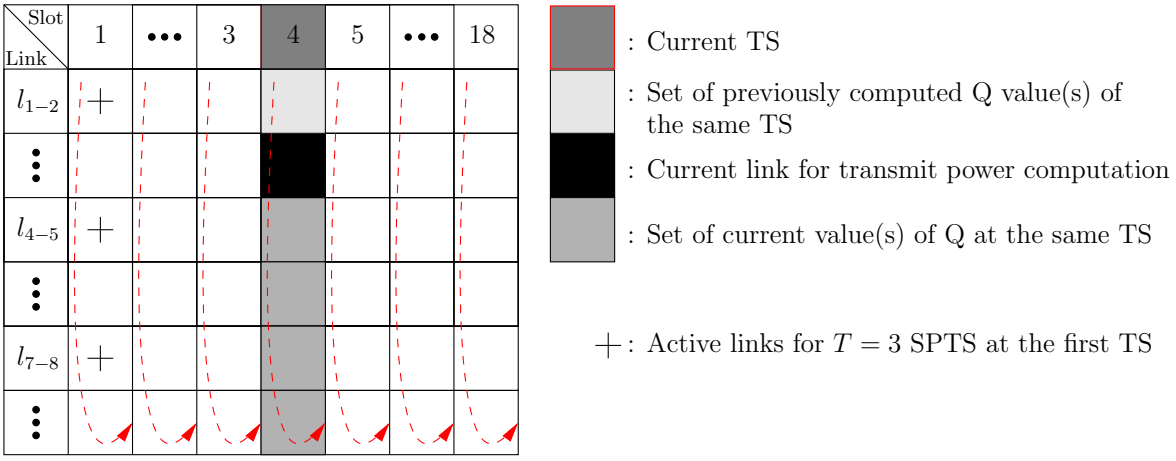

FIGURE 2.6: Computation order and variable dependency of the Gauss-Seidel Algorithm.

values in iteration t are yet to be updated or computed. These patterns can be observed in Fig. 2.6, which illustrates the computation order and the dependency of the variables relying on the Gauss-Seidel algorithm. More explicitly, considering the active links $l_{1,2}, l_{4,5}, l_{7,8}$ of Fig. 2.6 for $T = 3$ SPTS in the first TS, when the actual communication takes place on link $l_{1,2}$, the power value of the link $l_{1,2}$ relies on the current power values of link $l_{4,5}$ and $l_{7,8}$, respectively. On the other hand, when the actual communication is managed by the link $l_{4,5}$, the computation of the power value for $l_{4,5}$ relies on the future power value (previously computed, iteration $(t+1)$) of the link $l_{1,2}$ and the current power value of the link $l_{7,8}$. The generalized transmit power and rate equations in (2.89) and (2.90) are expected to converge to the optimal value with the aid of the Gauss-Seidel algorithm, which constitutes only one part of our generalized algorithm.

2.4.2 Gradient Ascent Algorithm

The dual objective function is defined as the minimum value of the Lagrangian (2.59) over z, $\boldsymbol{R}$, $\boldsymbol{Q}$ given by $g(\boldsymbol{\Omega}, \boldsymbol{\Psi}, \boldsymbol{\vartheta}, \boldsymbol{\mu}) = \inf_{z, \boldsymbol{R}, \boldsymbol{Q}} \mathcal{L}(z, \boldsymbol{R}, \boldsymbol{Q}, \boldsymbol{\Omega}, \boldsymbol{\Psi}, \boldsymbol{\vartheta}, \boldsymbol{\mu})$, which is a linear problem even if the primal problem is non-convex. The dual function $g(\boldsymbol{\Omega}, \boldsymbol{\Psi}, \boldsymbol{\vartheta}, \boldsymbol{\mu})$ may be maximized for the sake of finding a lower bound for the optimal value of the primal problem. Then, we can write the dual problem as follows,

$$\max_{\boldsymbol{\Omega}, \boldsymbol{\Psi}, \boldsymbol{\vartheta}, \boldsymbol{\mu}} \quad g(\boldsymbol{\Omega}, \boldsymbol{\Psi}, \boldsymbol{\vartheta}, \boldsymbol{\mu}) \tag{2.93}$$

$$\text{s.t.} \quad \boldsymbol{\Omega} \geq 0, \boldsymbol{\Psi} \geq 0, \boldsymbol{\vartheta} \geq 0, \tag{2.94}$$

which is a linear optimization problem. When the primal problem is convex, this lower bound is tight and so the duality gap is zero. Since the dual problem is continuously differentiable,

the gradient ascent algorithm [88] is utilized to solve the maximization problem by simply evaluating a series of closed-form expressions. The gradient of the Lagrangian function defines the search directions at the current point. Each dual variable is incremented in the direction of the positive gradient as shown in

$$\omega^{t+1} = \left[\omega^t + \Delta_\omega \left(\sum_{n=1}^{N}\left(\sum_{l\in\mathcal{O}(i)\cap\mathcal{L}_n}\left((1+\alpha)\cdot e^{Q^{t+1}_{l_{i,j},n}}\right)\right) - z\cdot\mathcal{E}_i\cdot N\right)\right]^+, \tag{2.95}$$

$$\psi^{t+1} = \left[\psi^t + \Delta_\psi \left(\left(\frac{N_0}{G_{i,j}} e^{r^{t+1}_{l_{i,j},n} - Q^{t+1}_{l_{i,j},n}} + \sum_{l_{i',j'}\in\mathcal{L}_n, i'\neq i} \frac{G_{i',j}}{G_{i,j}} e^{r^{t+1}_{l_{i,j},n} + Q^{t+1}_{l_{i',j'},n} - Q^{t+1}_{l_{i,j},n}}\right) - 1\right)\right]^+, \tag{2.96}$$

$$\vartheta^{t+1} = \left[\vartheta^t + \Delta_\vartheta \left(Q^{t+1}_{l_{i,j},n} - \log\Big((P_i)_{max}\Big)\right)\right]^+, \tag{2.97}$$

$$\mu^{t+1} = \left[\mu^t + \Delta_\mu \left(\sum_{l\in\mathcal{I}(i)}\left(\sum_{n=1}^{N} r^{t+1}_{l_{i,j},n}\right) - \sum_{l\in\mathcal{O}(i)}\left(\sum_{n=1}^{N} r^{t+1}_{l_{i,j},n}\right)\right)\right], \tag{2.98}$$

where t is the iteration index, and $[\cdot]^+$ denotes $\max(0,\cdot)$. Provided that $\Delta_{\boldsymbol{\Omega}} > 0, \Delta_{\boldsymbol{\Psi}} > 0, \Delta_{\boldsymbol{\vartheta}} > 0$ and $\Delta_{\boldsymbol{\mu}} > 0$ are sufficiently small positive step-sizes, the dual variables $\boldsymbol{\Omega}^t$, $\boldsymbol{\Psi}^t$, $\boldsymbol{\vartheta}^t$ and $\boldsymbol{\mu}^t$ converge to the dual optimal variables $\boldsymbol{\Omega}^*$, $\boldsymbol{\Psi}^*$, $\boldsymbol{\vartheta}^*$ and $\boldsymbol{\mu}^*$, respectively, as $t\to\infty$. In our case, the optimization problem shown in (2.46)–(2.52) is strictly convex, thus the duality gap is zero and the solution is unique.

2.4.3 Algorithm Structure

To solve the NL maximization problem for the optimal variables of z, $\boldsymbol{Q}$, $\boldsymbol{R}$, we describe our proposed algorithm in Algorithm 2.1. This algorithm is suitable both for AWGN and Rayleigh fading channels. In AWGN channels, we remove the fading gain matrix calculation and lines 21-23, while setting $\tau = 1$. First, we create the scheduling matrix for the string topology considered in Fig. 2.1 using the T SPTS parameter on line 3. Then, we acquire the index information of the active links and the TSs on line 4 and 5, since we have to compute both the transmit power and the rate of all those active links and TSs. We initialize all parameters considered in our specific scenario on line 6 and 7. The receive and transmit gain matrices of the interfering nodes are calculated on line 8, since the computation of (2.89) and (2.90) is based on $\mathbf{G}_r$ and $\mathbf{G}_t$. Initially, $\sum_{k=1}^{N}\mathbf{R}(k,\cdot)$ is set to a sufficiently high value so that abs $\left(\sum_{k=1}^{N}\mathbf{R}(k,\cdot) - NS_1\right) > \epsilon$ ensures the activation of the **while** loop on line 9 and 10, which controls the sum-rate of each link relying on (2.47). Once the sum-rate of each link is converged to an optimal value within a small margin of ϵ, then the convergence condition is satisfied and the **while** loop is terminated. Remembering that $P_{l_{i,j},n} = e^{Q_{l_{i,j},n}}$, the transmit power is computed using (2.89) in an iterative fashion based on the Gauss-Seidel algorithm on line 11. The reason for using the Gauss-Seidel method is because the

Algorithm 2.1 Solution algorithm for maximizing the NL.

Input: $\boldsymbol{\Omega}$ (A set of dual variables for energy conservation constraint in (2.49))
$\boldsymbol{\Psi}$ (A set of dual variables for transmission rate constraint in (2.48))
$\boldsymbol{\vartheta}$ (A set of dual variables for transmit power constraint in (2.50))
$\boldsymbol{\mu}$ (A set of dual variables for flow constraint in (2.47))
$\boldsymbol{Q}$ (transmission power matrix in (2.54))
$\boldsymbol{R}$ (transmission rate matrix in (2.53))
z_i (reciprocal of the lifetime of node i,$1/T_i$)
S_1 (source rate at the SN)
ϵ (convergence tolerance of the iterative algorithm)
$(P_i)_{max}$ (maximum affordable transmit power per node)
$\mathcal{E}_i$ (initial battery capacity of each sensor)
τ (number of trials for AWGN and fading scenarios)
$\mathbf{G}_r, \mathbf{G}_t$ (receiving and transmitting channel gain of the interferers, respectively)
α (power amplifier inefficiency)
d (Euclidean distance between two consecutive nodes)
T (SPTS parameter for fixed link scheduling)
N (total number of TSs per link frame)
c (counter of each trial)
$\mathcal{B}$ (predefined total number of iterations of each trial)

for i **from** 0 **until** τ **do**
  function kkt-solve()
  Create scheduling matrix of the string topology of Fig. 2.1
  Identify the activated links for each TS relying on T SPTS parameter
  Store index information of the links and the slots.
  Initialize all parameters $\rightarrow (\boldsymbol{\Omega}, \boldsymbol{\Psi}, \boldsymbol{\vartheta}, \boldsymbol{\mu}, \boldsymbol{Q}, \boldsymbol{R}, \mathbf{z}, S_1, \epsilon, (\mathrm{P}_i)_{max}, \mathcal{E}_i, \tau, \mathbf{G}, \alpha, N_0, d, T, c)$
  $\mathbf{z} = 0 \leftarrow$ Set initial value of the reciprocal of the lifetime of all nodes to zero
  $\mathbf{G}_r, \mathbf{G}_t \leftarrow$ Compute the channel gain matrices required by (2.89) and (2.90) using d
  $\beta \leftarrow \text{abs}\left(\sum_{k=1}^{N} \mathbf{R}(k,\cdot) - NS_1\right) \leftarrow k$-th row of the rate matrix is denoted by $\mathbf{R}(k,\cdot)$
    do while $(\beta > \epsilon) \leftarrow$Sum-rate of each link is constrained by S_1 over N TS
      $\mathbf{Q} \leftarrow$ Compute-transmit-power-Gauss-Seidel$(\mathbf{Q}, \boldsymbol{R}, \boldsymbol{\Omega}, \boldsymbol{\Psi}, \boldsymbol{\vartheta}, \boldsymbol{\mu}, \mathbf{G}_r)$ from (2.89)
      $\boldsymbol{R} \leftarrow$ Compute-transmit-rate$(\mathbf{Q}, \boldsymbol{\Psi}, \boldsymbol{\mu}, \mathbf{G}_t)$ from (2.90)
      $\mathbf{z} \leftarrow$ Compute-NL$(\alpha, N, \mathcal{E})$ Compute the reciprocal of the NL
      $z_i \leftarrow \max(\mathbf{z})$ Find the maximum z_i giving the minimum T_i, which defines T_{net}
      $\boldsymbol{\Omega} \leftarrow$ Update-gradient-energy-multiplier$(\boldsymbol{\Omega}, \mathbf{Q}, \alpha, N, \mathcal{E}, \Delta_\omega)$ in (2.95)
      $\boldsymbol{\Psi} \leftarrow$ Update-gradient-rate-multiplier$(\boldsymbol{\Psi}, \mathbf{Q}, \boldsymbol{R}, \Delta_\psi)$ in (2.96)
      $\boldsymbol{\vartheta} \leftarrow$ Update-gradient-power-multiplier$(\boldsymbol{\vartheta}, \mathbf{Q}, (P_i)_{max}, \Delta_\vartheta)$ in (2.97)
      $\boldsymbol{\mu} \leftarrow$ Update-gradient-flow-rate-multiplier$(\boldsymbol{\mu}, \boldsymbol{R}, \Delta_\mu)$ in (2.98)
      if $(c > \mathcal{B}) \leftarrow$ Each trial has a predefined number of iterations for convergence
        return kkt-solve() $\leftarrow$ Discard the current trial and repeat it again
      end if
      $c \leftarrow c + 1$
    end do
  return $T_{net} = 1/z_i = T_i$
end for
return $\sum_{a=1}^{\tau} (T_{net})_a/\tau \leftarrow$ Average NL over τ trials

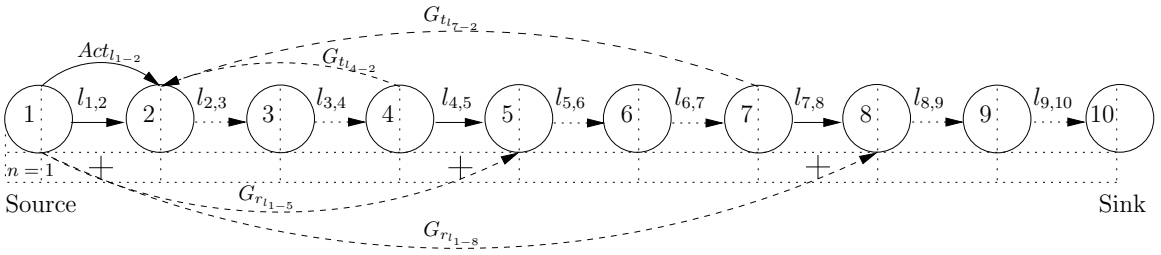

FIGURE 2.7: Receiver gain matrix $\mathbf{G}_r$ and transmitter gain matrix $\mathbf{G}_t$ of the interfering communication links.

computation of $\boldsymbol{Q}$ may be based on either the future or the current values of $\boldsymbol{Q}$ in the same iteration. Therefore, we use (2.91) for the computation of (2.89). In fact, (2.89) already indicates, which specific value of $\boldsymbol{Q}$ must be used for computing the current transmit power at the same TS. Fig. 2.7 illustrates the time instant, when an actual communication $Act_{l_{1,2}}$ is initiated between node-1 and node-2. Observe in Fig. 2.7 that the receiver gain matrix $\mathbf{G}_r$ is used for the computation of $\boldsymbol{Q}$, which is based on the receiver gain of the interfering communication links of the same TS. Similarly, the transmit rate $\boldsymbol{R}$ is computed based on the previously calculated future values of $\boldsymbol{Q}$ and on the transmitter gain $\mathbf{G}_t$ of the interfering links, as illustrated in Fig. 2.7. Therefore, the Gauss-Seidel algorithm is indirectly exploited for the computation of $\boldsymbol{R}$ on line 12. However, the computation of any element in $\boldsymbol{R}$ is not based on any other element in $\boldsymbol{R}$, hence the Gauss-Seidel algorithm does not have to be invoked. On line 13 of Algorithm 2.1, the reciprocal of the NL is computed for each node so that on line 14 the NL can be determined by finding the minimum lifetime of the nodes forming part of the string-topology considered. On line 15-18 of Algorithm 2.1, the dual variables $\boldsymbol{\Omega}, \boldsymbol{\Psi}, \boldsymbol{\vartheta}, \boldsymbol{\mu}$ are incremented in the direction of the positive gradient using sufficiently small positive step-sizes of $\Delta_{\boldsymbol{\Omega}} > 0, \Delta_{\boldsymbol{\Psi}} > 0, \Delta_{\boldsymbol{\vartheta}} > 0, \Delta_{\boldsymbol{\mu}} > 0$, as shown in (2.95)–(2.98), where the dual variables $\boldsymbol{\Omega}^t$, $\boldsymbol{\Psi}^t$, $\boldsymbol{\vartheta}^t$ and $\boldsymbol{\mu}^t$ converge to the dual optimal variables $\boldsymbol{\Omega}^*$, $\boldsymbol{\Psi}^*$, $\boldsymbol{\vartheta}^*$ and $\boldsymbol{\mu}^*$, respectively, as we have $t \to \infty$. If the channel only imposes AWGN, the NL is found on line 24. However, if the links operate over a fading channel, then the desired NL must be averaged over τ trials, as indicated on line 26.

2.5 Performance Results

In our experiments, we use the parameters of $\alpha = 0.01$, $N_0 = 1\,\text{dBm/Hz}$, $E_v = 5000\,\text{Joule}$[4], $s_1 = \{0.2, 0.3, 0.4, 0.5, 0.6, 0.7\}\text{nats/s/Hz} \approx \{0.29, 0.43, 0.58, 0.72, 0.87, 1.01\}\text{bits/s/Hz}$, $(P_i)_{max} = 50\,\text{W}$, $N = 18$, $d = 1\,\text{m}$, convergence tolerance of iterative algorithm $\epsilon = 10^{-5}$, $T = \{3, 4, 5, 6, 7, 8, 9\}$. A summary of parameters utilized in our simulations can be found in Table 2.3.

Fig. 2.8 shows the NL versus source rate trends for a fixed link schedule and for various

[4]For example, this is the energy storage capacity of an AAA alkaline long-life battery.

TABLE 2.3: Simulation parameters utilized for NL maximization.

Simulation parameter	Value
Path loss exponent, m	4
Euclidean distance between consecutive nodes, d [m]	1
Spectral noise power density, N_0 [dBm/Hz]	1
Initial battery energy per node, $\mathcal{E}_i$ [Joule]	5000
Maximum affordable transmission power per node, $(P_i)_{max}$ [W]	50
Number of slots per link frame, N	18
Number of nodes, V	10
Number of links, $L = V - 1$	9
Inefficiency of the power amplifier, α	0.01
Power dissipation of transmitter circuit, P_{ct} [W]	0
Power dissipation of receiver circuit, P_{cr} [W]	0
Source rate only at SN, S_1 [Nats/s/Hz]	$\{.2, .3, .4, .5, .6, .7\}$
SPTS parameter, T	$\{3, 4, 5, 6, 7, 8, 9\}$
Convergence tolerance of iterative algorithm, ϵ	10^{-5}
Number of trials, τ_{AWGN}, τ_{fading}	1, 5000

spatially periodic time sharing parameters, T, where the channel in each link is a LOS AWGN channel characterized by a fixed noise power. As expected, the NL decays as a function of the source rate, as shown in Fig. 2.8. This is because a higher source rate requires a higher transmission rate and hence a higher transmission power. Furthermore, in our model the weakly interfering nodes are scheduled to transmit simultaneously and hence each link becomes capable of transmitting at a lower rate, whilst still satisfying all the transmit requirements of the SN. This necessitates a lower transmission power. Using the $T = 9$ spatially periodic time schedule of Fig. 2.2 corresponds to a TDMA scheme, since there is only a single transmission in each TS, as shown in Fig. 2.2. However, since the time frame of Fig. 2.2 consists of 18 TSs, a specific link is scheduled to transmit twice during the whole time frame. Despite the fact that the $T = 9$ link schedule does not impose any interference, it results in the lowest NL according to Fig. 2.8. Although interference is present in the $T = 3$ scenario, since each link can be activated three times more often than in the $T = 9$ scenario, each link in the $T = 3$ scenario can be activated at a lower transmission power, while still satisfying the end-to-end rate constraint. Therefore, the spatial reuse

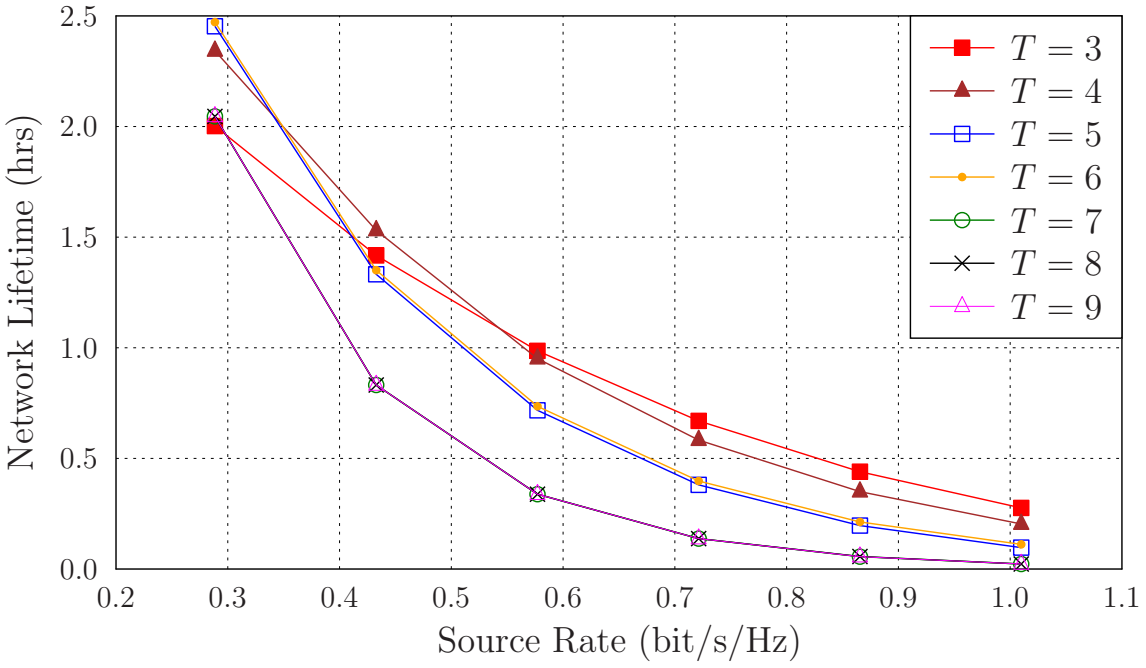

FIGURE 2.8: Network lifetime for different spatially periodic schedules and source rates in AWGN channel.

assisted us in the $T = 3$ scenario for increasing the NL. We can follow Fig. 2.2 to find out how many transmissions there are per link for a given value of T. For example, the $T = 3$ schedule allows a link to be scheduled 6 times, which requires a reduced transmission rate, since the total source rate delivered over different TSs is using 6 transmissions. From the flow conservation equality constraint of the optimization problem seen in Eq. 2.47, we have $\mathbf{A}(\mathbf{r}_1 + \mathbf{r}_2 + ... + \mathbf{r}_N) = \mathbf{s} \cdot N$. For example, let us assume that the source rate equals to 0.29 bits/s/Hz. Then we obtain $18 \cdot 0.29 = 5.22$ bits/s/Hz, which has to be divided into 6 transmissions, corresponding to a 0.87 bits/s/Hz per link transmission rate for $T = 3$. However, when we have $T = 9$, we obtain a 2.61 bits/s/Hz per link transmission rate, since a link is only activated twice during the whole time frame. Therefore, the transmission rate per link converges to 0.87 bits/s/Hz for $T = 3$ and 2.61 bits/s/Hz for $T = 9$. Hence, $T = 9$ requires three times as much transmission power as $T = 3$. The required transmit power in weakly interfering links is quite low compared to that for $T = 9$, which is the scenario requiring the highest transmission rate. Hence again, we surmise that simultaneous scheduling benefits from a reduced transmission power due to its reduced transmission rate per link. This is because the spatially periodic schedule allows us to schedule more transmissions during the same TS or to activate the same link more than once in different TSs. This explains the steep decay of the NL for $T = 9$. When considering the effects of node density on a given fixed link schedule, we expect a network supporting less than $V = 10$ nodes to be exposed to less interference. Therefore the transmission power of each link can be reduced without reducing the end-to-end transmission rate, which results in a higher NL. On the other hand, upon increasing the node density, we expect the NL to

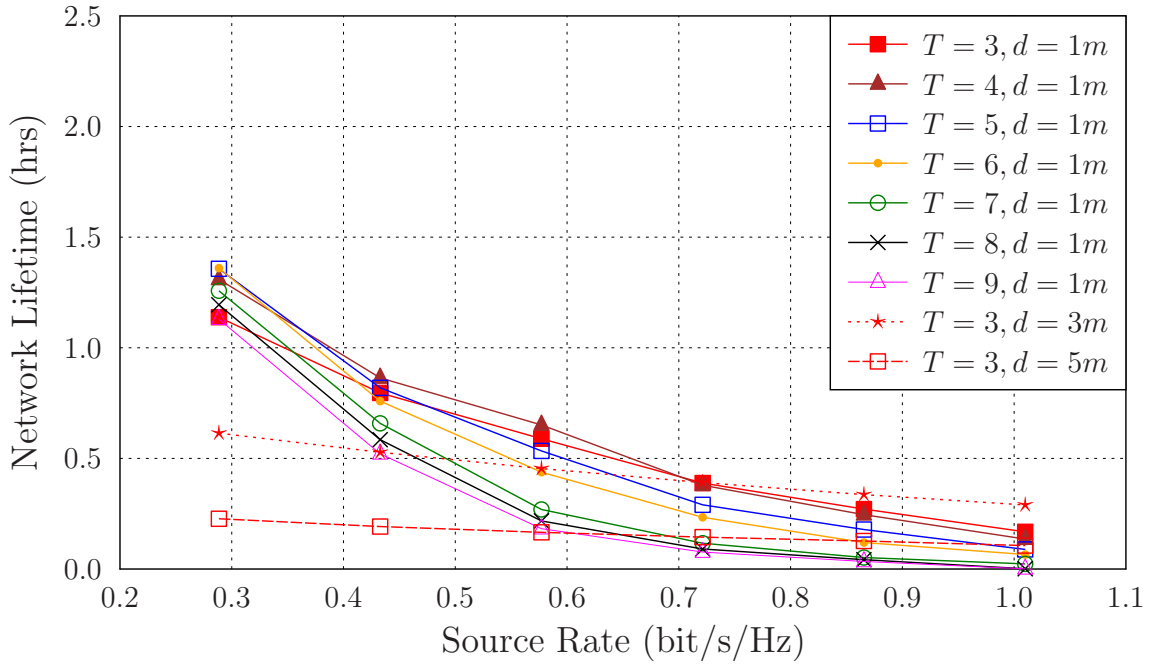

FIGURE 2.9: Network lifetime for different spatially periodic schedules and source rates in block-fading channel.

decrease, since more interferers are introduced, but the same transmission rate is required. Fig. 2.9 represents the NL versus source rate trade-off for a fixed link schedule and for various spatially periodic time sharing parameter values of T, when each link obeys an i.i.d. block Rayleigh fading channel. Naturally, the NL was reduced compared to the results of Fig. 2.8 recorded for an AWGN channel due to requiring a higher transmit power in order to combat the effects of fading. We also analyzed the impact of the inter-node distance on the NL for the $T = 3$-based link schedule, when communicating over a Rayleigh fading channel, as seen in Fig. 2.9. Increasing the distance between the consecutive nodes substantially reduced the NL, especially for lower source rates. However, quite surprisingly, increasing the distance between the consecutive nodes from 1m to 3m resulted in an improved NL for higher source rates. This is due to the reduced impact of the interferers located at a higher distance. More explicitly, even though the transmit power required had to be increased to satisfy the rate constraint, at the same time the interferers were moved a bit further away. Therefore the total energy dissipation of the $d = 3$m scenario is still lower than that of the $d = 1$m scenario associated with higher source rates. Furthermore, we comprehensively study the energy dissipation per node, the average transmission power per link and the lifetime of all sensor nodes in the network. Fig. 2.10 shows the energy dissipation per node, the average transmission power per link and the lifetime of all nodes in the network in both AWGN and fading channels for the $T = 3$ link schedule of Fig. 2.2 at a source rate of 0.29 bits/s/Hz. In the network topology considered, the transmissions from the first three nodes suffer from the highest amount of interference. This is because their receiving nodes are closer to their potential interferers, when compared to any other sets of nodes. Therefore,

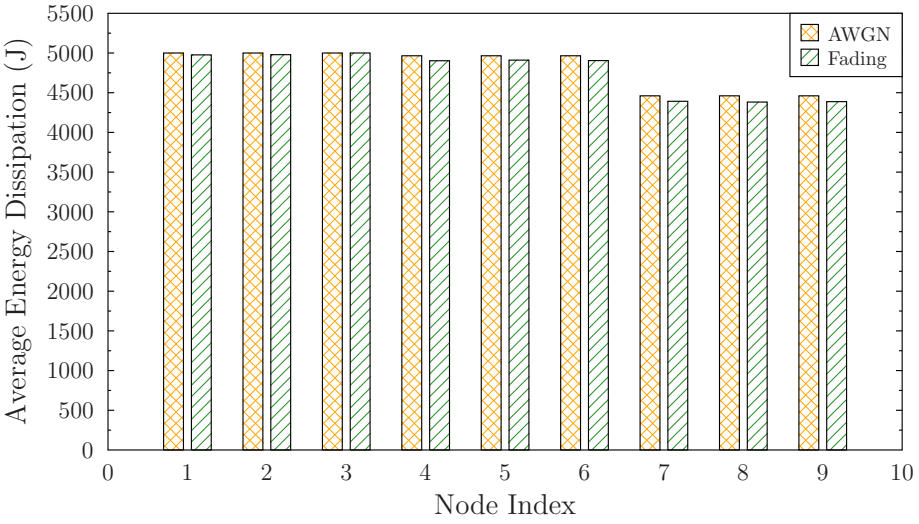

(a) Energy dissipated by each sequential node index of Fig. 2.1.

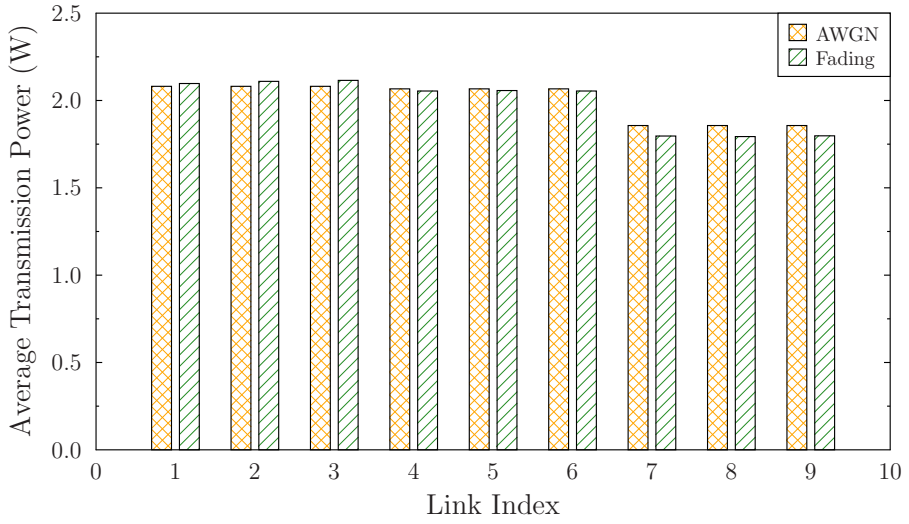

(b) Average transmit power required for each sequential link index of Fig. 2.1.

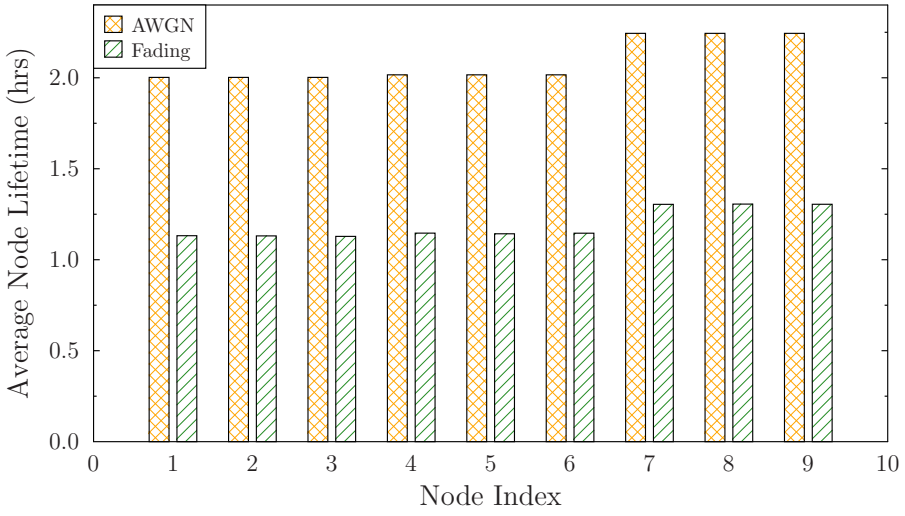

(c) Lifetime computed for each sequential node index of Fig. 2.1.

FIGURE 2.10: (a), Energy dissipation per node, (b), average transmit power per link and (c), lifetime of all nodes in the network in both AWGN and fading channels for the $T = 3$ link schedule at a source rate of 0.29 bits/s/Hz. We note that the terms *Links* and *Nodes* on the horizontal axis are referred to as the unique index of each sensor node forming part of the string-topology that is illustrated in Fig. 2.1.

to satisfy the flow conservation constraints, these nodes must transmit at a higher power, as seen in Fig. 2.10(b). Thus, in an AWGN channel the first three nodes in the network dissipate their 5000J initial amount of energy faster than the other nodes, since the energy dissipation is proportional to the transmit power, as seen in Fig. 2.10(a), whereas in the block Rayleigh fading channel the third node runs out of battery first, which also determines the lifetime of the WSNs. The required transmit power of the third link is higher than that in the AWGN channel scenario. This increase in transmit power is required to overcome the effect of fading.

The average transmit power per link is calculated by summing the transmit powers per link, and then dividing it by the number of TSs that the same link was allowed to transmit. For the first three links operating in the AWGN channel, the required transmission power per link is higher than that of the rest of the links. Since requiring a high transmit power results in dissipating more energy, the lifetime of those nodes is reduced, as illustrated in Fig. 2.10(c).

Upon comparing the AWGN and fading channel scenarios in Fig. 2.10, we observe that they follow a similar trend. An observation is that the average transmit power per link of the $7th$, $8th$ and $9th$ nodes in Fig. 2.10(b) is slightly lower for the fading channel than for the AWGN channel. However, interestingly the average transmit power per link of the $3rd$ node in Fig. 2.10(b) recorded for the fading channel is slightly higher than that of the AWGN channel. Therefore, the need for a high transmit power necessitates a higher energy dissipation for that particular node. Hence, the NL is reduced, which can also be observed by comparing Fig. 2.8 and Fig. 2.9. Fig. 2.8 illustrates that the NL of the WSN in the AWGN channel recorded for the $T = 3$ link schedule and for 0.29 bits/s/Hz source rate is approximately 2 hours (hrs). By contrast, Fig. 2.9 illustrates that the NL of the WSN operating in a Rayleigh fading scenario for the $T = 3$ link schedule and for 0.29 bits/s/Hz source rate indicates approximately a NL of $1.13hrs$. This earlier node failure of the fading scenario is due to the poor channel conditions, where the fading required a higher transmit power in the $3rd$ node, as seen in Fig. 2.10(b). Therefore, this earlier node failure shortened the NL of the WSNs in fading channels.

In order to put the above results into context, we apply our analysis to the environmental sensor networks of [58], where the relation between glaciers and climate change was studied. In their work, the authors of [58] transmit data only once per day for 0.5 second (s) TS. In this specific application and considering our results in Fig.2.10 for $T = 3$ and source rate of 0.29 bits/s/Hz, the battery will serve communications for $7200s$ which means that the NL will be around 4 years and 3 months in LOS AWGN channel. We also consider what NL we can achieve if the environmental conditions are more challenging and the channel is exposed to the severe environments mentioned in [58], which may be modeled by a NLOS Rayleigh block-fading channel. Activating the communication channel once per day in fading

conditions will lead us to a NL of around 2 years and 6 months.

2.6 Applicability of Optimal Scheduling

In this section we justify, why the transmit power must not be zero and why the node has no option of refraining from transmission[5]. This limitation is also the reason why optimal scheduling cannot be achieved based on the current system model formulated in (2.46)–(2.52). We recall the relaxed non-convex rate constraint, which is converted from

$$r_{l_{i,j},n} \leq \log\left(1 + \frac{G_{i,j}P_{l_{i,j},n}}{\sum_{i'\neq i, l_{i',j'}\in\mathcal{L}_n} G_{i',j}P_{l_{i',j'},n} + N_0}\right) \tag{2.99}$$

$$\text{into} \quad r_{l_{i,j},n} \leq \log\left(\frac{G_{i,j}P_{l_{i,j},n}}{\sum_{i'\neq i, l_{i',j'}\in\mathcal{L}_n} G_{i',j}P_{l_{i',j'},n} + N_0}\right) \tag{2.100}$$

by invoking an approximation of the SINR. Using this approximation may not cause any problems for high SINRs. However, the approximation has to be reconsidered for the links that experience a low SINR. When considering (2.100), if the rate $r_{l_{i,j},n}$ is allowed to be higher than or equal to zero, the term $\frac{G_{i,j}P_{l_{i,j},n}}{\sum_{i'\neq i, l_{i',j'}\in\mathcal{L}_n} G_{i',j}P_{l_{i',j'},n}+N_0}$ in (2.100) has to be at least equal to 1. Therefore, $P_{l_{i,j},n}$ always represents a non-zero transmit power, if the link is activated for transmission. This trend is illustrated in Fig. 2.11, where we plot the transmission rate versus the SINR. In fact, when $r_{l_{i,j},n} \geq 0$ is satisfied, the SINR always has to be higher than zero. Similarly, in (2.99) if the rate $r_{l_{i,j},n}$ is allowed to be higher than or equal to zero, the term $\left(1 + \frac{G_{i,j}P_{l_{i,j},n}}{\sum_{i'\neq i, l_{i',j'}\in\mathcal{L}_n} G_{i',j}P_{l_{i',j'},n}+N_0}\right)$ in (2.99) has to be at least equal to 1. This allows the term to obey $\frac{G_{i,j}P_{l_{i,j},n}}{\sum_{i'\neq i, l_{i',j'}\in\mathcal{L}_n} G_{i',j}P_{l_{i',j'},n}+N_0} \geq 0$. Therefore, $P_{l_{i,j},n}$ can be equal to zero. Given this type of system model, if a link is activated for transmission, it is allowed to opt for avoiding transmission for the sake of NL maximization. In fact, Fig. 2.12 indicates that when the rate obeys $r_{l_{i,j},n} \geq 0$, the SINR may become zero. Hence, if optimal scheduling is considered, then we can no longer invoke the approximation employed for the SINR. This is mainly because if a node is scheduled for transmission, it keeps transmitting based on the approximated SINR method. However, the system itself should be able decide either to transmit or not to transmit. More explicitly, if we schedule all links in all TSs for transmission, the system model should converge to an optimal scheduling, where some links and slots refrain from transmitting for the sake of NL maximization. However, when using the approximated SINR based method, this is no longer feasible, since all links scheduled

[5] A set of sensor nodes are activated according to, for example the $T = 3$ SPTS link scheduling scheme during the same TS. However, none of these sensor nodes is allowed to transmit by setting its transmit power to zero for the sake of maximizing the NL. Explicitly, these sensors are activated using the $T = 3$ SPTS link scheduling, but they may not be necessarily scheduled for the transmission.

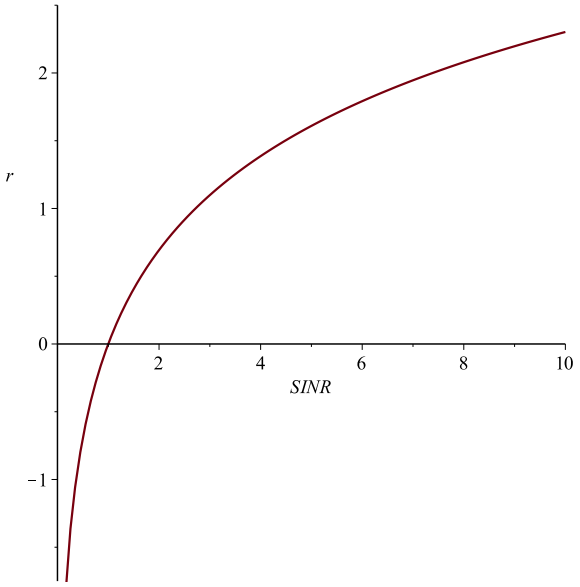

FIGURE 2.11: The plot of $r = \log(\text{SINR})$.

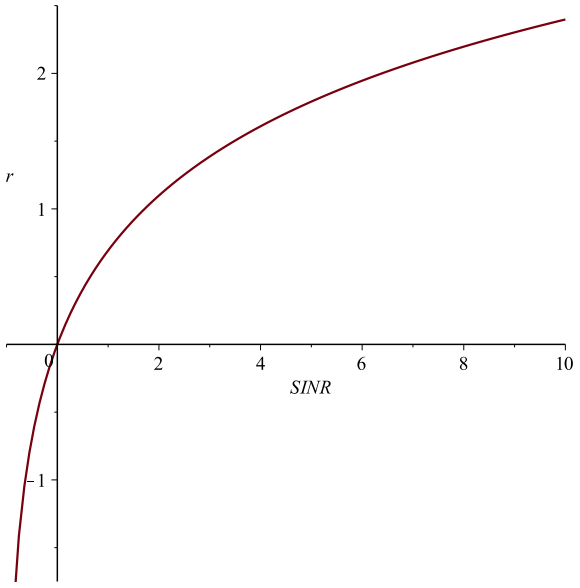

FIGURE 2.12: The plot of $r = \log(1 + \text{SINR})$.

for transmission in all TSs will continue transmission. In our case, when we consider the approximated SINR method, we can no longer achieve optimal scheduling due the constraints mentioned above. Additionally, as indicated in [30], a suboptimal scheduling scheme may be achieved. However, recall from Fig. 2.8 that a fixed link scheduling scheme based on the $T = \{3, 4\}$ SPTS parameters was able to achieve a similar performance compared to that of the suboptimal scheduling algorithm proposed in [30]. For this reason, in the following chapters we will consider a fixed link scheduling based on the $T = 3$ SPTS parameter.

2.7 Chapter Summary and Conclusions

In WSNs, the NL plays a vital role, since the sensor nodes usually rely on limited energy supply. Therefore, maximizing the NL is an important and challenging task due to the nature of the sensor nodes. Moreover, sensor nodes communicate unidirectionally on the same shared wireless channel with the aid of half-duplex transceivers and assuming that each node is constrained to transmit only in a single TS and within a fixed band of the spectrum. However, in larger networks a single physical channel will unavoidably be utilized by many other nodes. Therefore, link scheduling and multiple access schemes have to be invoked for mitigating the interference by controlling the channel access. One of the solution is to schedule weakly interfering links simultaneously and strongly interfering links at different TSs. We evaluated the optimal NL in an interference-limited scenario for an optimal transmit rate and power, when considering the so-called spatially periodic time sharing scheme of Fig. 2.2. The maximization of NL was formulated as a nonlinear optimization problem taking into account the link scheduling, the transmission rates as well as transmit powers of all active TSs. The original nonlinear problem was converted into a convex optimization problem by employing an approximation of the SINR. We then derived the Lagrangian form of the convex optimization problem and employed the KKT optimality conditions [129] of Section 2.3.8 for deriving analytical expressions of the globally optimal transmit rate and transmit power for our specific network topology. Exploiting the KKT optimality conditions significantly reduced the complexity of our algorithm, which requires the evaluation of $(n+1)$ expressions whilst the interior-point method requires the solution of a system of n linear equations, which has a complexity proportional to n^2. Finally, we obtained the maximum NL for both AWGN and Rayleigh fading channels. Our numerical results illustrated that as expected, fading has a detrimental impact on the achievable NL due to the poor channel conditions that require an increased transmit power in order to combat the effects of fading. Furthermore, the simultaneous scheduling of links that interfere with each other only weakly allowed us to take advantage of spatial reuse, where the activation of simultaneous transmissions at reduced rates necessitates a reduced transmission power, which results in extending the NL. Table 2.4 illustrates how the NL is reduced upon increasing the source rate due to the requirement of an increased transmission rate and power, regardless of the specific scheduling scheme employed. It also presents how the NL degrades due to fading. Hence, we may conclude that the choice of scheduling depends on the specific application considered, since a lower source rate favors infrequent transmissions requiring a low transmit power, which mitigates the interference, when aiming for extending the NL. However, for higher source rates, a higher NL can be achieved by invoking a more aggressive spatial reuse.

In this chapter, only the NL is considered as the QoS measure as a function of both the transmit rate and transmit power, where an adaptive scheme is assumed. At this stage,

S_1 [bits/s/Hz]	AWGN	Fading
0.29	2.0021	1.1383
0.43	1.4174	0.7960
0.58	0.9861	0.5888
0.72	0.6696	0.3886
0.87	0.4399	0.2708
1.01	0.2762	0.1682

TABLE 2.4: Maximum NL [hrs] comparison for increasing source rates of AWGN and fading channels, when $T = 3$.

the energy dissipation of the transceiver circuits was neglected. However, the system designers also have to investigate the impact of the signal processing power on the NL. On the other hand, achieving a reasonable NL at the cost of a tolerable end-to-end BER for various modulation and coding schemes is also important for the system designer in the light of the required QoS. Therefore, in Chapter 3, we will aim for maximizing the NL for a predetermined set of target SINR values, which guarantees a predefined QoS for each link operating over either an AWGN channel or a Rayleigh block-fading channel both with and without signal processing power.

Chapter 3

Cross-layer Network Lifetime Optimization Considering Transmit and Signal Processing Power in Wireless Sensor Networks

3.1 Introduction

In Chapter 2, we only considered the NL as the QoS measure as a function of the transmit rate and transmit power, where we assumed that each sensor node can adapt its transmission power, modulation scheme and duty cycle. However, we did not consider the ED of the signal processing operations, albeit system designers also have to consider the impact of the SPP on the NL. Additionally, it is also important to quantify, how different target BER affect both the NL and the overall network performance. Therefore, achieving a reasonable NL at the cost of a tolerable end-to-end BER for various MCSs is also of salient importance for the system designer considering the QoS required. Moreover, attaining a long NL along with a low target BER is crucial in WSNs, where regular battery replenishment can be impractical, or may even be futile in hostile environments. Therefore, battery depletion imposed by the inappropriate choice of the communication parameters may have a major effect on the lifetime of a sensor node. However, the impact of the physical layer parameters on the NL is not explicitly characterized in the literature and there is only a paucity of contributions on the desired BER performance of the selected MCSs as well as on its impact imposed on the NL in the context of WSNs. Explicitly, the choice of the system parameters has a vital effect on the BER, which in turn has a considerable impact on the number of retransmissions that may result in a high energy consumption. Therefore, in this chapter we

aim for maximizing the NL for a predetermined set of target SINR values, which guarantees the predefined QoS of each link operating over either an AWGN channel or a Rayleigh block-fading channel, both with and without SPP.

In [192], Chen *et al.* analyzed the NL of a low-complexity physical layer relying on amplify-and-forward (AF) relays between a SN and a DN, where the BER performance was analyzed in the low SNR regime. As detailed in [192], the relaying scheme between the transmitter and a receiver is capable of attaining a reduced-distance based path-loss gain and of conserving energy to prolong the NL, since the ED imposed on the transmitting sensor was reduced with the aid of relays. The appropriate modulation mode capable of maintaining the target BER was discussed in [193], while maintaining a high energy efficiency, where on-off keying (OOK) and pulse position modulation (PPM) were compared. The findings of [193] illustrate that the critical transmission range d_c can be readily found and that OOK is preferable to PPM for $d < d_c$. The constellation size and transmission power selection strategy conceived for energy-efficient communications over fading channels was discussed in [194]. Rosas *et al.* [194] demonstrated that the careful selection of the optimal constellation size is capable of extending the NL by as much a factor of five. The authors of [194] also showed that as expected, BPSK and QPSK constitute the optimal choice for long transmission distances, while for short distances the optimal choice of constellation size may be either 16-ary quadrature amplitude modulation (16-QAM) or even 64-QAM. In [195], Cui *et al.* proposed a modulation scheme selection strategy for minimizing the total energy consumption, including both the transmission and circuit energy consumption to deliver a predetermined number of bits. The authors of [195] demonstrated that optimized systems are capable of saving up to 80% energy compared to sub-optimum uncoded systems. The authors also observed that for coded systems, the impact of coding on the energy consumption depends both on the modulation scheme and the transmission range of the communication system. Additionally, increasing the tolerable symbol error ratio (SER) of the physical layer facilitated energy savings due to the reduced transmit power [196], while there was an increase in energy consumption due to the frame retransmissions. Plausible logic dictates that low-order modulation schemes like BPSK are energy efficient, unless achieving high data rates is necessary [197]. Nonetheless, the impact of the transmission rate on the NL is considered in [30], where an adaptive scheme is utilized for maximizing the NL with the aid of a cross-layer design in interference-limited WSNs. In [198], the authors analyzed the joint effect of the interference, power control and various forwarding strategies on the attainable NL. A similar study to ours was provided in [199], where the authors aimed for cooperatively maximizing the minimum device lifetime for M-ary phase shift keying (M-PSK) modulation under a specific BER constraint. An adaptive clustering technique maximizing the NL, while maintaining the network's connectivity was proposed in [200]. Similarly, as an application of WSNs, monitoring offshore wind farms was evaluated in [201], where a clustering protocol based on a three-level hierarchy and an algorithm

jointly considering information routing, the instantaneous energy level of each node and the spatial distribution of the sensor nodes was proposed. Li *et al.* [183] conceived an ED model for a generalized turbo decoder architecture as a function of numerous design parameters, while characterizing the trade-off between the ED of the SPP P_{sp} and transmit power. For our model, we adopted the ED of the SPP relying on [183].

3.1.1 Novel Contributions

The BER is one of the most salient QoS metrics of communication systems, but naturally, maintaining a longer NL for battery-limited devices is another important factor. Furthermore, the choice of the physical layer parameters, such as the MCSs, and transmit power substantially affect the NL and these parameters also have a direct impact on the attainable BER. Therefore, striking an attractive trade-off between the BER and the NL is crucial for network designers at an early design stage. The novel contributions of this chapter can be summarized as follows:

1. We quantify the effects of the physical layer parameters on the achievable NL, while considering an application-dependent target BER in both LOS AWGN and NLOS Rayleigh block-fading channels in interference-limited string-topology based WSNs.
2. We analyze the impact of the SPP on the NL for both AWGN and fading channels. Therefore, we show that the NL is substantially reduced due to the accumulated circuit ED and the transmit power. Here, we characterize the interplay between the transmit power and the SPP.
3. We examine the ED of each node, the required transmission power per link, the effects of the interference power on each node and the lifetime of all nodes forming part of the string-topology based network, while considering different target SINR requirements, SPP and channel characteristics.
4. We propose two types of BER performance metrics. The first one is the per-link BER requirement (PLBR), which defines the BER value attained by the weakest link. Hence, PLBR represents the worst BER that can be tolerated over the links. By contrast, the E2EB is defined as the BER accumulated along the route spanning from the SN to the DN. We demonstrate that a similar NL performance is achieved at a higher E2EB compared to the PLBR.
5. We also show how different target BER values affect both the NL and the overall network performance in the string topology considered.
6. Considering our proposed system model, depending on the required QoS and network performance, the network designer can make well-informed decisions concerning the type of modulation schemes that should be used for different types of networks and/or applications.

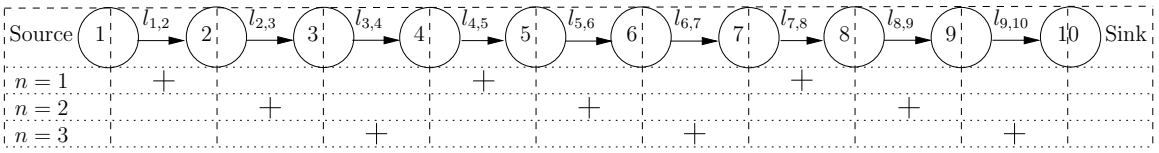

FIGURE 3.1: A string topology, where the SN and the DN is linearly connected by intermediate nodes relying on link scheduling associated with the SPTS parameter of $T = 3$, when $N = 3$ and $V = 10$.

3.1.2 Chapter Organization

The rest of this chapter is organized as follows. In Section 3.2 we describe our system model and define the integration of adaptive MCSs into our system model. Then, our problem formulation and solutions are presented in Section 3.3, while our experimental results characterizing a range of realistic application scenarios are discussed in Section 3.4. Finally, we conclude in Section 3.5.

3.2 System Model

In this section we first describe our network model in Section 3.2.1, which relies on a string-based network topology. Then, we provide the details of the channel and transmission scheduling models in Section 3.2.2. Finally, our NL definition is provided in Section 3.2.3.

3.2.1 Network Model

We consider V half-duplex sensor nodes in the string topology of Fig. 3.1, where the SN is linearly connected to the DN by relay nodes (RNs). This string topology is exemplified for $V = 10$ in Fig. 3.1. Given this simple network topology, $L = V - 1 = 9$ denotes the number of links. Unidirectional communication is considered between the links and omni-directional antennas are used by each node. Each link has only a single intended receiver. We denote the total number of TSs per TDMA frame by N.

3.2.2 Channel and MAC Layer Model

Each node can only transmit or receive in TS n. Due to the half-duplex nature of the transceivers, a receiver can only communicate with a transmitter over the shared wireless channel within the same TS. The channel gain of a link between the transmitter $i \in \{1, ..., V\}$ and receiver $j \in \{1, ..., V\}$ is given by $G_{i,j} = 1/\left(d_{i,j}\right)^m$, where $d_{i,j}$ is the geographic distance between the nodes i and j, while m is the path-loss exponent. Naturally, node i can only transmit at a limited power, which is lower than the maximum transmit power assigned to

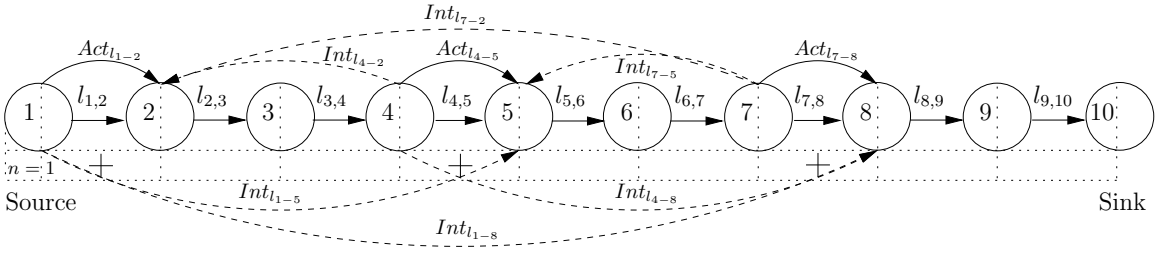

FIGURE 3.2: Interference model for 10-node string topology when $T = 3$.

that node. Each node has an initial battery energy that cannot be exceeded by the total ED of that node.

The LOS AWGN channel is defined by a certain propagation path-loss model and a fixed noise power at the receivers. The link quality is defined in terms of the SINR, which is denoted by Γ_l in the AWGN channel model and given by [181]

$$\Gamma_{l_{i,j},n} = \frac{G_{i,j} P_{l_{i,j},n}}{\sum_{i' \neq i, l_{i',j'} \in \mathcal{L}_n} G_{i',j} P_{l_{i',j'},n} + N_0}, \tag{3.1}$$

for a specific link l, where $P_{l_{i,j},n}$ denotes the transmit power of link l spanning from node i to node j in TS n and N_0 is the noise power at the receiver.

Additionally, for fading scenarios we assume a Rayleigh fading channel contaminated by the noise added at the receivers. A quasi-static fading or block-fading strategy is adopted here, where we keep the fading gain fixed for the whole duration of a transmission frame of the same link, which represents slow-fading channels. A modification of the SINR utilized in AWGN is necessary for formulating the SINR in Rayleigh fading channels, which is given by [184]

$$\widetilde{\Gamma}_{l_{i,j},n} = \frac{H_{i,j} G_{i,j} P_{l_{i,j},n}}{\sum_{i' \neq i, l_{i',j'} \in \mathcal{L}_n} H_{i',j} G_{i',j} P_{l_{i',j'},n} + N_0}, \tag{3.2}$$

where $H_{i,j} = |h_{i,j}|^2$ denotes the fading gain of the link between transmitter i and receiver j. Note that the SINR of each link in the network cannot be lower than the target SINR required for maintaining the target QoS, where the NL and the transmit power variables may vary. Given the SINR constraint and the deterministic path loss model, we can calculate the interference imposed on the intended receivers depending on the activated TS, as shown in Fig. 3.2. Three distinct types of communications occur over the string topology, namely $Act_{l_{1,2},1}$, $Act_{l_{4,5},1}$, $Act_{l_{7,8},1}$, where the actual communication taking place between node i and node j during the TS n is denoted by $Act_{l_{i,j},n}$, while their corresponding interferers are represented by $Int_{l_{i',j},n}$. For example, as illustrated in Fig. 3.2, the actual communication between node-1 (SN) and node-2 during the first TS is denoted by $Act_{l_{1,2},1}$. According to our transmission scheme $T = 3$ SPTS, the interfering nodes contaminating the reception of node-2 can be readily seen as node-4 and node-7 in Fig. 3.2, which is denoted by $Int_{l_{4,2},1}$

and $Int_{l_{7,2},1}$, respectively. More explicitly, when the transmitter of node-1 transmits to the receiver of node-2, node-4 and node-7 impose interference on node-2. Similarly, observe in Fig. 3.2 that $Act_{l_{4,5},1}$ is affected by the interferers $Int_{l_{1,5},1}$ and $Int_{l_{7,5},1}$, and $Act_{l_{7,8},1}$ is affected by the interferers $Int_{l_{1,8},1}$ and $Int_{l_{4,8},1}$. Having described the interference model, the total interference power at the receiver of node-2 is given by $P_{Int_{j=2}} = G_{4,2}P_{l_{4,5},1} + G_{7,2}P_{l_{7,8},1}$ and the received desired signal power at node-2 can be obtained by $P_{Rec_{j=2}} = G_{1,2}P_{l_{1,2},1}$. Upon considering a fixed noise power at the receiver, we can compute the SINR of link $l_{1,2}$ during the first TS for an AWGN channel as:

$$\Gamma_{l_{1,2},1} = \frac{P_{Rec_j}}{\sum_{w} P_{Int_j} + N_0} = \frac{G_{1,2}P_{l_{1,2},1}}{G_{4,2}P_{l_{4,5},1} + G_{7,2}P_{l_{7,8},1} + N_0}. \tag{3.3}$$

In Eq. (3.3), only two nodes interfere with node-2. However, this is a scenario, where more than three links are activated during the same TS, which requires the summation of all the interference power at the corresponding receiver node along with the fixed noise power. Eq. (3.3) can be generalized for a given string-topology based network in order to compute the SINR of any link in any TS, yielding

$$\Gamma_{l_{i,j},n} = \frac{G_{i,j}P_{l_{i,j},n}}{\sum_{i' \neq i, l_{i',j'} \in \mathcal{L}_n} G_{i',j}P_{l_{i',j'},n} + N_0}, \tag{3.4}$$

which defines the quality of the corresponding link. Therefore, we set $\Gamma_{l_{i,j},n} \geq \gamma$, so that the link quality is guaranteed for a given set of target SINR values of γ, which can be rewritten for an AWGN channel as follows,

$$\gamma \cdot \left(\sum_{i' \neq i, l_{i',j'} \in \mathcal{L}_n} G_{i',j}P_{l_{i',j'},n} + N_0 \right) - G_{i,j}P_{l_{i,j},n} \leq 0. \tag{3.5}$$

Similarly, it can be generalized for a Rayleigh block fading channel as follows,

$$\gamma \cdot \left(\sum_{i' \neq i, l_{i',j'} \in \mathcal{L}_n} H_{i',j}G_{i',j}P_{l_{i',j'},n} + N_0 \right) - H_{i,j}G_{i,j}P_{l_{i,j},n} \leq 0. \tag{3.6}$$

We rely on the SPTS technique of [30] for modeling periodic transmit-TS-activation-scheduling, where we consider a distance of T between pairs of nodes, which are transmitting in the same TS. The same TSs are reactivated after every T TSs. Fig. 3.1 illustrates the SPTS for $T = 3$, where $[n = 1, n = 2, n = 3, ..., n = N]$ describes each TS n for a given N-TS TDMA frame per link and "+" denotes the active links. For example, during the first TS, links $l_{1,2}$, $l_{4,5}$, $l_{7,8}$ are scheduled for simultaneous transmissions, which only moderately interfere with each other and each link is activated only once during the whole TDMA frame. For simplicity in our system model, we use $T = 3$ in our SPTS-aided interference-limited scenario.

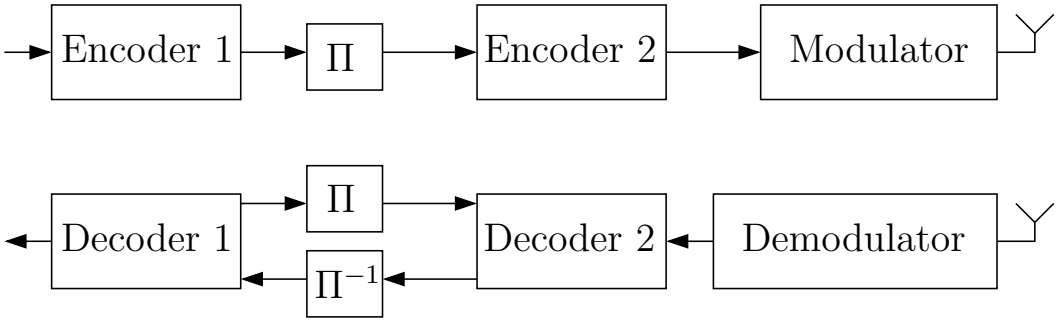

FIGURE 3.3: Block diagram of the iteratively decoded system.

We model the physical layer for the sake of characterizing the upper layers with the aid of a BER-SINR look-up table (LUT) relationship for the system model considered, which provides us with the SINR value required for maintaining a given target BER. Note that we consider the interference to be noise-like in the SINR calculation[1]. Explicitly, in this contribution we consider an uncoded BPSK modulated system and a 1/2-rate convolutional coded (CC) hard-decoded[2] [202] as well as soft-decoded[3] [202] QPSK scheme communicating over an AWGN channel. We also consider the BER-SINR LUTs of our iterative decoding aided system, as shown in Fig. 3.3 for 1/2-rate serially concatenated codes (SCCs) using 1, 5 and 10 decoding iterations, where the 1st iteration corresponds to the 1/2-rate-CC-Soft QPSK MCS [203]. We can determine the NL of any of the different MCSs by relying on their BER-SINR LUT for the system considered. Note that we invoke a decode and forward (DF) scheme in two different scenarios. In the first scenario we neglect the ED of the coding and decoding operations, which we refer to as *Scenario 1* in our forthcoming analysis. On the other hand, in the second scenario we include both the coding and decoding ED in our analysis, which we refer to as *Scenario 2*. Therefore, *Scenario 1* constitutes a benchmark of the NL, since it only considers the transmit power, hence giving us the best possible NL we can achieve. However, *Scenario 2* is a more realistic one, where we additionally consider the SPP. Therefore, we can evaluate the NL difference between the best case and the realistic scenarios. The SPP is modeled by the signal processing ED considered in [183]. At the DN, all ED is ignored, since we assume that the DN is plugged into the mains power source. The action of the BER-SINR LUT of the system model considered for both the AWGN and Rayleigh fading channels can be observed in Fig. 3.4 and Fig. 3.5, respectively.

[1]Since in practice WSNs rarely encounter a single dominant interferer, the interference is typically constituted by the sum of several interfering components, which allows us to approximate the interference by noise.

[2]Hard decoding compares the individual bits of the received bit sequence with all possible codewords with the aid of the Hamming distance approach.

[3]Soft decoding compares the received codeword with all possible codewords with the aid of the minimum Euclidean distance approach in order to attain a measure of confidence in terms of probabilities.

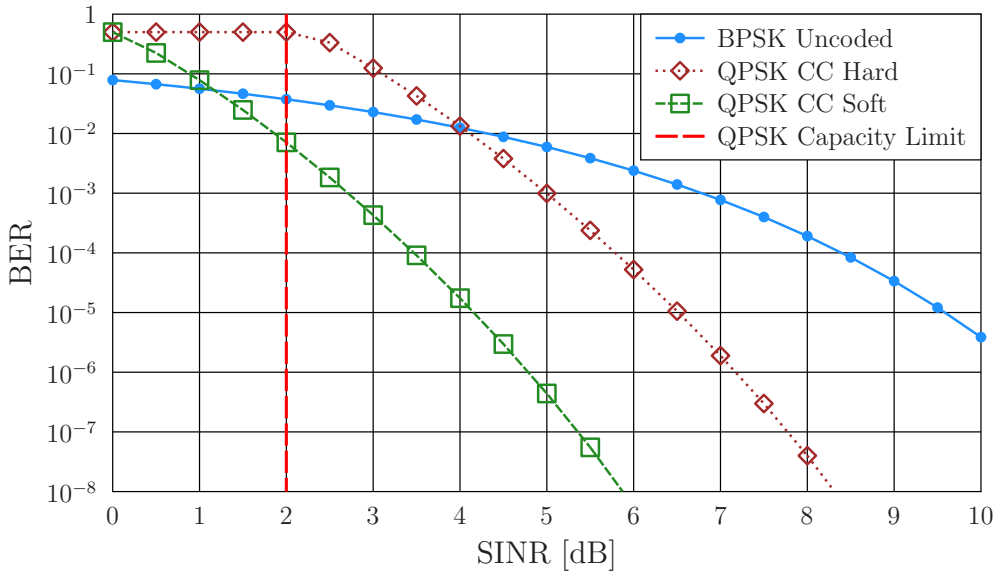

FIGURE 3.4: BER versus SINR [dB] for an AWGN channel.

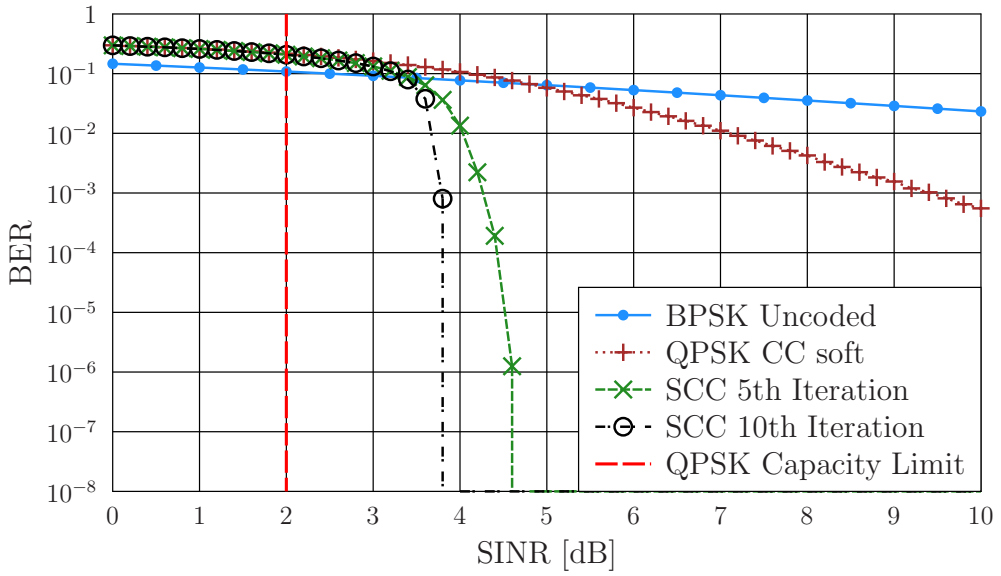

FIGURE 3.5: BER versus SINR [dB] for an independently Rayleigh block fading channel.

3.2.3 Network Lifetime Model

The network lifetime may be interpreted differently, depending on the specific application, as mentioned in [64,106,185,204]. For example, the NL may be maximized by incorporating energy awareness into each individual node [205]. Moreover, an optimal hop-length was obtained by the simultaneous computation of the optimal transmission power, the optimal SNR and the optimal BER in a Rayleigh fading environment in [206]. Specifically, Zhang *et al.* [206] demonstrated that in a relay-aided scheme, optimizing the hop-length is capable of significantly extending the NL. In our study, T_i is the lifetime of an individual node in the network, which corresponds to the time instant, when node i has completely discharged

its battery. The NL is then defined as the earliest time instant, at which any of the nodes drains its battery, which is given by $T_{net} = \min_{i \neq V, i \in \mathcal{V}} T_i$.

3.3 Problem Formulation

Having described the system model in Section 3.2, the NL maximization problem [30] can be formulated as

$$\text{max.} \quad T_{net} \tag{3.7}$$

$$\text{s.t.} \quad \Gamma_{l_{i,j},n} \geq \gamma, \, \forall n, l_{i,j} \in \mathcal{L}_n, \tag{3.8}$$

$$\frac{T_{net}}{N} \sum_{n=1}^{N} \left(\sum_{l \in \mathcal{O}(i) \cap \mathcal{L}_n} \Big((1 + (1 - \alpha)) \cdot P_{l_{i,j},n} + P_{sp} \Big) \right) \preceq \mathcal{E}_i, \, \forall i, \tag{3.9}$$

$$0 \preceq P_{l_{i,j},n} \preceq (P_i)_{max}, \, \forall n, i. \tag{3.10}$$

The links that are active in TS n are denoted by the set $\mathcal{L}_n$. The specific variables of the optimization problem are T_{net} and $P_{l,n}$ for $l \in \mathcal{L}_n$, $n = 1, \cdots, N$, where we have $N = 3$ TSs, say $l_{1,2}$, $l_{4,5}$ and $l_{7,8}$, per link. We assume that any operation other than the transmission and signal processing in the network incurs a negligible ED. The power amplifier's efficiency is denoted by α [190], while $l \in \mathcal{O}(i)$ and $l \in \mathcal{I}(i)$ represent the transmit link and the receive link of node i, respectively. Furthermore, $\{i : i \in \mathcal{O}^{-1}(l), \, l \in \mathcal{L}_n\}$ in (3.12) describes the set of nodes, where the transmit links are connected and activated in the same TS.

We can readily transform the NL maximization problem into the minimization of the reciprocal of the NL, which is formulated as $z = \frac{1}{T_{net}}$ by using a change of variable in order to avoid multiplication of the pair of optimization variables, which is generally non-convex, as exemplified in (3.9). We note that since each sensor forming part of the string-topology has a positive initial battery energy, and hence each node transmits at least for a certain amount of time, T_{net}, which is higher than zero. The energy preservation constraint of each node is formulated in (3.9), which represents how the initial battery energy $\mathcal{E}_i$ can be dissipated as a function of the system parameters, until the battery is discharged. Therefore, to transform the optimization problem into a convex one, (3.7)–(3.10) are rewritten as

$$\text{min.} \quad z \tag{3.11}$$

$$\text{s.t.} \quad \gamma \Big(\sum_{i' \neq i, l_{i',j'} \in \mathcal{L}_n} G_{i',j} P_{l_{i',j'},n} + N_0 \Big) - G_{i,j} P_{l_{i,j},n} \leq 0, \, \forall n, \{i : i \in \mathcal{O}^{-1}(l), \, l \in \mathcal{L}_n\}, \tag{3.12}$$

$$\sum_{n=1}^{N} \left(\sum_{l \in \mathcal{O}(i) \cap \mathcal{L}_n} \Big((1 + (1 - \alpha)) \cdot P_{l_{i,j},n} + P_{sp} \Big) \right) - z \cdot \mathcal{E}_i \cdot N \leq 0, \, \forall i, \tag{3.13}$$

$$0 \leq P_{l_{i,j},n} \leq (P_i)_{max}, \, \forall n, i, l_{i,j} \in \mathcal{L}_n, \tag{3.14}$$

where (3.8) and (3.12) represent the lower bound of the signal quality required for each link with a range of target SINR values, which are denoted by γ. The maximum affordable transmit power of a node is given by (3.14). As a result, using (3.5) the general optimization problem for an AWGN channel is provided in (3.11)–(3.14).

Similarly, when considering the effect of the fading on the link quality based on (3.6) we can generalize the NL maximization problem for a block fading channel as

$$\text{min.} \quad z \tag{3.15}$$

$$\text{s.t.} \quad \gamma\Big(\sum_{i'\neq i, l_{i',j'}\in\mathcal{L}_n} H_{i',j}G_{i',j}P_{l_{i',j'},n}+N_0\Big)-H_{i,j}G_{i,j}P_{l_{i,j},n}\leq 0, \forall n, \{i : i \in \mathcal{O}^{-1}(l), l\in\mathcal{L}_n\}, \tag{3.16}$$

$$\sum_{n=1}^{N}\left(\sum_{l\in\mathcal{O}(i)\cap\mathcal{L}_n}\Big((1+(1-\alpha))\cdot P_{l_{i,j},n}+P_{sp}\Big)\right)-z\cdot\mathcal{E}_i\cdot N\leq 0,\ \forall i, \tag{3.17}$$

$$0\leq P_{l_{i,j},n}\leq (P_i)_{max},\ \forall n, i, l_{i,j}\in\mathcal{L}_n. \tag{3.18}$$

Our optimization problem is solved with the aid of the interior point method described in [191], which can be used for solving both linear and non-linear convex optimization problems, for each link of a spatially periodic link schedule defined by the specific SPTS considered for the string network topology of Fig. 3.1.

3.4 Performance Results

In this section we analyze the NL of both *Scenario 1* and of *Scenario 2* versus the attainable BER performances for different MCSs under both AWGN and Rayleigh fading channels. We compute two types of BER performances. The first one is the PLBR, which defines the BER value attained by the weakest link. This represents the worst BER that can be tolerated over the links. In other words, the BER of each link must be lower than the PLBR. By contrast, the E2EB is defined as the BER accumulated along the route spanning from the SN to the DN, which is calculated as

$$BER_{end} = 1 - \prod_{l=1}^{V-1}\left(1 - BER_l\right), \tag{3.19}$$

where BER_l is a function of the SINR ($BER_l = f_{MCS}[SINR_l]$) that may be fetched from the LUT selected for the specified MCS and $(V-1)$ is the number of links along the route. Each target SINR returns $(V-1)$ number of actual link SINRs and each link SINR corresponds to a BER value read from the given LUT. Finally, the $(V-1)$ BERs provide us with a single accumulated E2EB. A PLBR, an E2EB and a single NL value are hence computed for each corresponding target SINR. The experimental results are for 'continuous-time' NL, which corresponds to the NL obtained by continuous transmission.

TABLE 3.1: System parameters used in our simulations.

Simulation parameter	Value
Path loss exponent, m	3
Geographic distance between consecutive nodes, d [m]	30
Noise power, N_0 [dBm]	-60
Initial energy per node, $\mathcal{E}_i$ [Joule]	5000
Maximum affordable transmit power of a node, $(P_i)_{max}$ [mW]	10 [207]
Number of slots per frame, N	3
Number of nodes, V	10
Number of links, $V-1$	9
Efficiency of the power amplifier, α	0.6 [190]
SPTS parameter, T	3
SPP, P_{sp} [mW]	0.44 [183]
Number of trials for fading scenario, τ_{fading}	2000

For our simulations, we use the system parameters of Table 3.1 for both the AWGN and Rayleigh fading channels of *Scenario 1* and *2*. The initial battery energy per node is $\mathcal{E}_i = 5000$Joule, which corresponds to the capacity of an AAA alkaline long-life battery. Additionally, the SPP utilized in *Scenario 2* is $P_{sp} = 0.44$mW [183] and the number of simulation trials used for the fading scenario is $\tau_{fading} = 2000$.

3.4.1 NL vs BER for an AWGN Channel

We present our NL results for *Scenario 1* and *2* versus the PLBR and E2EB for uncoded BPSK, as well as for hard-decoded and soft-decoded 1/2-rate CC QPSK MCSs for transmission over an AWGN channel in Fig. 3.6 and Fig. 3.7, respectively. Note that in all figures, BER values higher than 10^{-3} are deemed to be inadequate for practical application scenarios. They are only illustrated for the sake of highlighting the explicit trade-offs between the NL and the BER performances. Again, in *Scenario 1* we first neglect the SPP and then include it in the analysis of *Scenario 2*, which we refer to by using the notation of SPP-X in Fig. 3.6 and Fig. 3.7. These figures show that as expected, the NL decays, when requiring a reduced target BER, since the transmit power must be increased to achieve the target BER and vice versa. Having illustrated the trade-off between the NL and both the PLBR and the E2EB in Fig. 3.6 and Fig. 3.7, respectively, the designer can decide upon the optimal

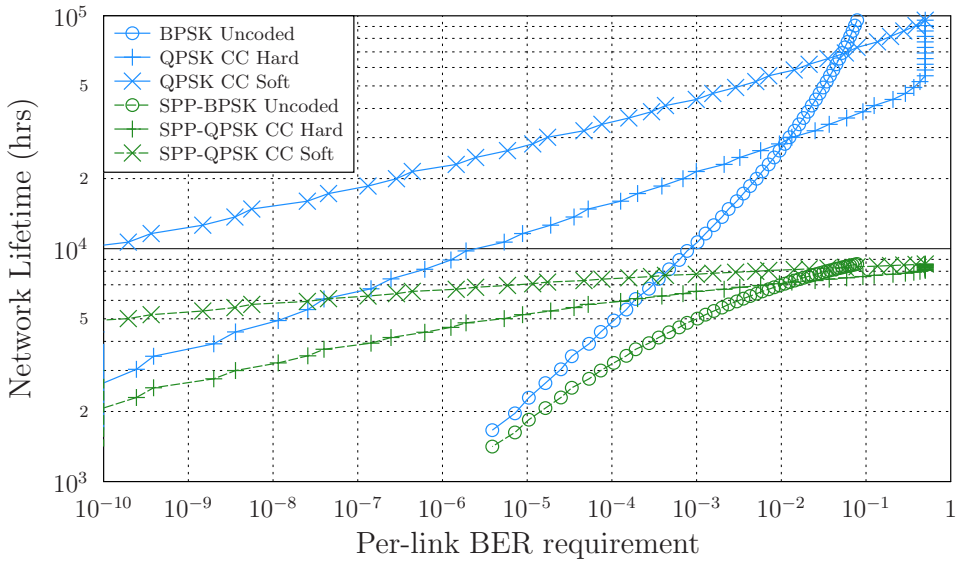

FIGURE 3.6: NL for *Scenario 1* and *Scenario 2* versus PLBR for uncoded BPSK as well as for both hard-decoded and soft-decoded 1/2-rate CC QPSK MCSs under AWGN channel.

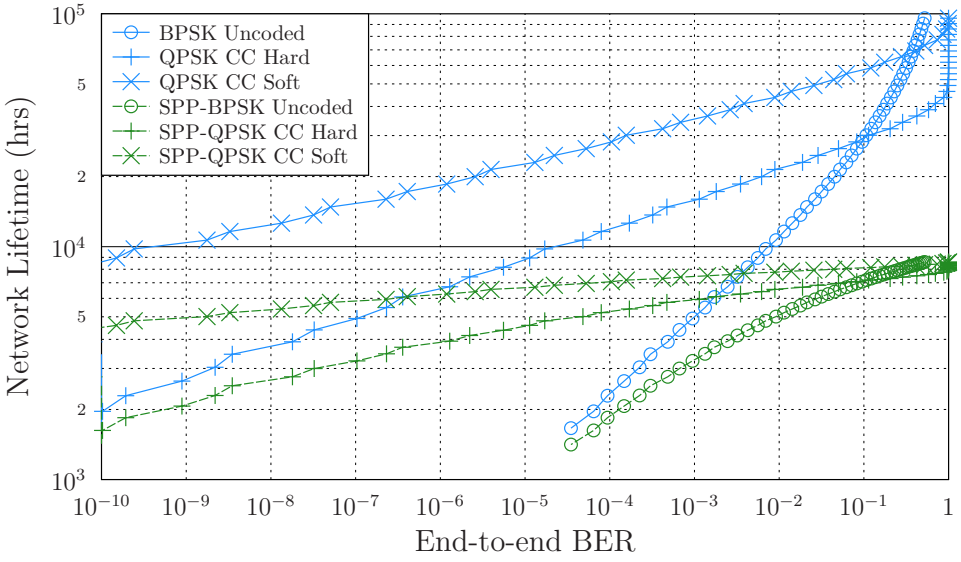

FIGURE 3.7: NL for *Scenario 1* and *Scenario 2* versus E2EB for uncoded BPSK as well as for both hard-decoded and soft-decoded 1/2-rate CC QPSK MCSs under AWGN channel.

choice of MCS for maximizing the NL. In *Scenario 1*, when aiming for a target BER of 10^{-3}, the best NL is achieved by the soft-decoded 1/2-rate CC QPSK MCS, which is about 43773 hours (hrs) = 4.99 years (yrs) in terms of the PLBR and 35140hrs = 4yrs in terms of the E2EB for an AWGN channel. On the other hand, considering the more realistic *Scenario 2*, and hence including the SPP in the analysis, the achievable NL is reduced to 0.89yrs for PLBR and to 0.85yrs for E2EB. The lowest NL for an AWGN channel and a PLBR of 10^{-3} is attained by the uncoded BPSK in *Scenario 2*, which is about 0.57yrs, and it increases to 1.2yrs of NL, where we only consider the transmit power in *Scenario 1*.

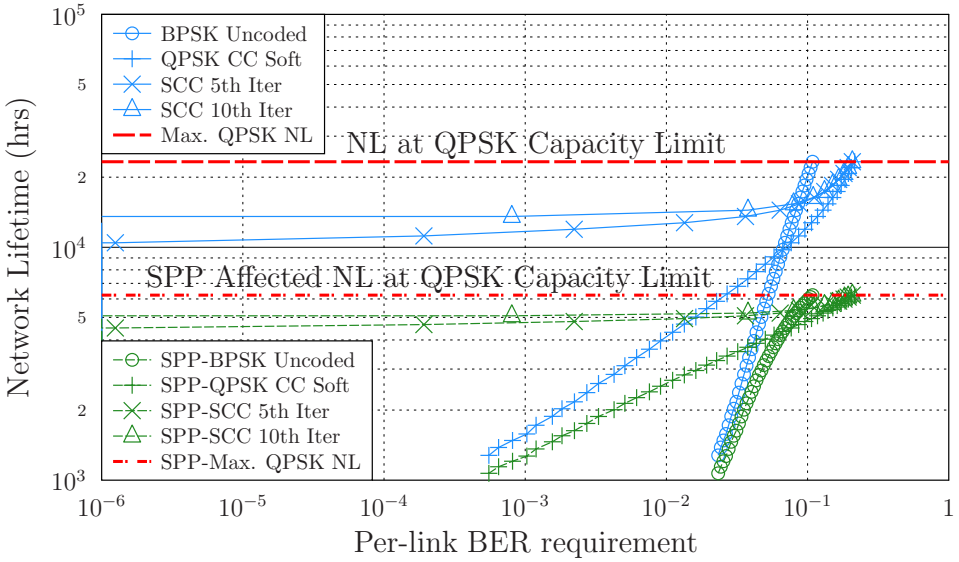

FIGURE 3.8: NL for *Scenario 1* and *Scenario 2* versus PLBR for uncoded BPSK and the maximum achievable NL for soft decoded 1/2-rate CC QPSK and 1/2-rate SCC using 5 and 10 decoding iterations with QPSK for a Rayleigh fading channel.

3.4.2 NL vs BER for Rayleigh Fading Channels and the Maximum Achievable NL

Let us now consider the NL of *Scenario 1* and *2* versus the PLBR and E2EB for uncoded BPSK, as well as the upper bound of the NL for soft decoded 1/2-rate CC, and 1/2-rate SCC [203] using 5 and 10 decoding iterations in conjunction with QPSK MCSs for Rayleigh fading channels in Fig. 3.8 and Fig. 3.9, respectively. Upon comparing Fig. 3.8 and Fig. 3.9 for the same NL values, the E2EB is seen to be substantially higher than the PLBR due to the bit errors accumulated, while relaying the information bits over intermediate nodes all the way, through to the DN. For a target BER of 10^{-3}, the best NL for *Scenario 1* is achieved by 1/2-rate SCC using 10 decoding iterations for QPSK MCS, which is about 1.55yrs in terms of the PLBR under Rayleigh fading channels, whereas upon considering the SPP of *Scenario 2* about 0.58yrs of NL is achieved for the same PLBR. The maximum NL that can be achieved is approximately 2.66yrs in *Scenario 1*, while in *Scenario 2*, the maximum achievable NL is reduced to 0.71yrs, which is computed according to the SINR that corresponds to the capacity limit of the QPSK system considered.

3.4.3 Network Analysis Without SPP Considering Low and High Target SINR Values

In this section, we analyze both the ED of each node as well as the required transmission power per link, the interference power experienced by each node and the lifetime of all nodes forming part of the string-topology for the target SINR values of $\gamma = 2$dB and $\gamma = 10$dB

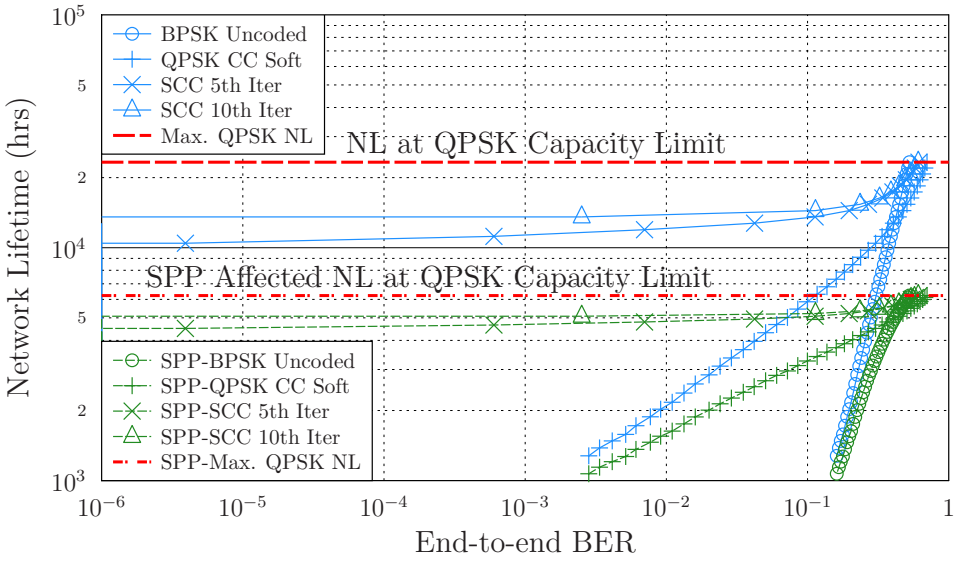

FIGURE 3.9: NL for *Scenario 1* and *Scenario 2* versus E2EB for uncoded BPSK and the maximum achievable NL for soft decoded 1/2-rate CC QPSK and 1/2-rate SCC using 5 and 10 decoding iterations with QPSK for a Rayleigh fading channel.

determining the QoS, while operating over an AWGN channel and without considering the SPP. Fig. 3.10 portrays the average required transmit power versus sequential unique index number of each link[4], as seen in Fig. 3.1, when the target SINR values are $\gamma = 2$dB and $\gamma = 10$dB, respectively. Due to the target SINR constraint of (3.12), the required transmit power is proportional to the predetermined target SINR. Therefore, when the network operates at a $\gamma = 10$dB target SINR QoS requirement, the required transmit power becomes much higher than that in the $\gamma = 2$dB scenario. We can readily observe these substantial transmit power differences of both cases for each node in Fig. 3.10. This also explains why the ED is much higher for the $\gamma = 10$dB scenario in Fig. 3.11. Observe in Fig. 3.11 that the total ED of the $\gamma = 2$dB scenario is higher than the $\gamma = 10$dB scenario, where the first three nodes of Fig. 3.1 depleted their batteries first in both cases. However, the ED of the rest of the nodes is much higher for the $\gamma = 2$dB scenario. This is because the ED of $\gamma = 10$dB is much higher than that of $\gamma = 2$dB. In the $\gamma = 10$dB case, the first three nodes' batteries are depleted much quicker than for the $\gamma = 2$dB case. Therefore, in the $\gamma = 10$dB scenario the other nodes still have a higher residual energy in their batteries compared to the $\gamma = 2$dB case, since the NL is determined by the earliest battery depletion. Moreover, Fig. 3.12 shows how rapidly a battery is depleted, where the lifetime of the first three nodes determines the NL for both cases, respectively. Lastly, the interference power imposed on each node is illustrated in Fig. 3.13, where the first three nodes of Fig. 3.1 are exposed to the highest amount of interference for the $\gamma = 10$dB case, whereas for the $\gamma = 2$dB case the first 6 nodes are exposed to the highest amount of interference. To summarize, the optimal transmit power required is increased due to the interference power

[4]In our analysis, *Links* and *Nodes* on the x-axis are referred to as the sequential unique index number of each sensor node forming part of the string-topology that is illustrated in Fig. 3.1.

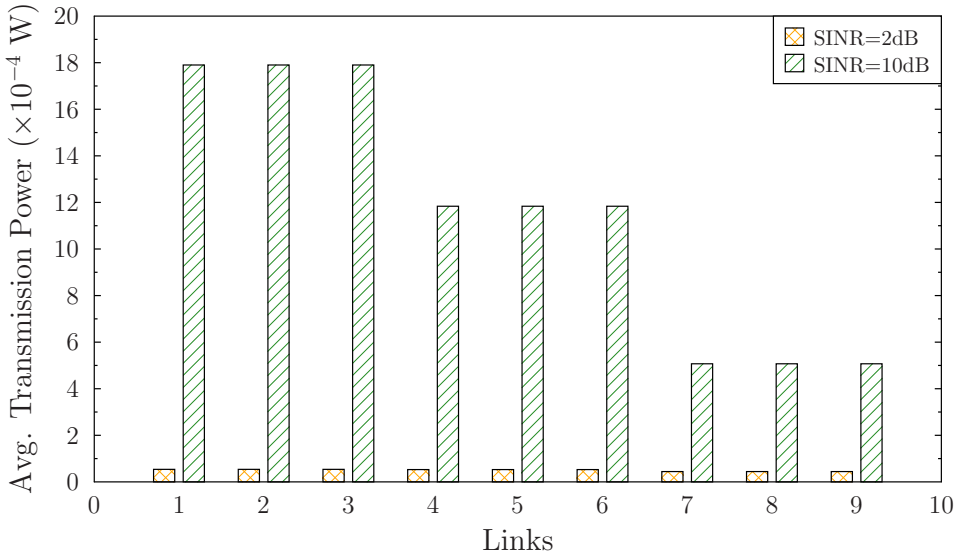

FIGURE 3.10: Average transmission power per link for target SINR values of $\gamma = 2$dB and $\gamma = 10$dB.

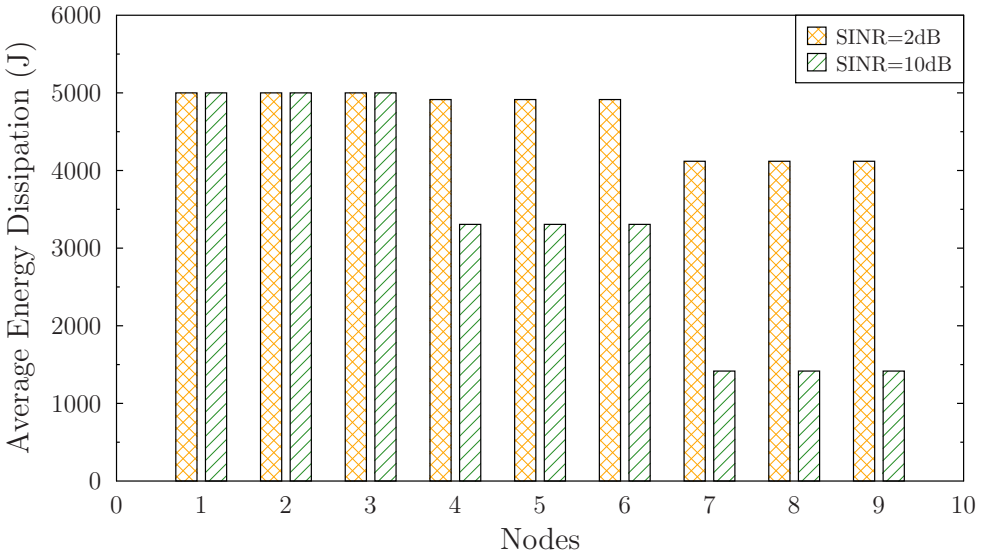

FIGURE 3.11: Average ED of each node for target SINR values of $\gamma = 2$dB and $\gamma = 10$dB.

imposed on a particular node when aiming to satisfy the target SINR QoS requirement, which results in a higher ED for that node. Hence, the lifetime of a node is reduced and the minimum lifetime amongst all nodes forming part of a string-topology based network determines the NL.

3.4.4 Network Analysis Considering the Impact of the SPP

Let us now analyze the effect of the SPP further on the ED of each node as well as the required transmission power per link, the interference power imposed on each node and the lifetime of all nodes forming part of the string-topology for a target SINR of $\gamma = 2$dB, while

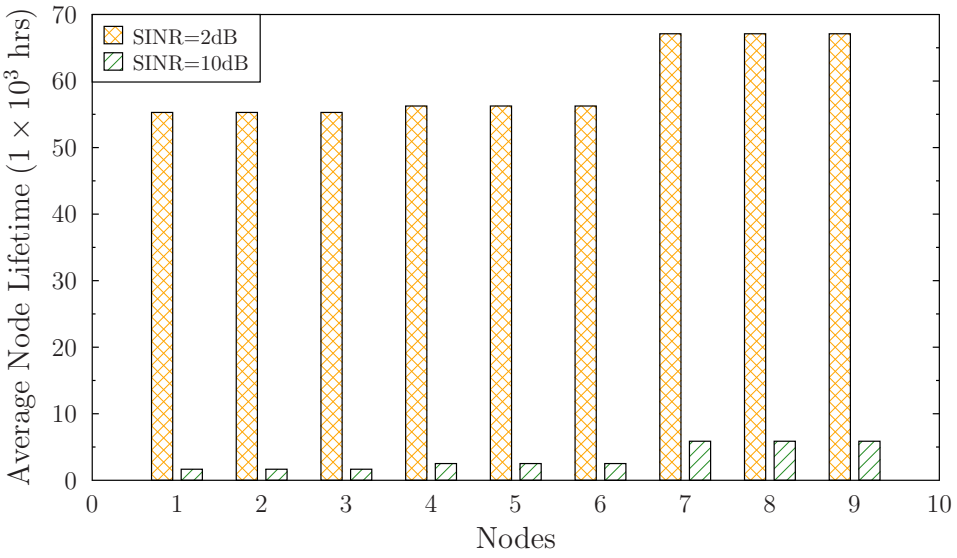

FIGURE 3.12: Average lifetime of each node for target SINR values of $\gamma = 2$dB and $\gamma = 10$dB.

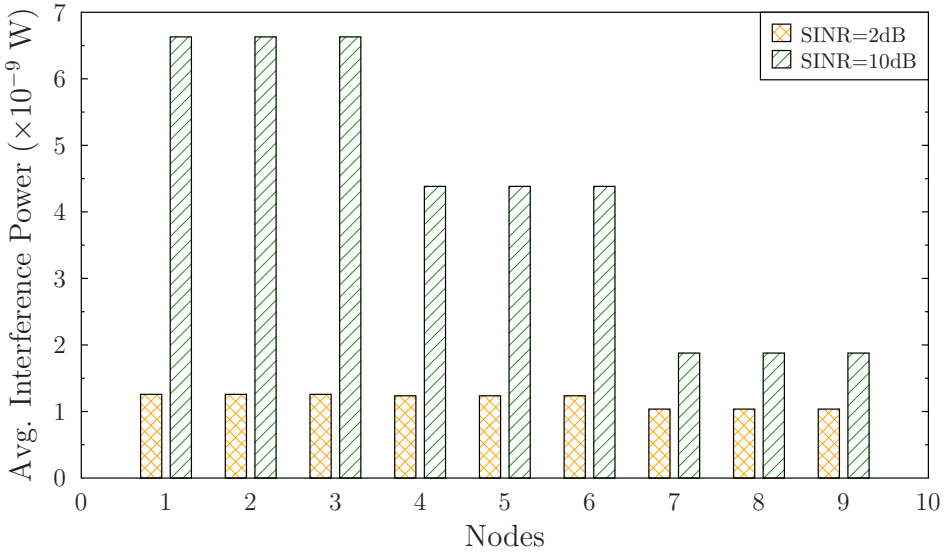

FIGURE 3.13: Average interference power imposed on each node for target SINR values of $\gamma = 2$dB and $\gamma = 10$dB.

operating over an AWGN channel. Therefore, we compare the scenario, where we neglect the SPP, to the explicit consideration of the SPP. Considering (3.12) and (3.13), we can readily see that the effect of the SPP is independent of the that imposed by the transmit power and the interference power. We can observe this trend both from Fig. 3.14 and Fig 3.17, where each link requires the same optimal transmit power, when the interference power imposed on all nodes is similar. One noticeable result is that the ED rate for SPP case becomes similar for each node. Explicitly, all the nodes approximately deplete their battery energy at the same time. This is mainly due to the dominant impact of the SPP compared to that of the required transmit power, where a lower target SINR QoS requirement results in a

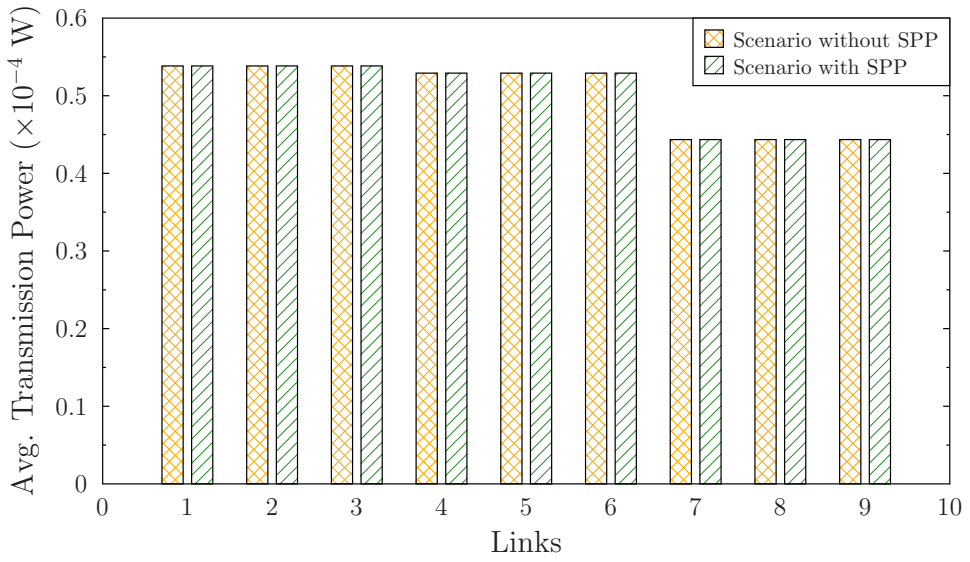

FIGURE 3.14: Average transmission power per link in the absence and in the presence of SPP.

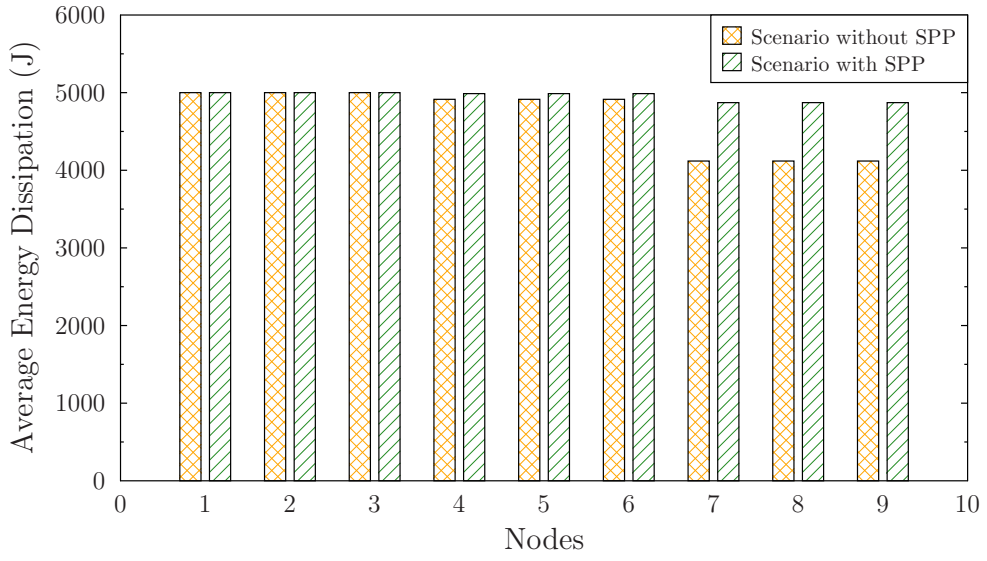

FIGURE 3.15: Average ED of each node in the absence and in the presence of SPP.

lower required transmit power. We can also see the same pattern by checking the lifetime of every node lying in the string topology from Fig. 3.16, where the lifetime of each node is reduced compared to that of the case without SPP, and hence the lifetime of all nodes becomes similar. Fig. 3.16 also presents the substantial impact of the SPP on the lifetime of all the nodes in the network, where the lifetime of each node is declined by about $7 - 8$ times.

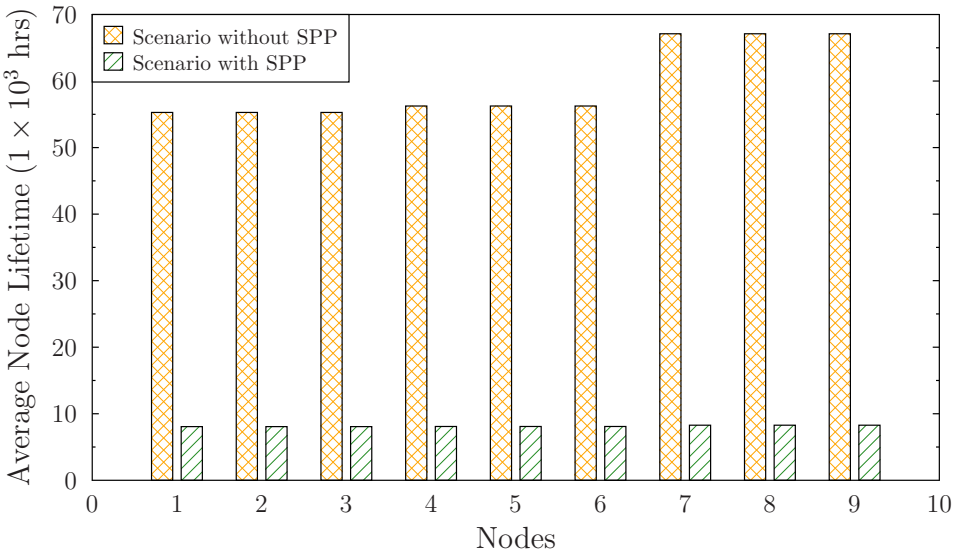

FIGURE 3.16: Average lifetime of each node in the absence and in the presence of SPP.

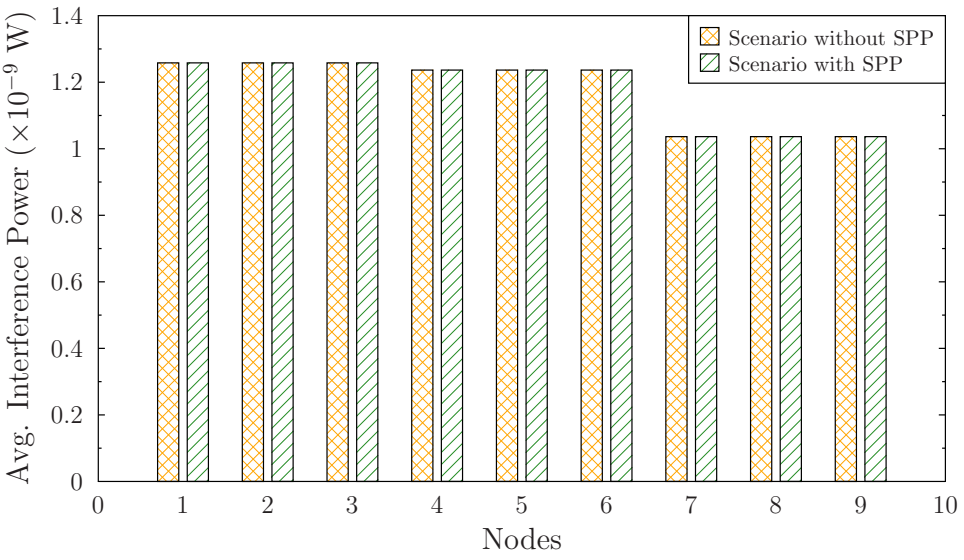

FIGURE 3.17: Average interference power imposed on each node in the absence and in the presence of SPP.

3.4.5 Network Analysis Considering Channel Characteristics

We also examine the effect of both the channel characteristics on the ED of each node as well as of the transmission power per link, the interference power imposed on each node and the lifetime of all nodes forming part of the string-topology for a target SINR of $\gamma = 2$dB, while considering the scenario without SPP. We present our results both for AWGN and Rayleigh fading channels. Fig. 3.18 illustrates the transmission power per link required for both AWGN and fading channels, which is about 2.9 times higher than to that of the AWGN channel. This increase in the transmit power is required for overcoming the detrimental impact of the fading and of the interference, while satisfying the target SINR requirement.

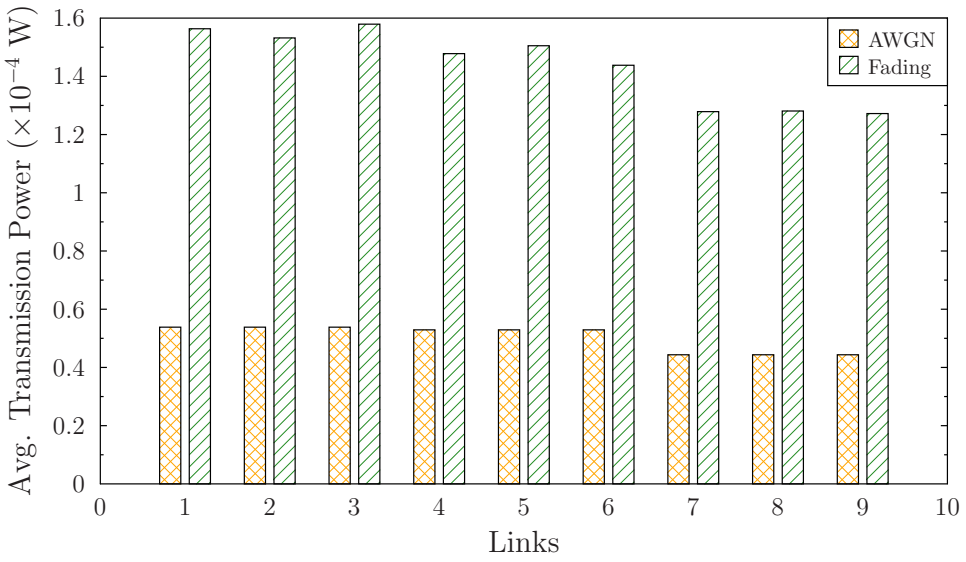

FIGURE 3.18: Average transmission power per link, when the network operates over AWGN and fading channels.

Observe in Fig. 3.19 that the first three nodes of Fig. 3.1 drain their battery faster than the rest of the nodes for the AWGN channel. For fading channels, the amount of ED per node is accumulated as well as averaged over several fading trials and the result is normalized to the maximum amount of energy that can be depleted per node (5000J) in Fig. 3.19. Therefore, we can claim that on average the first three nodes of Fig. 3.1 tend to dissipate their battery energy faster than the other nodes in fading channels. Moreover, the interference power imposed on each node is illustrated in Fig. 3.21, where the first three nodes of Fig. 3.1 were exposed to the highest amount of interference for both AWGN and fading channels, since their receiver nodes are closer to their potential interferers, when compared to the rest of the nodes. Consequently, the lifetime of each node is reduced by a factor of 1.45 to 1.61 due to the fading channel characteristics, which can be explicitly seen in Fig. 3.20.

3.4.6 Discussions

Again, the results of Figs. 3.6 to 3.9 illustrated that the NL is reduced upon reducing the target BER, which is owing to the increased transmit power required. More explicitly, the NL becomes undesirably short for low target BER values, which is due to the increased transmit power required to satisfy the target BER. As expected, the NL is longer for an AWGN channel than for a Rayleigh fading channel for the same SINR values and configurations due to the higher ED required for combating the deleterious effects of fading. Hence, provided that the application considered is capable of tolerating a higher BER, the NL becomes higher due to requiring a lower SINR value. Furthermore, the NL is substantially reduced due to the accumulated ED of SPP and transmit power. In other words, when considering higher target BER values requiring lower SINRs, the transmit power becomes negligible compared

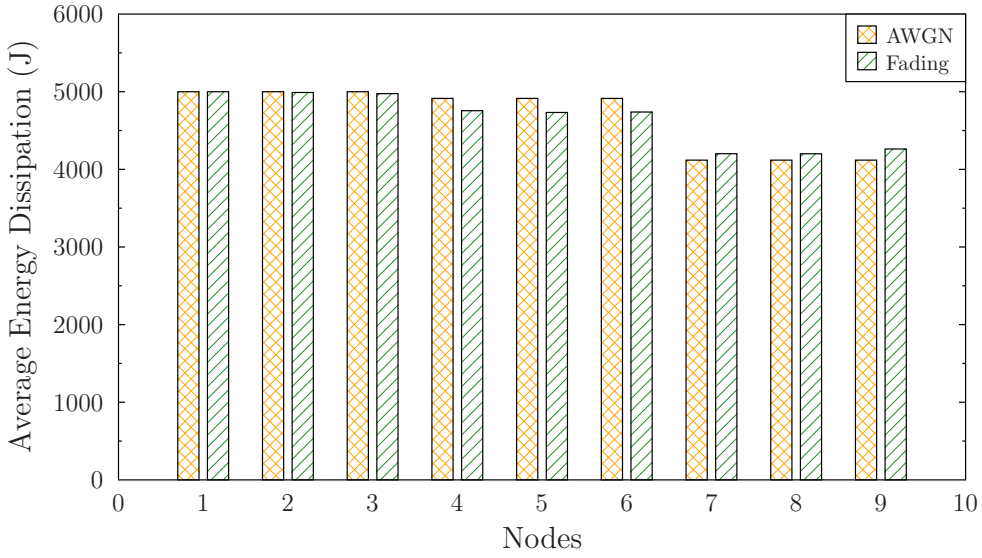

FIGURE 3.19: Average ED of each node, when the network operates over AWGN and fading channels.

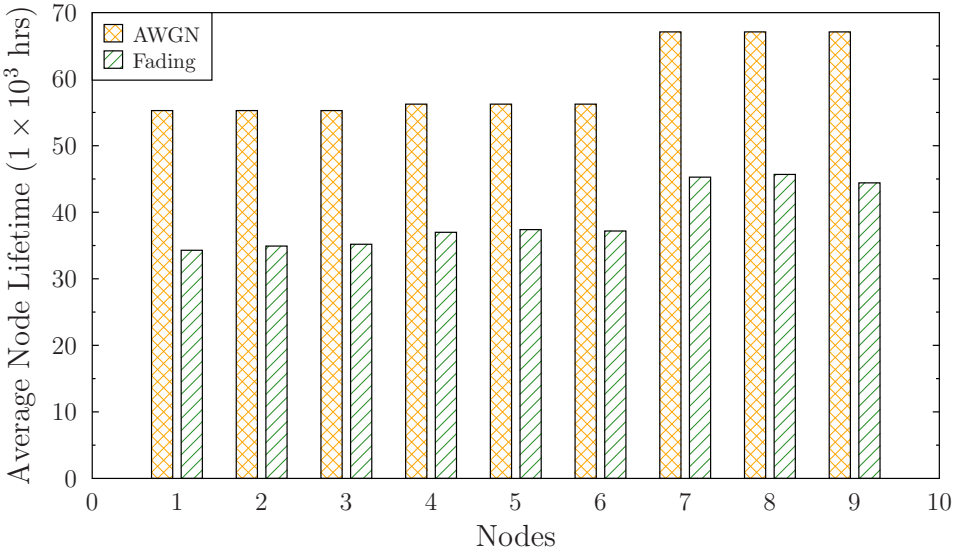

FIGURE 3.20: Average lifetime of each node, when the network operates over AWGN and fading channels.

to the SPP. This is why there is a substantial difference between the NL values of *Scenario 1* and *2* at higher BER values. On the other hand, when considering lower target BER values, the required transmit power increases and it becomes more dominant than the SPP in the analysis and this is why the difference between the NL values of *Scenario 1* and *2* reduces, as the BER reduces. Nonetheless, when aiming for achieving the same target PLBR and E2EB, the NL is always shorter for E2EB due to the higher SINR required, which necessitates a higher transmit power. It is observed that for an AWGN channel and for both a PLBR as well as for an E2EB of 10^{-3}, 1/2-rate CC soft-decoded QPSK doubles the NL of its hard-decoded counterpart, when we ignore the SPP. Similarly, it has an up to four times longer NL than uncoded BPSK for an AWGN channel and a PLBR of 10^{-3}, when

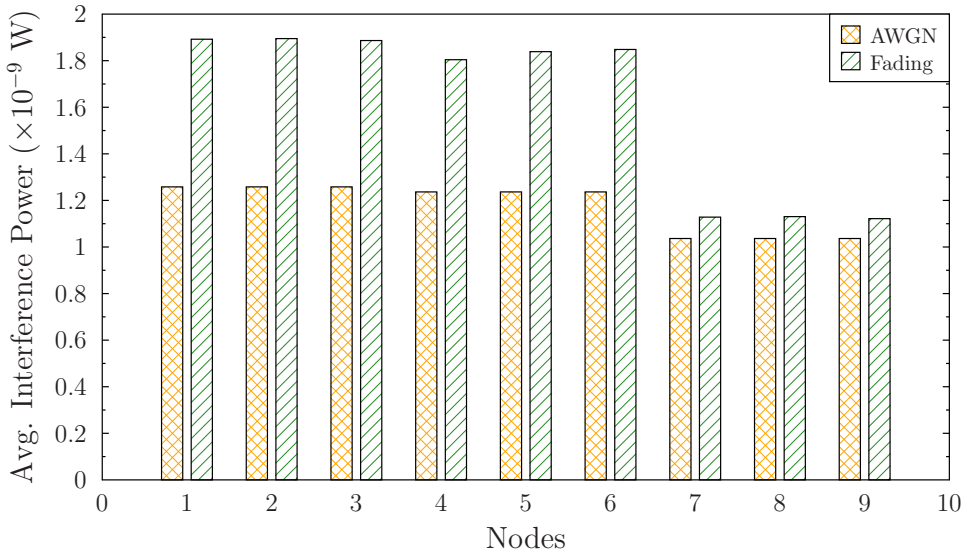

FIGURE 3.21: Average interference power imposed on each node, when the network operates over AWGN and fading channels.

TABLE 3.2: The 'continuous-time' NL (in years) evaluation for WSNs with given configurations.

	Scn 2	Scn 1	Scn 2	Scn 1	Scn 2	Scn 1	Scn 2	Scn 1	
	10^{-4} PLBR		10^{-4} E2EB		10^{-3} PLBR		10^{-3} E2EB		AWGN
Uncoded-BPSK	0.36	0.55	0.21	0.27	0.57	1.2	0.37	0.57	
QPSK-CC-Soft	0.85	3.97	0.80	3.20	0.89	4.99	0.85	4.00	
QPSK-CC-Soft	0.30	0.47	0.18	0.24	0.14	0.18	–	–	Fading
SCC-10th-Iter	0.58	1.57	0.58	1.55	0.58	1.55	–	–	
	10^{-2} PLBR		10^{-2} E2EB		10^{-3} PLBR		10^{-3} E2EB		

only considering the transmit power. On the other hand, when the more realistic scenario of including the SPP in the analysis is considered, the 1/2-rate CC soft-decoded QPSK has a factor of 1.2 higher NL than its hard-decoded counterpart at a PLBR and E2EB of 10^{-3}, while achieving a 1.5 times higher NL for a PLBR of 10^{-3} and 2.3 times more NL for a E2EB of 10^{-3} than uncoded BPSK.

Table 3.2 presents the 'continuous-time' NL, in years for different MCSs and different target BER values in terms of both the PLBR and E2EB, and provides an overview of the systems, indicating both the longest and the shortest NL in *Scenario 1* and *2* for both AWGN and fading channels, where '*Scenario*' is abbreviated by 'Scn'. Therefore, the designer can readily determine, which systems and configurations are more NL-aware for a realistic application.

For example, observe in Table 3.2 that the longest NL is achieved for an AWGN channel by soft decoded 1/2-rate CC for a PLBR of 10^{-4} in *Scenario 1*, which is nearly 3.97yrs. By contrast, the lowest NL for an AWGN channel is accomplished by uncoded BPSK at a E2EB of 10^{-4} in *Scenario 2*, which is about 0.21yrs. Uncoded BPSK results in an even lower NL in a Rayleigh fading scenario, but the exact PLBR and E2EB values cannot be provided, since this would require an excessive transmit power. The longest NL is achieved for Rayleigh fading channels by 1/2-rate SCC using 10 decoding iterations at a PLBR of 10^{-2} in *Scenario 1*, which corresponds to NL=1.57yrs. Nonetheless, up to 4.99yrs of NL can be accomplished by soft decoded 1/2-rate CC for a PLBR of 10^{-3} for AWGN channels in *Scenario 1*, which is reduced to 0.18yrs for Rayleigh fading channels.

We have shown how the requirement of different target BER values at the physical layer affected both the NL and the network performance in the string topology considered. We also illustrated the dominant impact of the SPP on the NL compared to that of the transmission power. A useful further investigation would be to ascertain, what type of modulation schemes should be used for what type of networks or applications. Therefore, depending on the QoS requirements, the network designer can make beneficial decisions for specific systems, depending on the network performance required.

3.5 Chapter Summary and Conclusions

We evaluated the NL for both *Scenario 1*, where we consider the required transmit power only, and for *Scenario 2*, where we considered an additional SPP, versus the BER target of WSNs for a fixed rate of different MCSs for both AWGN and Rayleigh fading channels. The NL maximization problem was formulated with the aid of a set of lower bounded target SINR values for each link for characterizing the BER-dependent QoS and the impact of the physical layer parameters on the NL in the string topology considered. We also analyzed the ED of each node, the required transmission power per link, the interference power imposed on each node and the lifetime of all nodes forming part of the string-topology, while considering different target SINR requirements, SPP and channel characteristics. Moreover, we presented experimental results for assisting the network designer in making informed decisions as to which MCS works well for the application supported. The experimental results illustrated that 1/2-rate CC soft-decoded QPSK MCS provided the longest NL for an AWGN channel, which is nearly 4.99yrs of 'continuous-time' NL at 10^{-3} of PLBR in *Scenario 1*. On the other hand, SPP has a substantial impact on the NL, which reduced the NL to 0.89yrs in *Scenario 2*.

In this chapter, we considered a string-topology based network, where the distances between consecutive nodes were fixed. However, in a more realistic network, there may be thousands of routes spanning over various distances between consecutive sensor nodes, each of which

is assigned to a string-topology. Moreover, in such a complex network we also have to reconsider our NL definition. Therefore, in the next chapter we maximize the NL of a random uniformly distributed fully connected WSN, where the fully connected WSN imposes an exponentially increasing complexity upon increasing the number of nodes.

Chapter 4

Network-Lifetime Maximization of Wireless Sensor Networks Relying on Low-Complexity Routing

4.1 Introduction

As described in Chapter 1, the NL is a crucial metric for enabling the network designer to make informed decisions for the sake of maintaining the desired network performance and QoS in WSNs. The NL usually relies on the limited battery capacity of the sensor nodes within the WSN. Moreover, in realistic applications, such as for example in case of sensors embedded into the glaciers for measuring the climate changes, replenishing the battery energy of the sensors and/or replacing the sensors is usually impractical and/or costly. Therefore, the NL is constrained by the battery of the individual sensors in the WSN [2, 3]. Hence, in Chapter 2 we proposed an adaptive scheme for striking a compelling trade-off between the attainable transmit rate and the power dissipated. In Chapter 3, we examined a fixed-rate system considering the impact of various physical layer parameters on the NL, including the signal processing power dissipated by each sensor. In such scenarios, only the SN was allowed to generate information, while the rest of the nodes acted as relays aligned in a string-topology for conveying the source data to the sink node, which is also referred to as the DN. Therefore, the data can only reach the sink node by guaranteeing the connectivity between the SN and the DN in order to maintain a longer NL.

In this chapter we consider routing optimization algorithms conceived for maximizing the NL. We invoke a high-complexity exhaustive search algorithm (ESA) for quantifying the upper bound on the NL achieved by a reduced-complexity genetic routing algorithm operated in an interference limited WSN. Moreover, since in both Chapters 2 and 3 a string-topology

was considered, here we extend our network topology to a WSN having random uniformly distributed nodes that are fully connected, so that the routing behavior of the algorithms can be investigated. In the literature, there is a paucity of contributions on NL maximization relying on low-complexity routing optimization in interference limited WSNs, when maintaining a target QoS for each transmission link and having sensors that are random uniformly distributed. For example, the authors of [30] considered the joint optimal design of the transmit rate and power, while in [82] scheduling and routing was combined for maximizing the NL in an interference-limited WSN communicating over an AWGN channel. In [208] the aim of the authors was to minimize the ED, which is not the same objective as the maximization of the NL, as discussed in [186]. However, [30] and [82] simply considered a rhombus network topology[1] for illustrating the routing behavior of their proposed algorithm. Similarly, the authors of [208] also considered a simplified network topology, where a low-complexity distributed algorithm was developed for minimizing the ED. In [31], we formulated the NL maximization problem as a non-linear optimization problem encompassing the routing, scheduling, as well as the transmission rate and power allocation operations for transmission over both AWGN and Rayleigh block fading channels using the Lagrangian form and the KKT optimality conditions. However, in [31] we only considered a string topology, where the impact of the routing on the NL cannot be observed. Similarly, in [39] we optimized the NL of a string topology given the lower bound SINR values per link by analyzing the impact of the physical layer parameters along with the signal processing power dissipation on the NL, while operating both in AWGN and Rayleigh block-fading channels.

The authors of [209] proposed a low-complexity near-optimal genetic algorithm for analyzing the joint link scheduling and routing strategies for the sake of maximizing the traffic delivery from a SN to a specific DN within a given delay-deadline in the context of WMNs. By contrast, in [210] a low-complexity genetic algorithm was advocated for jointly optimizing the channel assignment, power control and routing operations for the sake of throughput maximization in cognitive radio based WMNs. Even though both [209] and [210] proposed genetic algorithms for solving complex cross-layer operation problems at a reduced complexity, neither the energy efficiency nor the NL were considered in the context of the low-complexity routing optimization of WSNs.

The authors of [211] and [212] investigated beneficial uplink scheduling and transmit power control techniques for maximizing the NL of battery driven machine to machine (M2M) devices deployed in long-term evolution (LTE) networks, where both an optimal solution as well as a low-complexity suboptimal solution were presented. To elaborate a little further, the suboptimal solution was capable of accomplishing a near-optimal NL performance at a significantly reduced complexity than the optimal one. In [33], [34] and [35] the authors considered an optimal routing algorithm as well as a reduced-complexity near-optimal routing

[1] A rhombus network topology is a diamond shaped network topology retaining equal length for all four edges.

optimization algorithm designed for maximizing the NL, while guaranteeing the end-to-end delivery-success probability of WSNs. However, they did not take the inter-node interference into account. Similarly, the authors of [213] presented a utility-based nonlinear optimization problem formulation for the sake of NL maximization and proposed a fully distributed routing algorithm for solving the optimization problem, which can of course only provide a near-optimal solution compared to a centralized technique. Nonetheless, the authors of [26] succeeded in conceiving a distributed algorithm for maximizing the NL, which was capable of approaching the performance of the optimal solution at a lower computational complexity. But again, in [26] the impact of the inter-node interference as well as that of the network size was not considered. The authors of [214] proposed a tree-cluster-based data-collection algorithm for WSNs in conjunction with a mobile sink, where the traffic load of the entire network was balanced, since the sink node was able to move around the network for a certain period in order to collect data and avoid the utilization of the same hot-spots in order to prolong the NL. Similarly, in [215] the authors advocated a low-complexity genetic algorithm for achieving both an enhanced coverage and an improved NL for multi-hop mobile WSNs, but their OF is to minimize was the ED, which also improved the NL.

However, as discussed in [186], even though energy conservation is beneficial in terms of extending the NL, it has subtle differences with respect to the NL maximization. Furthermore, Shi *et al.* in [218] proposed a low-complexity genetic algorithm for jointly optimizing the power control, the scheduling and the routing to maximize the end-to-end throughput in cognitive radio networks (CRNs). Moreover, Guo *et al.* [216] studied the options for beneficial base station placement for extending the NL based on a specific problem formulation, given the flow routing and energy conservation constraints. Hence, the authors of [216] developed a heuristic algorithm for solving the NL maximization problem at a reduced complexity, but at the cost of a small reduction in NL compared to the optimal NL solution. A multi-objective routing optimization approach was proposed in [217] for extending the lifetime of disaster response networks (DRNs), where a low-complexity genetic algorithm was utilized for analyzing the trade-off between the ED and the packet delivery delay. Similarly, the authors of [106] formulated the maximum-NL routing challenge as a linear programming problem, where the optimal NL was obtained and compared to the near-optimal NL acquired by the proposed routing algorithm. However, the goal in [106] was to only find the specific flow that maximizes the NL relying on the flow conservation constraint. In [219], the authors considered a distributed ED balancing algorithm based on a game-theoretical approach for data gathering and routing in WSNs, where the inter-node interference was not taken into account. Our study shows some similarities with [209] and [218] in terms of the solution approaches applied to the problems considered, but our main objective is the NL maximization in WSNs, while the authors of [218] aimed for maximizing the end-to-end throughput of CRNs. By contrast, the authors of [209] focused their attention on the computational complexity of the traffic delivery maximization problem. However, compared

TABLE 4.1: Key approaches of NL maximization techniques with reduced-complexity algorithm design.

Year	Authors	Summary
2005	Kwon *et al.* [33], [34]	An optimal routing algorithm as well as a reduced-complexity near-optimal routing optimization algorithm was designed for maximizing the NL, while guaranteeing the end-to-end delivery-success probability of WSNs.
2006	Cui *et al.* [213]	A utility-based nonlinear optimization problem formulation was conceived for the sake of NL maximization and a fully distributed routing algorithm was proposed for solving the optimization problem, which can only provide a near-optimal solution compared to a centralized technique.
	Madan *et al.* [26]	A distributed algorithm was proposed for maximizing the NL, which was capable of approaching the performance of the optimal solution at a lower computational complexity.
2007	Khanna *et al.* [215]	A low-complexity genetic algorithm was advocated for achieving both an enhanced coverage and an improved NL for multi-hop mobile WSNs.
2008	Hua *et al.* [107]	Routing and data aggregation were jointly optimized in order to maximize the lifetime of the WSN considered using a distributed gradient algorithm.
2013	Gu *et al.* [216]	The options for beneficial base station placement were studied with the objective of extending the NL based on a specific problem formulation given specific flow routing and energy conservation constraints. A heuristic algorithm was proposed for solving the NL maximization problem at a reduced complexity, but at the cost of a small reduction in NL compared the optimal NL solution.
2014	Chenji *et al.* [217]	A multi-objective routing optimization approach was proposed for extending the lifetime of disaster response networks, where a low-complexity genetic algorithm was utilized for analyzing the trade-off between the energy dissipation and the packet delivery delay.
2015	Yetgin *et al.* [31]	The NL maximization problem was formulated as a non-linear optimization problem encompassing the routing, scheduling, as well as the transmission rate and power allocation operations for transmission over both AWGN and Rayleigh block fading channels using the Lagrangian form and the KKT optimality conditions for reduced-complexity.
	Zhu *et al.* [214]	A tree-cluster-based data-collection algorithm was conceived for WSNs with a mobile sink, where the traffic load of the whole network was balanced, since the sink node was able to move around the network for a certain period in order to collect data and to avoid the utilization of the same hot-spots in order to prolong the NL.
	Azari *et al.* [211], [212]	Beneficial uplink scheduling and transmit power control techniques were investigated for maximizing the NL of battery driven M2M devices deployed in LTE networks, where both an optimal solution as well as a low-complexity suboptimal solution were presented.

to [218], our NL maximization algorithm is capable of achieving a longer NL. The major NL maximization techniques with reduced-complexity algorithm design are summarized in Table 4.1.

The network model provided in the above contributions mostly considered simplified topologies of low-complexity networks. In this chapter, we consider a WSN relying on randomly distributed and fully connected sensor nodes, which exponentially increases the computational complexity required for the network design and optimization with the number of sensor nodes due to the fully connected nature of the WSN. Explicitly, a fully connected WSN is considered, where one sensor can communicate with any other sensor in the network. This chapter considers a low-complexity algorithm designed for maximizing the NL, while guaranteeing a specific worst-case E2EB, which provides the BER upper bound of the interference limited WSN considered. We also characterize the trade-off between the proposed low-complexity algorithm and its optimal exhaustive search based benchmarker. Moreover, we compare the NL performance of the different WSN scenarios consisting of various numbers of sensors. Note that in the scenarios considered each transmission link has to satisfy a predefined target SINR, which determines the QoS of the WSN. For the sake of clarity, in the rest of the chapter we consider the route lifetime (RL) as the lifetime of a single route spanning from a SN to a DN, which can be considered as a string topology, whereas the NL is defined as the lifetime of a WSN, consisting of many other routes.

4.1.1 Novel Contributions

This chapter focuses on the cross-layer optimization of the power allocation, scheduling and routing operations for the sake of NL maximization for predetermined per-link target SINR values. We propose an optimal algorithm, namely the above-mentioned ESA at a high complexity for high number of nodes and a near-optimal single objective genetic algorithm (SOGA) exhibiting a reduced complexity in fully connected WSNs. The contributions of this chapter are summarized as follows.

1. We propose an extended-NL algorithm capable of exploiting alternative routes exhibiting the longest RL for end-to-end transmission in a fully connected WSN, where the aim is to carry the information generated at the SN to the DN, until the SN's battery becomes completely depleted. More explicitly, the addition of the maximum RL computed over the entire range of alternative routes provides us with an extended NL, since the NL is determined by the RL values, until the SN's battery becomes entirely depleted. Therefore, in this chapter, the NL values are expected to be higher than those in Chapters 2 and 3.
2. We optimize the power, the scheduling and the routing for the sake of NL maximization, where we propose the above-mentioned ESA and SOGA algorithms conceived for random

network topologies relying on fully connected nodes. Each SN-DN route is passed to an optimization function, namely the so-called dual-simplex function for finding the optimal RL for the corresponding route, where by definition the ESA finds the best route and its RL by searching through all the possible solutions provided by the given number of nodes in the fully connected WSN. On the other hand, the SOGA finds the best solution, given a predetermined number of generations and genetic algorithm (GA) individuals. We show that the SOGA is capable of finding a near-optimal solution at a significantly reduced complexity compared to ESA, specifically when the number of nodes is larger than 7.

3. During the iterations of the ESA and SOGA algorithms, more than one maximum NL value may be returned. Therefore, the selection of the best route is required, where the selection process determines the best SN-DN route for the end-to-end transmission. The selection process also determines the battery drain of the sensors, which has to be updated after each iteration for the forthcoming RL computation relying on the residual battery charges. Hence, we conceive beneficial route selection schemes (RSSs) for finding the specific route with the least total energy dissipation (LTED), the least number of hops (LNOH), the largest remaining SN battery (LRBAT) charge and the random route selection (RANR). For simplicity, we assume that each hop introduces one unit of delay.
4. We provide the E2EB as an upper bound on the BER of the interference-limited fully connected WSN using both uncoded BPSK, as well as 1/2-rate CC hard-decoded and soft-decoded QPSK MCSs for the proposed RSSs. We will demonstrate that the 1/2-rate CC soft-decoded QPSK MCS has a higher NL than the other MCSs in all scenarios of the ESA and SOGA.
5. We also demonstrate that the RSS-LRBAT and RSS-LTED outperforms other RSSs in terms of their NL, since they are the most NL-aware RSSs. The E2EB of the RSS-LNOH exhibits a slightly better E2EB versus SINR performance, which is due to its reduced bit error accumulation over the associated lower number of hops.
6. Since we assume that the ED of any operation is negligible, compared to the transmit power, introducing an additional sensor into the WSN extends the NL, since this creates more opportunities for relaying the information over alternative routes. We observe that the NL gain achieved by an additional sensor, when for example the 5th sensor enters the WSN having 4 sensors, provides an approximately 5500 extra hours of NL, when the WSN operates at SINR=10dB.
7. For a network size given by $V = 7$ the computational complexity is similar for both the ESA and SOGA. However, for larger networks the complexity starts to increase exponentially for the ESA, while it is only increased modestly for the SOGA at the cost of a small NL-reduction compared to the optimal NL for WSNs composed of $V > 7$ nodes.
8. The fully connected network model considered can also be applied to any distributed network having more nodes but less distinct routes. We opted for a fully connected

WSNs due to the exponentially increased number of the distinct routes, which provides us with a complex network yet tractable even for a low number of nodes to characterize the capability of our SOGA. Therefore, in our scenarios the performance analysis of the SOGA and ESA is based on the total number of distinct routes.

4.1.2 Chapter Organization

The rest of this chapter is organized as follows. Our system model is described in Section 4.2, which is characterized by its network topology, transmission scheme, physical layer, BER and NL. We also provide an example of the interference model and define the integration of the specific MCSs considered into our system model. Then, our problem formulation and the ESA as well as SOGA are presented in Section 4.3, while our experimental results are provided in Section 4.4. Finally, we summarize our findings in Section 4.6.

4.2 System Model

We consider a fully connected stationary WSN, where the sensors are randomly and uniformly distributed over the sensor field, as illustrated in Fig. 4.1, which also portrays how the sensor nodes may join the WSN. Once a pending sensor node becomes capable of initiating a communication session with a sensor node in the network, we assume that the pending sensor node can also communicate with any other sensor node in the WSN. Furthermore, we also assume that a sensor node stores the distance information $(d_1, d_2, d_3, ...)$ with respect to any other node in the WSN and any changes in the distance information is relayed to the control center, which maintains all the global knowledge concerning the WSN considered at the DN. A communication link can be established between nodes i and j, when node $i \in \{1, ..., V\}$, $(i \neq j)$ transmits at its optimum transmit power and node $j \in \{1, ..., V\}$ receives a signal with a power higher than a predetermined threshold, where V denotes the number of nodes in the fully connected WSN. We consider a low threshold for guaranteeing that the WSN remains fully connected, as illustrated in Fig. 4.1, where each sensor is capable of communicating with any other sensor in the network. A fully connected WSN has an exponentially increased complexity upon increasing the number of nodes V. Again, our goal is to study the behavior of our algorithms in a high-complexity fully connected WSN composed of a large number of distinct non-looping routes[2]. Note that the SN and

[2]The term "non-looping route" defines the route with the dissimilar sensor nodes lying in, where one sensor node can only transmit once on the same route, i.e. $SN - 1 - 2 - 3 - DN$ is non-looping, but $SN - 1 - 2 - 3 - 1 - DN$ is looping, since node-1 repeats in the same route. The term "distinct route" indicates different routes having dissimilar sensor nodes in the same WSN. For example, suppose we can only generate $SN-1-2-3-DN$ and $SN-1-2-3-4-DN$ routes in the same WSN. Then, $SN-1-2-3-DN$ and $SN-1-2-3-4-DN$ are distinct routes, since the second route obtains node-4, which the first route does not have. Therefore, the term "distinct non-looping routes" indicates the routes with non-repeating or dissimilar sensor nodes within the same route and this route differs from another route due to its dissimilar

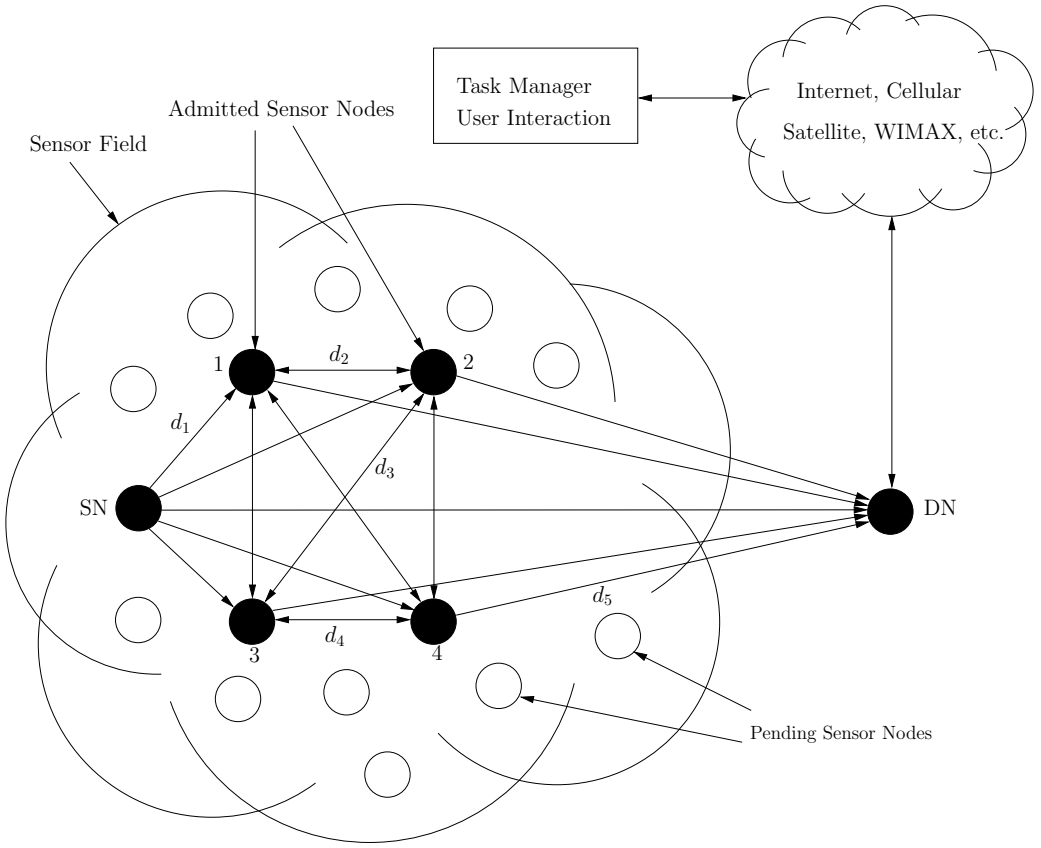

FIGURE 4.1: Distributed fully connected WSN illustrating the node admission and awaiting sensor nodes.

the destination node, which is termed as the DN in the rest of the chapter, are located at the opposite corners for ensuring that the geographic distance between the SN and the DN is the longest. The rest of the $(V-2)$ nodes are randomly distributed according to the uniform distribution. Additionally, we assume that only the SN generates information to be transmitted to its neighboring nodes with the aid of a multi hop relaying scheme through to the DN. Therefore, apart from the SN, all nodes in the network act as a relay, which carries information to the DN, as illustrated in Fig. 4.1. We note that the SN is also capable of directly transmitting to the DN, without the need of a relay node, due to the fully connected nature of the WSN.

Since we assume that only the SN generates information and all the other sensor nodes share a single frequency band, carrying data to the DN requires careful consideration due to the interference. Considering a fully connected network, the SN may have numerous alternative routes for delivering the data to the DN. However, relying on the constrained lifetime of the sensors, choosing the best-lifetime route plays a significant role in keeping the network operational, whilst efficiently utilizing the limited resources of the WSN. Owing to the full connectivity of the WSN, the data generated at the SN can be transmitted until the SN

sensor nodes within the same WSN.

fully drains its battery. We assume that as long as at least one SN-DN route exists in the WSN and the battery of the SN is not fully drained, the data transmission from the SN to the DN continues. This process requires the addition of the computed RL values, until the source battery is fully drained. In our system model, at most one SN-DN route can be activated at a time for delivering data to the DN, i.e. we consider a unicast network, and each route is associated with a specific RL value calculated based on the optimization problem to be described in Section 4.3.1. Hence, the maximum RL pair is selected for the transmission of data to the DN. More explicitly, observe in Fig. 4.2 that there are five distinct non-looping routes, namely Route-1, Route-2, Route-3, Route-4 and Route-5. The term RL refers to the lifetime of any route based on the minimum lifetime of nodes forming part of that particular route, as illustrated in Fig. 4.2. Additionally, the NL is calculated by the summation of the longest RL values, until the SN's battery is completely drained. For example, we start computing the lifetime of all the routes in the network and assuming that in the first iteration we obtain Route-1=1000 hours (hrs), Route-2=2000hrs, Route-3=3000hrs, Route-4=4000hrs, Route-5=5000hrs of RL values for each of those specific routes. During this iteration, Route-5 will be selected for the end-to-end transmission, since it is the highest RL value computed and hence using that particular route is beneficial for extending the duration of the network's operation. Since our NL model is strictly constrained by the SN's battery energy capacity, we have to check the battery level of the SN after each RL calculation and sum up the longest RL values computed after each iteration. Let us assume for a moment that after the first iteration we still conserved some energy in the SN's battery, therefore the network is still capable of transmitting its information to the DN via alternative routes, which do not rely on the specific sensor node that ran out of battery. Hence, we compute the lifetime of all routes in the current WSN by avoiding the drained sensor node. Let us assume for example that node-1 was the one that completely drained its battery. Then, in the second iteration we assume that we have the following RL values: Route-1=2000hrs and Route-2=4000hrs, which requires Route-2 to be utilized for the next end-to-end transmission. At this stage, if there is no energy left in the SN's battery, then the NL is defined by the summation of the RL values of Route-5 in the first iteration and of Route-2 in the second iteration, which results in $(5000 + 4000 = 9000)$hrs of NL.

4.2.1 Transmission Scheme

Again, in a fully connected WSN there are numerous alternative routes for the end-to-end transmission. However, selecting the highest-NL route for end-to-end transmission is crucial. Therefore, lifetime of every possible SN-DN route is considered as the RL, which is defined as the time instant at which the first node lying on a given route fully drains its battery. The specific route having the best RL is selected for the final end-to-end transmission, as explained in Fig. 4.2 of Section 4.2. Moreover, the battery-information of the sensor nodes actually utilized for the end-to-end transmission is updated. After each end-to-end trans-

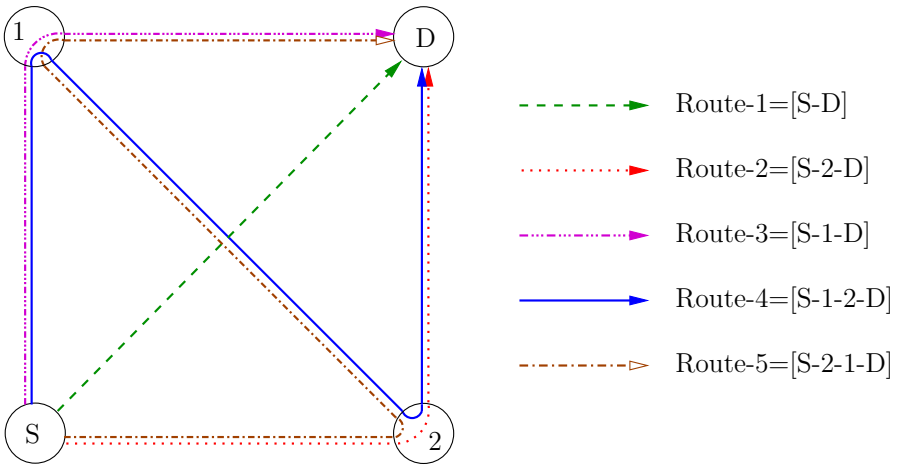

FIGURE 4.2: A simple WSN having 4 sensor nodes, which exemplifies the RL and NL computation.

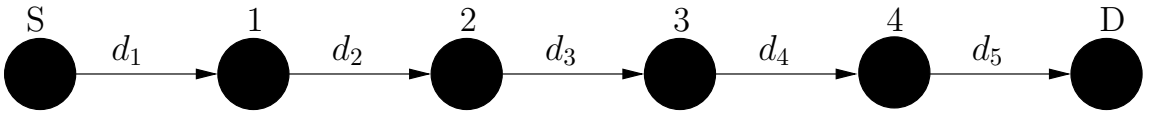

FIGURE 4.3: A random example of the route extracted from Fig. 4.1

mission, the battery level of the SN is checked and if the SN battery is not fully depleted, RL computation is updated with the remaining battery power. Here, each maximum RL computation corresponds to one iteration of the algorithm considered. On the other hand, the NL is a function of the RL, until the SN fully depletes its battery. Therefore, the computation of the resultant NL may require a few iterations of the RL computations. Once again, the RL corresponds to the computation of any SN-DN route. Hence, the NL is dependent on the lifetime of the routes of the WSN considered. A unidirectionally communicating route extracted from the omni-directionally communicating network of Fig. 4.1 is illustrated in Fig. 4.3. More explicitly, NL computation relies on the unidirectional links of the available routes extracted from the WSN of Fig. 4.1, despite the fact that the communication of the WSN is omni-directional. In Fig. 4.3 the nodes are only capable of transmitting unidirectionally to their consecutive neighboring nodes. We note that a specific SN-DN route of Fig. 4.3 extracted from the WSN of Fig. 4.1 can be considered as a single string-topology. Each string-topology extracted from Fig. 4.1 is utilized for the RL computation by exploiting their distance values, which are correspondingly assigned to the extracted route in Fig. 4.3, and illustrated as the distances of $(d_1, d_2, d_3, d_4, d_5)$ in Fig. 4.1.

The computation of the RL for each extracted route relies on the SPTS technique of [30] for modeling the periodic TS activation scheduling used, where we consider a distance of T hops between the pairs of nodes, which are transmitting in the same time TS. The same TSs are reactivated after every T TSs. Fig 4.4 illustrates the SPTS for $T = 3$, where $[n = 1, n = 2, n = 3, ..., n = N]$ describes each TS n for a given N-TS TDMA frame per

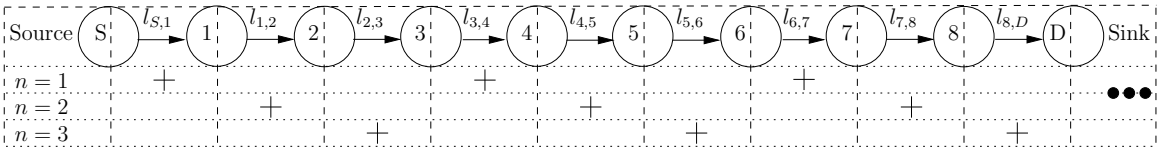

FIGURE 4.4: SPTS with time sharing parameters of $T = 3$ and $N = 3$ for $V = 10$ nodes.

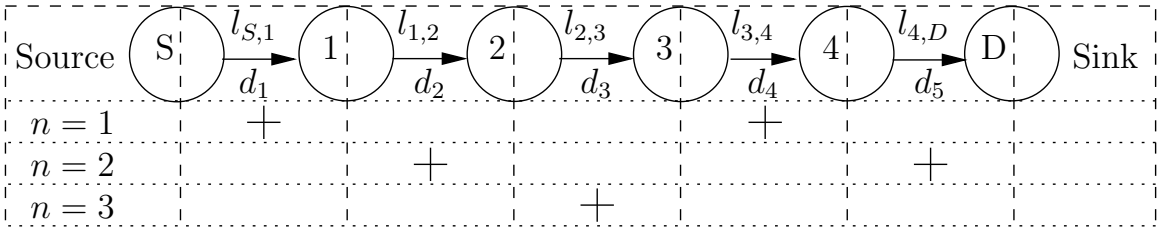

FIGURE 4.5: TS-centric view of the SPTS for the 6-node route string-topology of Fig. 4.1, which is illustrated in Fig. 4.3, when $T = 3$ and $N = 3$.

link and "+" denotes the active links. Therefore, a link l, spanning from node i to node j, scheduled for TS n, is denoted by $(l_{i,j}, n)$. For example, during the first TS ($n = 1$), the links $(l_{1,2}, 1)$, $(l_{4,5}, 1)$, $(l_{7,8}, 1)$ are activated for simultaneous transmissions, which only moderately interfere with each other and each link is activated only once during the whole TDMA frame. For the simplicity of our system model, we use $T = 3$ in our SPTS-aided interference-limited scenario and the total number of TSs per link frame is assumed to be $N = 3$ due to its low computational complexity. This means that each link can be scheduled for one of $N = 3$ TSs and in each TS the distance between the scheduled links has to be $T = 3$ hops. We assume that an ongoing transmission is capable of interfering with any other transmission in the extracted route, if they are scheduled during the same TS, as shown in Fig. 4.5. Naturally, the analysis presented here applies to any arbitrary T value.

For the sake of simplicity, we provide two different illustrations of the same transmission scheme seen in Fig. 4.3, which allows the reader to readily observe which specific links are activated in a particular TS, giving us a TS-centric view, as illustrated in Fig 4.5 and which TSs are activated for a particular link, providing us with a link-centric view, as illustrated in Fig. 4.6. More explicitly, we illustrate the TS-centric view of the SPTS strategy for the route illustrated in Fig. 4.3 in the context of the topology seen in Fig. 4.1, where we can observe how many links are activated per TS in Fig 4.5. Due to the periodic nature of the SPTS for $T = 3$, the third TS ($n = 3$) contains only a single active link for the 6-node scenario of Fig. 4.5. If a 7-node route were to be considered, another link would have appeared in the third TS obeying the $T = 3$ scheduling scheme, which can be clearly inferred from the 10-node scenario of Fig. 4.4.

As a further insight, we provide the link-centric view of the SPTS strategy in Fig. 4.6, so that we can clearly observe how many times a specific link is activated in each TS. Since this specific scenario is proposed for $N = 3$ TDMA frames and $T = 3$, observe in Fig. 4.6 each

Slots / Links	$n=1$	$n=2$	$n=3$
$l_{S,1}$	•		
$l_{1,2}$		•	
$l_{2,3}$			•
$l_{3,4}$	•		
$l_{4,D}$		•	

• : T=3 SPTS parameter

FIGURE 4.6: Link-centric view of the SPTS for the 6-node route string-topology of Fig. 4.1, which is illustrated in Fig. 4.3, when $T = 3$ and $N = 3$.

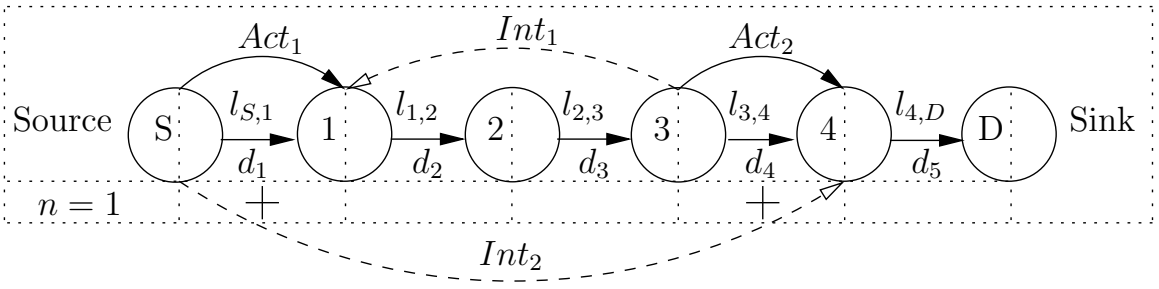

FIGURE 4.7: Interference model for the extracted 6-node route string-topology of Fig. 4.1, when $T = 3$.

link only has been activated once in different TSs. When the first TS ($n = 1$) is activated obeying the SPTS of $T = 3$, the links $l_{S,1}$ and $l_{3,4}$ start their actual transmission actions Act_1 and Act_2 over their arbitrary link-distances d_1 and d_4, respectively in Fig. 4.7. However, during Act_1, node-3 initiates an interfering transmission to node-1 denoted by Int_1. In the mean time, during Act_2, SN concurrently initiates an interfering transmission to node-4, which is denoted by Int_2. Therefore, we can readily see that the interferers (interfering nodes) of the link $l_{S,1}$ and $l_{3,4}$ are node-3 and node-SN, respectively. Since there are only 2 scheduled links in the same TS, one link interferes with another one. If there were 3 links scheduled in the same TS obeying the SPTS of $T = 3$, one link would have been concurrently interfered with the other two. More explicitly, a receiving node would have been exposed to more interference emanating from additional interferers.

4.2.2 Physical Layer

The sensor nodes of the fully connected WSN rely on using omni-directional antennas. This implies that a SN-DN route selection process takes place with the aid of omni-directional

communication. Once a route is selected, the communication is handed over to uni-directional links, because information can only flow from a SN to a DN along the selected route. Additionally, the nodes use half-duplex communications, where each node can either transmit or receive in the same TS n. We note that the sensor nodes communicate via the same shared wireless channel. The channel gain of a link between the transmitter i and the receiver j is given by $G_{i,j,\,i\neq j} = 1/(d_{i,j})^m$, which encapsulates the path loss, where the power diminishes with $d_{i,j}^m$ as a function of the distance $d_{i,j}$ between the transmitter i and receiver j, with the path loss exponent denoted by m. In addition, each node is capable of transmitting at an adjustable transmit power between the no-transmission state and the maximum affordable transmit power assigned to that node, given by $0 \leq P_{l_{i,j}} \leq (P_i)_{max}$. Each node has an initial battery capacity that cannot be exceeded by the total ED of the node.

The AWGN channel is defined by a certain propagation path-loss model and a fixed noise power at the receiver. The link quality is defined in terms of the SINR, which is denoted by Γ_l for the AWGN channel model and it is given by [181]

$$\Gamma_{l_{i,j},n} = \frac{G_{i,j} P_{l_{i,j},n}}{\sum_{i'\neq i, l_{i',j'}\in\mathcal{L}_n} G_{i',j} P_{l_{i',j'},n} + N_0}, \tag{4.1}$$

for a specific link l, where $P_{l_{i,j},n}$ denotes the transmit power of link l spanning from node i to node j in TS n and N_0 is the noise power at the receiver. Note that the SINR of each link in the extracted route cannot be lower than the target SINR γ given by $\Gamma_{l_{i,j},n} \geq \gamma$, $\forall n$, $l_{i,j} \in \mathcal{L}_n$, where $l_{i,j}$ denotes the link between transmitter i and receiver j, while $\mathcal{L}_n$ is the set of links activated in the same TS n. On the other hand, $G_{i',j}$ denotes the channel gain of a link between the interfering node and the receiving node of the desired communication, while $P_{l_{i',j'},n}$ is the transmit power of the interfering link l spanning from node i' to node j' in TS n, where i' is the transmitter and j' is the receiver of the link interfering with the desired communication.

In our system model, we rely on a BER-SINR LUT for characterizing the upper layers, which specifies the particular SINR value to be satisfied for the sake of maintaining a given target BER. Note that we consider the interference to be noise-like in the SINR calculation[3]. Upon knowing the SINR constraint and our deterministic path loss model, we can calculate the interference imposed on the intended receivers, depending on which TS is activated, as shown in Fig. 4.7, assuming that the actual communication occurs between the SN and node-1 during the first TS. Then, the interference power at the receiving node-1 can be expressed as $Int_1 = G_{3,1} P_{l_{3,4},1} = P_{l_{3,4},1}/(d_2 + d_3)^m$ and the power received at node-1 can be formulated as $Act_1 = G_{S,1} P_{l_{S,1},1} = P_{l_{S,1},1}/(d_1)^m$. Note that if we consider a fixed noise power at the receiver, then we can compute the SINR of link $l_{S,1}$ during the first TS as:

[3]Since in practice WSNs rarely encounter a single dominant interferer, the interference is typically constituted by the sum of several interfering components, which allows us to approximate the interference by noise.

$$\Gamma_{l_{S,1},1} = \frac{G_{S,1}P_{l_{S,1},1}}{G_{3,1}P_{l_{3,4},1} + N_0} = \frac{P_{l_{S,1},1}(d_2+d_3)^m}{(d_1)^m\left(P_{l_{3,4},1} + ((d_2+d_3)^m N_0)\right)} = \left(\frac{d_2+d_3}{d_1}\right)^m \frac{P_{l_{S,1},1}}{P_{l_{3,4},1} + (d_2+d_3)^m N_0}. \tag{4.2}$$

In Eq. (4.2), only a single node interferes with node-1. However, in a scenario, where more than two links are activated during the same TS, we have to sum up the interferences imposed on the corresponding receiver node, along with the fixed noise power. Now Eq. (4.2) invoked for calculating the SINR of any link in any TS can be generalized for any given route as

$$\Gamma_{l_{i,j},n} = \frac{G_{i,j}P_{l_{i,j},n}}{\sum_{i'\neq i, l_{i',j'}\in\mathcal{L}_n} G_{i',j}P_{l_{i',j'},n} + N_0}, \tag{4.3}$$

which defines the quality of the corresponding link. Therefore, we set $\Gamma_{l_{i,j},n} \geq \gamma$, which can be rewritten as follows,

$$\gamma \cdot \left(\sum_{i'\neq i, l_{i',j'}\in\mathcal{L}_n} G_{i',j}P_{l_{i',j'},n} + N_0\right) - G_{i,j}P_{l_{i,j},n} \leq 0. \tag{4.4}$$

Let us consider a communication session taking place between node i and j separated by a distance of $d_{i,j}$, where the BER of the link $l_{i,j}$ is denoted by $BER_{l_{i,j}}$. This error probability, plausibly depends on the SINR experienced at the receiver node j of the link $l_{i,j}$, on the modulation scheme, on the channel coding and on the characteristics of the channel. Considering a multi hop scenario, consisting of more than one link, we can derive an expression for the E2EB defined by the BER accumulated along the route spanning from the SN to the DN given by [220, 221],

$$E2EB_{route} = 1 - \prod_{l=1}^{V-1}(1 - BER_l), \tag{4.5}$$

where BER_l is a function of the SINR ($BER_l = f_{MCS}[SINR_l]$), which can be fetched from the LUT selected for the specific MCS employed and $(V-1)$ is the number of links along the *route*. In this contribution, we consider an uncoded BPSK modulated system and a 1/2-rate CC hard-decoded as well as soft-decoded QPSK scheme communicating over an AWGN channel. We can compute the NL of any of the different MCSs by relying on their BER-SINR LUT for the system considered. Note that since we can estimate the BER at the relay nodes, we invoke a DF scheme in our scenarios, where we neglect the ED of the coding and decoding operations. At the DN, all ED is ignored, since we assume that the DN is plugged into the mains power source. The BER-SINR relationship of the system model considered for transmission over the AWGN can be observed in Fig. 4.8, where for SINRs

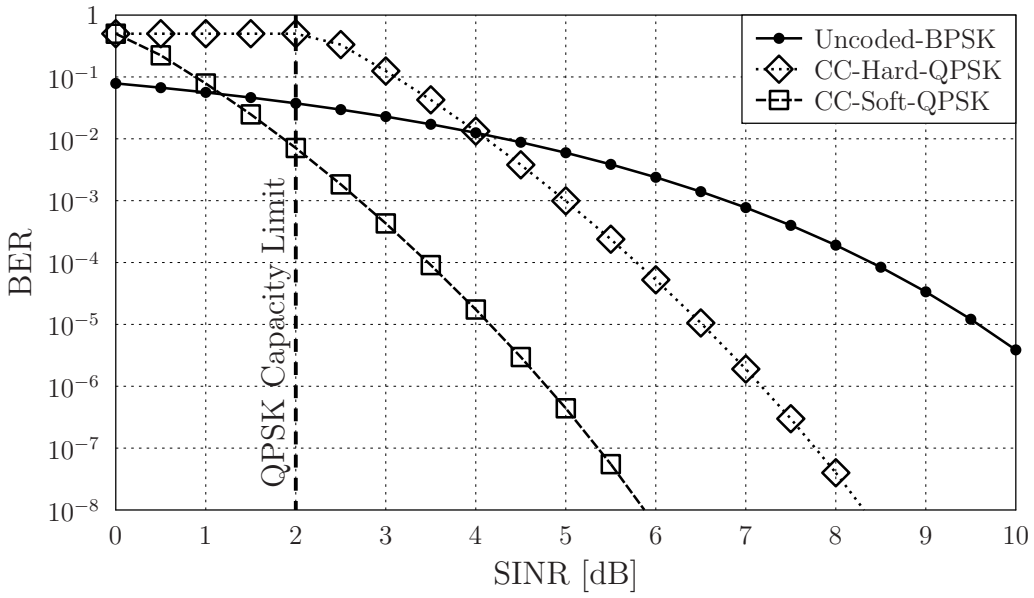

FIGURE 4.8: BER versus SINR performance of the MCSs considered for an AWGN channel.

in excess of 4dB, CC soft QPSK outperforms both CC hard QPSK and uncoded BPSK. Moreover, to guarantee a BER of 10^{-2} or lower, CC soft QPSK requires the lowest SINR, which is the most energy-efficient MCS amongst our MCSs considered. The CC hard QPSK is the second most energy-efficient MCS. Therefore, we also expect to see a similar pattern in terms of the NL for the system model considered, which will indeed be confirmed by the results of Section 4.4.

4.2.3 Lifetime Model

In our model, we consider a novel two-stage lifetime evaluation process, as exemplified by a simplified scenario in Fig. 4.2 of Section 4.2. The first stage is related to the RL, which is based on the maximization of the minimum node lifetime given by $T_R = \min_{i \neq \text{DN}, i \in V} T_i$, where T_i denotes the lifetime of node i lying on the route R. This lifetime definition is realistic, especially if the failure of any node in the route disconnects the SN and the DN. More explicitly, in a route, where the information generated at the SN has to be relayed to the DN via multiple hops, this NL definition is feasible, since a node in the route cannot communicate with the node that is two hops away.

The second stage of the lifetime computation is strictly dependent on the RL computation of the first stage, where each computed maximum RL is summed up, until the SN battery is fully depleted. More explicitly, the best route associated with each maximum RL computation is relied upon for the end-to-end transmission and the sensor nodes lying on those best routes are updated with the remaining battery-levels for the next RL computation. Each maximum RL is summed up in order to calculate the NL, until the SN battery is fully

depleted. Since our only concern is that of carrying the SN's information to the DN with the aid of alternative routes, the NL is strictly dependent on the SN's battery level. Therefore, until the SN fully depletes its battery, the maximum RL values are added for calculating the NL in the second stage, as exemplified in Fig. 4.2 of Section 4.2. Note finally that there are also other alternative NL definitions, which were discussed in Section 1.1.

4.3 Problem Formulation

Our NL maximization problem is divided into two stages. The first stage considers the formulation of the system model described in the context of the route extracted, which forms a string topology, followed by the selection of the best RL-aware route. The second stage includes the specific design of the algorithm conceived for maximizing the NL by summing up the RL values, until the SN battery becomes entirely depleted in the WSN considered. We detail the RL computation in Section 4.3.1, followed by the maximum NL computation in Section 4.3.2, where the complexity of a fully connected WSN is also characterized as a function of V. Furthermore, we study the details of both the ESA and SOGA of Section 4.3.2 followed by the run-time simulation analysis of both algorithms in Section 4.3.2.

4.3.1 Route Lifetime Computation

Let us first discuss the problem formulation regarding the routes extracted, which are the SN-DN routes obtained from the fully connected WSN illustrated in Fig. 4.1, for a given number of nodes per network. Having discussed the system model in Section 4.2, we focused our attention on the general optimization problem formulation for the first stage of maximizing the NL in (4.6) subject to the constraints of (4.7)–(4.9) as follows,

$$\begin{aligned}
\text{max.} \quad & T_R && (4.6)\\
\text{s.t.} \quad & \Gamma_{l_{i,j},n} \geq \gamma,\ \forall n, l_{i,j} \in \mathcal{L}_n, && (4.7)\\
& \frac{T_R}{N} \sum_{n=1}^{N} \left(\sum_{l \in \mathcal{O}(i) \cap \mathcal{L}_n} \Big((1 + (1-\alpha)) \cdot P_{l_{i,j},n} + P_{sp} \Big) \right) \preceq \mathcal{E}_i,\ \forall i, && (4.8)\\
& 0 \preceq P_{l_{i,j},n} \preceq (P_i)_{max},\ \forall n, i, l_{i,j} \in \mathcal{L}_n. && (4.9)
\end{aligned}$$

We maximize T_R in (4.6) in order to maximize the minimum lifetime of nodes lying on the route extracted, while obeying the constraints mentioned in our system model. For example, (4.4) formulates the link quality, given the relationship between the attainable rate, the signal power and the interference imposed as well as the noise power encountered at the receiver, which can be associated with the QoS. Therefore, (4.7) may be formulated

as a constraint to be satisfied for guaranteeing the QoS at a specific predetermined target SINR value. Additionally, each sensor node relies on limited batteries, which cannot be replenished. Therefore, the ED of a single sensor cannot exceed its initial battery charge level $\mathcal{E}_i$, which can be readily written as $\sum_{u_i}^{U} f_{ED}(x_{u_i}) \leq \mathcal{E}_i$, where $u_i = \{1, ..., U\}$ characterizes the sensor operations imposing a specific ED and $f_{ED}(x)$ is the ED function. We assume that any operation other than the transmission of information across the network incurs a negligible ED. Therefore, the signal processing power dissipation P_{sp} is set to 0 and u_i can be set to 1, since the transmit power is the only reason for dissipating energy in the sensor. Then, $f_{ED}(x)$ can be characterized by (4.8), representing how the initial battery energy is dissipated as a function of both the system parameters and of the transmit power $P_{l_{i,j}}$, where α denotes the power amplifier's efficiency and N corresponds to the total number of TSs per link, $n = \{1, ..., N\}$.

For simplicity, in our scenarios we consider $N = 3$. For example, for the topology defined in Fig. 4.5, links $l_{S,1}$ and $l_{3,4}$ are activated in the first TS ($n = 1$), links $l_{1,2}$ and $l_{4,D}$ are activated in the second TS ($n = 2$), and link $l_{2,3}$ is activated in the third TS ($n = 3$). Moreover, (4.9) indicates that the transmit power can be adjusted to the no-transmission state of $P_{l_{i,j}} = 0$ or to the maximum affordable transmit power at any sensor $P_{l_{i,j}} = (P_i)_{max}$ or to any value between 0 and $(P_i)_{max}$, depending on the SPTS parameter of $T = 3$ and on the other optimization variables. Explicitly, the variables of the optimization problem are the RL T_R and the transmit power $P_{l_{i,j},n}$ of the link spanning from sensor node i to node j in TS n. It is clear that (4.6)–(4.9) is non-convex owing to their reliance of the product of two optimization variables, which is generally non-convex [129].

We can readily transform the non-convex[4] NL maximization problem into a convex[5] one by minimizing the reciprocal of the RL, which is formulated as $z = \frac{1}{T_R}$ in (4.10) by using a change of variable in order to avoid the product of the two variables. In fact, the optimization problem is converted into a linear programming problem, which is also a special case of convex optimization problems. Note that T_R cannot be zero in the reciprocal domain, since the SN has a battery capacity of $\mathcal{E}_i > 0$ and a positive lifetime, implying that the SN definitely transmits information for a non-zero amount of time. This is also applicable to any other sensor nodes in the WSN considered. Additionally, Eq. (4.7) is rearranged into (4.11). Most importantly, the optimization variables contained in the product are appropriately separated so that (4.8) becomes linear in (4.12), which is a special case of convex problems, where $l \in \mathcal{O}(i)$ represents the transmit link of node i. Furthermore, $\{i : i \in \mathcal{O}^{-1}(l), l \in \mathcal{L}_n\}$ in (4.11) represents the set of nodes, which the transmit links are connected to and that are activated in the same TS.

[4]Non-convex optimization problems may have local optimal points. However, these local optimal points mostly will not be the global optimal solutions. Additionally, proving that there is no feasible solution can be time consuming and is not guaranteed.

[5]Convex optimization problems can only have one global optimal solution and one can easily prove if there is no feasible solution to the convex problem.

$$\text{min.} \quad z \tag{4.10}$$

$$\text{s.t.} \quad \gamma\Big(\sum_{i'\neq i, l_{i',j'}\in\mathcal{L}_n} G_{i',j}P_{l_{i',j'},n} + N_0\Big) - G_{i,j}P_{l_{i,j},n} \leq 0,\ \forall n, \{i : i \in \mathcal{O}^{-1}(l),\ l \in \mathcal{L}_n\}, \tag{4.11}$$

$$\sum_{n=1}^{N}\left(\sum_{l\in\mathcal{O}(i)\cap\mathcal{L}_n}\Big((1+(1-\alpha))\cdot P_{l_{i,j},n} + P_{sp}\Big)\right) - z\cdot\mathcal{E}_i\cdot N \leq 0,\ \forall i, \tag{4.12}$$

$$0 \leq P_{l_{i,j},n} \leq (P_i)_{max},\ \forall n, i, l_{i,j} \in \mathcal{L}_n. \tag{4.13}$$

We compute the maximum RL of the routes obtained from the fully connected WSN using the dual simplex method of the CPLEX library[90], which is a powerful solution method conceived for linear programming problems, as a special case of convex problems. Therefore, the first phase of the NL maximization problem is based on the computation of the RL and on the selection of the best RL-aware route. Generally speaking, based on the transmission scheme proposed in Section 4.2.1, we maximize the NL of an arbitrarily created and uniformly distributed WSN composed of V nodes, where the SN and the DN have their positions fixed at the opposite corners of the sensor field, while the nodes lying on a route adjust their transmit powers for a predetermined target SINR γ for guaranteeing at least the minimum signal quality required for each link, until the NL of the WSN is exhausted due to the depleted SN battery.

4.3.2 Maximum Network Lifetime

In this section, we propose a pair of algorithms for maximizing the NL of our fully connected WSNs. The first technique considered is the so-called ESA, which searches for all the possible distinct routes in the given network. The second algorithm, which we refer to as the SOGA, intelligently searches through a fraction of the potentially excessive solution space for finding the optimum at a low complexity. The general structure of our algorithms can be seen in Fig. 4.9, where each algorithm starts with a fully connected network-creation. Then, beneficial route discovery and route evaluation processes are provided by the proposed algorithms. The route information obtained is utilized for RL computation for each route selection scheme. Since the NL is strictly dependent on the SN, the battery level of the SN is updated by both algorithms. Having a large number of nodes in a fully connected network leads to an exponential increase of the number of routes, which imposes an exponentially increasing complexity. Therefore, we first provide the complexity analysis of the fully connected network before describing our proposed algorithms.

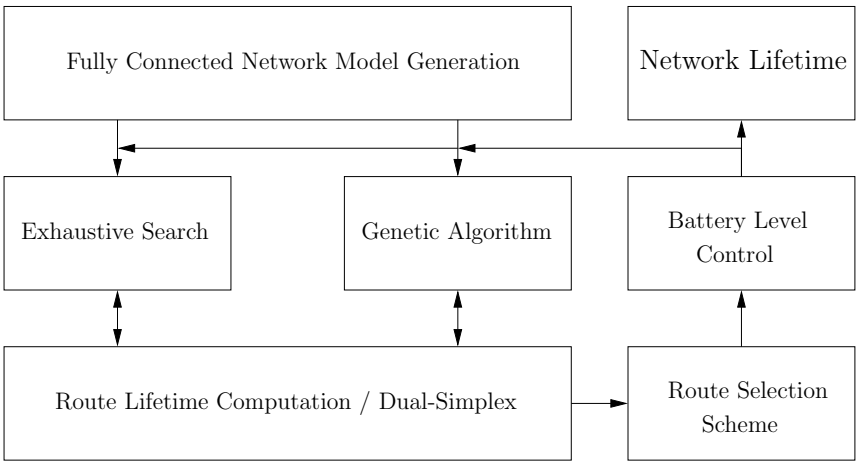

FIGURE 4.9: A single trial of the general NL computation framework for ESA and GA.

4.3.2.1 Fully Connected WSN and Complexity Analysis

Short-range densely deployed sensor networks can be used for numerous realistic applications [2, 3], where any sensor between the SN and DN may act as a relay to forward the information of the SN. For example, in battle fields non-rechargeable sensors can be densely deployed for maintaining the lowest battery consumption and for keeping the network operative as long as possible. Another example of densely deployed short-range networks can be found in a football stadium, where each person carries a sensor for health and security reasons. Finally, earth quake monitoring requires a dense sensor deployment for measuring the backscattered wave fields [222]. Therefore, all of these applications may necessitate communication of a node with any other node in the network, which leads to a fully connected WSN. More explicitly, a WSN associated with numerous communication links can be represented by a tractable fully connected WSN. However, the complexity is an important issue in fully connected networks, since the number of distinct non-looping routes increases exponentially upon increasing V. The term "distinct non-looping routes" indicates the routes associated with distinct sensor nodes within the same route and this route differs from any other route due to its unique sensor nodes within the same WSN. The total number of distinct and non-looping routes is given by

$$R_V = \sum_{h=0}^{V-2} \frac{(V-2)!}{(V-2-h)!}, \tag{4.14}$$

which is basically the aggregation of all the route permutations for each route having $(h+1)$ links or hops, given the total number of V nodes in the network. As an example, we provide the route permutations of a 4-node fully connected WSN in Fig. 4.10, where Eq. (4.14) constructed for a scenario associated with $V = 4$ leads to:

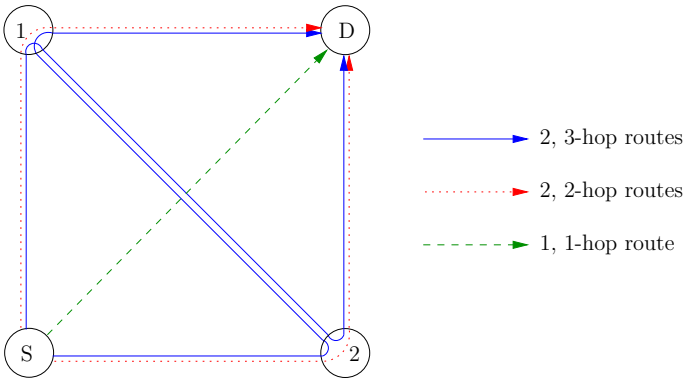

FIGURE 4.10: An example of distinct route permutations for a 4-node fully connected WSN.

$$R_{V=4} = \sum_{h=0}^{4-2} \frac{(4-2)}{(4-2-h)} = \sum_{h=0}^{2} \frac{2!}{(2-h)!} = \frac{2}{(2-0)!} + \frac{2}{(2-1)!} + \frac{2}{(2-2)!} = 1+2+2 = 5, \tag{4.15}$$

which can also be verified with the aid of Fig. 4.10. It is clear from the equation that the permutation is calculated in a hop-by-hop manner. We know that the values of 0, 1 and 2 are denoted by h in the denominator of $\frac{2}{(2-0)!}$, $\frac{2}{(2-1)!}$, $\frac{2}{(2-2)!}$ and $(h+1)$, i.e. 1, 2 and 3, represents the number of hops. Therefore, Eqs. (4.14) and (4.15) indicate that {1, 2, 2} number of distinct route permutations are calculated for the corresponding number of hops {1, 2, 3}, respectively. This can also be confirmed using Fig. 4.10, which is illustrated by the blue solid lines for the 3-hop, by the red dotted lines for the 2-hop, by the green dashed line for the 1-hop communication scenarios, respectively. It is observed that there are two 3-hop, two 2-hop and one 1-hop distinct routes, which is summed up to 5, as seen in Eq. (4.15) using Fig. 4.10. Naturally, we can also say that any route constructed for a given network can have a maximum of $(V-1)$ hops starting from 1-hop communication.

We provide Table 4.2 for V nodes as a reference for evaluating the associated complexity trade-offs, representing how the total number of distinct non-looping routes changes as a function of the number of nodes using (4.14). Table 4.2 also portrays that the complexity increases exponentially as a function of V. Since we quantify the complexity of the algorithms in terms of the total number of function calls to the RL evaluation, i.e. by the number of CFEs, the complexity is linearly proportional to the number of distinct non-looping routes.

4.3.2.2 Exhaustive Search Algorithm

Algorithm 4.1 shows the ESA used for maximizing the NL, which can be summarized as follows;

V	Number of distinct non-looping routes
3	2
4	5
5	16
6	65
7	326
8	1,957
9	13,700
10	109,601
15	1.6927×10^{10}
20	1.7403×10^{16}

TABLE 4.2: Total number of distinct non-looping routes as a function of V.

- We initialize the parameters in the "input" section of Algorithm 4.1 for V, such as the target SINR γ, number of trials τ and the initial battery capacity $\mathcal{E}_i$ of each sensor. Note that the SN is always considered to be the first node and the DN is always set as the last node. Let us assume that a fully connected WSN is composed of 10 sensor nodes. Then the SN has the unique identifier of 0, while the DN has the unique index of 9.
- Then, a fully connected network conceived for a given number of V nodes is created at line 3 of Algorithm 4.1. We consider a single SN, which is fixed at a coordinate of $(0, 0)$, and a single DN is located at the coordinate of (x_{max}, y_{max}), where $(x_{max} \times y_{max})\text{m}^2$ describes the size of the sensor field, guaranteeing that SN and DN are far apart having the longest distance in between. All the other sensors are stationary and randomly distributed according to a uniform distribution. Therefore, the distance of a node from any other node in the network can be readily recorded with the aid of a distance matrix. This scenario may correspond to a network illustrated in Fig. 4.1, where the Euclidean distance between the SN and the DN is given by $d_{S,D} = \sqrt{(x_{max})^2 + (y_{max})^2}$, which coincides with the diagonal of the sensor field. We rely on the same distance matrix, until we compute the accumulated NL. More explicitly, since the WSN considered is stationary, once the network is created, the distances of all sensors are fixed for a given NL computation.
- The SN can transmit the information to the DN along with all possible distinct routes given by Eq. (4.14). Therefore, all possible SN-DN routes, which can be seen from Table. 4.2 for V number of nodes, are passed on to an optimization function, one at a time. On line 8, the optimization function, namely the so-called dual-simplex, computes the RL according to (4.10)–(4.13). Each route associated with a different number of hops in the fully connected network is automatically and appropriately arranged according to it scheduling matrix for RL computation. For example, the active links are determined for each TS n corresponding to the SPTS parameter T, discussed in Section 4.2.1, so

Algorithm 4.1 ESA for maximizing the NL based on the battery level of the SN

Input: γ (target SINR)
τ (number of trials)
$\mathcal{E}_{init}$ (initial battery of each sensor in the WSN)
V (number of nodes)
$(x_{max} \times y_{max})\text{m}^2$ (size of the sensor field starting from $(0,0)$ to (x_{max}, y_{max}))
κ (total number of RSS, while i indicates each of the RSS)
T_{net} (network lifetime)

1: **for** i **from** 0 **until** κ **do**
2: **for** j **from** 1 **until** τ **do**
3: Create a fully connected, randomly and uniformly distributed network for V
4: $d_{all} \leftarrow$ Get distance matrix using coordinates of sensors lying on $(x_{max} \times y_{max})\text{m}^2$
5: $T_{net} = 0 \leftarrow$ Set initial value of NL to zero per created network
6: $\mathbf{R} \leftarrow$ Discover all possible non-looping routes using (4.14)
7: **function** ESA($\mathcal{E}_{init}$, T_{net}, γ)
8: dual-simplex($\mathbf{R}$, d_{all}, $\mathcal{E}_{init}$, γ) $\rightarrow$ Pass $\mathbf{R}$ to the dual-simplex function
9: **if** $infeasible$
10: **eliminate** $\mathbf{R}_{infeasible}$
11: **else**
12: $\mathbf{T_R} \leftarrow$ Return the route lifetime of $\mathbf{R}$
13: $\mathbf{E_R} \leftarrow$ Return the energy usage per node of $\mathbf{R}$
14: $\mathbf{P_R} \leftarrow$ Return the transmit power per link of $\mathbf{R}$
15: **end if**
16: $T_R \leftarrow$ Obtain maximum $\mathbf{T_R}$
17: $\mathbf{R}_{best} \leftarrow$ Reserve the best RL aware routes with T_R
18: **do while** $\mathcal{E}_{SN} > 0 \leftarrow$ NL strictly depends on the SN battery level
19: $T_{net} = T_{net} + T_R \leftarrow$ Accumulate each RL value for building the NL
20: $R_{best} \leftarrow$ Select the best route using RSS_i from $\mathbf{R}_{best}$ for end-to-end transmission
21: $\mathbf{R}_{final} \leftarrow$ Copy R_{best} to a final array for each iteration of RL.
22: Update the batteries of all sensors with $E_{R_{best}}$ to obtain $\mathcal{E}_{residual}$
23: **return** ESA($\mathcal{E}_{residual}$, T_{net}, γ)
24: **end do**
25: **return** each T_{net} to an array for averaging NL τ times for given RSS_i
26: $h_{\mathbf{R}_{final}} \leftarrow$ size($\mathbf{R}_{final}$) Gather the hop length of each final route
27: $\text{SINR}_{link} \leftarrow$ Compute SINR of each link using (4.11) of γ for $\mathbf{R}_{final}$ with $\mathbf{P}_{\mathbf{R}_{final}}$
28: $\text{BER}_{link} \leftarrow$ Obtain BER_{link} of SINR_{link} with the aid of LUT for considered MCSs
29: $\text{E2EB}_{\mathbf{R}_{final}} \leftarrow$ Compute E2EB of each final route using (4.5) of BER_{link} with $h_{\mathbf{R}_{final}}$
30: $\text{E2EB}_{worst-case} \leftarrow$ Attain the highest E2EB of $\mathbf{R}_{final}$
31: **return** each $\text{E2EB}_{worst-case}$ to an array for averaging E2EB τ times for given RSS_i
32: **end for**
33: **end for**
34: **return** averaged T_{net} and worst case E2EB over τ trials for each RSS

that we are capable of identifying the interfering nodes and their gain matrices $G_{i,j}$ in the same TS to compute the interference terms, as shown in (4.2). Since our objective is to maximize the RL for all possible routes identified by the ESA, each optimization function call returns a RL value as its output, as indicated in Algorithm 4.1 on line 12. This implies that we obtain RL values for all the distinct routes in the fully connected WSN considered.

- Then, we choose the route associated with the highest RL on line 17. Additionally, since there may be more than one route having the same maximum RL value, we have introduced the RSSs. Four different RSSs are introduced for their appropriate employment

in different application scenarios. The first one is based on the total energy usage of the routes having the maximum RL. We basically select the specific route having the least total ED. In the second RSS, the route associated with the least number of hops is chosen, since here we assume that each sensor incurs a delay of a single time unit due to queuing delays both at the SN and intermediate nodes. The third RSS relies on the SN battery level. The route associated with the largest remaining SN battery is selected. The last RSS is based on a random route selection strategy. A random route is selected amongst all the routes having the maximum RL value. Note that the selection process exclusively relies on the specific routes having the maximum RL value. Therefore, we expect the NL results of these various RSSs to be similar, which will indeed be confirmed in Section 4.4. For each of the RSS, we run τ number of trials for averaging the NL results, as indicated on line 25 of Algorithm 4.1. Moreover, for convenience we term the four route selection schemes mentioned above as RSS-LTED, RSS-LNOH, RSS-LRBAT and RSS-RANR, respectively.

- The best selected RL route, based on its RSS, is used for the end-to-end transmission as indicated on line 20 of Algorithm 4.1. Let us refer to this end-to-end transmission as the "transmission phase". Therefore, a single evaluation of the best RL-aware route indicates that a transmission phase will take place over the reference route, which is the best RL-aware route. During the transmission phase, the battery level of the sensor nodes utilized during this transmission is reduced. Therefore, on line 22 of Algorithm 4.1, those battery levels have to be updated relying on their appropriately adjusted transmit power conforming to (4.10)–(4.13), respectively. Since we consider a scenario, where the NL is strictly dependent on the SN battery level considered on line 18 of Algorithm 4.1, the SN battery level has to be checked after every transmission phase. If the SN battery is not fully depleted, the ESA continues searching for the next best RL-aware route in the fully connected WSN with its residual (updated) batteries, commencing from the previous transmission phase. Basically, if there is sufficient battery charge at the SN, Algorithm 4.1 recursively searches for the next best route in the next iteration on line 23. If the SN battery is fully depleted, then the NL is determined by the summation of the maximum RL values gleaned from the previous iterative transmission phases, as indicated on line 19 of Algorithm 4.1. Note that each NL computation may require a few iterations of the RL-aware route computation or transmission phase, depending on the SN battery status after each iterative transmission phase.
- Since we know what the best RL-aware routes are from the various iterations of this specific transmission phase, on line 29 of Algorithm 4.1 we can invoke (4.5) for the E2EB calculation of the best RL-aware routes. Note that we assume the best RL-aware routes are indeed reserved by the SN after each transmission phase, as indicated on line 20 and 21 of Algorithm 4.1. We aim for finding the highest E2EB in the network to determine the upper bound of the BER in our WSN. Therefore, the route associated with the largest E2EB amongst the best RL routes is utilized on line 30 of Algorithm 4.1. More explicitly,

the best RL-aware routes possibly carry the highest E2EB, because these routes are the most power-efficient routes, since the only objective of the optimization problem is to maximize the NL, while maintaining a required QoS. Therefore, finding the highest E2EB amongst these best RL-aware routes is adequate for determining the upper bound of the E2EB in the WSN considered. Additionally, Eq. (4.11) guarantees maintaining the required signal quality of each link, which has to maintain the predefined target SINR. However, in our results we will confirm that each link attains the exact target SINR values, so that the transmit power per link can be minimized. Minimizing the transmit power can only be achieved by keeping the SINR per link as close as possible to the target SINR, which is given by the Eq. (4.11) and shown on line 27 of Algorithm 4.1. Therefore, it is demonstrated on line 28 of Algorithm 4.1 that the BER per link can be obtained from the LUT of the corresponding SINR, which can then be utilized for the E2EB computation using (4.5). Therefore, we conclude that for a given MCS and for a specific target SINR per link, the E2EB can be readily determined using (4.5) along the best RL routes and the route associated with the largest E2EB is used as the upper bound of the BER for the WSN considered, which describes the worst-case E2EB performance of the network, as indicated on line 30 of Algorithm 4.1.

4.3.2.3 Run-time Example of the ESA

We consider a 6-node fully connected network, where the SN has the unique identifier of 0 and the DN has the unique index of 5. In order to exemplify the NL computation, we select a target SINR of $\gamma = 0\,\text{dB}$, where the discrete-input continuous-output memoryless channel (DCMC) [223] capacity of QPSK is about 0.5 bit/symbol. The battery capacity per sensor is initialized to 5000 Joule. This simulation example only covers a single trial[6] ($\tau = 1$) of the NL computation for a path loss exponent of $m = 3$ and for the system model considered in Section 4.2.

The size of the sensor field is given by $40 \times 40m^2$, where the sensors are randomly and uniformly deployed over the sensor field. However, the SN is fixed at a coordinate of $(0, 0)$, while the DN is placed at the other corner of the sensor field associated with the coordinate of $(40, 40)$. Therefore, the distance between the SN and the DN corresponds to the largest possible distance in the network, which is approximately $d_{SN,DN} \approx 56.57\text{m}$, as illustrated in Fig. 4.11.

We can readily observe from Table 4.2 that the SN has 65 alternative routes for transmitting its data to the DN for $V = 6$. Therefore, the ESA looks for all those possible routes and computes their RL by passing the route information to the optimization function. For this specific scenario, the symmetric distance matrix of the fully connected WSN seen in

[6] A NL computation *trial* may be constituted by several RL computation *iterations*.

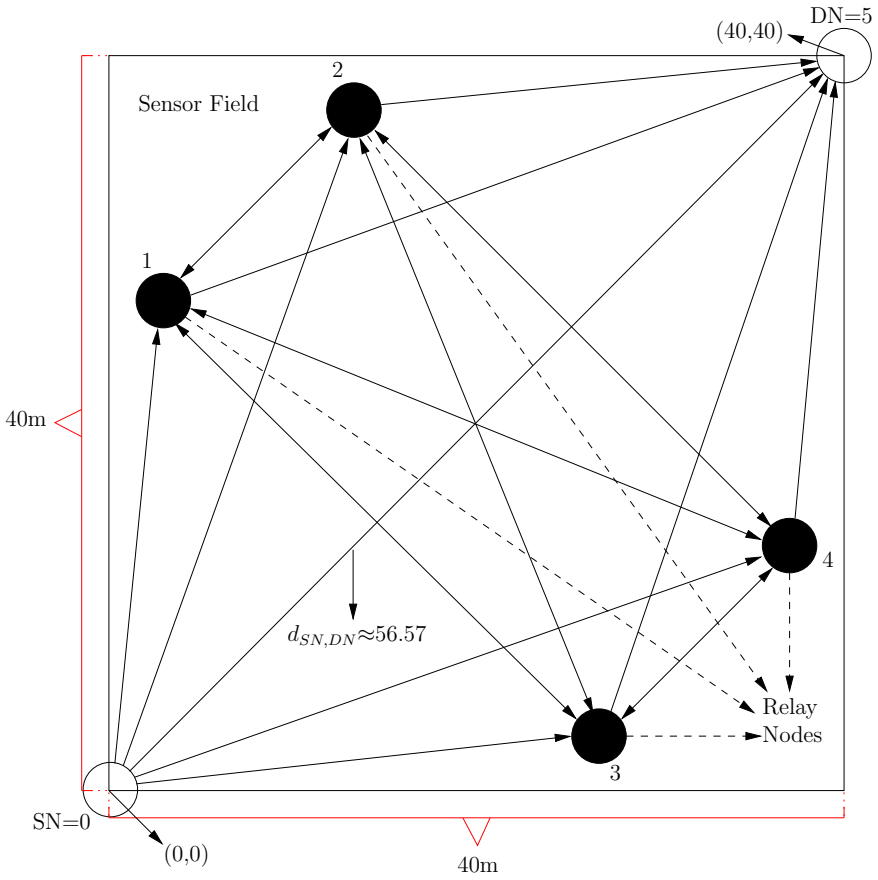

FIGURE 4.11: Example of a fully connected WSN consisting of 6 nodes (not to scale).

nodes $i \setminus j$	0	1	2	3	4	5
0	0	9.03	41.87	42.15	23.64	56.57
1	9.03	0	33.21	33.23	18.38	47.54
2	41.87	33.21	0	4.77	36.12	19.82
3	42.15	33.23	4.77	0	33.67	16.41
4	23.64	18.38	36.12	33.67	0	42.73
5	56.57	47.54	19.82	16.41	42.73	0

TABLE 4.3: Distance matrix $d_{i,j}$ of a 6-node fully connected WSN.

Fig. 4.11 can be exported, as observed in Table 4.3, where we can look up all the distance information of any relevant sensor node. For the sake of clarity, we present the distance conversion matrix (DCM) of a single actual route $R_{act} = [0-4-1-2-3-5]$ out of the 65 possible routes. For the sake of computing the RL in dual-simplex optimization function, arranging the corresponding matrix elements of the distance and $G_{i,j}$ of the WSN is one of the challenging parts of the problem due to the presence of the interference terms.

nodes $i \setminus j$	0	4	1	2	3	5
0	0	23.64	0	0	42.15	0
4	23.64	0	18.38	36.12	0	42.73
1	0	18.38	0	33.21	33.23	0
2	0	36.12	33.21	0	4.77	0
3	42.15	0	33.23	4.77	0	16.41
5	0	42.73	0	0	16.41	0

TABLE 4.4: Distance matrix d_{act} of R_{act} including the distance information of the interferers extracted from $d_{i,j}$.

Therefore, in our approach we utilize the DCM, where each sensor along the route having a unique identifier is reordered. Let us clarify this with the aid of an example by referencing it to the original distance matrix of Table 4.3. Firstly, a distance matrix is extracted from Table 4.3, which is only specified for the route R_{act}. In the mean time, the actual route R_{act} associated with the actual distance matrix d_{act} in Table 4.4 is converted to the ordered route $R_{ord} = [0-1-2-3-4-5]$ having the distance d_{ord} in Table 4.5. This approach provides us with the converted route R_{ord} along with the actual distance matrix d_{act} of the route R_{act}. The ordered route R_{ord} exploits the simplified indices of the corresponding sensors, while reserving the required distance values of the actual route R_{act}. Basically, each time when a route R_{act} is passed to the optimization function, its distance information is assigned to the converted route R_{ord}. Note that the reordered routes can be in the range of $\{0-1, 0-1-2, 0-1-2-3,...,0-1-2-3-4-5-6-7,...\}$, depending on the size of the actual route R_{act}. Additionally, a zero is placed in Table 4.4 and Table 4.5, if there are no direct communication links between the nodes lying on the route.

Then, we estimate the gain matrix seen in Table 4.6 of the reordered route using the distance matrix of Table 4.5, which is calculated using $G_{i,j} = 1/d_{i,j}^{m}$, as discussed in Section 4.2.2.

Moreover, given the gain matrix of Table 4.6, the optimization function handles (FHs) are automatically created by the optimization tool, namely the dual simplex function of the CPLEX library[90], by exploiting the specific relationship between the optimization variables in order to obtain the optimal values of the transmit power and the RL, as shown in Table 4.7. Note that optimization FHs are constituted by the mathematical expressions describing the relationship between the optimization variables, where each part of the optimization problem and its constraint is transformed so that they can be readily interpreted and solved by the optimization function. We exemplify the optimization FHs of our optimization problem

nodes $i \setminus j$	0	1	2	3	4	5
0	0	23.64	0	0	42.15	0
1	23.64	0	18.38	36.12	0	42.73
2	0	18.38	0	33.21	33.23	0
3	0	36.12	33.21	0	4.77	0
4	42.15	0	33.23	4.77	0	16.41
5	0	42.73	0	0	16.41	0

TABLE 4.5: Distance matrix d_{ord} of R_{ord}, including the distance information of interferers converted from d_{act} using DCM.

$i \setminus j$	0	1	2	3	4	5
0	∞	7.6×10^{-5}	∞	∞	1.3×10^{-5}	∞
1	7.6×10^{-5}	∞	1.6×10^{-4}	2.1×10^{-5}	∞	1.3×10^{-5}
2	∞	1.6×10^{-4}	∞	2.7×10^{-5}	2.7×10^{-5}	∞
3	∞	2.1×10^{-5}	2.7×10^{-5}	∞	9.2×10^{-3}	∞
4	1.3×10^{-5}	∞	2.7×10^{-5}	9.2×10^{-3}	∞	2.3×10^{-4}
5	∞	1.3×10^{-5}	∞	∞	2.3×10^{-4}	∞

TABLE 4.6: Gain matrix $G_{i,j}$ of the route R_{ord}, which is transformed from R_{act}.

considered in (4.10)–(4.11), where the OF and the constraint functions are transformed into a series of mathematical expressions, as illustrated in Tables 4.7, 4.8 and 4.9. Additionally, we can follow the link-centric view of Fig. 4.6 or the TS-centric view of Fig. 4.5 for a clear understanding of the variable relationships for Table 4.7, which is obtained by using Eq. (4.11). For example, only the specific link spanning from node $i = 2$ to node $j = 3$ in TS $n = 3$ denoted by $(l_{2,3}, 3)$ is activated in Fig. 4.6. Therefore, link $(l_{2,3}, 3)$ in Table 4.7 contains only the desired transmission, since there is no interfering node. We note that the FHs of Tables 4.7 and 4.9 are taken from our run-time simulation outputs. Thus, let us confirm under the target SINR constraint of link $(l_{1,2}, 2)$, whether the optimization FHs are correctly obtained from our run-time simulation trial for the corresponding elements taken from Table 4.6.

Hence, here we commence by deriving the expected FH of the target SINR constraint for the link $l_{1,2}, 2$ by following Fig. 4.6, where both link $l_{1,2}$ as well as link $l_{4,D}$ are activated in TS $n = 2$, nothing that node $i' = 4$ interferes with node $i = 2$. Therefore, the constraint

$l_{i,j}, n$	Target SINR constraint FHs
$l_{0,1}, 1$	$[-7.56 \times 10^{-5} \times q(1) + \gamma \times 2.12 \times 10^{-5} \times q(4)] \leq -(\gamma \times N_0)$
$l_{1,2}, 2$	$[-1.61 \times 10^{-4} \times q(2) + \gamma \times 2.72 \times 10^{-5} \times q(5)] \leq -(\gamma \times N_0)$
$l_{2,3}, 3$	$[-2.73 \times 10^{-5} \times q(3)] \leq -(\gamma \times N_0)$
$l_{3,4}, 1$	$[-9.21 \times 10^{-3} \times q(4) + \gamma \times 1.33 \times 10^{-5} \times q(1)] \leq -(\gamma \times N_0)$
$l_{4,5}, 2$	$[-2.26 \times 10^{-4} \times q(5) + \gamma \times 1.28 \times 10^{-5} \times q(2)] \leq -(\gamma \times N_0)$

TABLE 4.7: Optimization FH of the target SINR considering Eq. (4.11), when $V = 6$, $T = 3$ and $N = 3$.

$P_{l_{0,1},1}$	$P_{l_{1,2},2}$	$P_{l_{2,3},3}$	$P_{l_{3,4},1}$	$P_{l_{4,5},2}$	z
$q(1)$	$q(2)$	$q(3)$	$q(4)$	$q(5)$	$q(6)$

TABLE 4.8: Transmit power and the corresponding reciprocal of the RL variables, which are denoted by the optimization variable vector $\mathbf{q}$.

for link $l_{1,2}$ and TS $n = 2$ inferred from Eq. (4.11) is given by $-G_{1,2} \times P_{l_{1,2},2} + \gamma \times G_{4,2} \times P_{l_{4,D},2} \leq -(\gamma \times N_0)$ in conjunction with $\gamma = 10^{(0.1 \times SINR[dB])}$, where $SINR = 0\,\text{dB}$ is considered for this specific scenario. By substituting in the corresponding elements from Table 4.6, we arrive at $-1.61 \times 10^{-4} \times P_{l_{1,2},2} + 1 \times 2.72 \times 10^{-5} \times P_{l_{4,D},2} \leq -(1 \times N_0)$, where we have $P_{l_{1,2},2} = q(2)$ and $P_{l_{4,D},2} = q(5)$ from Table 4.8, and $\mathbf{q}$ is the vector of the corresponding transmit power $\mathbf{P}_{l_{i,j},n}$ and z variables, which is denoted by the set of $\mathbf{q} = \{\mathbf{P}_{l_{i,j},n}, z\}$ for $\{\mathbf{q} \in \mathbb{R} : 0 \preceq \mathbf{q} \preceq \infty\}$, since the unique identifier of the SN is 0 and of the DN is 5, as illustrated in Figs. 4.5 and 4.6. The final version of the constraint becomes $[-1.61 \times 10^{-4} \times q(2) + \gamma \times 2.72 \times 10^{-5} \times q(5) \leq -(\gamma \times N_0)]$, which is the value of link $(l_{1,2}, 2)$ in Table 4.7. Note again that the transmit power variables are linked to their corresponding variables of $\mathbf{q}$ in the optimization FHs of Table 4.7. For convenience, we provide the corresponding variable relationships in Table 4.8. To sum up, using the set of mathematical expressions in Tables 4.7, 4.8 and 4.9, we can find the optimal solutions for the variables of our original optimization problem.

Furthermore, we provide the FHs of the ED constraints as well as maximum transmit power constraints for the parameters considered in Section 4.3.2.3. Note that we aim for minimizing the reciprocal of the RL z, which is the main objective function of our optimization problem and corresponds to $q(6)$. The constraint FHs required for minimizing $z = q(6)$ provided in Tables 4.7 and 4.9 must be satisfied at all time for $V = 6$, $T = 3$, $N = 3$ and for the other parameters of this particular scenario. Having discussed the ESA, let us now move on to

$l_{i,j}, n$	Energy dissipation constraint FHs	Transmit power constraint FHs
$l_{0,1}, 1$	$1.4 \times q(1) - 15000 \times q(6) \leq 0$	$q(1) \leq (P_i)_{max}$
$l_{1,2}, 2$	$1.4 \times q(2) - 15000 \times q(6) \leq 0$	$q(2) \leq (P_i)_{max}$
$l_{2,3}, 3$	$1.4 \times q(3) - 15000 \times q(6) \leq 0$	$q(3) \leq (P_i)_{max}$
$l_{3,4}, 1$	$1.4 \times q(4) - 15000 \times q(6) \leq 0$	$q(4) \leq (P_i)_{max}$
$l_{4,5}, 2$	$1.4 \times q(5) - 15000 \times q(6) \leq 0$	$q(5) \leq (P_i)_{max}$

TABLE 4.9: The FHs for the variables of the ED formulated in (4.12) and for the maximum transmit power constraints of (4.13) per node.

the calculation of the NL and of the residual battery capacity.

4.3.2.4 NL Computation and Battery State Update

In the first step of the NL computation, the ESA searches for the best RL-aware routes. For the 6-node fully connected scenario of Fig. 4.11, ESA finds four different routes having the same maximum RL. These four routes of Fig. 4.11 are $[0-1-2-5]$, $[0-1-2-3-5]$, $[0-4-1-2-5]$, $[0-4-1-2-3-5]$ with a RL of $81,292.4$ hours (hrs) for a predefined target SINR value of $\gamma = 0\,\text{dB}$, as evaluated by the optimization tool. To further elaborate on this specific example, we consider a target SINR value of $\gamma = 0\,\text{dB}$[7]. However, this can be extended for any of the target SINR values of $\gamma = \{0, 0.5, 1, 1.5, ..., 9, 9.5, 10\}\,\text{dB}$. In Section 4.3.2.2, we introduced four RSSs to deal with the route selection process, which we referred to as RSS-LTED, RSS-LNOH, RSS-LRBAT and RSS-RANR. However, for this specific example we will only consider RSS-LTED, which reserves the route associated with the least total ED. Therefore, we can identify the best RL-aware route by checking the total ED of each route.

From Table 4.10, we can observe 3 iterations (iters) of the RL computation, which constitutes one trial NL computation for the $V = 6$-node fully connected WSN. Each iteration of the RL computation evaluates how much of the SN battery (initialized to 5000J) has been dissipated by the route that is selected as the best RL-aware route after each iteration. For example, route $[0-1-2-3-5]$ is selected with the aid of RSS-LTED, since it consumes a total of 5733J energy, which is the least amount of ED among all the routes. Moreover, since the NL is strictly dependent on the level of the SN battery, the remaining battery (RBAT)

[7]We compute the NL for the target SINR values of $\gamma = \{0, 0.5, 1, 1.5, ..., 9, 9.5, 10\}\,\text{dB}$. However, as an example here we use only 0 dB SINR to present the routing information, the remaining battery charge and other related operations during the NL computation. We note that for a target SINR value of 0dB, the discrete-input continuous-output memoryless channel (DCMC) [223] capacity of QPSK is about 0.5 bit/symbol.

Iters	The best RL routes	RSS-LTED [J]	RL [hrs]	The best route	RBAT at SN [J]
1st	$[0-1-2-5]$	6163	$81,292$	$[0-1-2-3-5]$	4887
	$[0-1-2-3-5]$	5733			
	$[0-4-1-2-5]$	9131			
	$[0-4-1-2-3-5]$	8444			
2nd	$[0-4-3-5]$	7310	$77,985$	$[0-4-3-5]$	3155
	$[0-4-3-2-5]$	8164			
3rd	$[0-2-5]$	3490	$25,595$	$[0-2-3-5]$	0
	$[0-2-3-5]$	3350			

TABLE 4.10: One trial of NL computation is composed of three dependent steps of RL computation, while illustrating the level of SN battery after each iteration.

of the SN after each iteration of the RL computation is provided in Table 4.10. During the first iteration, 112J of energy is utilized at the SN, while in the second iteration, an amount of 1731J is depleted from the SN, which had an instantaneous RBAT of 4887J. The RBAT of the SN is reduced to 3155J. Finally, in the third iteration an amount of 3155J energy is consumed from the RBAT of 3155J. Since there is no more energy left in the SN battery, the information cannot be generated and transmitted to the DN. Therefore, the network becomes inoperative and hence the NL is determined and accumulated to arrive at $81,292 + 77,985 + 25,595 \approx 184,873$hrs after terminating the RL computation. Note that a single trial of the NL computation may be composed of a few iterations of the RL computations and it is not fixed to three iterations. It can vary depending on how much energy is utilized at the SN after each RL computation.

To elaborate further on how the sensor batteries are depleted after each iteration using the best route shown in Table 4.10, in Table 4.11 we provide the battery states for all sensors lying in the best route. We consider three states for the battery of sensor nodes lying on the best route. The "After" and "Before" states represent the level of all the sensor batteries in the network, except for the DN. The "Used" state represents the amount of battery dissipation for the sensors lying on the best route utilized for the end-to-end transmission. Recall that node-0 is the SN and node-5 is the DN in Fig. 4.11. Since we assume that the ED at the DN is unimportant, because it is plugged into the mains power supply, the DN is removed from the battery charge update list. Therefore, only the first 5 nodes of the 6-node fully connected WSN of Fig. 4.11 is reserved for the battery charge update list. For example, each battery of the sensor nodes, in the order of $[0-1-2-3-4]$ is initialized with $[5000-5000-5000-5000-5000]$Joules battery capacity, respectively and these nodes

Iters	The best route	State	Sensor nodes except DN $[0-1-2-3-4]$
1st	$[0-1-2-3-5]$	Before	$[5000-5000-5000-5000-5000]$
		Used	$[112-5000-14-606]$
		After	$[4887-0-4985-4393-5000]$
2nd	$[0-4-3-5]$	Before	$[4887-0-4985-4393-5000]$
		Used	$[1731-5000-578]$
		After	$[3155-0-4985-3815-0]$
3rd	$[0-2-3-5]$	Before	$[3155-0-4985-3815-0]$
		Used	$[3155-4-189]$
		After	$[0-0-4980-3625-0]$

TABLE 4.11: The battery state of all the sensor nodes after each iteration of RL computation in the WSN of Fig. 4.11.

are always reserved in order and are updated, when a node is on the route utilized for the end-to-end transmission.

Explicitly, depending on which route is used for an end-to-end transmission after each iteration of the RL computation, the corresponding battery of the sensor node is depleted in the WSN. For example, assuming that the sensors $[0-1-2-3-5]$ are utilized for the end-to-end transmission, only the actively utilized sensor battery charges are reduced by the amount of $[112-5000-14-606]$, respectively, as illustrated in Table 4.11. The battery of node-4 is never utilized in the first iteration, therefore in the state "After" of the first iteration it remains 5000J, while the residual battery charge of the other nodes becomes $[4887-0-4985-4393-5000]$.

Furthermore, for the sake of clarity we provide Fig. 4.12(a), 4.12(b), 4.12(c), and 4.12(d) for illustrating which particular routes are utilized for end-to-end transmission, and hence which sensor batteries are updated after each iteration of the RL computation. Note that the hollow batteries represent the fully-depleted batteries after each iteration. Surprisingly, node-2 and node-3 were capable of preserving their battery levels as close as possible to their initial battery levels. This is due to the smaller distance between the transmitting node-2 and its receiver for the routes selected as the best RL-aware ones in each iteration. A similar trend is observed for node-3. For example, for the first iteration the distance between node-2 and node-3, as well as node-3 and node-5 is lower than those of others on the same route. Similar trends can be observed during the second and third iterations. Additionally, in the first iteration node-1, in the second iteration node-4 and in the third iteration SN (node-0) communicates over longer distances with their receivers compared to that of node-2 and

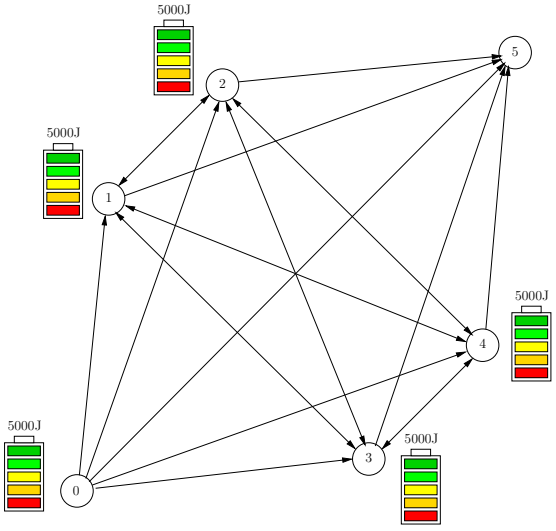

(a) Initial battery level of all sensors in the WSN

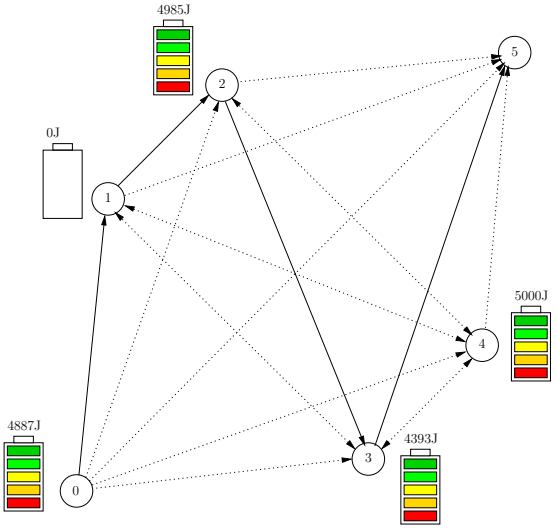

(b) The battery levels after the first iteration of RL computation

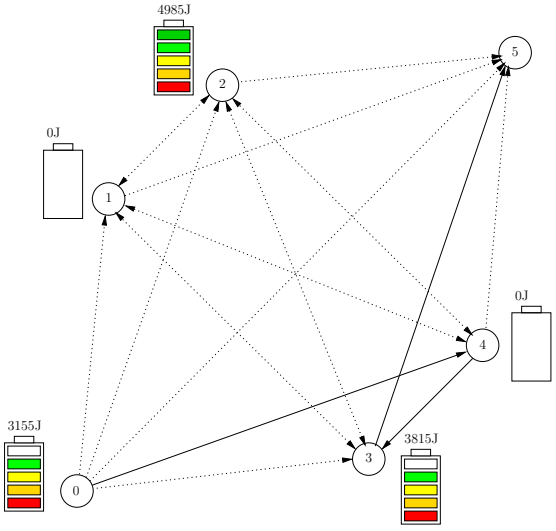

(c) The battery levels after the second iteration of RL computation

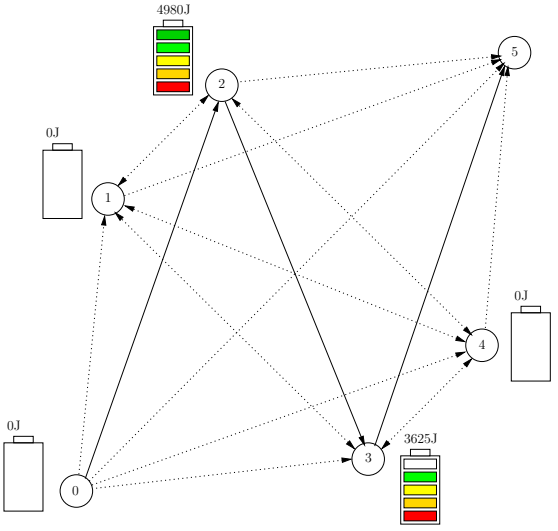

(d) The battery levels after the third iteration of RL computation

FIGURE 4.12: Illustration of the changes in the level of the battery-energy (not to scale).

node-3, respectively. Therefore, those sensor nodes depleted their batteries earlier than the other nodes lying on their respective routes, which are illustrated by the hollow batteries in Fig. 4.12(b), 4.12(c), and 4.12(d), respectively.

4.3.2.5 Single Objective Genetic Algorithm

The above run-time simulation analysis of ESA is based on $V = 6$ nodes, but it can be readily generalized for any arbitrary number of nodes. However, the computation of the NL strictly depends on the specific route's complexity in the WSN considered. For example, the $V = 6$ scenario of Fig. 4.11 examines 65 distinct non-looping alternative routes, whilst according to Table 4.2 $V = 10$ introduces $109,601$ distinct routes for the NL computation

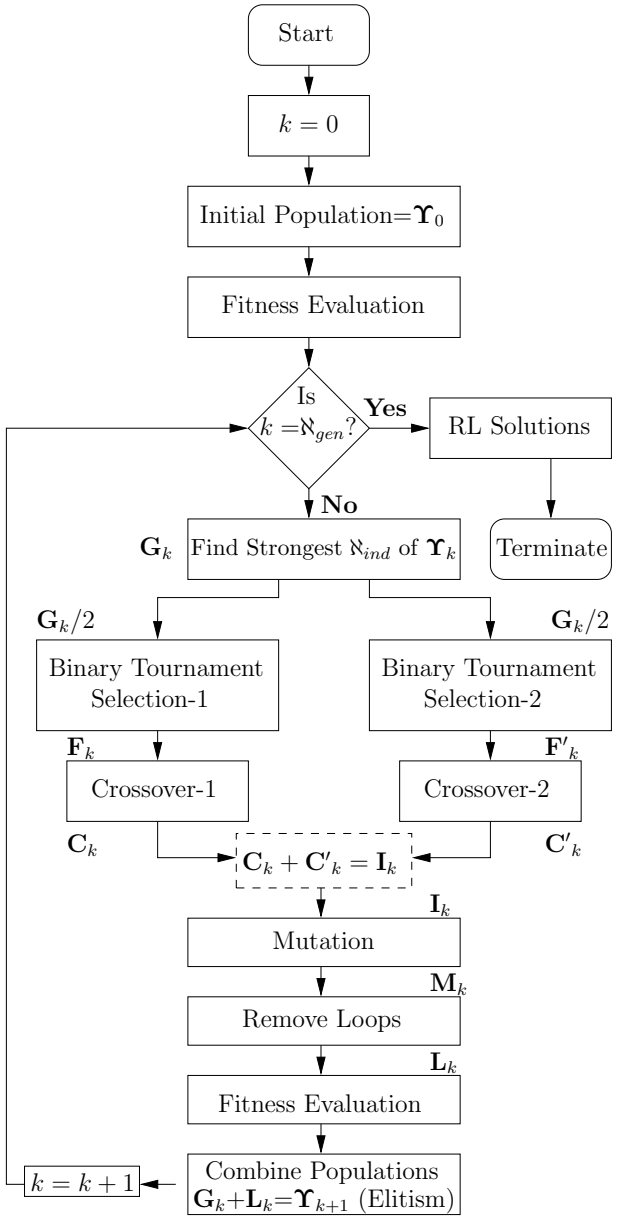

FIGURE 4.13: A flowchart presenting the general overview of the SOGA adopted for our NL maximization technique, which the flow of the genetic operations can also be followed for more details in Fig. 4.16.

using ESA. Therefore, the exponential increase in the number of distinct routes from 65 to 109,601 may impose an excessive complexity, especially when each NL computation requires more than a few RL computation iterations, which invokes a full search of the fully connected WSN during each iteration. This large number of distinct routes may correspond to a larger partially connected distributed network with many more sensor nodes. Therefore, our fully connected WSN approach can also be applied to any other realistic network without being limited to fully connected networks.

In order to circumvent the computational complexity of ESA encountered in realistic WSNs

composed of a vast number of distinct routes we invoke a SOGA, which relies on genetic operations inspired by evolutionary biology, such as inheritance, selection, crossover, mutation and recombination. Before moving on to the intricate details of the SOGA considered, let us familiarize ourselves with the terms of evolutionary biology and its exploitation in our context. For example, a chromosome of the SOGA is composed of sequences of integers, which represent a specific route consisting of a unique sensor node index. Hence we refer to a sensor node as a gene, each of which belongs to the chromosome. We also refer to a chromosome as an individual of the SOGA having a specific route's path (chromosome) information. Moreover, a fitness function evaluates the quality of a chromosome in terms of achieving the desired objective. In our scenarios, we evaluate the route information of each individual using a fitness function (FF) or OF to acquire the RL fitness value. Therefore, we can say that the FF quantifies the quality of a chromosome (individual), where the FF is expected to have a higher fitness value in maximization problems for a better solution, i.e. route.

A general overview of how our SOGA operates is outlined in Fig. 4.13. The process commences with the initialization of a population, which is constituted by the individuals that are evaluated in terms of their specific fitness functions in order to identify the quality of the corresponding solutions. Note that we deploy a regular genetic algorithm, including some modifications of its operators. In a GA, a termination rule has to be set, so that it can terminate when a certain condition is satisfied, i.e. a sufficiently high quality solution has been found or the affordable number of generations has been exhausted. Specifically, in the SOGA we can adjust the number of generations $\aleph_{gen}$, as illustrated in Fig. 4.13, which allows us to strike a performance versus complexity trade-off. Additionally, since there are numerous individuals in a population, the specific selection amongst the candidate solutions (individuals) plays a significant role in terms of converging to an improved solution. Basically, the selection operator is invoked for improving the quality of the population by giving the high-quality individuals a higher chance of passing on their fitness characteristics to the next generations, as seen in Fig. 4.13. Consequently, we obtain the population $\mathbf{G}_k$ containing $\aleph_{gen}$ high-quality individuals, as illustrated in Fig. 4.13.

Following the inclusion of these high-quality individuals in the current population, we invoke the binary tournament selection (BTS) of Fig. 4.13, where the individuals of the current population are divided into two sets $\mathbf{G}_k/2$. Then, a specific individual is randomly selected from each of the two sets for a competition in terms of their fitness values. Finally, the particular individual having a better fitness value is selected as a parent individual for creating the next generation, which forms the populations $\mathbf{F}_k$ and $\mathbf{F}'_k$. Then, as seen in Fig. 4.13, the crossover operation is applied to each of these populations $\mathbf{F}_k$ and $\mathbf{F}'_k$ containing the parent individuals, respectively, for examining the current solutions in order to find more fit individuals, which may also introduce a certain grade of solution diversity for the current population. We use the single-point cross-over method, where a common gene (sensor

node) is used for dividing the chromosomes into two parts for merging a certain fraction of the individual constituted by a route with the other half of the other individual and vice versa. These newly created individuals are termed as child individuals, which are expected to inherit the beneficial characteristics of the parent individuals. We note that as illustrated in Fig. 4.13, the BTS and crossover operations are applied twice for increasing the solution diversity as well as for acquiring a sufficient number of individuals. Then, the populations $\mathbf{C}_k$ and $\mathbf{C}'_k$, which are subjected to both the BTS and crossover operations, are combined in order to create the population $\mathbf{C}_k + \mathbf{C}'_k = \mathbf{I}_k$, which is then subjected to mutation, as seen in Fig. 4.13.

Finally, as seen in Fig. 4.13, a mutation operation is applied to the child individuals constituting the population $\mathbf{I}_k$, where each one of the genes of each child individual is mutated with a certain mutation probability, so that entirely new individuals constituting the population $\mathbf{M}_k$ can be introduced into the next generation. When the mutation operation is applied to a particular gene, we opt for one of three different mutation operations in our scenarios with equal probability, namely for node replacement, for node removal and for node insertion. Their specific details will be provided along with our more elaborate explanations of SOGA later in this section. Basically, the mutation operation further increases the diversity of the population by examining the fitness of new candidate solutions. Therefore, we may conclude that a population is created in the first generation (iteration) consisting of several individuals (candidate solutions) and throughout the successive generations by using the genetic operations described above. As a benefit, the individuals are expected to gradually create better solutions [177, 224, 225]. After the mutation operation, any potential node repetitions are removed from the routes, which leads to the population $\mathbf{L}_k$, as illustrated in Fig. 4.13. Then, the fitness of the individuals in population $\mathbf{L}_k$ is evaluated before proceeding to the forthcoming generation. Ultimately, as seen in Fig. 4.13, the newly created population $\mathbf{L}_k$ and the current population $\mathbf{G}_k$ are combined, since we do not want to lose any of the current high-quality solutions. The specific process of combining the new and current populations as well as the technique of selecting the high-quality individuals from this combined population is referred to as elitism, which will be discussed later. Having summarized the general structure of a genetic algorithm and the SOGA considered, the diverse terminologies concerning the above genetic operations, including the individuals, populations, fitness values, binary tournament selection, crossover and mutation operations will be exemplified later in this section.

We simplified the multi-objective genetic algorithm described in [177] so that it can be utilized for single-objective optimization. We further modified the genetic operations in a manner similar to our work in [182]. One of the main differences between the SOGA and ESA is that SOGA intelligently searches through the solution space relying on the above-mentioned genetic operators, while ESA performs a brute-force full search by means of looking for all possible permutations in the solution space. As illustrated in Fig. 4.14, SOGA

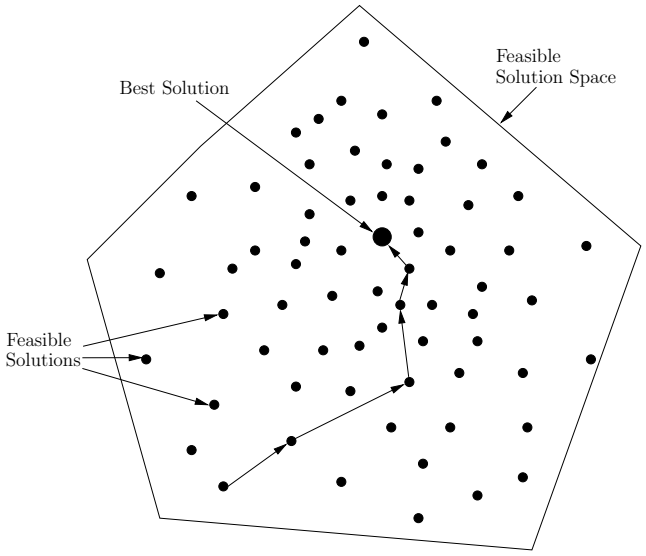

FIGURE 4.14: Solution search strategy of ESA and SOGA within the feasible solution space.

is capable of arriving at the best solution (marked by the largest dot filled with black color) after 5 generations, whereas ESA has to search though the entire solution space constituted by each dot for finding the best solution. However, the reduced-complexity SOGA may produce suboptimal results for large networks. Nonetheless, it may be configured to strike the required performance versus complexity trade-offs approaching the optimal NL. Let us now discuss the SOGA as described in Algorithm 4.2, where we mostly focus our attention on the genetic operators of the algorithm.

At the "input" section of Algorithm 4.2, we define the simulation parameters as well as the genetic operation constants, such as $\aleph_{ind}$, $\aleph_{gen}$, Pr_c, Pr_m denoting the number of individuals, number of generations, the crossover probability and the mutation probability, respectively. In each generation of a population, $\aleph_{ind}$ individuals are created, each of which represents a candidate solution, which is randomly initialized with feasible values during the initial population. After each iteration of $\aleph_{gen}$, these initialized individuals are expected to converge to superior fitness values by applying the genetic operators of inheritance, selection, crossover, mutation and recombination, which also assist us in increasing the diversity of the solutions, so that the algorithm would not miss the improved solutions. Firstly, we create a fully connected, randomly and uniformly distributed WSN and obtain the distance matrix of it with the aid of coordinates of the sensors, as indicated on line 3 and 4 of Algorithm 4.2. Then, an initial population associated with $\aleph_{ind} = 48$ individuals is created and each individual is associated with a route randomly selected from the fully connected WSN, as shown on line 7–9 of Algorithm 4.2 and in Table. 4.12. Here, we only gather the route information of the individuals, but the RL objective function or synonymously the fitness function, is not evaluated. Hence we have no knowledge of the fitness values for the corresponding individuals. Therefore, on line 10 of Algorithm 4.2 these routes are passed to

Algorithm 4.2 SOGA for maximizing the NL based on the battery level of the SN

Input: γ (target SINR)
τ (number of trials)
$\mathcal{E}_{init}$ (initial battery of each sensor in the WSN)
V (number of nodes)
$(x_{max} \times y_{max})\text{m}^2$ (size of the sensor field starting from $(0,0)$ to (x_{max}, y_{max}))
κ (total number of RSS, while i indicates each of the RSS)
T_{net} (network lifetime)
$\aleph_{gen}$ (number of generations)
$\aleph_{ind}$ (number of individuals)
Pr_c (probability of crossover)
Pr_m (probability of mutation)

1: **for** i **from** 0 **until** κ **do**
2: **for** j **from** 1 **until** τ **do**
3: Create a fully connected, randomly and uniformly distributed network for V
4: $d_{all} \leftarrow$ Get distance matrix using coordinates of sensors lying on $(x_{max} \times y_{max})\text{m}^2$
5: $T_{net} = 0 \leftarrow$ Set initial value of NL to zero per created network
6: **function** run($\mathcal{E}_{init}$, T_{net}, γ) $\rightarrow$ Start SOGA
7: create($\boldsymbol{\Upsilon}_0$) $\leftarrow$ Create an initial population
8: $\boldsymbol{\Upsilon}_0 \rightarrow \mathbf{R} \leftarrow$ Create $\aleph_{ind}$ random routes for setting up the population
9: $\boldsymbol{\Upsilon}_0 \rightarrow T_{\mathbf{R}} = 0 \leftarrow$ Initialize the RL of each individuals in the population
10: dual-simplex($\boldsymbol{\Upsilon}_0 \rightarrow \mathbf{R}$, d_{all}, $\mathcal{E}_{init}$, γ) $\rightarrow$ Evaluate RL of $\boldsymbol{\Upsilon}_0 \rightarrow \mathbf{R}$
11: **for** k **from** 0 **until** $\aleph_{gen}$ **do**
12: $\mathbf{G}_k \leftarrow$ get-strongest-$\aleph_{ind}$($\boldsymbol{\Upsilon}_k$)
13: $\mathbf{F}_k \leftarrow$ get-$\aleph_{ind}$/2-parents($\mathbf{G}_k$), binary tournament selection
14: $\mathbf{C}_k \leftarrow$ get-$\aleph_{ind}$/2-crossover-$\aleph_{ind}$/4-by-$\aleph_{ind}$/4($\mathbf{F}_k$) using Pr_c
15: $\mathbf{F}'_k \leftarrow$ get-$\aleph_{ind}$/2-parents($\mathbf{G}_k$), binary tournament selection
16: $\mathbf{C}'_k \leftarrow$ get-$\aleph_{ind}$/2-crossover-$\aleph_{ind}$/4-by-$\aleph_{ind}$/4($\mathbf{F}'_k$) using Pr_c
17: $\mathbf{I}_k \leftarrow$ complete-individuals-to-$\aleph_{ind}$($\mathbf{C}_k + \mathbf{C}'_k$)
18: $\mathbf{M}_k \leftarrow$ mutate-individuals-get-$\aleph_{ind}$($\mathbf{I}_k$) using Pr_m
19: $\mathbf{L}_k \leftarrow$ remove-loops-of-$\aleph_{ind}$($\mathbf{M}_k$)
20: dual-simplex($\mathbf{L}_k \rightarrow \mathbf{R}$, d_{all}, $\mathcal{E}_{init}$, γ)
21: $\boldsymbol{\Upsilon}_{k+1} \leftarrow$ combine-populations-get-2 $\times$ $\aleph_{ind}$($\mathbf{L}_k$, $\mathbf{G}_k$)
22: **end for**
23: $\mathbf{T_R} \leftarrow$ Return the route lifetime of $\boldsymbol{\Upsilon}'_{\aleph_{\mathbf{gen}}} \rightarrow \mathbf{R}$
24: $\mathbf{E_R} \leftarrow$ Return the energy usage per node of $\boldsymbol{\Upsilon}'_{\aleph_{\mathbf{gen}}} \rightarrow \mathbf{R}$
25: $\mathbf{P_R} \leftarrow$ Return the transmit power per link of $\boldsymbol{\Upsilon}'_{\aleph_{\mathbf{gen}}} \rightarrow \mathbf{R}$
26: $T_R \leftarrow$ Obtain maximum $\mathbf{T_R}$
27: $\mathbf{R}_{best} \leftarrow$ Reserve the best RL aware routes with T_R
28: **do while** $\mathcal{E}_{SN} > 0 \leftarrow$ NL strictly depends on the SN battery level
29: $T_{net} = T_{net} + T_R \leftarrow$ Accumulate each RL value for building the NL
30: $R_{best} \leftarrow$ Select the best route using RSS_i from $\mathbf{R}_{best}$ for end-to-end transmission
31: $\mathbf{R}_{final} \leftarrow$ Copy R_{best} to a final array for each iteration of RL.
32: Update the batteries of all sensors with $E_{R_{best}}$ to obtain $\mathcal{E}_{residual}$
33: **return** run($\mathcal{E}_{residual}$, T_{net}, γ)
34: **end do**
35: E2EB computation as between line 26 and 31 of the Algorithm 4.1
36: **end for**
37: **end for**
38: **return** averaged T_{net} and worst case E2EB over τ trials for each RSS

Individual index	Route Information
0	$[0-4-1-2-5]$
1	$[0-4-1-3-2-5]$
2	$[0-4-1-3-5]$
⋮	⋮
35	$[0-1-3-2-4-5]$
⋮	⋮
46	$[0-1-2-4-3-5]$
47	$[0-3-1-2-4-5]$

TABLE 4.12: Random route initialization of the 48 individuals in the first iteration of the first trial of the SOGA.

the dual-simplex optimization function in conjunction with their respective distance matrices for the RL evaluation, where each RL evaluation is characterized in terms of its fitness value. Hence, in our case each function call to the dual-simplex optimization function produces a fitness array consisting of the RL, the energy used per node and the transmit power per link utilized. The $\aleph_{ind}$ number of individuals (candidate solutions) are selected from population $\boldsymbol{\Upsilon}_k$ as the set of strongest individuals denoted by $\mathbf{G}_k$. As the iterations (generations) progress, Υ' is returned in conjunction with $(2 \times \aleph_{ind})$ individuals at the end of each generation. Therefore, the selection process[8] of the strongest individuals guarantees having $\aleph_{ind}$ individuals for the current population associated with the strongest attributes. The population $\mathbf{G}_k$ having $\aleph_{ind}$ individuals is randomly divided into two halves each having $\aleph_{ind}/2$ individuals of the population $\mathbf{F}_k$ in order to find the parents based on the BTS, as illustrated in Table 4.13 for crossover operation on line 13. We note that in Table 4.13 each index value represents an individual. Despite the fact that the index of 48 individuals is uniquely divided into two pairs of $Pair_1$ and $Pair_2$, the route information these individuals refer to can be exactly the same. For example, in Fig. 4.13, the individuals 24 and 30 are supposed to be different individuals due to their unique index values. However, the route information of the individuals 24 and 30 can be exactly the same. Nonetheless, the genetic operations can be extended to a strategy for creating arbitrary non-replicative individuals in the genetic algorithm considered, which provides us with a potentially faster convergence, since the algorithm is naturally forced to provide a higher grade of diversity of solutions

[8]This selection process introduces elitism to SOGA, where the better individuals from previous generations are carried over the next generations, unchanged. Therefore, the solution quality will never decrease from one generation to the next, since the best solution from previous generations is kept throughout the next generations. This selection strategy is known as elitist selection, which is not to be confused with the BTS.

Pairs	The index order of the individuals for BTS
$Pair_1$	$\{24, 12, 23, 29, 18, 8, 17, 6, 22, 1, 4, 20, 14, 11, 25, 0, 5, 16, 44, 9, 41, 2, 35, 34\}$
$Pair_2$	$\{30, 46, 28, 3, 45, 40, 37, 33, 7, 42, 21, 38, 47, 27, 43, 31, 36, 10, 26, 19, 32, 15, 13, 39\}$
Parents	$\{24, 12, 23, 3, 18, 8, 17, 6, 7, 1, 4, 20, 14, 11, 25, 0, 5, 16, 26, 9, 32, 2, 13, 34\}$

TABLE 4.13: The indices of the selected parents after BTS operation of $Pair_1$ and $Pair_2$ in the first iteration of the first trial of the SOGA.

at the initial stage. Note that BTS assists us in obtaining moderately stronger parent individuals associated with better fitness values for crossover operation. However, the BTS cannot guarantee that the selected individuals will always be stronger. More explicitly, in Table 4.13, $Pair_1$ and $Pair_2$ are compared in terms of their fitnesses and the better individuals are listed as "Parents". For example, individuals 24 and 30 are compared in terms of their fitnesses and 24 is selected as a better individual, since its RL evaluation produced a better fitness value for its route information. However, the fitness value of eliminated individual 30 for its route could have been better than that of the next elected individual, namely 12 in the current population $\mathbf{F}_k$. Therefore, BTS can only advocate the selection of fairly stronger individuals, while maintaining a beneficial solution diversity, which prevents early convergence by exploring much of the search-space. On line 14 of Algorithm 4.2 ($\aleph_{ind}/2$) individuals of the population $\mathbf{F}_k$ are consecutively divided into two halves, each of which now contains $\aleph_{ind}/4$ parent individuals. The pair sets of parent individuals, i.e. $\{(24, 12), (23, 3), (18, 8), ..., (13, 34)\}$ of Table 4.13, are then mated with the aid of the crossover operation as exemplified in Fig. 4.15 using Pr_c in order to create two child individuals, which may inherit attributes of both fairly strong parents selected by the BTS. Explicitly, assume that two consecutive arbitrary parents $\{...(1, 35)...\}$ selected from Table 4.12 exist in the population $\mathbf{F}_k$ for the sake of illustrating the crossover operation in Fig. 4.15. At the instant of the crossover operation, we use a similar strategy to that of our work in [182], where a common sensor node is chosen for the crossover point in our scenarios considered. We assume that the parents $Parent_1$ and $Parent_2$ represent the individuals 1 and 35 of $\mathbf{F}_k$, respectively. In this particular scenario, as illustrated in Fig. 4.15 the common node is selected as 3 for both $Parent_1$ and $Parent_2$. Then, $Child_1$ is created by the concatenation of the specific parts of the individuals representing the nodes leading up to and including the common node 3 from $Parent_1$ with the nodes following 3 in $Parent_2$ and similarly for $Child_2$. Then, the newly created two sets of child individuals are merged to a total number of $\aleph_{ind}/4 + \aleph_{ind}/4 = \aleph_{ind}/2$ individuals. However, to obtain the original population size of $\aleph_{ind}$, lines 15 and 16 of Algorithm 4.2 are applied again as the operations on lines 13 and 14 of Algorithm 4.2. More explicitly, both BTS and the crossover operations are applied twice to the current population in order to obtain $\aleph_{ind}$ individuals of the population $\mathbf{I}_k$, as indicated on line 17 of Algorithm 4.2. Further clarifications concerning

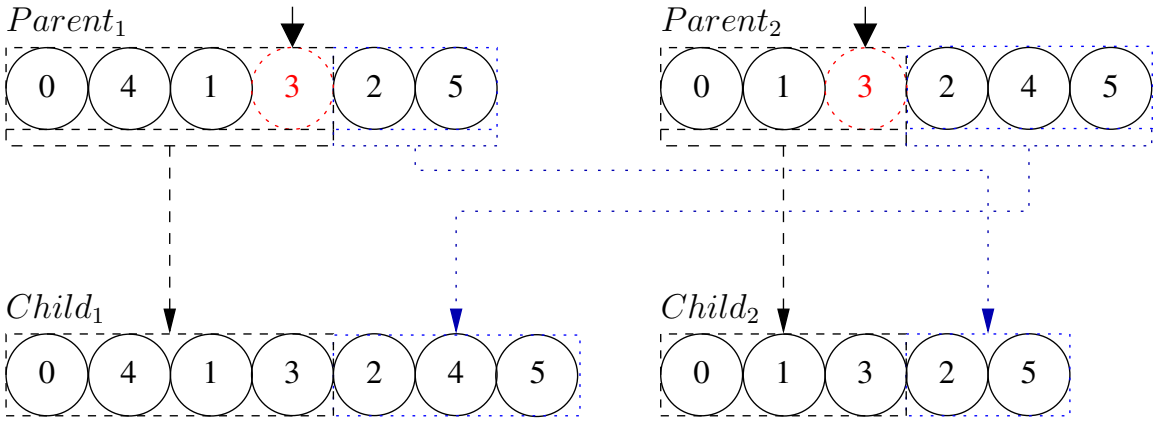

FIGURE 4.15: Crossover operation of parent individuals $(1, 35)$, where $Parent_1$ and $Parent_2$ represent individual 1 and 35 of $\mathbf{F}_k$, respectively.

the changes of the population size are provided in Fig. 4.16, while the genetic operators continue to iterate from the initial population $\boldsymbol{\Upsilon}_0$ to the final population $\boldsymbol{\Upsilon}'_k$ throughout k generations. Moreover, in our scenarios a similar mutation method to that of our work in [182] is applied to each sensor node (gene) lying on a route of an individual (candidate solution, chromosome or route) with the probability of Pr_m. In the implementation of the mutation operator, three possible modifications are invoked with equal probability, such as the node replacement, node removal and node insertion. In case of node replacement, the current node is replaced with a randomly selected node, as shown in Fig. 4.17. In node removal, the current node is removed from its route and the previous node is linked with the latter node. In case of node insertion, a randomly selected new node is inserted before the current node. After mutation is applied to each individuals, any potential node repetitions imposed are removed from each route in the interest of improving the population-diversity.

4.4 Performance Results

We consider a fully connected network associated with $V = \{4, 5, 6, 7, 8, 10, 15, 20\}$ nodes, where for example $V = 7$ is composed of 326 and $V = 10$ is composed of 109,601 distinct non-looping routes, as indicated in Table 4.2. A fully connected network is considered, because it may have an excessive number of links upon increasing the number of sensor nodes, when we aim for investigating the complexity of the distinct routes for a given WSN. Therefore, our implementation of a fully connected network may be applied to any distributed network having more nodes, but with less number of communicating links. Specifically, we consider a sensor field of $40 \times 40\text{m}^2$ for a WSN having V sensor nodes. The SN and the DN are placed at the opposite corners of the sensor field, where the SN is placed at the coordinate of $(0, 0)$ and the DN is located at the coordinate of $(40, 40)$, which guarantees having the longest distance between the SN and the DN at all time. This specific SN and DN placement is

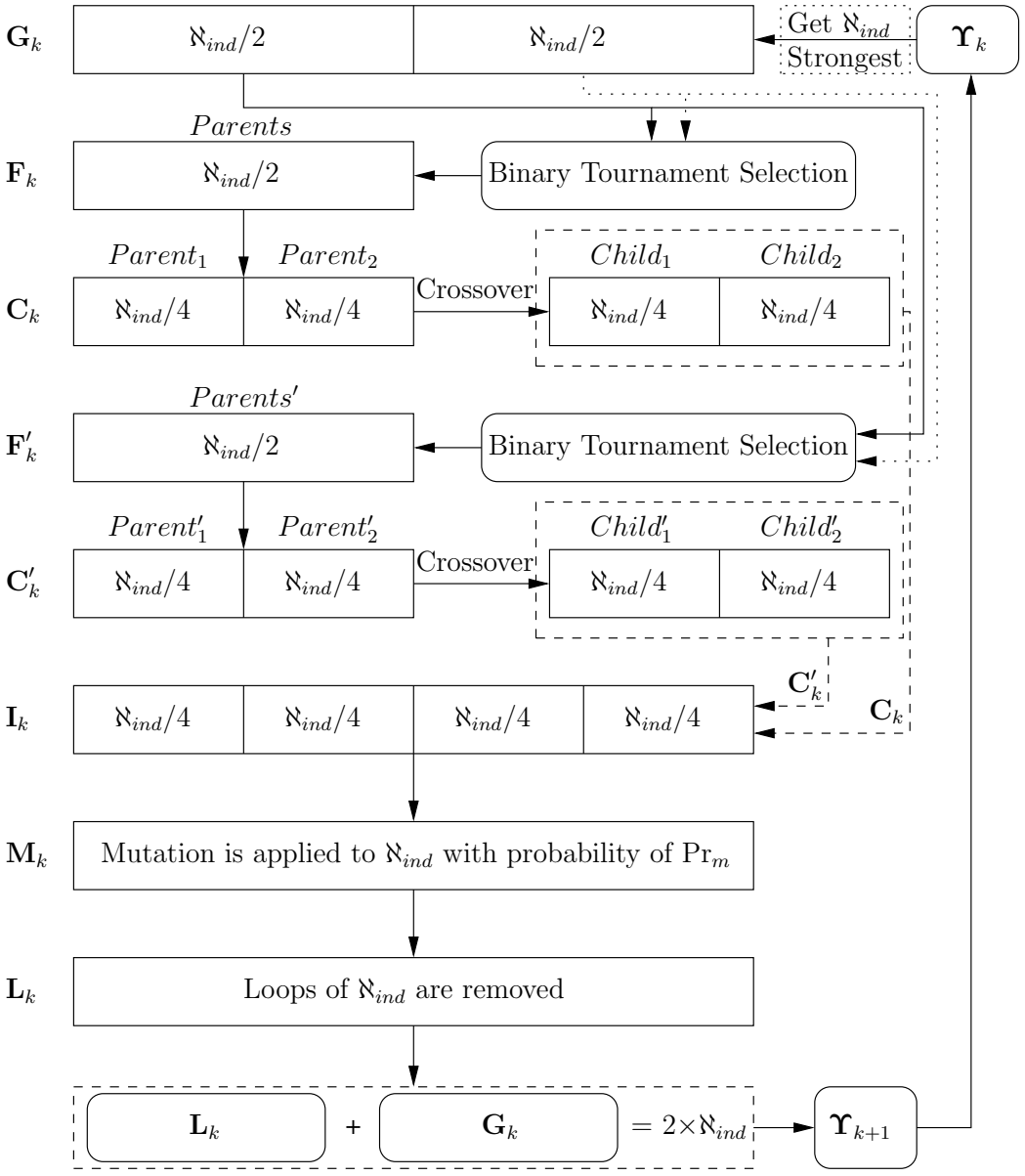

FIGURE 4.16: Illustration of the changes in the population size, while the genetic operations iterate.

important, because a single-hop transmission from SN to DN is not a favorable option due to its highest transmit power required over the longest distance amongst all the other distinct routes. Therefore, the end-to-end transmission across the network is designed for the sake of NL maximization by the evaluation of the various routes across the WSN considered. We note that the performance results of the NL are obtained for a continuous transmission scenario, termed as 'continuous-time NL'. For brevity, we simply use the term 'NL' for 'continuous-time NL'. On the other hand, in this chapter the NL values are expected to be much higher compared to those of Chapters 2 and 3 owing to the specific NL definition considered. Explicitly, in both Chapters 2 and 3 the NL is computed for a string topology, where the distances are fixed, hence a sensor does not have the option of transmitting over

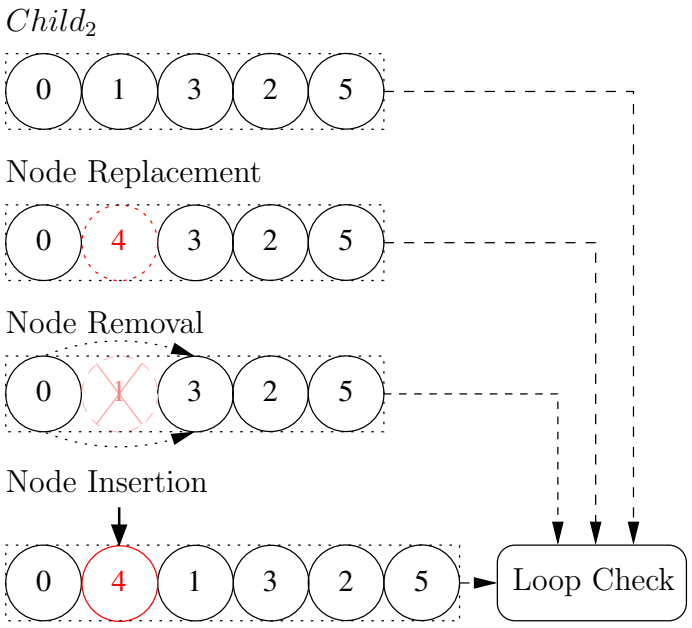

FIGURE 4.17: Mutation operations of $Child_2$, which is created by the crossover operation of the parent individuals $(1, 35)$ of $\mathbf{F}_k$.

another lower-dissipation route. However, in our scenario the SN is capable of exploiting alternative routes with the aid of a greedy-ED approach, by selecting the maximum RL-aware route for the end-to-end transmission in a fully connected WSN, where the aim is to carry the information generated at the SN to the DN until the SN battery is fully depleted. More explicitly, the accumulation of the maximum RL computed over the alternative routes provides us with a substantially extended NL, since the NL computation is composed of the summation of the several RL values, until the SN battery is fully depleted. Moreover, the maximum affordable transmit power of each node is set to $(P_i)_{max} = 0.01$W, as in the IEEE Standard 802.15.4 [207]. We consider an AWGN channel, which is defined by a certain propagation path loss model having the path loss exponent of $m = 3$ and a fixed noise power of $N_0 = -60$dBm at the receiver. Since the sensors communicate over the same shared channel, we utilize a TDMA based scheduling scheme we defined in Section 4.2.1, namely the SPTS with $T = 3$, where each link relies on a TDMA frame consisting of $N = 3$ TSs. The target SINR thresholds per link are defined as $\gamma = \{0, 0.5, 1, ..., 9, 9.5, 10\}$dB in order to investigate the NL performance of the WSN considered, where each link operates over different sets of target SINR values. Each sensor is equipped with an AAA long-life alkaline battery having the capacity of 5000J. For convenience, we summarize the system parameters used in our simulations in Table 4.14. In all scenarios of the SOGA, we set $\aleph_{ind} = 48$. These parameters are utilized in each iteration of the RL computation for each NL trial and the NL is averaged over $\tau = 5000$ trials. We use the number of CFEs to measure the complexity by accumulating each fitness evaluation call to the dual-simplex function, until a NL value is calculated by the ESA and SOGA described in Algorithm 4.1 and Algorithm 4.2, respectively. In some of our analysis, target SINR value or RSS is not

TABLE 4.14: System parameters utilized in our simulations.

Simulation parameter	Value
Channel model	AWGN
Path loss exponent, m	3
Target SINR per link $l_{i,j}$, γ [dB]	$\{0, 0.5, 1, ..., 9, 9.5, 10\}$
Noise power, N_0 [dBm]	-60
Battery capacity per sensor, $\mathcal{E}_i$ [Joule]	5000
Maximum transmit power of a node, $(P_i)_{max}$ [mW]	10 [207]
Number of TSs per frame, N	3
The field size of the WSN [m^2]	40×40
Number of nodes, V	$\{4, 5, 6, 7, 8, 10, 15, 20\}$
Number of trials per NL, τ	5000
Efficiency of the power amplifier, α	0.6 [190]
SPTS parameter, T	3
Number of total RSSs	4
Number of generations, $\aleph_{gen}$	$\{3, 6, 9, 12, 15, 18, 21, 24\}$
Number of individuals, $\aleph_{ind}$	48
Probability of crossover, Pr_c	0.9
Probability of mutation, Pr_m	0.5

specified, because we only compare the complexity of the algorithms. Therefore, as an example we choose the results of $\gamma = 0$dB and/or RSS-LTED, unless stated otherwise. For example, for any SINR value other than $\gamma = 0$dB, we observe the same complexity for the same algorithm, hence the number of CFEs is independent of both the target SINR value and of the RSS.

4.4.1 Difference with Respect to the Optimal NL versus Complexity

The optimality analysis of the SOGA is provided in Fig. 4.18 for the sake of NL maximization, while considering $\aleph_{gen} = \{3, 12\}$ generations for $V = \{4, 6\}$ sensor nodes, as well as $\aleph_{gen} = \{3, 15, 18\}$ generations for $V = 8$ sensor nodes, and $\aleph_{gen} = \{9, 21, 24\}$ generations for $V = 10$ sensor nodes. The target SINRs are set to $\gamma = \{0, 0.5, 1, ..., 9, 9.5, 10\}$. Note that here we consider the NL achieved by the RSS-LTED, but the other RSSs also exhibit similar

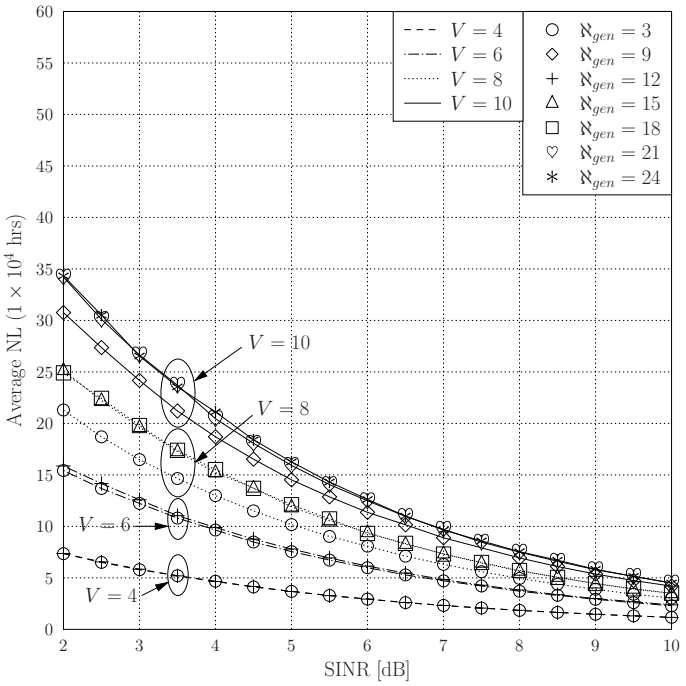

FIGURE 4.18: The NL of the SOGA invoked for the sake of NL maximization considering various parameter values of $\aleph_{gen}$, γ and V. Unless stated otherwise, in the rest of the numerical analysis we illustrate the NL values at the SINR of 2dB, which corresponds to the QPSK capacity limit.

trends. It is observed that for a lower number of nodes the convergence to the optimal NL can be readily obtained with the aid of a lower number of generations. For example, in Fig. 4.18 we can see for $V = 4$ that the NL results always match the optimal NL values after a few generations. Therefore, for $V = 4$ this emphasizes that there is no further improvement in the NL results upon increasing N_{gen}, which would introduce unnecessary additional complexity. However, upon increasing V, increasing the complexity becomes inevitable for the sake of attaining the optimal NL. For instance, for $V = 6$ there is a slight reduction in the performance of the SOGA for $\aleph_{gen} = 3$, when aiming for attaining the optimal NL obtained using the ESA. For a fixed number of generations, such as $\aleph_{gen} = 3$, the gap between the optimal and the suboptimal NL values further increases upon increasing V. This is because the number of distinct non-looping routes exponentially increases, as indicated in Table 4.2. Hence obtaining a near-optimal NL necessitates investing a higher computational complexity, where a higher $\aleph_{gen}$ is required. For example, for $V = 10$ the difference between the NL solutions for various $\aleph_{gen}$ values is significant, especially for $\aleph_{gen} = \{9, 21\}$. This is because the SOGA leads to a suboptimal NL at a reduced complexity, i.e. for $V = 10$ and $\aleph_{gen} = 9$, whereas the SOGA is capable of approaching the optimal NL value, which is only possible at the cost of a higher complexity, i.e. for $V = 10$ and $\aleph_{gen} = 21$. Therefore, the complexity versus the discrepancy with respect to the optimal NL plays a significant role in characterizing the system model considered, which will be discussed later in this section. Nonetheless, when the WSN operates at SINR=2dB, a NL improvement of approximately

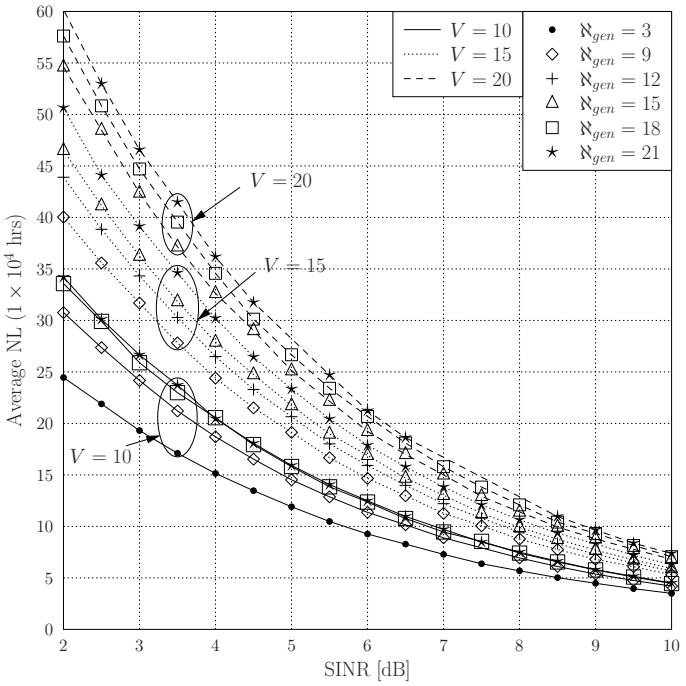

FIGURE 4.19: The NL of the SOGA invoked for the sake of NL maximization considering various parameter values of $\aleph_{gen}$ and γ, where more sensor nodes, i.e. $V = \{10, 15, 20\}$ are considered compared to Fig. 4.18.

45,000hrs is achieved with the aid of an additional sensor node, for example when a 5th sensor is admitted to the 4-node fully connected WSN or a 6th sensor node is admitted to the 5-node fully connected WSN and so on. However, the NL improvement is reduced to about 5,500hrs, when the WSN operates at SINR=10dB for the system model considered. Another significant finding is that to obtain a near-optimal NL when V increases, we have to increase $\aleph_{gen}$, which in turn increases the computational complexity imposed. Furthermore, the NL versus complexity trade-off becomes even more noticeable in Fig. 4.19 upon increasing V, especially for $V = \{15, 20\}$. For $V = 10$, the NL reaches a near-optimal value, where no improvement is observed upon increasing $\aleph_{gen}$, i.e. increasing the computational complexity. However, increasing $\aleph_{gen}$ provides further improvements for the NL of the $V = \{15, 20\}$ scenarios, as illustrated in Fig 4.19. Although the NL discrepancy with respect to the optimal recorded for $V = \{15, 20\}$ is reduced between the consecutive trials, due to the high complexity of WSNs composed of $V = \{15, 20\}$ nodes, it still remains suboptimal even for $\aleph_{gen} = 21$. Near-optimal NL solutions may be obtained for the $V = \{15, 20\}$ scenarios at a vast complexity by steeply increasing both $\aleph_{gen}$ and $\aleph_{ind}$. The ESA is considered as the best possible solution for the NL evaluation, which is an upper bound to the true NL attained by the SOGA. In Fig. 4.20, the SOGA is seen to be capable of achieving the optimal NL with the aid of $\aleph_{gen} = 3$ for $V = \{4, 5\}$. However, the $V = \{6, 7, 8, 10\}$ scenarios require a larger $\aleph_{gen}$ for approaching the optimal NL. For example, when considering $V = \{6, 7\}$, the SOGA is only capable of achieving suboptimal NL solutions for $\aleph_{gen} = 3$, but when we have $\aleph_{gen} = 6$, the NL becomes near-optimal for $V = 6$ and for $\aleph_{gen} = 9$ the NL gap with respect

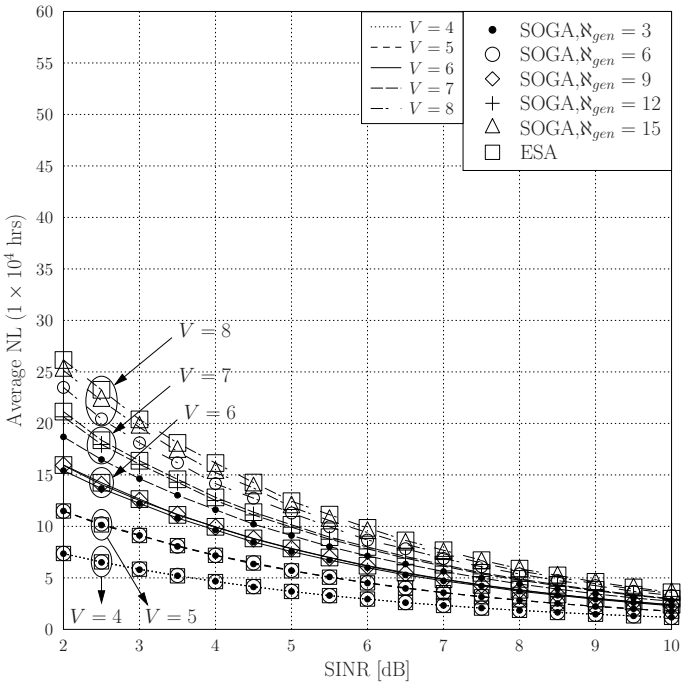

FIGURE 4.20: ESA as an upper bound for the true NL compared to the NL of SOGA for various $\aleph_{gen}$ and V values.

to the ESA benchmark becomes extremely small for $V = 7$. Therefore, in the following investigations, we consider that for $V = \{4, 5\}$ using $\aleph_{gen} = 3$, for $V = 6$ using $\aleph_{gen} = 6$, for $V = 7$ using $\aleph_{gen} = 9$, for $V = 8$ using $\aleph_{gen} = 15$ and for $V = 10$ using $\aleph_{gen} = 21$ constitute an attractive compromise, when aiming for obtaining a near-optimal NL value at the cost of a reasonable complexity.

4.4.2 NL Performance of Various RSSs Using the ESA and SOGA

Fig 4.21 characterizes the NL of the RSSs of ESA considering various V and γ values. As mentioned in Section 4.3.2.2, RSSs are introduced due to multiple routes having the same maximum RL. Therefore, the selection of the route in this stage plays a significant role in determining the NL, because the best route selected will be utilized for the end-to-end transmission and therefore the battery of the sensors utilized is correspondingly drained and updated for the next iteration. For a lower V, such as for example $V = 4$, the differences between the RSSs are negligible. However, for $V = 7$ we only have small differences in the NL of the RSSs considered. This is because there are many distinct non-looping routes for the fully connected network composed of a higher number of nodes V, and hence the probability of having a variety of best routes in each iteration of RL computations is high in terms of the LTED, LNOH, LRBAT and RANR. For example, for $V = 7$ at SINR of 2dB the optimal NL for RSS-LTED is the highest, followed by RSS-LRBAT, then RSS-RANR and finally, RSS-LNOH. We expect that the NL of RSS-LRBAT and RSS-LTED

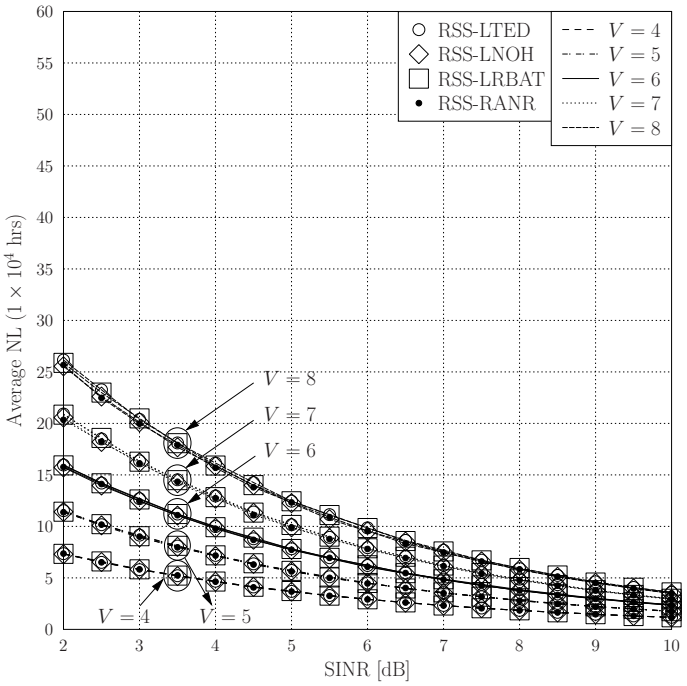

FIGURE 4.21: NL of different RSSs in the ESA for various V and γ values.

becomes moderately better than the other two RSSs owing to their energy awareness. More explicitly, RSS-LTED is based on the least total ED of the route, while RSS-LRBAT relies on the SN's battery level. Therefore, we observe that in our scenarios RSS-LRBAT and RSS-LTED typically outperform RSS-RANR and RSS-LNOH in terms of their NL, which can be readily seen in Fig. 4.21 and Fig. 4.22. Specifically, when a higher number of nodes V is considered, the difference in NL can be readily observed. Rather than providing the NL results associated with all $\aleph_{gen}$ values for different WSNs composed of V sensor nodes, as previously mentioned, we only consider the near-optimal NL characteristics of SOGA associated with their near-optimal $\aleph_{gen}$ choices, as indicated in Fig. 4.22. It becomes clear in Fig. 4.22 that for the near-optimal $\aleph_{gen}$ choices and for their respective WSNs composed of V sensor nodes, the maximum NL attained by SOGA approaches that of its benchmark NL values, as illustrated in Fig. 4.20. We observe that similar to Fig. 4.21 a near-optimal NL is obtained for the corresponding RSSs by SOGA in Fig. 4.22.

4.4.3 The NL versus Complexity Trade-off

The NL versus routing complexity trade-off plays a significant role in characterizing the system model considered. It will be demonstrated that SOGA is capable of achieving a near-optimal NL in conjunction with $\aleph_{gen} = 15$ at a much lower complexity for a WSN having $V = 8$ nodes, as illustrated in Fig. 4.20. Furthermore, SOGA is capable of finding route resulting in a near-optimal NL value for a WSN consisting of $V = 10$ nodes. Here, due to the high computational complexity of ESA, the optimal NL achieved by the ESA

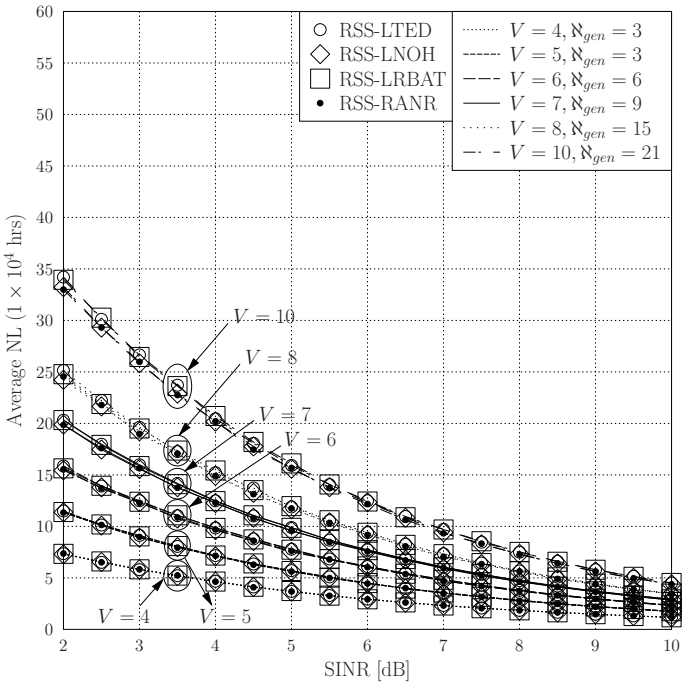

FIGURE 4.22: NL of different RSSs in the SOGA for various V and γ values.

is not provided for WSNs having $V > 8$ nodes, which consist of more than $1,957$ distinct non-looping routes. One may think that increasing V from 8 to 10 imposes an insignificant change in complexity. However, in our scenarios we consider the distinct non-looping routes of a fully connected WSN, which leads to an exponential increase in the computational complexity. Correspondingly, increasing V from 8 to 10 increases the number of distinct non-looping routes from $1,957$ to $109,601$, which is a substantial escalation of the computational complexity, and whilst the SOGA can cope with it, the ESA cannot. The computational complexity of both the ESA and SOGA is proportional to the average number of CFEs required for the computation of a specific NL value. Therefore, the attainable NL associated with their required number of CFEs is illustrated in Fig. 4.23. More explicitly, the convergence of the computed NL to the optimal achieved at the cost of the complexity required by the SOGA can be readily seen from Fig 4.23, which also explains the optimal choices of $\aleph_{gen}$ provided in Fig. 4.22. Note that in Fig 4.23, the vertical points of the different markers represent the computed NL value for each $\aleph_{gen}$, which is incremented by 3 from left to the right for each fully connected WSN composed of V nodes. In terms of the attainable NL, increasing $\aleph_{gen}$ from 3 to 12 with intervals of 3 for $V = \{4, 5\}$ does not improve the NL, but imposes unnecessary complexity, while the NL of the $V = \{6, 7\}$ scenarios barely improves upon increasing $\aleph_{gen}$ from 3 to 12. However, the $V = 10$ scenario results in a significant NL improvement for each increase of $\aleph_{gen}$ from $\aleph_{gen} = 3$ to $\aleph_{gen} = 21$, when it is seen to converge to its optimal NL value at $\aleph_{gen} = 21$.

The number of CFEs required for the NL computation by the ESA and SOGA for V number

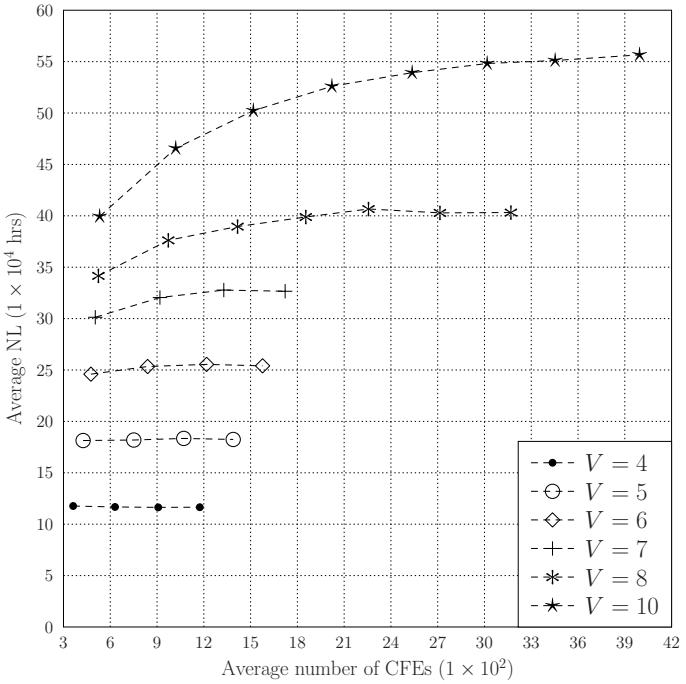

FIGURE 4.23: The NL versus complexity of SOGA for a WSN composed of V sensor nodes.

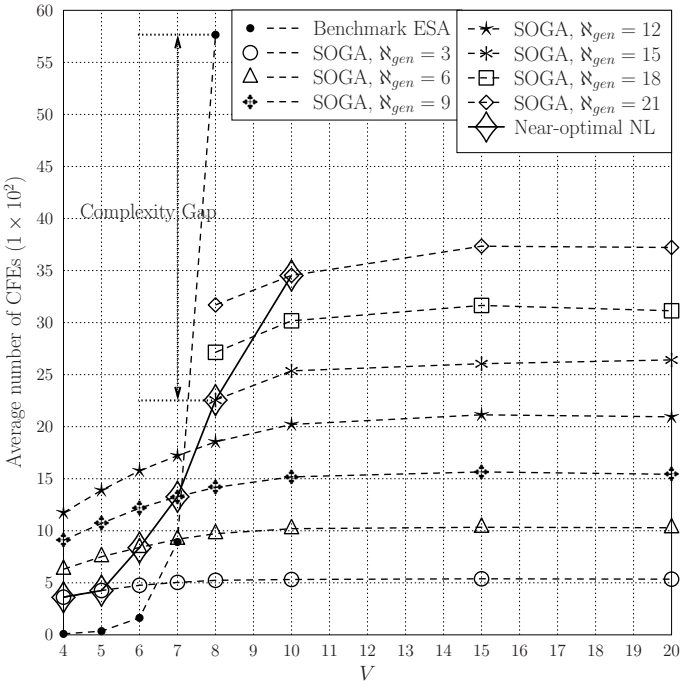

FIGURE 4.24: Complexity analysis of the ESA and the SOGA for V nodes, given $\aleph_{gen}$ for the SOGA.

of nodes is illustrated in Fig. 4.24, where the NL of SOGA is computed for each of the $\aleph_{gen}$ values considered. For each fully connected WSN composed of V nodes, the number of CFEs required for achieving the optimal NL can be compared to that of ESA as an upper bound to the true NL. We also illustrated in Fig. 4.24 number of the CFEs required for attaining the near-optimal NL for each WSN composed of V sensor nodes. Moreover, Fig. 4.24 illustrates that the ESA outperforms the SOGA for $V \leq 7$, when aiming for near-optimal NL values. This is a benefit of the higher number of individuals $\aleph_{ind} = 48$ evaluated in each iteration of $\aleph_{gen}$. Therefore, in each iteration of the RL computation, the routes represented by the $\aleph_{ind} = 48$ individuals are evaluated and this requires at least 48 CFEs. Note that a single NL computation may require a few RL computation iterations, hence it may lead to a higher number of CFEs. However, in the least complex scenario, where a single iteration of RL computation fully drains the SN battery and produces the NL value, 48 CFEs will be required, which already necessitates a larger number of CFEs than in the scenarios of $V \leq 7$ for the ESA. In Fig. 4.24, we can observe that $V = 7$ is the point, where the computational complexity of the ESA is similar to that of the SOGA and increases exponentially, when $V > 7$. Therefore, we may conclude that the SOGA imposes a lower complexity than the ESA for WSN having $V > 7$ nodes. For example, observe in Fig. 4.24 that the SOGA is capable of finding a near-optimal NL for $V = 8$ at a 2.56 times lower complexity than the ESA. Another important conclusion is that the complexity imposed by finding the near-optimal NL values in SOGA increases near-linearly upon increasing V, whereas the complexity of spotting the optimal NL values in the ESA increases exponentially. For example, the complexity of the optimal NL, when moving from $V = 6$ to $V = 7$ in the SOGA is provided in Fig. 4.24, where the number of CFEs is increased 1.58 times. Similarly, the complexity of the optimal NL upon extending the network from $V = 7$ to $V = 8$ in the SOGA is increased 1.70 times. We expect this gap to be much larger for the ESA due to its exponentially increasing complexity. For example, upon extending the network from $V = 6$ to $V = 7$ the complexity is increased by a factor of 5.46, whereas the complexity of obtaining the optimal NL for $V = 8$ is increased 6.46 times compared to $V = 7$. The scenario of $V = 10$ characterized in Fig. 4.24 and associated with different vertically stacked markers representing the $\aleph_{gen} = \{3, 6, 9, 12, 15, 18, 21\}$ generations incremented by 3 from bottom to the top corresponds to the line associated with the star marker at the top in Fig. 4.23, which commences from 40×10^4hrs of NL with $\aleph_{gen} = 3$ and converges to 55×10^4hrs of near-optimal NL in conjunction with $\aleph_{gen} = 21$. Therefore, one can readily observe that the "Near-optimal NL" points are selected in Fig. 4.24 based on their convergence to the near-optimal NL values extracted from Fig. 4.23. For example, convergence to the optimal NL at $\aleph_{gen} = 21$ for the $V = 10$ scenario can be clearly seen from Fig. 4.23, which is explicitly marked as the "Near-optimal NL" point in Fig. 4.24 by a diamond-marker.

4.4.4 E2EB versus SINR Performance per WSN

In this section, we provide the E2EB versus SINR performance analysis of the WSNs operated with the aid of uncoded BPSK, a 1/2-rate CC hard-decoded as well as soft-decoded QPSK communicating over an AWGN channel. Fully connected WSNs consisting of $V = \{4, 7\}$ nodes for the ESA and $V = \{4, 10\}$ nodes for the SOGA are considered for various RSSs in Figs. 4.25(a)–4.25(b) and Figs. 4.26(a)–4.26(b), respectively. In all scenarios of both the ESA and SOGA, the E2EB is the lowest for 1/2-rate-CC soft-decoded QPSK at a given SINR value, which can be seen both from Figs. 4.25(a)–4.25(b) and Figs. 4.26(a)–4.26(b). The E2EB of the system model considered slightly decreases upon increasing V, which is due to the higher chances of selecting a longer hop for the end-to-end transmission, yielding more accumulated bit errors during the passage of the message through to the DN. Furthermore, in most of the scenarios, especially for lower V values, RSS-LNOH performs slightly better in terms of its E2EB performance compared to the other RSSs. The main reason behind this is a natural consequence of using RSS-LNOH as a delay-aware scheme, which relies on the route having the lowest number of hops. Consequently, on the routes, where each link operates at the same SINR, less bit errors are accumulated over less hops. Another important point is that for a higher V, e.g. $V = 10$ the E2EB curves overlap in Fig. 4.26(b), which means that the difference between the E2EB performances of the RSSs is barely noticeable. The fundamental reason behind this is that for a higher V having a larger number of distinct routes, the probability of requiring a RSS is low, because the chance of having only a single route associated with the maximum NL is extremely high. More explicitly, there may only be a single route having the maximum NL or routes having the same number of hops. Therefore, RSSs will always provide the same E2EB due to the selection of the specific route having the same number of hops in each RL iteration. Consequently, the E2EB performance will be similar, regardless of the RSSs.

Observe that Fig. 4.25(a) recorded for the ESA and Fig. 4.26(a) for the SOGA do not provide exactly the same RSS-LNOH performance, even though they are measured for the same WSN composed of $V = 4$ nodes. This is due to the strategy they follow for searching through the solution space taking different routes as the reference points. More explicitly, ESA searches through the entire solution space and finds the specific route having the best RSS-LNOH performance amongst the best routes having the best RL, which may provide a diversity of routes having different number of hops, possibly a small number of hops so that both the delay as well as the E2EB is reduced. On the other hand, the SOGA intelligently searches through the solution space with the aid of $\aleph_{ind} = 48$ randomly initialized routes, which constitutes only a small part of the solution space. Therefore, since the routes associated with the maximum RL are selected amongst the $\aleph_{ind} = 48$ routes of the individuals, the SOGA may find several maximum-RL routes having the same number of hops, which potentially results in the same RSS-LNOH performance. More explicitly,

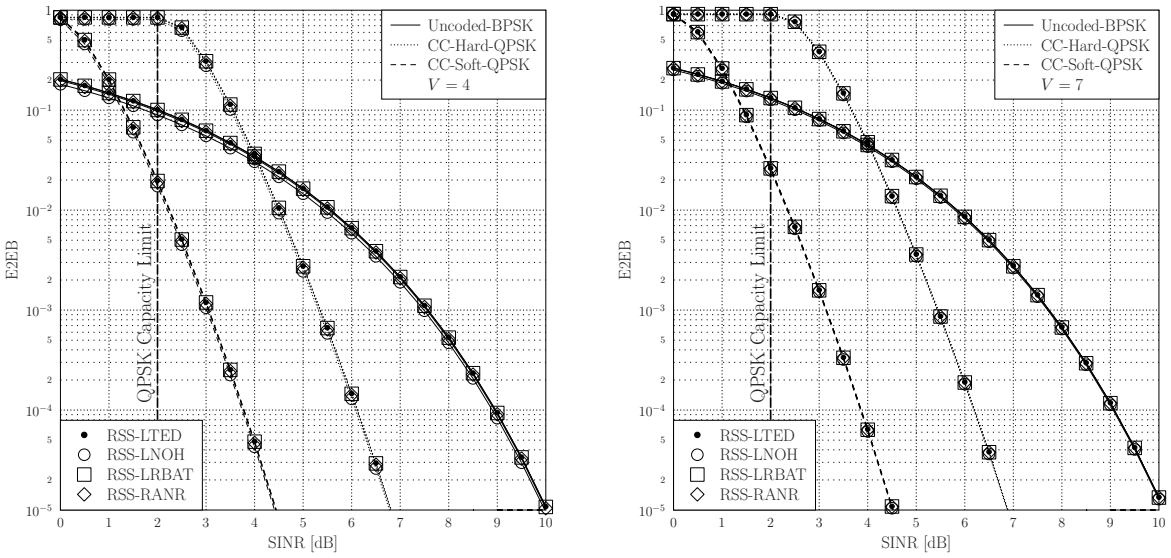

(a) For $V = 4$ (b) For $V = 7$

FIGURE 4.25: E2EB versus SINR performance of MCSs for each RSSs of ESA in a fully connected WSN having $V = \{4, 7\}$ nodes.

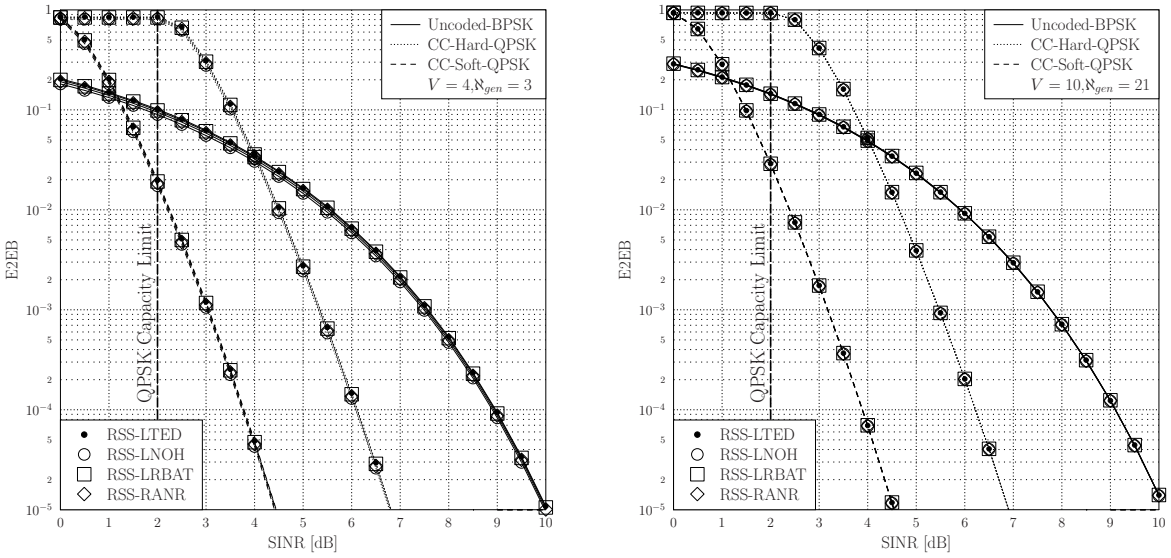

(a) For $\aleph_{gen} = 3$ and $V = 4$ (b) For $\aleph_{gen} = 21$ and $V = 10$

FIGURE 4.26: E2EB versus SINR performance of MCSs for each RSSs of SOGA using $\aleph_{gen}$ generations specifically chosen for the corresponding WSN having V nodes.

missing a maximum-RL route associated with less hops is possible, when using the SOGA, and hence the E2EB performance of all RSSs may become similar. Hence, for $V = 4$, the performance difference of the RSS-LNOH compared to other RSSs observed in Fig. 4.25(a) for the ESA is not noticeable in Fig. 4.26(a) for the SOGA.

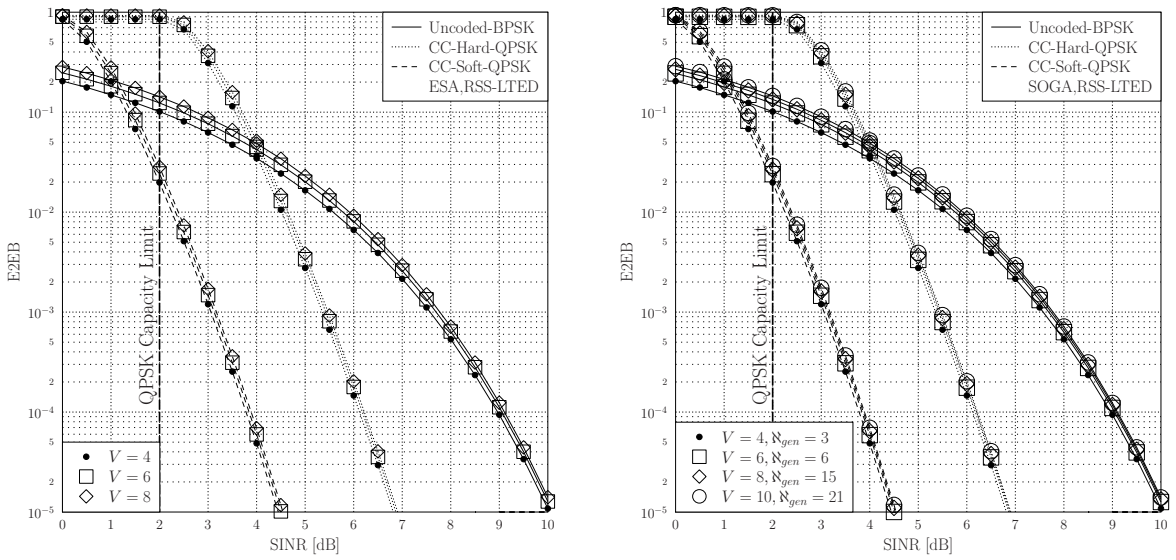

(a) ESA (b) SOGA

FIGURE 4.27: E2EB versus SINR performance of MCSs for each WSNs composed of V sensor nodes considering RSS-LTED in ESA and SOGA.

4.4.5 E2EB versus SINR Performance for RSS-LTED

Here, we consider the E2EB versus SINR performance analysis of various WSNs composed of V sensor nodes operating with the aid of uncoded BPSK, a 1/2-rate CC hard-decoded as well as soft-decoded QPSK MCSs communicating over an AWGN channel. Fully connected WSNs consisting of $V = \{4, 6, 8\}$ nodes in the ESA and $V = \{4, 6, 8, 10\}$ nodes in the SOGA are considered for only RSS-LTED in Fig. 4.27(a) and Fig. 4.27(b), respectively. Explicitly, Fig. 4.27(a) and Fig. 4.27(b) illustrate the E2EB performance upon increasing the number of nodes. At the same SINR value, the highest E2EB belongs to the WSN composed of $V = 8$ nodes in the ESA and $V = 10$ nodes in the SOGA compared to the WSNs consisting of a lower number of nodes. One of the main reasons behind this is that the WSNs composed of larger number of nodes have a higher chance of achieving the maximum RL with the aid of the best route having longer hops in each iteration of the RL computation. The other main reason is that of relying on the worst-case E2EB computation strategy. We select the final route amongst the best routes obtained by each RL computation providing the longest hop. More explicitly, let us assume that the NL computation requires 3 iterations for RL computation. Then, each iteration provides us both with its best route and with the associated RL value, depending on the RSS. Once 3 iterations have been completed, the E2EB of these 3 best routes is calculated, respectively and the route that provides us with the worst E2EB value is selected, since we aim for finding the upper bound of the E2EB for the WSN considered. Here, the selection of the worst E2EB requires the selection of the route associated with the longest hop due to the specific nature of the E2EB computation. Therefore, the selection of the route having the worst-case E2EB requires longer hops, which

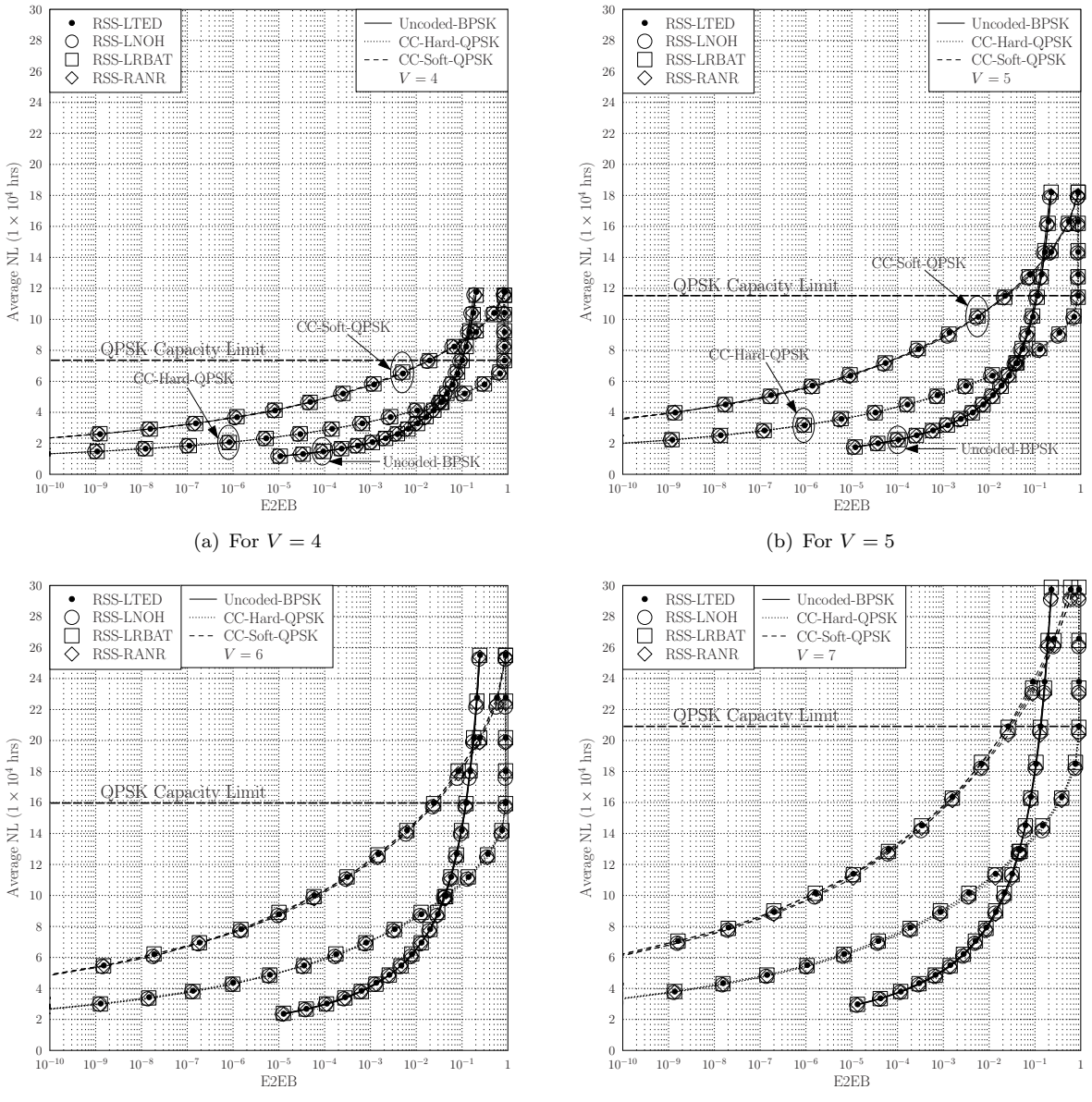

(a) For $V = 4$

(b) For $V = 5$

(c) For $V = 6$

(d) For $V = 7$

FIGURE 4.28: Average NL versus E2EB performance of MCSs for each RSSs of ESA in a fully connected WSN having $V = \{4, 5, 6, 7\}$ nodes.

in turn yields higher E2EB for larger networks, as illustrated in Fig. 4.27(a) and Fig. 4.27(b).

4.4.6 Average NL versus E2EB Performance per WSN

The average NL versus E2EB trade-off is of salient importance, since it characterizes the QoS of the system model considered. In this section, we provide the average NL versus E2EB performance analysis of the WSNs operated with the aid of uncoded BPSK, a 1/2-rate CC hard-decoded as well as soft-decoded QPSK MCSs communicating over an AWGN channel. The fully connected WSNs composed of $V = \{4, 5, 6, 7\}$ nodes for the ESA and

$V = \{4, 7, 10\}$ nodes for the SOGA are considered for various RSSs in Figs. 4.28(a)–4.28(d) and Figs. 4.29(a)–4.29(c), respectively. The E2EB performance of the 1/2-rate CC soft-decoded QPSK MCS is better than any of the other MCSs in all scenarios of both the ESA and the SOGA. For example, in the $V = 4$ scenario of ESA, at the same E2EB of 10^{-3}, approximately 4×10^4hrs of NL gain is achieved by the 1/2-rate CC soft-decoded QPSK MCS compared to uncoded BPSK and nearly 2.4×10^4hrs of NL gain compared to the 1/2-rate CC hard-decoded QPSK MCS. For an E2EB of 10^{-3}, the NL gain of 1/2-rate CC soft-decoded QPSK MCS for the $V = 5$ scenario is increased to approximately 6×10^4hrs compared to uncoded BPSK and to about 4×10^4hrs compared to 1/2-rate CC hard-decoded QPSK MCS. The NL gain further increases upon introducing additional sensor nodes, namely for a $V = 6$ scenario approximately to 8×10^4hrs of NL compared to uncoded BPSK and to about 5×10^4hrs compared to 1/2-rate CC hard-decoded QPSK MCS. Similarly, for $V = 7$ this gain increases to about 10×10^4hrs of NL compared to uncoded BPSK and to about 7×10^4hrs of NL compared to the 1/2-rate CC hard-decoded QPSK MCS. Since the NL results converged to their optimal values under the SOGA, the E2EB performance of the ESA seen in Figs. 4.28(a)–4.28(d) and that of the SOGA recorded in Figs. 4.29(a)–4.29(b) become similar. Therefore, the E2EB performance analysis of ESA provided for $V = \{4, 5, 6, 7\}$ nodes is also carried out for the corresponding SOGA scenarios. Finally, for the $V = 10$ scenario of the SOGA, a NL gain of 17×10^4hrs is attained compared to uncoded BPSK and 10×10^4hrs compared to 1/2-rate CC hard-decoded QPSK MCS at the same E2EB of 10^{-3}. Note that we were not able to generate the NL versus E2EB performance curves for $V = 10$ for the ESA due to its excessive computational complexity. We may conclude that the average NL versus E2EB trade-off for the various RSSs and MCSs in the considered fully connected WSNs composed of V sensor nodes provides the network designer with insights concerning the interplay between the NL and E2EB, depending on the application considered.

4.5 Application Scenarios

Our NL maximization approach significantly extends the lifetime of the WSN considered, compared to our previous studies in [31] and [39]. Therefore, our NL maximization approach is particularly well-suited for the applications that require longer network connectivity and operations in military battlefields, in monitoring climate changes and so on. For instance, the longevity of network operations in the military battlefield is crucial, since the hostile territory may become inaccessible and thus the battery of the sensors cannot be replaced. Therefore, a significant piece of information may be captured by a specific sensor and relaying its information to the base station is vital. More particularly, a specific sensor or a group of sensors that are located closer to the hostile targets may in fact carry the most significant information. Therefore, using these sensor(s) as the more significant sensor(s) and assuming

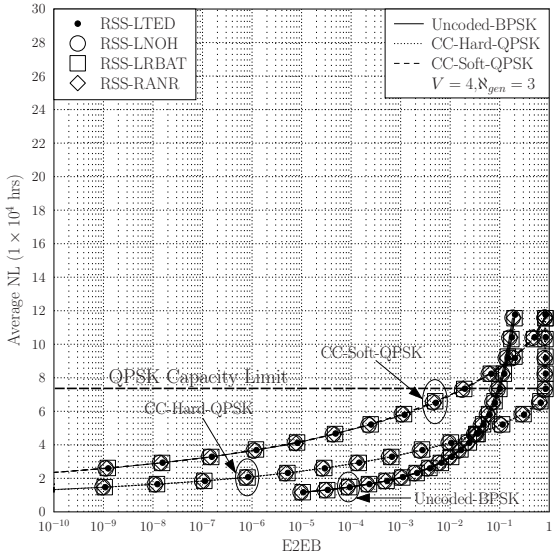

(a) For $\aleph_{gen} = 3$ and $V = 4$

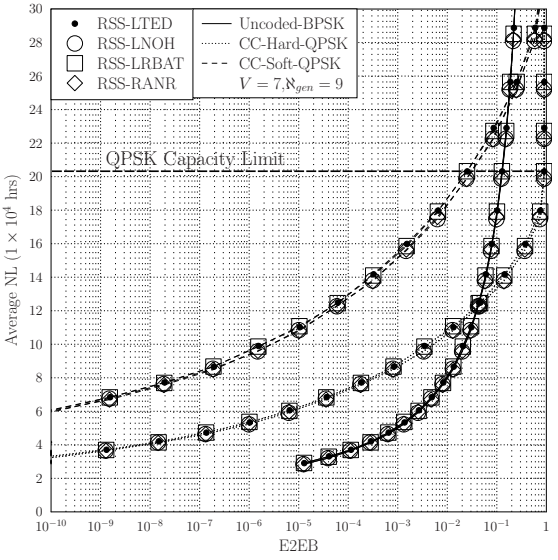

(b) For $\aleph_{gen} = 9$ and $V = 7$

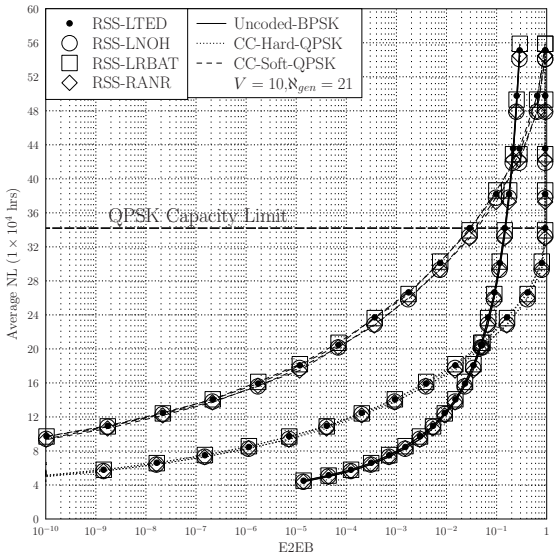

(c) For $\aleph_{gen} = 21$ and $V = 10$

FIGURE 4.29: Average NL versus E2EB performance of MCSs for each RSSs of SOGA using $\aleph_{gen}$ generations specifically chosen for the corresponding WSN having V nodes.

that the rest of the sensors relay these significant pieces of information can conserve more energy and this can assist us in extending the NL, as described in our NL maximization technique.

Another example of densely deployed WSNs may be found in a football stadium, where each user carries a RFID sensor for health and safety reasons. Whenever a predefined threshold is exceeded, as exemplified by a high temperature, the information is relayed to the base station by hundreds of sensors. Again, only the most crucial information is transmitted to the base station by selecting the most lifetime-efficient route amongst thousands of potential alternative routes. Nonetheless, there are numerous other applications [13, 14] for the employment of our NL maximization framework, including environmental monitoring [58], surveillance [226], smart water quality monitoring, smart environment sensing, smart metering, smart agricultural applications, health monitoring and smart cities [227], just to name a few.

4.6 Chapter Summary and Conclusions

In this chapter, the NL maximization of interference-limited fully connected WSNs composed of V nodes associated with a single source and destination is considered, where the SN and the DN are located at the opposite corners of the sensor field of Fig. 4.11 to ascertain the longest distance between them, so that the system model guarantees the utilization of alternative routes for the end-to-end transmission. The information to be transmitted is only generated at the SN and the aim of the system model considered is to carry the SN's information to the DN via the relays, which are also capable of decoding and forwarding the information relayed. For the sake of mitigating the interference, we use the SPTS TDMA scheduling method, where on each route a node can only interfere with another node at the distance of T, if they are scheduled during the same TS. Moreover, each sensor node is equipped with a limited battery capacity and we only consider the transmit power as the main ED factor. Moreover, the E2EB constituting the worst-case BER of the fully connected WSN considered is formulated in (4.5) for uncoded BPSK, 1/2-rate CC hard-decoded and soft-decoded QPSK MCSs, as described in Section 4.2.2. Naturally, the NL versus E2EB performance can be obtained for any arbitrary MCSs. In the system model described in Section 4.2, we proposed the ESA and the SOGA for solving the linear optimization problem formulated for each route given by (4.10)–(4.13) in Section 4.3.1. Note that the ESA finds the optimal NL, where the best possible NL can be achieved by checking all the possible solution candidates of the entire solution search space, which the NL performance of the SOGA is benchmarked against. However, the SOGA is designed in a way that it can intelligently search through a limited fraction of the solution space using genetic operators. Since the NL is strictly dependent on the battery level of the SN, it is described in two

stages; first stage is responsible for the computation of the RL, until the SN fully drains its battery, because the system model is only subjected to the end-to-end transmission of the information generated at the SN with the aid of the maximum-RL-aware routes. The second stage is involved in the accumulation of RLs during the iterations of the RL computation, until the SN battery is fully depleted. Thus, the NL computation may consist of a few RL computation iterations, where in each iteration the best route is selected from the set of routes having the maximum RL for end-to-end transmission. This selection process may rely on several criteria, which are described as the set of RSSs methods constituted by the RSS-LTED, RSS-LNOH, RSS-LRBAT, RSS-RANR of Section 4.3.2.2.

The computation of the NL in such networks may be challenging due to its computational complexity for a large V, which might result in numerous alternative routes that have to be evaluated in terms of their RL. Moreover, considering the exponential increase of the number of distinct routes upon increasing the number of nodes, an algorithm associated with a much reduced complexity is required for NL maximization. Therefore, the SOGA of Section 4.3.2.5 was introduced for circumventing the shortcomings of the ESA for larger network sizes. Upon using the parameter values of Table 4.14 discussed in Section 4.4, an approximately $45,000$hrs of NL gain is attained for the WSN considered, when operating at SINR=2dB by inserting an additional sensor node into a WSN having an arbitrary size. This NL gain is reduced to about $5,500$hrs, when the WSN operates at SINR=10dB. We also observed that for $V \leq 7$ using the ESA is a better option due to its lower computational complexity at a specific target-performance. Observe from Table 4.15 that for $V = 7$ the computational complexity of the ESA and SOGA is similar. As illustrated in Fig. 4.30, the NL discrepancy of the SOGA with respect to the optimal NL value of the ESA is as low as 3.17%, which corresponds to 1.07×10^4hrs of NL. We say that the NL is converged to its optimal NL value, if the NL discrepancy is less than 3.5%. For example, in the $V = 8$ scenario the NL gap of the SOGA with respect to the upper bound ESA is 3.02%. Hence, in the $V = 8$ scenario of Fig. 4.20 the NL computed by the SOGA becomes near-optimal at a 2.56 times lower complexity compared to the ESA. Nonetheless, observe in Fig. 4.24 that the SOGA imposed a lower complexity than the ESA for any WSN having $V > 7$. For convenience, Table 4.15 summarizes the computational complexity of both the ESA and SOGA imposed for different V values, when relying on the RSS-LTED. Again, the convergence of SOGA to a near-optimal NL value is achieved at a much reduced complexity.

Furthermore, observe in Figs. 4.21 and 4.22 that both RSS-LTED and RSS-LRBAT have a higher NL owing to their energy-awareness compared to the other RSSs. Additionally, as illustrated in Figs. 4.25(a)–4.25(b), Figs. 4.26(a)–4.26(b), Figs. 4.28(a)–4.28(d) and Figs. 4.29(a)–4.29(c), RSS-LNOH tends to exhibit a better E2EB performance than the other RSSs due to its delay-awareness, which naturally results in the accumulation of less bit errors as a benefit of selecting the route having the least number of hops. However, one

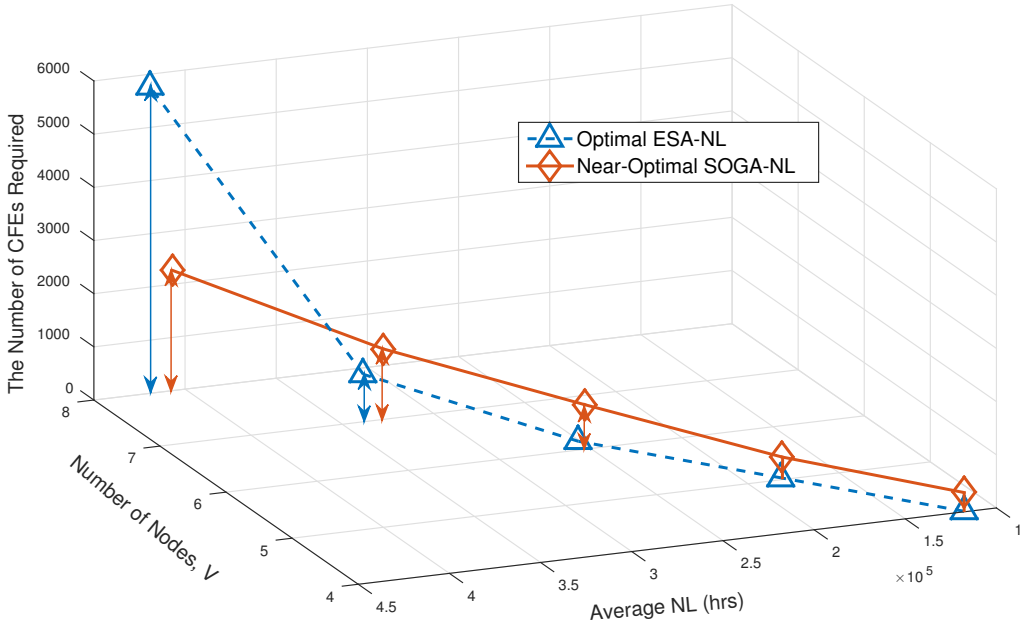

FIGURE 4.30: Discrepancy from the ESA as a benchmark of the NL, upon increasing V.

can conclude that since the objective function is formulated for achieving RL maximization, the RSSs presented attain a similar NL. More explicitly, as long as the RL is maximized, any route associated with the maximum RL amongst the routes having the same maximum RL can be selected for the end-to-end transmission. On the other hand, the decision concerning the route selection significantly affects the E2EB performance, since the computation of the E2EB strictly relies on the number of hops and the MCSs considered.

Nonetheless, the 1/2-rate CC soft-decoded QPSK MCS outperforms the other MCSs in all scenarios for the ESA and SOGA. For example, in the $V = 4$ scenario of the ESA, at the same E2EB of 10^{-3} the 1/2-rate CC soft-decoded QPSK MCS achieves an approximately 4×10^4hrs of NL gain compared to uncoded BPSK and nearly 2.4×10^4hrs of NL gain compared to the 1/2-rate CC hard-decoded QPSK MCS. This gain is further increased upon increasing the number of nodes. Moreover, WSNs composed of larger number of nodes result in higher E2EB. The main reason for this is that the route selection strategy associated with the worst-case E2EB requires longer hops, which in turn yields a higher E2EB for larger networks. Another reason is that WSNs composed of larger number of nodes have a higher chance of achieving the maximum RL with the aid of the best route having longer hops in each iteration of the RL computation.

In this chapter, we considered the NL maximization of a fully-connected WSN, where the NL was strictly dependent on the SN battery level, since we only transmit information generated at the SN to the DN via alternative routes, depending on their RL. Moreover, the NL was

V	ESA-CFEs	SOGA-CFEs	Optimal ESA-NL [hrs]	Near-optimal SOGA-NL [hrs]
4	9	362	117,682	117,682
5	35	425	181,886	181,385
6	163	839	256,745	253,381
7	892	1,328	338,474	327,753
8	5,765	2,256	419,264	406,622
10		3,453		551,086

TABLE 4.15: The number of CFEs required for the convergence of the ESA and SOGA for different V values and for the RSS-LTED only.

computed by the accumulation of the maximum RL values of these alternative routes, until the SN battery was fully depleted, where the RL was defined by the earliest time, at which a sensor node lying in the route fully drains its battery charge. Therefore, depending on the size of the network, the lifetime models in our previous studies were based on a single-objective NL or RL maximization problem. However, other several pertinent objectives, such as the end-to-end delay were not considered in the context of our NL maximization, since a large end-to-end delay may lead to a significant end-to-end throughput reduction during the lifetime of the network. Therefore, in Chapter 5 we will revisit our NL definition in order to reflect the effect of the end-to-end delay on the NL along with the aggregate energy dissipation of the same route. Another distinctive aspect of this study is the simultaneous optimization of the energy and the delay, as a multi-objective optimization problem in order to provide the system designer with a trade-off between the Pareto optimal energy and delay, which determines the set of Pareto optimal NL aware routes.

Chapter 5

Multi-Objective Network Lifetime Design Relying on Routing Optimization Using Evolutionary Algorithms

5.1 Introduction

In Chapter 4, we considered the network lifetime (NL) maximization of a fully-connected wireless sensor network (WSN), where the NL was strictly dependent on the battery energy level of the source node (SN). Therefore, the NL was computed based on the accumulation of the lifetime of the alternative routes spanning from the SN to the destination node (DN), whereas the route lifetime (RL) was determined by the earliest time instant, at which a sensor node forming part of the route fully depletes its battery energy. Therefore, the lifetime definitions used in previous chapters were based on a single optimization objective, such as the energy dissipation (ED) of a particular node lying in the route or in the string topology network. However, several other significant optimization objectives, such as the end-to-end delay were not considered during the NL maximization. Therefore, in this chapter we aim for providing the system designer with a trade-off relying on the interplay between the energy dissipation and the end-to-end delay in order to obtain the set of Pareto optimal NL aware routes using multi-objective routing optimization algorithms.

5.1.1 Motivation and Related Works

Routing is one of the most important design issues of multi-hop wireless networks, which has a significant impact on their achievable performance. Hence, efficient routing techniques should be designed for ensuring that the data packets propagate in an "optimal" manner in terms of several metrics, such as energy dissipation, delay, delay jitter, bandwidth and packet loss ratio. In conventional multi-hop networks, only one of the desired objectives is optimized, whereas other objectives are assumed to be constraints of the problem [228]. Nonetheless, in some practical applications finding multiple solutions, each of which is optimal in terms of a single metric may be better than finding a single meritorious solution, which strikes a trade-off amongst several conflicting factors. The way to strike a meritorious trade-off is to consider the multiple design objectives as the components of a single aggregate objective function (OF), for example, using the weighted linear sum based method [176,229]. However, choosing the most appropriate weights for the various constituent design objectives requires careful consideration depending on the specific importance of the individual design objectives. Naturally, this method only provides a single solution per simulation [230]. In certain applications multi-objective optimization (MO) algorithms that provide several optimal solutions may be preferred, since these methods do not necessarily require user-defined objective weights. Furthermore, the drawback of focusing on a single design objective, whilst ignoring other important objectives may be circumvented by multi-objective optimization techniques [228]. We can consider all the objectives simultaneously and generate a set of optimal solutions, which are known as the Pareto-optimal solutions [176–178, 231] of multi-objective problems. However, finding optimal routes satisfying multiple OFs in networks is an NP-Complete problem [232]. Hence, there is a need for efficient heuristic search algorithms based on reduced-complexity evolutionary algorithms (EAs) [177, 233–238].

At the time of writing there is a paucity of contributions in the literature on the issue of multi-objective optimization conceived for routing-related issues in WSNs. One of the earliest study considering the simultaneous optimization of multiple quality of service (QoS) objectives in the context of wireless networks was proposed by Roy *et al.* in [239], where the authors considered a *multi-cast QoS routing algorithm* based on the *non-dominated sorting based genetic algorithm* (MQRA-NSGA), which simultaneously optimizes the end-to-end delay, the bandwidth requirement and the bandwidth exploitation. On the other hand, Cui *et al.* [240] studied MO relying on genetic algorithms (MOGAs) for finding specific routes, which satisfied different QoS requirements, with a special emphasis on how close their algorithm was capable of approaching the global minimum of each objective, as the number of nodes in the network increased. As a further development, Xue *et al.* [175] conceived a novel multi-objective differential evolution (MODE) algorithm for solving the routing problems of multi-hop networks by simultaneously optimizing both the delay and the energy consumption. Additionally, Kotecha and Popat [232] employed a multi-objective genetic algorithm

for improving the QoS in mobile ad-hoc networks (MANETs). Their solution considered the bandwidth, the delay, the traffic emanating from the neighboring nodes and the number of hops. They demonstrated that the proposed GA-aided QoS-based routing (GAQR) protocol performs better than conventional methods, such as the ad-hoc on-demand distance vector (AODV) and QoS-AODV techniques. Camelo *et al.* [230] proposed a new method for solving routing problems by considering the QoS in wireless mesh networks (WMNs). In [230], the non-dominated sorting based genetic algorithm-II (NSGA-II) was invoked for finding different routing alternatives for guaranteeing the QoS requirements of both the voice over Internet protocol (VoIP) and of file transfer. Nevertheless, in [182] we investigated the performance of the NSGA-II and MODE algorithms for finding the optimal routes spanning from a given source node to a given destination node based on the conflicting design objectives, such as the delay and the energy dissipation.

Liu *et al.* [241] investigated energy-efficient capacity optimization problems using a multi-objective optimization method in a general large-scale multi-hop, multi-radio, multi-channel wireless network. The authors of [241] firstly considered a single-objective capacity optimization problem and then compared its energy efficiency performance to that of its multi-objective optimization counterpart, where the OFs were based on the energy efficiency and on the capacity. They observed that depending on the number of available radios and channels, simultaneous optimization of the capacity and the energy efficiency was capable of saving 20% to 60% of the energy compared to that of the single-objective capacity optimization. Moreover, Alanis *et al.* [242] proposed a near-Pareto-optimal multi-objective quantum-assisted algorithm, namely the so-called non-dominated quantum optimization algorithm (NDQO) for simultaneously optimizing the performance of a self-organizing network in terms of its delay, BER and energy dissipation.

Additionally, there are comprehensive studies of MO problems that investigate different aspects of WSNs [2, 235, 243]. For example, Jourdan *et al.* [244] proposed a MOGA for sensor node placement, where the objectives were constituted by maximizing the sensor coverage quality and the lifetime of the network considering the trade-off between transmission over longer distances at increased powers and the lifetime. Similarly, in [245, 246] the authors considered multi-objective node-deployment and power assignment problems by simultaneously maximizing the conflicting objectives, which are the NL and the network coverage quality, where the algorithms considered, namely multi-objective evolutionary algorithm based on decomposition hybridized with a problem-specific generalized subproblem-dependent heuristic (MOEA-D/GSH) were characterized using various network instances including the network size, the number of sensors and the node-density. On the other hand, Aitsaadi *et al.* employed a multi-objective node-deployment optimization algorithm (MODA) [247] considering the cost-reduction of WSN deployments and the desired event detection probability, in order to maintain the network's connectivity and to maximize the NL. Moreover, Masazade *et al.* [228] studied the distributed detection problem and the choice of the appropriate sen-

sor thresholds, which was also solved with the aid of MO algorithms, namely the so-called NSGA-II and the normal boundary intersection (NBI) method. Minimizing both the error probability and energy consumption of the network was the author's objective. In [248], the authors proposed a cluster-based routing algorithm for maintaining the desired QoS by considering the battery energy constraints of WSNs. The authors of [248] formulated their multi-objective optimization problem relying on the end-to-end delay, the path reliability and the energy dissipation. They concluded by providing a set of Pareto optimal solutions using the NSGA-II.

Jin *et al.* [249] investigated the so-called redundant overlapping coverage problem in terms of the network's high-quality coverage and the power consumption of the network with the aid of the MODE algorithm. Additionally, Martins *et al.* [250] proposed a hybrid multi-objective optimization algorithm, namely multi-objective global on-demand algorithm with a local on-line algorithm (MGoDA-LoA) for improving the performance of WSNs. This algorithm provided a solution for the dynamic coverage and connectivity problem (DCCP) of WSNs subjected to node failures. They concluded that the MO approach provides an attractive solution for extending the network's lifetime at a slight degradation of the network's coverage quality. Similarly, in [251] the authors aimed for maximizing both the coverage quality and the NL, while simultaneously minimizing the deployment cost. The multi-objective optimization problem of [251] was solved using the NSGA-II as well as the strength Pareto evolutionary algorithm-II (SPEA-II) and multi-objective ant colony optimization (MOACO) algorithm to obtain the set of Pareto front solutions, where the coverage quality and the NL were maximized, while the deployment cost was minimized.

Moreover, Perez *et al.* [252] described a MO model conceived for jointly minimizing both the number of sensors employed and the total energy dissipation of the sensor network, which allowed them to minimize the total deployment cost. Abidin *et al.* [253] compared single-objective territorial predator scent marking algorithm (SO-TPSMA) and multi-objective TPSMA (MO-TPSMA) optimization problems, where the single-objective optimization problem only aimed for maximizing the coverage quality, whereas the multi-objective optimization problem simultaneously optimized multiple objectives, such as the maximization of coverage quality and the minimization of the energy dissipation. The authors of [253] demonstrated that the energy dissipation is significantly reduced, despite the fact that the coverage quality is slightly degraded in multi-objective optimization compared to that of single-objective optimization. Chenji *et al.* [217] investigated the attainable system performance and its energy dissipation using multi-objective optimization of the system's lifetime and its packet delivery latency in disaster response networks. The authors of [217] solved the multi-objective optimization problem considered using the NSGA-II and demonstrated that the system's lifetime was increased by 162 minutes at the cost of 61 minutes increase in packet delivery latency, while maintaining a similar packet delivery ratio performance. Additionally, Lu *et al.* [254] formulated a multi-objective optimization problem considering

the fuzzy and random nature of the routing in WSNs, which simultaneously optimized several objectives, such as the end-to-end delay, the delay jitter, link reliability, the interference levels and the balanced residual energy distribution of a path. Lu *et al.* [254] solved the problem considered using a multi-objective routing algorithm, namely fuzzy-random multi-objective optimization (FRMOO), which is a hybrid routing algorithm that was alternating between a fuzzy and a random state of the WSN. This hybrid algorithm was capable of finding the Pareto optimal paths based on the objectives considered. Rahat *et al.* [255] proposed a multi-objective routing optimization approach using evolutionary algorithms to obtain the Pareto optimal solutions of the minimum lifetime of the nodes in the network and the average lifetime of the WSN. The authors of [255] demonstrated that their approach was capable of providing better trade-offs than the minimization of the energy dissipation and the simultaneous optimization of the minimum lifetime of the nodes in the network. Hence, the average lifetime of the network as a whole was improved. Moreover, in [256] the authors employed a multi-objective approach, namely the so-called SPEA for simultaneously optimizing the QoS requirements, such as the end-to-end delay and the expected transmission count (ETX) for finding paths that minimize the objectives considered. They also characterized the interplay of the conflicting design factors. The major contributions of the multi-objective optimization techniques are summarized in Table 5.1.

To elaborate a little further, various multi-objective optimization approaches have been considered in the literature, where the simultaneous optimization of the multiple objectives was converted to either the minimization or the maximization of the weighted function of each objective considered. For example, in [257] the authors considered a minimum-power routing method, which optimally allocates the transmit power in a multi-hop network. The multi-objective optimization of the transmit power allocation of each node was evaluated in [257], while maintaining the link's QoS quantified in terms of the capacity outage probability for transmission over Nakagami-m faded channels. However, the power allocation of each node was converted to a weighted power-sum minimization problem. Additionally, in [258] the authors employed a data forwarding protocol, which traded-off the energy dissipation against the delay by the simultaneous minimization of the energy dissipation and the delay, while maintaining a uniform battery power depletion across the network. However, despite the fact that the author of [258] derived the multiple objectives separately, these objectives were incorporated into a weighted function. This reduced the problem considered to a single-objective function, which had a specific weighting coefficient for each objective function.

5.1.2 Novel Contributions

Although there are numerous examples of employing multi-objective evolutionary algorithms (MOEAs) in the literature, no comparative study exists for a sufficiently diverse

TABLE 5.1: The major contributions of the multi-objective optimization techniques.

Year	Author(s)	Objective functions	Optimization algorithm(s)
2002	Roy *et al.* [239]	Delay, bandwidth	MQRA-NSGA
2003	Cui *et al.* [240]	Delay, bandwidth, packet loss ratio	MOGA
2004	Jourdan *et al.* [244]	Coverage quality, NL	MOGA
2006	Xue *et al.* [175]	Delay, energy dissipation	MODE
2007	Kotecha *et al.* [232]	Delay, bandwidth, traffic, number of hops	GAQR
2010	Jin *et al.* [249]	Coverage quality, power consumption	MODE
	Aitsaadi *et al.* [247]	Deployment cost, event detection probability, network connectivity, NL	MODA
	Masazade *et al.* [228]	Error probability, energy dissipation	NBI, NSGA-II
	Ekbatani-Fard *et al.* [248]	Delay, path reliability, energy dissipation	NSGA-II
	Camelo *et al.* [230]	Delay, bandwidth, packet loss ratio, power consumption	NSGA-II
2011	Martins *et al.* [250]	Network connectivity, coverage quality, NL	MGoDA-LoA
	Le Berre *et al.* [251]	Deployment cost, coverage quality, NL	NSGA-II, SPEA-II, MOACO
	Konstantinidis *et al.* [246]	Coverage quality, NL	MOEA-D/GSH
2012	Yetgin *et al.* [182]	Delay, energy dissipation	MODE, NSGA-II
2013	Abidin *et al.* [253]	Energy dissipation, coverage quality	SO-TPSMA, MO-TPSMA
2014	Chenji *et al.* [217]	Delay, NL	NSGA-II
	Lu *et al.* [254]	Delay, delay jitter, link reliability, interference, residual energy distribution	FRMOO
	Alanis *et al.* [242]	Delay, BER, energy dissipation	NDQO
2015	Magaia *et al.* [256]	Delay, expected transmission count	SPEA

range of algorithms conceived for our specific routing problem. In this light, the novel contributions of this chapter are summarized as follows.

1. We investigate two MO algorithms. The first is based on the above-mentioned NSGA-II, while the second one is the MODE algorithm [174, 175]. We invoke both algorithms for jointly optimizing the delay and energy dissipation of a fully connected network relying on randomly distributed nodes.
2. We compare both algorithms in terms of the proximity of their solutions to the true Pareto front [176–178].
3. We evaluate their complexities and their rates of convergence, as the number of nodes in the network increases. We also demonstrate that at the same complexity, the MODE algorithm provides solutions approaching the true Pareto front more closely than the NSGA-II, and in general exhibits a higher convergence rate.
4. Additionally, we demonstrate that both algorithms require substantially less cost-function evaluations to approach the true Pareto front for networks of 10 or more nodes, when compared to an exhaustive search algorithm (ESA).
5. We propose a novel multi-objective NL definition, where the system designer can foresee a trade-off between the energy dissipation and the end-to-end delay. Therefore, depending on the specific application and target QoS required, the set of NL aware routes lying on the Pareto front is the Pareto optimal set maximizing the NL by considering the interplay between the energy dissipation and end-to-end delay.

5.1.3 Chapter Organization

The rest of this chapter is organized as follows. In Section 5.2, we illustrate the ideas behind multi-objective optimization and provide the mathematical definition of the multi-objective optimization problems. In Section 5.3, we describe our network model and quantify the fitness of each routing solution in order to obtain the set of optimal NL solutions. Moreover, we describe the NSGA-II and MODE algorithms conceived for routing optimization in Section 5.4, followed by the simulation setup and present our performance evaluation of the MOEAs considered in Section 5.5. Finally, we conclude in Section 5.6.

5.2 Multi-objective Optimization

Multi-objective optimization defines decision problems, which deal with the simultaneous optimization of multiple objectives in order to strike a trade-off between these objectives. Multi-objective optimization has been exploited in diverse fields, including engineering, finance, economics, radio resource management, logistics and so on, where an optimal decision has to be made upon considering the trade-off between conflicting objectives. Nonetheless,

real-world optimization problems usually have to meet multiple objectives to identify an attractive solution. For example, assuming that we want buy a car by looking at several of its attributes (objectives) and assuming that these attributes are simply related to its fuel consumption and its price. Hence, in order to find this car, we look for the minimum fuel consumption and the minimum price. Therefore, fuel consumption and price are two separate objectives we have to evaluate before buying the car. However, finding a car with the minimum fuel consumption may lead to an increased price, which we also want to minimize simultaneously. This indicates the conflicting nature of the two objectives[1]. Suppose we have to make a decision to buy the car, thus we have to construct a list of the cars, which is composed of the minimum fuel consumption and minimum price attributes regardless of their color and brand [231]. Then, we can obtain the list of the cars striking a compelling trade-off between the fuel consumption and the price, as portrayed in the stylized Fig. 5.1, where we can choose a car with a reasonable fuel consumption and price. This list will definitely eliminate the cars with high fuel consumption and high price. Observe in Fig. 5.1 that we can formulate a car selection decision that either has a high fuel consumption or a high price, which we refer to as *poor decisions*. However, from the whole list of cars, if at least one of the cars is better in terms of fuel consumption and price, then we include this car in a separate list, namely in the so-called *superior decisions* set. Here, *superior decisions* define the best possible solutions in terms of fuel consumption and price. None of the decisions amongst these superior decisions may be deemed to be better than the others. The decision can be made by the buyer using Fig. 5.1, where he/she can buy a car from the set of *superior decisions* with the highest fuel consumption but for the cheapest price, or with the lowest fuel consumption but for the highest price, or one with a reasonable price and reasonable fuel consumption.

In a nutshell, a specific problem that arises using a single weighted function is how to weight the various objectives for a final decision. Returning to the selection of the car, some of these objectives, such as the color and the size of the car or fuzzy objectives, such as the comfort and elegance of the car cannot be readily quantified. Since the selection of the car is strictly dependent on the weighting factors, the inappropriate choice of the factors might lead to suboptimal or misleading solutions in practice. Therefore, the simultaneous optimization of these objectives plays a vital role in making a decision, where MO provides the decision maker relying on informed decisions striking a trade-off amongst several objectives.

5.2.1 Multi-Objective Definition

In this section, we provide the general mathematical formulation of multi-objective optimization problems. A multi-objective optimization produces a set of solutions for objective

[1]Here, we assume an inverse-proportion relation between the fuel consumption and the price of the car. We assume that if a car is more expensive, it can only be due to its less fuel consumption.

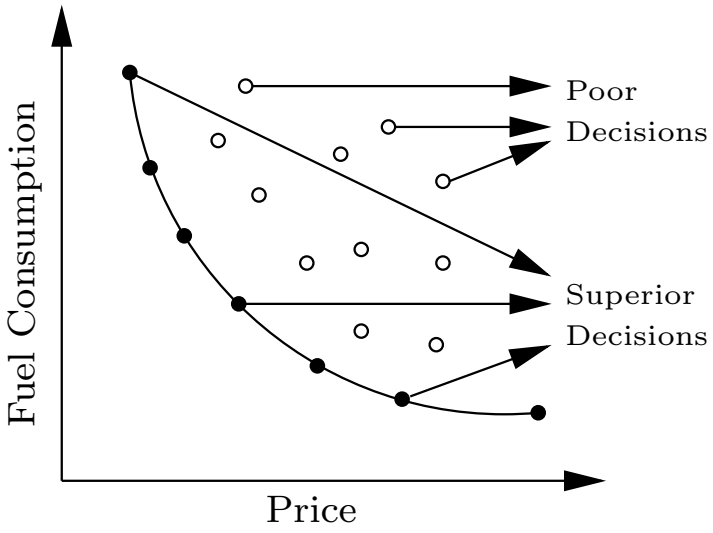

FIGURE 5.1: Decision making in buying a car using multiple objectives, namely the fuel consumption and price of the car.

functions relying on multiple conflicting parameters. By contrast, in conventional single-objective optimization we find the global optimum by satisfying a single-component objective function. A multi-objective problem can be formulated as follows [178, 234]

$$\text{min.} \quad f(\mathbf{x}) = [f_1(\mathbf{x}), f_2(\mathbf{x}), f_3(\mathbf{x}), \cdots, f_{n_f}(\mathbf{x})] \tag{5.1}$$

$$\text{st.} \quad g_j(\mathbf{x}) \leq 0, j = 1, \cdots, n_g, \tag{5.2}$$

where $\mathbf{x} = [x_1, x_2, x_3, \cdots, x_N]^T \in \mathbb{R}^N$ is the vector of variables that has to be optimized, f_i, $i = 1, \cdots, n_f$, are the OFs and g_j, $j = 1, \cdots, n_g$, are the constraint functions. Multi-objective optimization problems can be solved using the Pareto optimality technique, which was proposed by Edgeworth and Pareto [259], as defined below for the case of a minimization problem [231].

Definition 1. Pareto dominance[2]: A particular solution vector

$$f(\mathbf{x}_1) = [f_1(\mathbf{x}_1), f_2(\mathbf{x}_1), f_3(\mathbf{x}_1), \cdots, f_{n_f}(\mathbf{x}_1)] \tag{5.3}$$

is said to dominate another particular solution vector

$$f(\mathbf{x}_2) = [f_1(\mathbf{x}_2), f_2(\mathbf{x}_2), f_3(\mathbf{x}_2), \cdots, f_{n_f}(\mathbf{x}_2)] \tag{5.4}$$

if and only if $f(\mathbf{x}_1) \preceq f(\mathbf{x}_2)$, i.e. we have $\forall i \in 1, \cdots, n_f$, $f_i(\mathbf{x}_1) \leq f_i(\mathbf{x}_2) \wedge \exists i \in 1, \cdots, n_f$: $f_i(\mathbf{x}_1) < f_i(\mathbf{x}_2)$, where n_f is the number of OFs in the optimization problem.

[2]The terminology of *dominance* is a natural one in the context of a maximization problem. However, when aiming for finding the minimum in an optimization problem, a *dominant* solution is one, which is associated with a lower OF value.

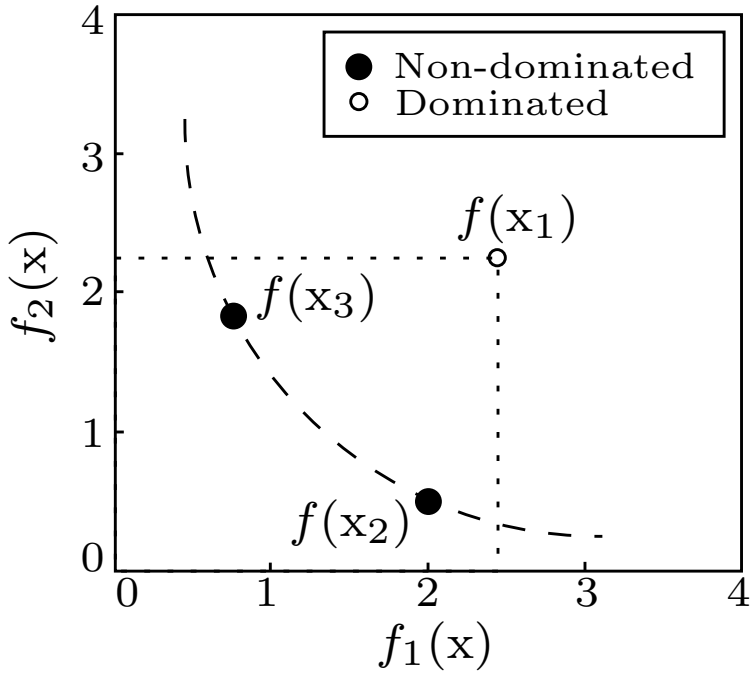

FIGURE 5.2: Optimal Pareto front for two OFs and their dominance relationship.

To elaborate further, let us consider three solution vectors $f(\mathbf{x}_1)$, $f(\mathbf{x}_2)$ and $f(\mathbf{x}_3)$, given that $f(\mathbf{x}_1) = [2.4, 2.3]$, $f(\mathbf{x}_2) = [2.1, 0.3]$ and $f(\mathbf{x}_3) = [0.8, 1.6]$. From the definition of Pareto dominance, we can say that $f(\mathbf{x}_2)$ dominates $f(\mathbf{x}_1)$, since each element of $f(\mathbf{x}_2)$ is unambiguously lower than the corresponding element of $f(\mathbf{x}_1)$. However, $f(\mathbf{x}_2)$ neither dominates nor it is dominated by $f(\mathbf{x}_3)$, since we have $f_1(\mathbf{x}_3) < f_1(\mathbf{x}_2)$, but $f_2(\mathbf{x}_3) > f_2(\mathbf{x}_2)$.

Definition 2. Pareto optimality: A particular solution $f(\mathbf{x}_1)$ is said to be Pareto optimal, if and only if there is no $f(\mathbf{x})$ for which $f(\mathbf{x}_1)$ is dominated by $f(\mathbf{x})$.

For the three solution examples given above, solutions $f(\mathbf{x}_2)$ and $f(\mathbf{x}_3)$ are both Pareto optimal, since they are not dominated by any other solution. In this case, they are said to lie on the Pareto front of the objective space. Additionally, solution $f(\mathbf{x}_1)$ is dominated, and the relationships between $f(\mathbf{x}_1)$, $f(\mathbf{x}_2)$ and $f(\mathbf{x}_3)$ are shown in Fig. 5.2. The aim of multi-objective optimization is to generate a diverse set of Pareto-optimal solutions so that the user can evaluate the trade-offs between the different objectives.

5.3 System Model

We consider a fully-connected network having a single source and a single destination in a $100 \times 100\text{m}^2$ area, as seen in Fig. 5.3, where all the nodes are stationary and randomly distributed according to the uniform distribution. They can communicate bidirectionally on the same shared wireless channel. Each node has a unique identifier for its transmitter

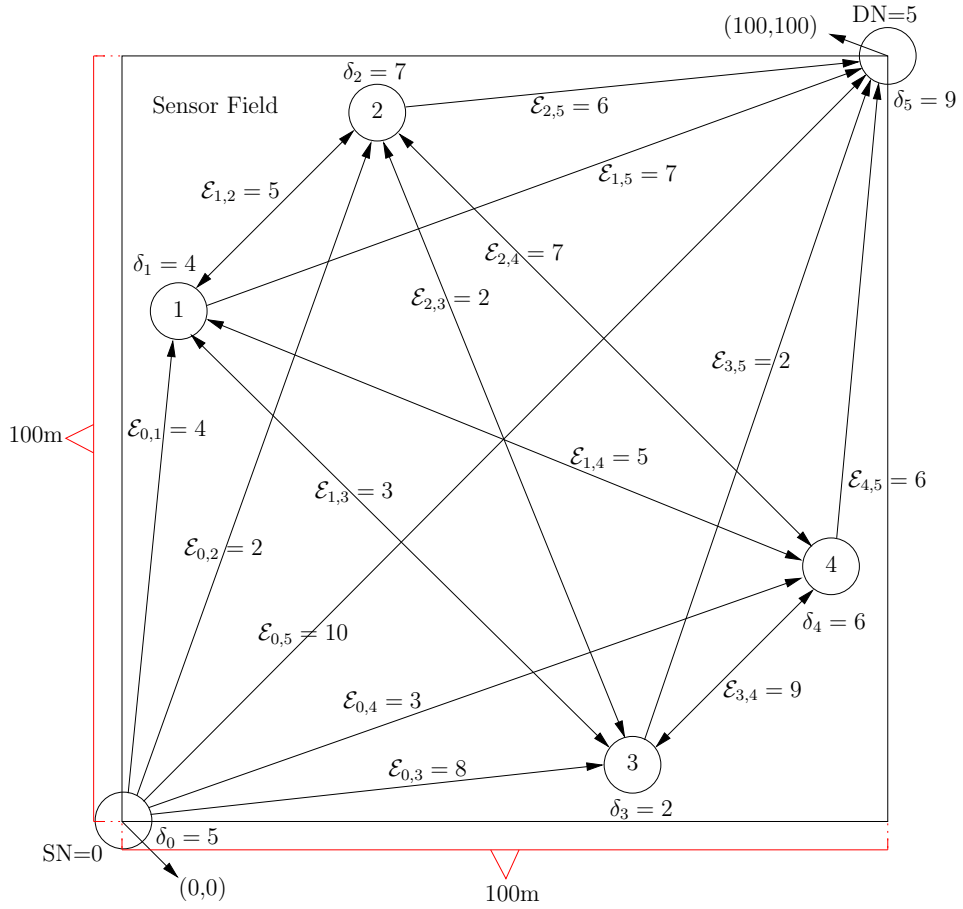

FIGURE 5.3: Fully connected network, where δ is the number of packets that may be stored in the queue and $\mathcal{E}$ is the energy cost (not to scale).

and receiver. The SN and the DN are placed at opposite corners. Transmission between any two nodes is assumed to incur an energy cost of $\mathcal{E}_{i,j}$, which is proportional to $(d_{i,j})^m$, where $d_{i,j}$ is the Euclidean distance between the nodes i and j ($i \neq j$), while m is the path-loss exponent, which is dependent on the propagation environment. We assume that all other network operations incur a negligible energy dissipation cost. Furthermore, the ith node has a queue length of δ_i packets, and we assume a propagation delay of one time unit. Therefore, given a link between nodes i and j, the total transmission delay $D_{i,j}$ is given by $D_{i,j} = \delta_i + 1$. We note that the values of $\mathcal{E}_{i,j}$ and δ_i are randomly initialized, as illustrated in Fig. 5.3. In Section 5.5, for simplicity we set δ_i to zero so that the end-to-end delay is equal to the number of hops in units of time.

Given these assumptions, we can now describe the "cost" of a particular $(V-1)$-hop route formulated as, $R = v_0, v_1, ..., v_{V-2}, v_{V-1}$, which is a vector containing both the aggregate energy dissipation, $\mathcal{E}_t$ and the delay, D_t, of each link along the route given by

$$\mathcal{E}_t = \sum_{i=0}^{V-2} \mathcal{E}_{i,i+1}, \; D_t = \sum_{i=0}^{V-2} (\delta_i + 1). \tag{5.5}$$

Therefore, (5.5) determines the aggregate energy and the delay cost of each link in the WSN considered in Fig. 5.3. Given the definition of multi-objective optimization described in Section 5.2.1, the lifetime of the network considered in Fig. 5.3 is defined by the set of routes, each of which having the minimum aggregate energy and end-to-end delay costs. Therefore, our NL model is based on the simultaneous optimization of the aggregate energy dissipation and the end-to-end delay. However, since the energy dissipation and end-to-end delay costs are conflicting objectives, a set of Pareto optimal solutions can be found. Moreover, we stipulate the idealized simplifying assumption that our routing protocols have global knowledge of the node-positions, so that the SN can evaluate the cost of each potential route leading to the DN.

5.4 Evolutionary Algorithms

Many realistic applications require the simultaneous optimization of several conflicting objectives. For this type of problems, finding a single optimal solution is not satisfactory, but rather a set of optimal solutions is required. These solutions strike a trade-off amongst several objectives and there are no other solutions in the entire solution space that are superior to these solutions. Therefore, these solutions are known as Pareto optimal solutions, as described in Section 5.2.1. As mentioned in [176, 229, 231, 234], MOEAs are well-suited for such problems, since they are capable of finding a set of Pareto optimal solutions. In this study, we appropriately adapt the MOEAs of NSGA-II and MODE for our routing optimization problem. We note that we have considered a single objective version of the NSGA-II algorithm in Chapter 4. Here we adopt the genetic operators in a similar manner to that in Chapter 4 for our multi-objective routing optimization problem. The main differences between the single-objective and multi-objective versions of NSGA-II are the non-dominated sorting and the crowding distance method of the algorithm considered in Section 5.4.1. The rest of the genetic operators are used in a similar way and therefore, the illustrations of genetic operations, such as selection, crossover, mutation, recombination and the change in the population size are the same as these described in Chapter 4.

5.4.1 Non-Dominated Sorting Based Genetic Algorithm-II

In genetic algorithms, there is an initial population of candidate solutions, which are termed as *individuals*, and the performance of a solution in terms of a given objective function is quantified in terms of its *fitness*. These individuals are initialized to random values and after each iteration (*generation*) of the algorithm the values tend to converge upon those corresponding to better solutions given an OF by applying the genetic operators: *crossover*, *mutation* and *selection*, which help to diversify the values of the population and guide them towards higher-fitness solutions.

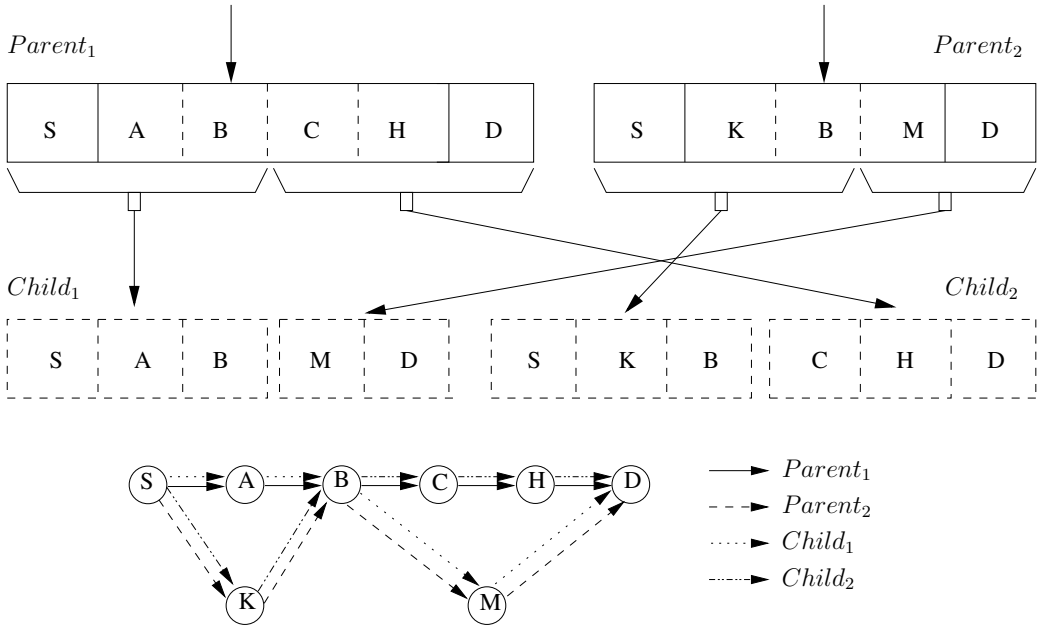

FIGURE 5.4: In the crossover operation, exchanging components of the candidate solutions after the common-node was selected.

The NSGA-II is a multi-objective evolutionary algorithm based on non-dominated sorting of the population, which was proposed by Deb *et al.* [177]. Each individual represents a route emerging from a given SN and leading to a given DN.

In Fig. 5.4, $Parent_1$ and $Parent_2$ represent a sequence of nodes for the fully-connected multi-hop network, assuming that S is the SN and D is the DN. The candidate solutions in the population are arbitrarily initialized to a random length, i.e. to a random number of hops, with the SN in the first position and the DN in the last position. Naturally, routing loops are prevented, since any individual associated with a loop would perform poorly both in terms of delay and energy dissipation. Then, the population is sorted into fronts, $\mathcal{F}_1, \mathcal{F}_2, \cdots, \mathcal{F}_N$, by ensuring that individuals in each preceding front dominate all individuals of all subsequent fronts, as shown in Fig. 5.5.

Given this definition, individuals in the first front, $\mathcal{F}_1$, belong to the Pareto front of the current solution set, where the dominated individuals representing longer and higher-energy routes are denoted by small symbols. Furthermore, the concept of *crowding distance* [177] is introduced in NSGA-II, which is the normalized Euclidean distance of an individual from its immediate neighbors in the same front of the solution space. After each generation, the algorithm preserves the specific solutions having the highest crowding distance in each front, which ensures that a high grade of individual-diversity is maintained in the solution space, corresponding to routes consisting of dissimilar links. The difference between NSGA-II and its predecessor, NSGA [260], is that the diversity of candidate solutions is maintained without requiring a user-selected parameter.

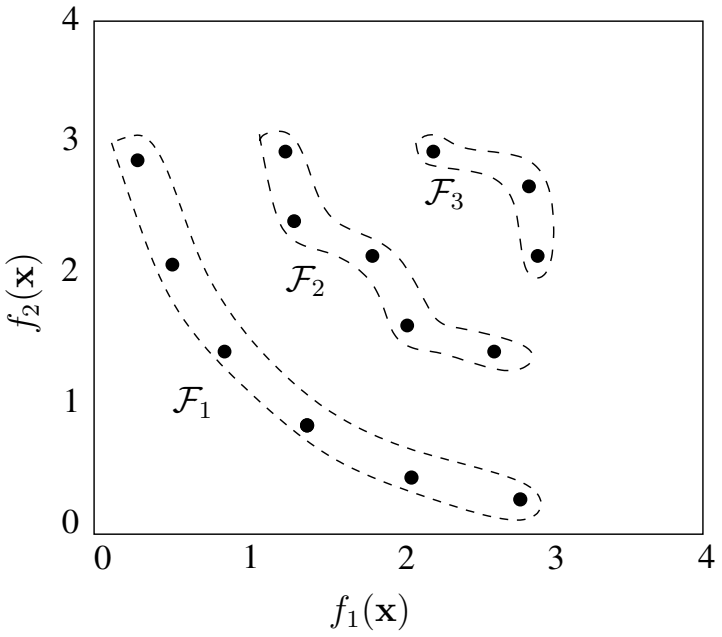

FIGURE 5.5: Individuals are arranged into fronts based on their dominance relationship.

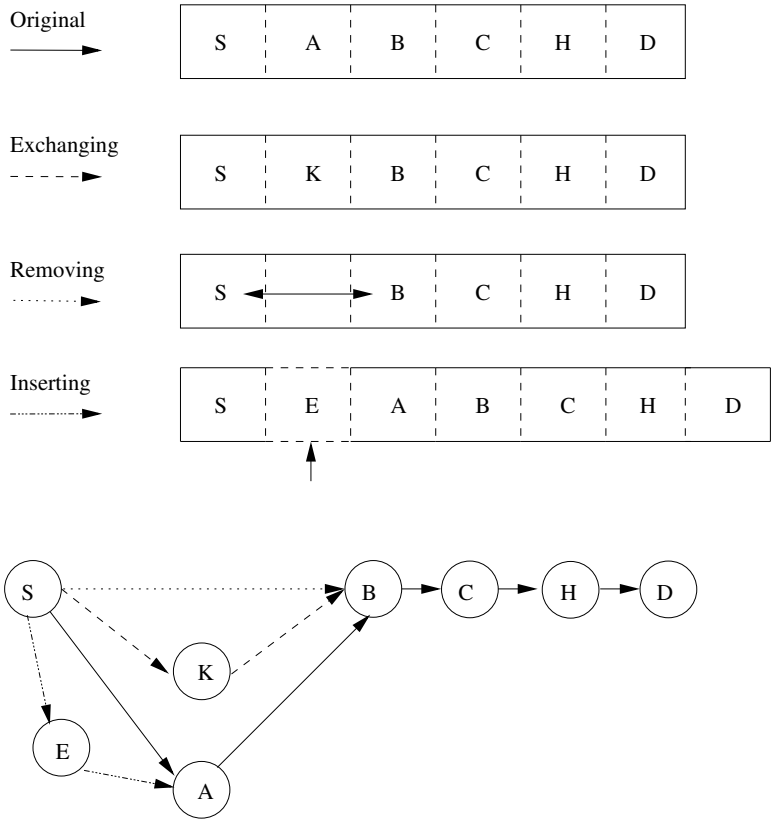

FIGURE 5.6: Exchanging, removing and inserting node stages during the mutation operation.

For more details on NSGA-II, the readers are referred to [177], since we now focus our attention on the modified parts of NSGA-II in order to adapt the algorithm to our specific optimization problem. The classic GA operators, such as the crossover and mutation, assists us in evolving the individuals of a specific population by producing new individuals - i.e. new routes - from the existing ones in order to find improved solutions. The classic genetic operators are applied to the so-called parent solution pairs, which are obtained here by the so-called binary tournament selection [177]. We use a common-node, single-point crossover mask with a crossover probability of Pr_c, and highlight the reasoning behind this choice as follows. Routes are formed from the links between the SN and DN passing through intermediate nodes, and the cost of each route is dependent on the cost of the individual links themselves. Therefore, it is more logical to find nodes that are common for both parent routes to perform the crossover operation at, in order to ensure that all but one of the already established links in both parent routes are preserved. Given this method, the crossover operation intelligently searches through the candidate-solution space, rather than doing this haphazardly. For example, in Fig. 5.4, the common node between $Parent_1$ and $Parent_2$ is B, therefore it is chosen as the crossover point. Then $Child_1$ is created by the concatenation of the nodes leading up to and including B from $Parent_1$ with the nodes following B in $Parent_2$, and vice-versa for $Child_2$. Note that the SN and DN cannot be chosen as crossover points, since applying crossover to them does not provide any new solutions. In the NSGA-II algorithm, both tournament selection and crossover are applied twice to the current population of individuals in order to provide $\aleph_{ind}$ new solutions, if the original population size was $\aleph_{ind}$. Further details on the change of the population size can be found in Fig. 4.16. The mutation operator is applied to each new individual. For each node - excluding the SN and DN - mutation is applied with a probability of Pr_m. In our implementation of the mutation operator, there are three possible modifications, which occur with equal probability: *node exchange*, as well as *node removal* or *insertion*. In case of *node exchange*, the current node is exchanged for a randomly-selected node, as shown in Fig. 5.6, where node A in the original individual is exchanged to node K. In *node removal* or *node insertion*, either the current node is deleted from the route, or a new node is inserted before this node. For example, in Fig. 5.6, node A is removed in the related example. In the *insertion* example, node E is inserted before node A. After mutation has been applied to each new individual, any potential routing loops are removed from each solution. In our fully-connected network, these GA operators are straightforward to implement, since any new route is valid. Our specific NSGA-II is summarized in Algorithm 1, where the general overview of the algorithm is that the initial population $\boldsymbol{\Upsilon}_1$ containing $\aleph_{ind}$ individuals iterates over $\aleph_{gen}$ number of generations, each of which constitutes a new population with better individuals after each generation using genetic operators, such as inheritance, selection, crossover, mutation and combination.

Algorithm 1: The NSGA-II algorithm adapted to our routing problem.

initialize($\boldsymbol{\Upsilon}_1$);
for $g := 1$ **to** $\aleph_{gen}$ **do**
  $\mathcal{F}$ = non-dominated-sort(Υ_g);
  $\mathcal{F}$ = calculate-crowding-distance($\mathcal{F}$);
  R_g = get-strongest-N-individuals($\mathcal{F}$);
  S_g = selection(R_g) $\cup$ selection(R_g);
  C_g = crossover(S_g);
  M_g = mutation(C_g);
  R_g = remove-loops(M_g);
  $\Upsilon_{g+1} = \Upsilon_g \cup R_g$
end for

5.4.2 Multi-Objective Differential Evolution Algorithm

The philosophy of Differential Evolution (DE) is that of relying on the individuals in the current population for guiding the optimization process. In classic DE [261], the new individuals are created using the appropriately weighted difference between the current individuals of the specific generation. We follow a similar methodology to [174, 175], which used both the current population as well as the non-dominated solutions for generating new solutions. By contrast, we only use the non-dominated solutions, because applying common-node, single-point crossover using a solution also from the current population may produce a solution has no relation to either the original individual or the non-dominated solution. In order to generate new individuals, with reference to Fig. 5.7, we use the common-node, single-point crossover for each parent individual $f(x_1)$ of the current generation and a randomly selected node from the set S_i, which consists of individuals in the Pareto front that dominate $f(x_1)$. If the set S_i is empty, in other words $f(x_1)$ lies on the Pareto front, then no crossover is performed. However, apart from the crossover process the rest of the algorithm operates like our implementation of NSGA-II in Algorithm 1.

5.5 Performance Results

We generate a WSN supporting V random uniformly distributed nodes. Each node has a queue length of δ packets and each link has an energy cost, as previously detailed in Section 5.3. Therefore, our conflicting OFs that have to be concurrently minimized are given by (5.5) and they are determined as the aggregate energy dissipation as well as the end-to-end delay in Section 5.3. For our simulations, a path-loss exponent of $m = 3$ is selected. To simplify the analysis, we set the queue length of each node to zero, therefore

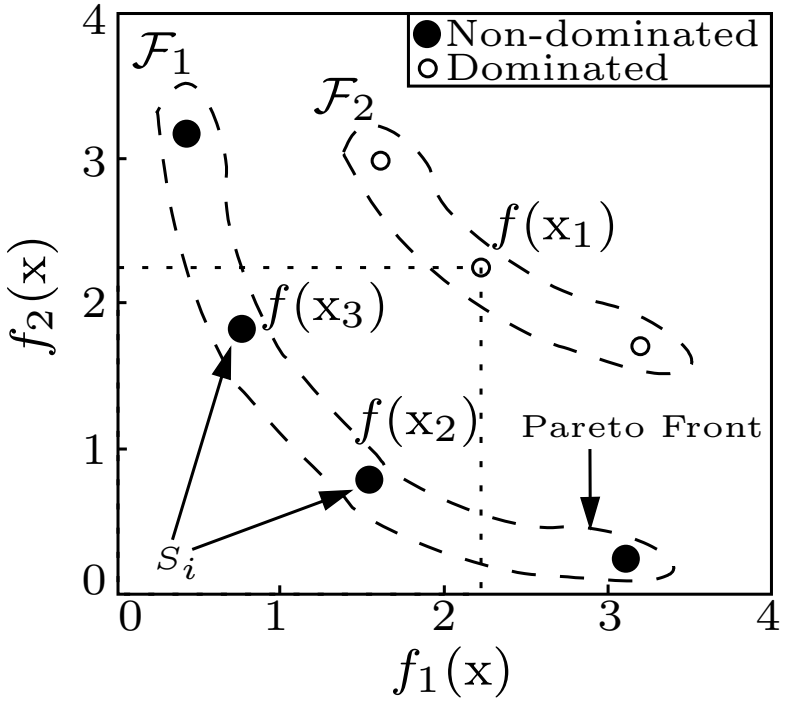

FIGURE 5.7: The set S_i consists of individuals in the Pareto front that dominate $f(x_1)$.

the delay is equal to the number of hops in units of time. For our MOEAs, the probability of crossover was set to $Pr_c = 0.9$, and the probability of mutation was $Pr_m = 0.5$.

5.5.1 True Pareto Front

Let us now continue by invoking our MOEA for the optimization of the routing in networks of V nodes, $V \in \{6, 8, 10, 12\}$. We used the true Pareto front, as the best-case performance lower-bound relying on an ESA. As described in Chapter 4, for V nodes the number of distinct routes R_V, excluding loops, is given by

$$R_V = \sum_{h=0}^{V-2} \frac{(V-2)!}{(V-2-h)!}, \tag{5.6}$$

which is simply the summation of the total number of route permutations for each route having $(h+1)$ hops, given a total of V nodes. In Fig. 5.8, we can follow the summation of route permutations per hop. As an illustration, we find the number of distinct routes for 4 fully-connected nodes. Further details on the complexity of the fully-connected networks and the computation of the total number of distinct and non-repeating routes can be found in Section 4.3.2.1. For clarity, the number of hops for each route is denoted by $\widehat{h} = (h+1)$.

$$\widehat{h} = 1, \text{ while } h = 0 \quad \blacktriangleright \quad \frac{2!}{2!} = 1 \tag{5.7}$$

$$\widehat{h} = 2, \text{ while } h = 1 \quad \blacktriangleright \quad \frac{2!}{1!} = 2 \tag{5.8}$$

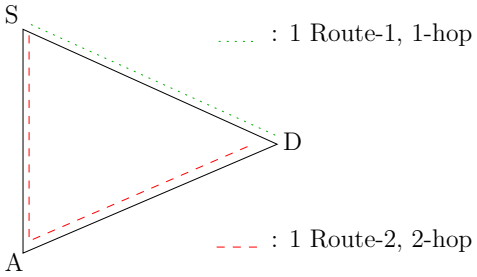

(a) WSN composed of 3 fully-connected nodes.

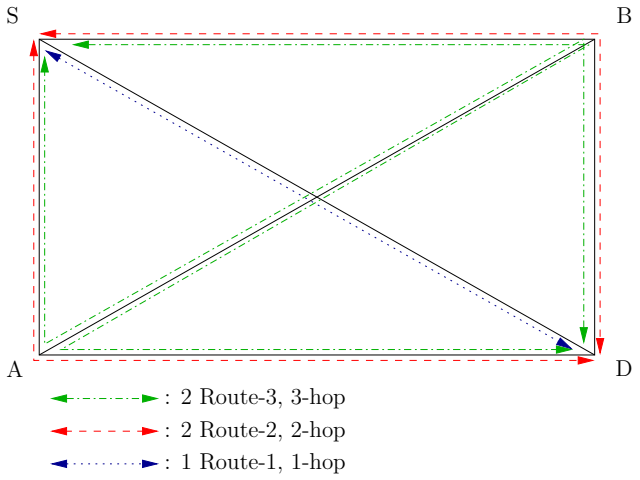

(b) WSN composed of 4 fully-connected nodes.

FIGURE 5.8: Total number of distinct routes for a given source and destination.

$$\widehat{h} = 3, \text{ while } h = 2 \quad \blacktriangleright \quad \frac{2!}{0!} = 2 \tag{5.9}$$

$$\text{Total Distinct Routes} \quad \blacktriangleright \quad 1 + 2 + 2 = 5. \tag{5.10}$$

From this simple calculation, we can easily observe the distinct lines, namely Route-1, Route-2, Route-3 and Route-$\widehat{h}$ in Fig. 5.8(b) for each possible number of hops of 4 fully-connected nodes.

As it will be shown in Section 5.5.2, even for a modest-size network of $V = 12$ nodes the number of route evaluations becomes prohibitively high. For our randomly generated uniformly distributed nodes, the Pareto solutions obtained using ESA are presented in Table 5.2. These solutions may be used for evaluating the performance of our MOEAs, when employed within the same network deployments.

As shown in Table 5.2, in a small-size network, for example $V = 6$, there are less Pareto solutions, since the network is not dense enough to provide many attractive routing solutions. As the network size increases above $V = 8$, the number of Pareto solutions becomes generally higher, and furthermore, the achievable energy reduction is improved, since there is a higher diversity of routes available. For example, when considering $V \in \{10, 12\}$ and increasing the number of hops $\widehat{h}$ from 1 to 2 provides an energy reduction of 75%. However, as the

		Delay					
		1	2	3	4	5	6
Nodes	6	1.00	0.31	0.18	-	-	-
	8	1.00	0.38	0.21	0.15	0.11	-
	10	1.00	0.25	0.13	0.08	-	-
	12	1.00	0.26	0.12	0.08	0.06	0.06

TABLE 5.2: Pareto optimal solutions for different number of nodes. The values in the table depict the lowest energy dissipation of the routes having the same delay cost, normalized to the single-hop case.

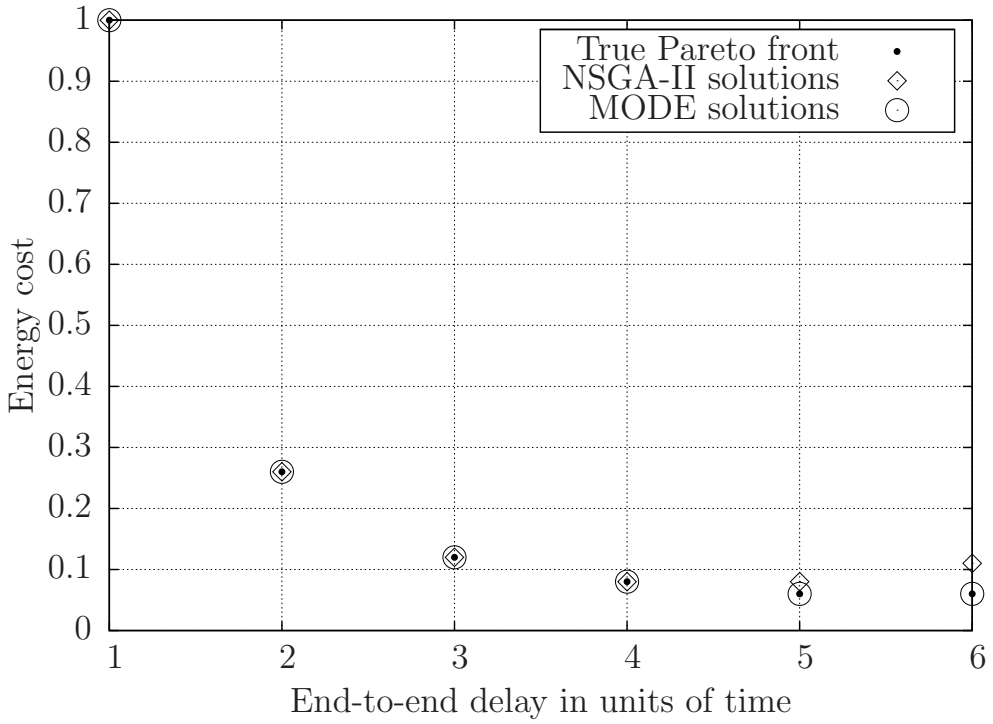

FIGURE 5.9: Comparison between the solutions obtained by NSGA-II and MODE to the true Pareto front for $V = 12$.

value of $\widehat{h}$ increases beyond 2, the potential energy reduction generally results in diminishing returns.

5.5.2 Performance evaluation of MOEAs

We present the results of applying our MOEAs in Fig. 5.9 for the optimization problem of $V = 12$. For these results, the number of individuals for both MOEAs is $\aleph_{ind} = 48$, whilst the number of generations is fixed to $\aleph_{gen} = 50$, so that the difference in performance can be illustrated. It is clear from Fig. 5.9 that increasing the number of hops reduces the

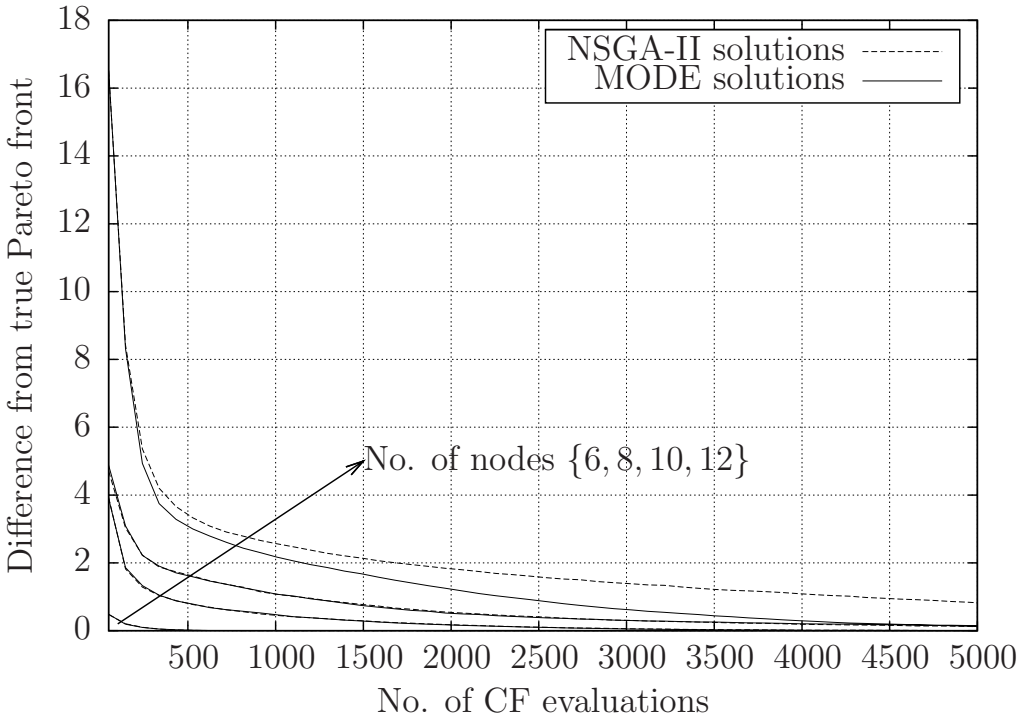

FIGURE 5.10: Convergence rate comparison of MODE and NSGA-II for different number of nodes averaged over 1000 runs. The lines for $V \in \{6, 8, 10\}$ are overlapping.

energy cost, which is expected due to the reduced-distance-based relaying gain. However, the reduction in energy cost exhibits diminishing returns upon increasing the number of hops beyond $\widehat{h} > 4$. Additionally, the end-to-end delay increases as the number of hops $\widehat{h}$ increases, and this represents a fundamental trade-off in this multi-hop network. This trade-off and solutions lying in the Pareto front provide the set of optimal NL-aware routes, since the route with the minimum energy dissipation and the minimum end-to-end delay determines our NL model. Depending on the application and the QoS required, the network designer can decide which NL-aware route is the best option to transmit.

At the same complexity, the MODE algorithm provides solutions that are closer to the true Pareto front than the NSGA-II for $\widehat{h} \geq 5$, namely when the search space becomes larger. MODE is capable of searching through this increased solution-space efficiently by combining each generation with the individuals in the current Pareto front, whereas NSGA-II uses only tournament selection, which may not find sufficiently meritorious individuals that would provide improved routes with the aid of crossover.

The algorithms may also be compared on the basis of their average rates of convergence and complexities. We may define the proximity of the solutions obtained to the true Pareto front in terms of the percentage difference between them. Let us define the set of Pareto solutions obtained from Section 5.5.1 as $\mathcal{P}_V$, which contains elements of $p_{V,\widehat{h}}$, where V is the number of nodes in the network, while the subscript $\widehat{h}$ indicates the number of hops associated with that particular solution. Furthermore, let us define the current solutions

Number of nodes, V	NSGA-II	MODE	ESA
6	395	446	65
8	4,557	4,377	1,957
10	1,186	1,112	109,601
12	10,950	10,680	9,864,101

TABLE 5.3: The average number of CFEs required for approaching the Pareto front within 1% averaged over 1000 runs.

in the MOEAs as $c_{V,\widehat{h}}$, which have the minimum energy cost. Then we may define the difference, $\Delta_{V,g}$, between the current solutions of the MOEAs and the true Pareto front for a V node network as

$$\Delta_{V,g} = \sum_{\widehat{h}=1}^{V-2} \frac{c_{V,\widehat{h}} - p_{V,\widehat{h}}}{p_{V,\widehat{h}}}. \tag{5.11}$$

As shown in Fig. 5.10, although both the NSGA-II and the MODE algorithms are capable of approaching the Pareto front, the rate of convergence for MODE is higher at $V = 12$ than that of the NSGA-II. However, as shown in Table 5.3, the average number of cost function evaluations (CFEs) required for approaching the Pareto front within 1% are similar for both algorithms. This illustrates that although the convergence rate of MODE is initially higher, the number of generations needed for approaching the Pareto front is ultimately similar for both algorithms. We can also see that the number of CFEs is significantly lower for the MOEAs than that of the ESA.

5.6 Chapter Summary and Conclusions

WSNs suffer from a higher end-to-end delay than their single-hop counterparts. Furthermore, since they rely on batteries and can be affected by long aggregate queuing times at each node along the route, minimizing their energy requirements is of prime importance. Therefore, in our scenario prolonging the NL is strictly dependent on the simultaneous optimization of the aggregate energy dissipation and the end-to-end delay of a route in the WSN considered. In this chapter, we optimized the routing using the combined CFE of (5.5) with the aid of novel multi-objective optimization algorithms in a fully-connected arbitrary WSN in order to identify the set of NL-aware routes using the NSGA-II and of the MODE algorithms, which were appropriately adapted to suit our routing problem. We demonstrated that both the MODE and NSGA-II are applicable for these kind of routing problems and that they are capable of finding the Pareto-optimal solutions at a significantly lower complexity than an exhaustive search method, when the number of nodes is higher than or equal

to 10. We also proposed a novel multi-objective NL definition, where the system designer can foresee a trade-off between the energy dissipation and the end-to-end delay. Therefore, depending both on the application and on the target QoS required, the set of NL aware routes lying on the Pareto front is the set of Pareto optimal solutions identified for optimizing the NL by considering the interplay between the energy dissipation and the end-to-end delay. Additionally, we demonstrated that at the same complexity, the MODE algorithm is capable of finding solutions closer to the Pareto front and in general, converges faster than the NSGA-II. The Pareto optimal solutions we obtained from the results demonstrated that the conflicting multiple objectives may indeed be beneficially reconciled.

Chapter 6

Conclusions and Future Research

6.1 Summary and Conclusions

In WSNs, NL maximization plays a significant role in striking a compelling compromise between maximizing the overall throughput and minimizing the energy dissipation, while extending the duration of communications, when the sensor nodes rely on limited energy supply. In this specific context, most contributions in the literature focus on minimizing the energy dissipation, while considering various network topologies [30, 189, 195]. Therefore, this treatise has broadened the scope of NL maximization by considering the design of several NL maximization methods. For example, the NL maximization method of Chapter 2 was based on rate versus power allocation, while Chapter 3 and Chapter 4 were considering an SINR constraint as the target QoS requirement rather than a transmission rate requirement. Chapter 5 proposed multi-objective NL function in order to optimize the routing based on the trade-off between the energy dissipation and the end-to-end delay.

6.1.1 Chapter 2

In this chapter, we evaluated the lifetime of the interference-limited WSN of Fig. 6.1, as a function of the transmit rate and power using the SPTS scheduling scheme of Section 2.2.2. The string topology of Section 2.2.1 was considered, where we defined the incidence matrix of the network characterized in Table 2.1. The path loss model, the channel characteristics

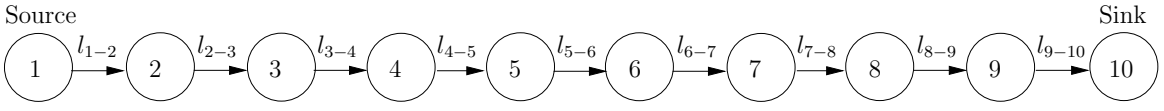

FIGURE 6.1: String topology having $V = 10$ nodes including a SN and a DN.

Links \ Slots	1	2	3	4	5	6	7	8	9	10	11	12	13	14	15	16	17	18
l_{1-2}	•+			•			•			•+			•			•		
l_{2-3}		•+			•			•			•+			•			•	
l_{3-4}			•+			•			•			•+			•			•
l_{4-5}	•			•+			•			•			•+			•		
l_{5-6}		•			•+			•			•			•+			•	
l_{6-7}			•			•+			•			•			•+			•
l_{7-8}	•			•			•+			•			•			•+		
l_{8-9}		•			•			•+			•			•			•+	
l_{9-10}			•			•			•+			•			•			•+

• : $T = 3$ SPTS + : $T = 9$ SPTS

FIGURE 6.2: Link scheduling with SPTS parameter $T = 3$ and $T = 9$, when $N = 18$ time slots (TSs) per link and $V = 10$ number of nodes.

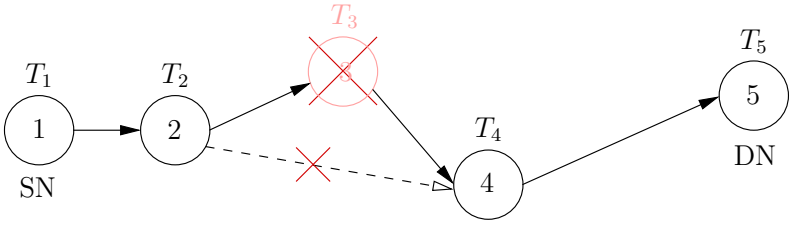

FIGURE 6.3: SN cannot relay its data to the DN due to a route-failure caused by the depleted battery of node-3.

and the scheduling scheme were described in Section 2.2.2, where a LOS AWGN channel subjected to a certain propagation path-loss law and a fading channel was considered. The SINR of both channels was discussed in Section 2.2.2, where we also described the SPTS scheduling scheme for $T = 3$ and $T = 9$, as illustrated in Fig. 6.2. Moreover, we justified the choice of the NL model considered in Section 2.2.3. Explicitly, Fig. 6.3 justifies why this NL model is a realistic NL model for the string topology considered in Fig. 6.1. Furthermore, the NL maximization problem was formulated in Section 2.3 as a nonlinear optimization problem taking into account the link scheduling, the transmission rates as well as transmit powers of all active TSs, as given by (2.8)–(2.12) for an AWGN channel. Later in Section 2.3, the rate constraint was generalized for a fading channel scenario using (2.19). The original nonlinear problem was converted into a convex optimization problem by employing an approximation of the SINR, as given by (2.30)–(2.36) for AWGN and (2.37)–(2.43) for fading channels. We also appraised the convexity of these problem formulations in Section 2.3.5.1. We then derived the Lagrangian form of the convex optimization problem in Section 2.3.7 and invoked the KKT optimality conditions [129] for deriving analytical expressions of the

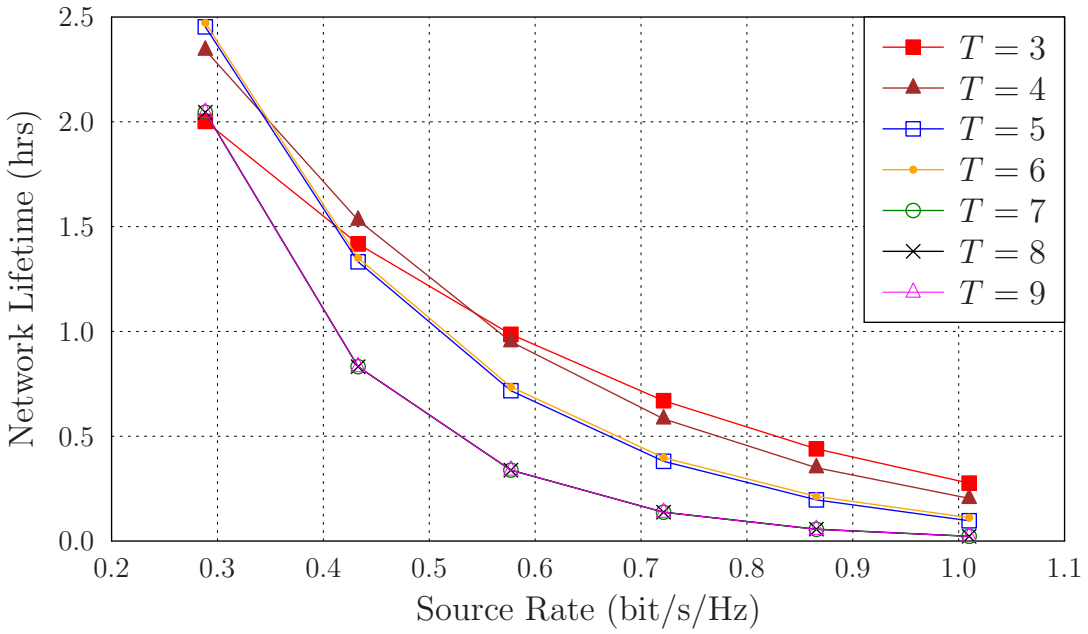

FIGURE 6.4: Network lifetime for different spatially periodic schedules and source rates in AWGN channel.

globally optimal transmit rate and power for our specific network topology in Section 2.3.8.1. Exploiting KKT optimality conditions significantly reduced the complexity of our algorithm, which requires the evaluation of $(n+1)$ expressions compared to an interior-point method requiring at least on the order of n^2 operations to solve n linear equations, as discussed in Section 2.3.8. Finally, we quantified the maximum NL for both AWGN and Rayleigh fading channels using Algorithm 2.1 of Section 2.4.3.

The effects of the fading and the source rate on the NL can readily be observed in Figs. 6.4 and 6.5, respectively. Our numerical results provided in Section 2.5 illustrated that fading has a detrimental impact on the achievable NL due to the poor channel conditions that require an increased transmit power in order to combat the effects of fading. The degradation of the NL due to fading and due to increasing the source rate is presented for $T = 3$ and $T = 9$ in Table 6.1. For example, Table 6.1 shows that at a source rate of 0.29bits/s/Hz, the NL of about 2hrs recorded for an AWGN channel is reduced to approximately 1.14hrs due to the impact of fading. Furthermore, as illustrated in Table 6.1, the simultaneous scheduling of links that interfere only weakly allowed us to take advantage of spatial reuse, where the activation of simultaneous transmissions at reduced rates necessitates a reduced transmission power, which resulted in extending the NL. More explicitly, Table 6.1 indicates that at the same source rate and for the same channel, the NL achieved in $T = 3$ was higher than that of $T = 9$. This is due to the simultaneous scheduling of 3 links for $T = 3$ in the same TS and the scheduling of one link for $T = 9$. Therefore, concurrently scheduling more transmission links was capable of exploiting the spatial reuse for extending the NL. Table 6.1 also illustrates how the NL is reduced upon increasing the source rate due to the requirement of higher transmission rate and power, regardless of the choice of channel and the scheduling

S_1 [bits/s/Hz]	$T = 3$		$T = 9$	
	AWGN	Fading	AWGN	Fading
0.29	2.0021	1.1383	2.0458	1.1292
0.43	1.4174	0.7960	0.8318	0.5206
0.58	0.9861	0.5888	0.3382	0.1824
0.72	0.6696	0.3886	0.1375	0.0767
0.87	0.4399	0.2708	0.0559	0.0342
1.01	0.2762	0.1682	0.0227	0.0009

TABLE 6.1: Maximum NL [hrs] comparison for increasing source rates of AWGN and fading channels, when $T = 3$ and $T = 9$.

scheme. For example, the NL of about 2hrs found for the source rate of 0.29bits/s/Hz, is gradually reduced to approximately 0.28hrs, when the source rate is 1.01bits/s/Hz. To summarize, the choice of the scheduling depends on the application, since a lower source rate favors infrequent transmissions requiring a low transmit power, which do not suffer from interference, when aiming for extending the NL. However, for higher source rates, a higher NL can be achieved by aggressive spatial reuse. For example, following Table 6.1, we can readily observe that in an AWGN channel, for a lower rate of 0.29bits/s/Hz, the $T = 3$ scenario achieved about 2hrs of NL, while $T = 9$ accomplished 2.05hrs of NL, which are quite similar performances. However, when encountering the same channel and a 3.5 times higher rate of 1.01bits/s/Hz, $T = 3$ achieved about 0.28hrs of NL, while $T = 9$ accomplished 0.02hrs of NL. Therefore, in order to extend the NL in applications requiring higher source rates, aggressive spatial reuse is necessary, where $T = 3$ allows 3 links to be scheduled in the same TS, while $T = 9$ schedules only a single link in a TS at a time.

6.1.2 Chapter 3

In Chapter 2, we only considered the NL as a function of the transmit rate and of the power, where an adaptive transmission scheme was assumed. However, the energy dissipation of the signal processing operations was neglected. But in practice the system designers also have to take into account the impact of the SPP on the NL. On the other hand, achieving a reasonable NL at the application-specific end-to-end target BER for a fixed-rate system using various MCSs is also of significant importance for the system designer in the interest of maintaining the required QoS. Therefore, in this chapter we aimed for maximizing the NL for a set of target SINR values, which guarantees a predefined QoS for each link modeled either by an AWGN channel or by a Rayleigh block-fading channel, while considering two

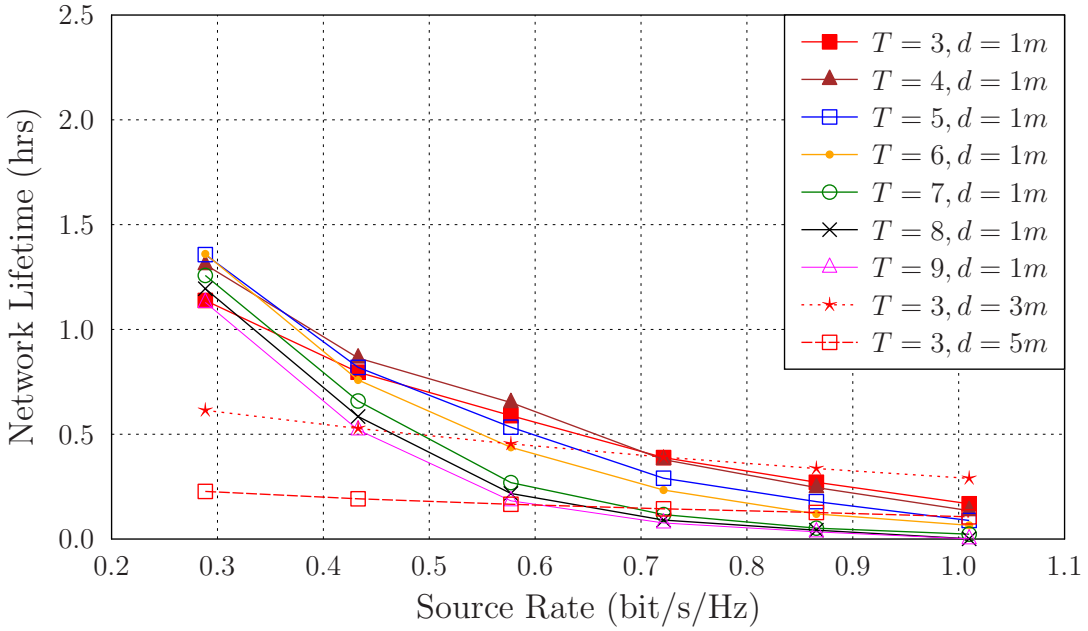

FIGURE 6.5: Network lifetime for different spatially periodic schedules and source rates in block-fading channel.

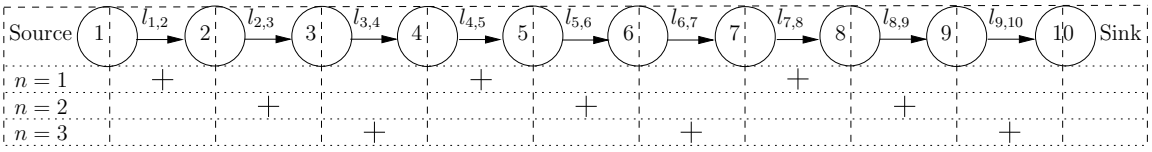

FIGURE 6.6: A string topology, where the SN and the DN is linearly connected by intermediate nodes relying on link scheduling associated with the SPTS parameter of $T = 3$, when $N = 3$ and $V = 10$.

scenarios; *Scenario 1*, where we considered the required transmit power only, and *Scenario 2*, where we considered the SPP in addition to the transmit power. The NL maximization problem was formulated in Section 3.3 with the aid of a set of lower bounded target SINR values for each link for the sake of characterizing the BER-dependent QoS and the impact of the physical layer parameters on the NL in the string topology of Fig. 6.6. We also analyzed the ED of each node, along with the required transmission power per link, the interference power imposed on each node and the lifetime of all nodes forming part of the string topology, while considering different target SINR requirements, SPP and channel characteristics. Moreover, we presented experimental results in Section 3.4 for assisting the network designer in making informed decisions as to which MCS works well for the application supported.

Table 6.2 presents the 'continuous-time' NL expressed in years for different MCSs and different target BER values in terms of both the PLBR as well as E2EB, and provides an overview of the systems, indicating both the longest and the shortest NL in *Scenario 1* and *2* for both AWGN and fading channels, where '*Scenario*' is abbreviated as 'Scn'. Therefore, the designer can readily determine, which systems and configurations are more NL-aware in

TABLE 6.2: The 'continuous-time' NL (in years) evaluation for WSNs with given configurations.

	Scn 2	Scn 1	Scn 2	Scn 1	Scn 2	Scn 1	Scn 2	Scn 1	
	10^{-4} PLBR		10^{-4} E2EB		10^{-3} PLBR		10^{-3} E2EB		AWGN
Uncoded-BPSK	0.36	0.55	0.21	0.27	0.57	1.2	0.37	0.57	
QPSK-CC-Soft	0.85	3.97	0.80	3.20	0.89	4.99	0.85	4.00	
QPSK-CC-Soft	0.30	0.47	0.18	0.24	0.14	0.18	–	–	Fading
SCC-10th-Iter	0.58	1.57	0.58	1.55	0.58	1.55	–	–	
	10^{-2} PLBR		10^{-2} E2EB		10^{-3} PLBR		10^{-3} E2EB		

a realistic application. For example, observe in Table 6.2 that the longest NL is achieved for an AWGN channel by soft decoded 1/2-rate CC for a PLBR of 10^{-4} in *Scenario 1*, which is nearly 3.97yrs. By contrast, the lowest NL for an AWGN channel is accomplished by uncoded BPSK at a E2EB of 10^{-4} in *Scenario 2*, which is about 0.21yrs. Uncoded BPSK results in an even lower NL in a Rayleigh fading scenario, but the exact PLBR and E2EB values cannot be provided, since this would require an excessive transmit power. The longest NL is achieved for Rayleigh fading channels by 1/2-rate SCC using 10 decoding iterations at a PLBR of 10^{-2} in *Scenario 1*, which corresponds to NL=1.57yrs. Nonetheless, up to 4.99yrs of NL can be achieved by soft decoded 1/2-rate CC for a PLBR of 10^{-3} for AWGN channels in *Scenario 1*, which is reduced to 0.18yrs for Rayleigh fading channels. On the other hand, SPP has a substantial impact on the NL, which reduced the NL of 4.99yrs of *Scenario 1* to 0.89yrs in *Scenario 2*.

In conclusion, we presented the trade-off between NL and BER in order to observe, how the requirement of different target BER values at the physical layer affected both the NL and the network performance in the string topology considered. We also illustrated the dominant impact of the SPP on the NL compared to that of the transmission power. A useful finding was to determine what type of MCSs should be used for what type of networks or applications in order to maximize the NL, while maintaining the target BER requirement. Therefore, with the aid of our experimental results discussed in Section 3.4, the network designer can make beneficial decisions for specific systems, depending on the QoS requirements and on the desired network performance.

6.1.3 Chapter 4

In Chapter **3**, we considered the string topology of Fig. 6.6, where the distances between consecutive nodes were fixed. However, in a more realistic WSN there may be thousands of

routes consisting of various distances between consecutive sensor nodes, each of which can be assigned to a string topology. Moreover, in such a complex network we may also have to reconsider our design of the NL model. In Chapter **4** we maximize the NL of a randomly and uniformly distributed fully-connected WSN, as exemplified in Fig. 6.7, which may lead to an exponentially increased complexity upon increasing the number of nodes (V). In such a network, we considered a single source and destination, where the SN and the DN were located at the opposite corners of the sensor field to guarantee the longest distance between them, so that the system model guarantees the utilization of diverse alternative routes for end-to-end transmission, as portrayed in Fig. 6.7. The information was only generated at the SN and the aim of the system model considered was to carry the SN's information to the DN via relay nodes, which were also capable of decoding and forwarding the relayed information. To mitigate the interference imposed on sensors, we used a TDMA scheduling method, namely the so-called SPTS regime described in Section 4.2.1, which allows each node lying on a route to moderately interfere with another node at the distance of T, if they were scheduled during the same TS. Additionally, each sensor node was equipped with a limited battery capacity and we only considered the transmit power as the main ED factor. Moreover, the worst-case BER, namely E2EB, of the fully connected WSN considered was computed in (4.5) for an uncoded BPSK, 1/2-rate CC hard-decoded and for soft-decoded QPSK MCSs, as described in Section 4.2.2. Therefore, the network designer was capable of observing the NL versus E2EB performance of each MCS considered.

For the system model described in Section 4.2, we proposed the ESA based benchmarker of Section 4.3.2.2 and the SOGA of Section 4.3.2.5 as our solution algorithms to keep the network operational as long as possible via solving the linear optimization problem for each route given by (4.10)–(4.13) in Section 4.3.1. Note that ESA was considered as an upper bound for the optimal NL, where the best possible NL was achieved by checking all the possible solution candidates in the whole solution search space. On the other hand, the SOGA of Section 4.3.2.5 was designed for intelligently searching through the entire solution space using genetic operators. Since the NL was strictly dependent on the battery level of the SN, the NL optimization was described in two stages, as discussed in Section 4.2.3. The first stage was responsible for the computation of RL until the SN fully drains its battery, because the system model was only considered for the end-to-end transmission of the information generated at the SN via the maximum-RL routes. The second stage accumulated the RLs during the iterations of the RL computation, until the SN battery was fully depleted. Thus, the NL computation was constituted by a number of RL computation iterations, where in each iteration the best route was selected amongst the routes having the maximum RL for the corresponding end-to-end transmission. This selection process includes several criteria, which were described in terms of the RSSs relying on the LTED, the LNOH, the LRBAT and the RANR regimes, namely the RSS-LTED, RSS-LNOH, RSS-LRBAT, RSS-RANR. The computation of the NL in such networks is indeed challenging due to the computational

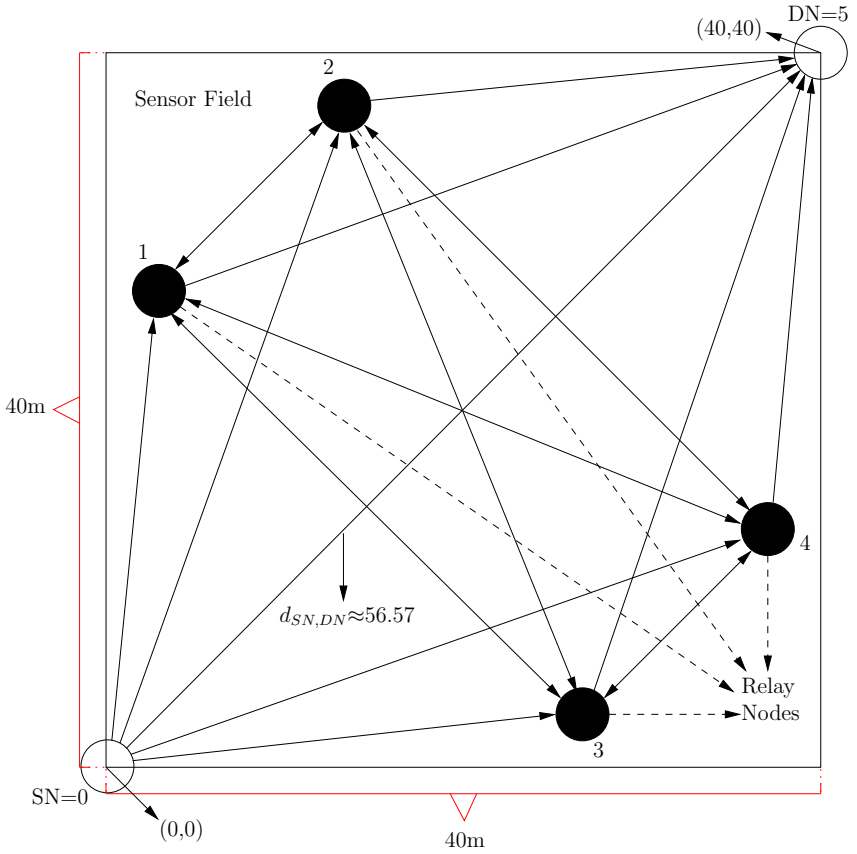

FIGURE 6.7: Example of a fully connected WSN consisting of 6 nodes (not to scale).

V	NL of 2dB	NL gain of 2dB SINR	NL of 10dB	NL gain of 10dB SINR
4	73,499.94	$(4 \rightarrow 5)$ 41,782.21	11,713	$(4 \rightarrow 5)$ 5,758
5	115,282.15	$(5 \rightarrow 6)$ 44,368.49	17,471	$(5 \rightarrow 6)$ 6,020
6	159,650.64	$(6 \rightarrow 7)$ 49,460.48	23,491	$(6 \rightarrow 7)$ 5,596
7	209,111.12	$(7 \rightarrow 8)$ 52,455.78	29,087	$(7 \rightarrow 8)$ 5,737
8	261,566.90	$(8 \rightarrow 9)$ $(9 \rightarrow 10)$ 80,479.45	34,824	$(8 \rightarrow 9)$ $(9 \rightarrow 10)$ 10,174
10	342,046.35	Total: 268,546.41	44,998	Total: 33,285
Average	-	$\frac{268,546.41}{6} = 44,757.74$	-	$\frac{33,285}{6} = 5,547.5$

TABLE 6.3: The NL **[hrs]** and NL gain achieved by the fully-connected WSNs composed of $V = \{4, 5, 6, 7, 8, 10\}$, when the network operates at 2dB and 10dB SINR. The number of hours included in this table has to be divided by $\approx 8,760$ to convert them to **years**.

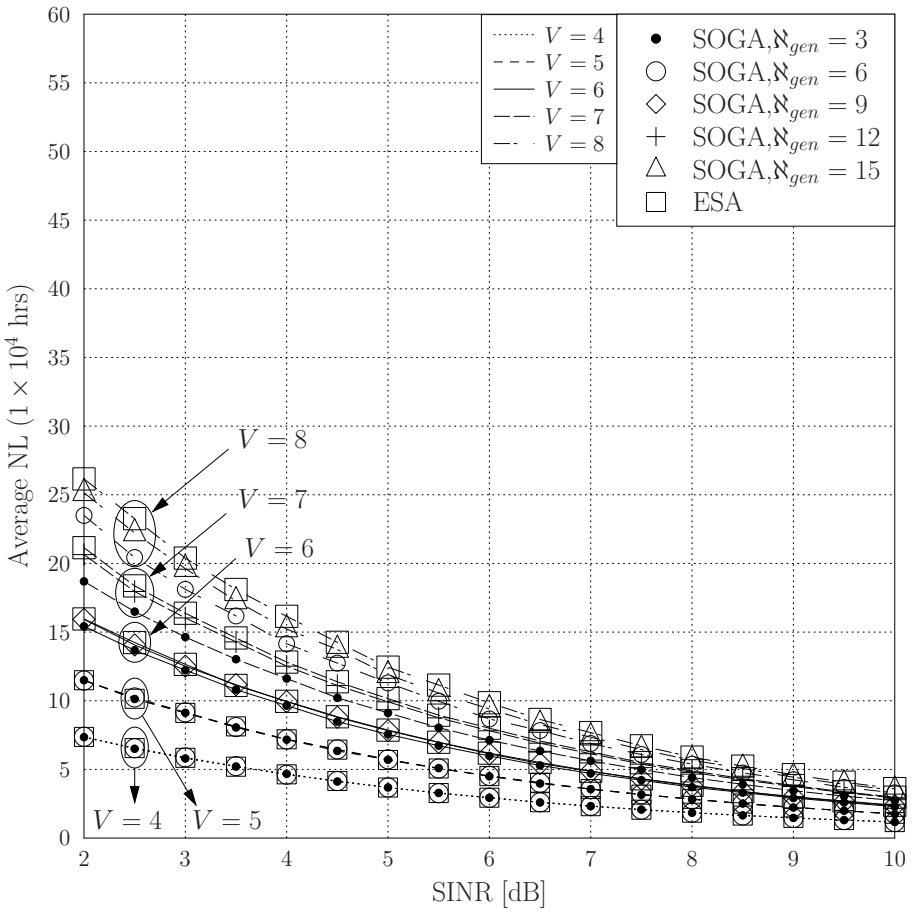

FIGURE 6.8: ESA as an upper bound for the true NL compared to the NL of SOGA for various number of generations $\aleph_{gen}$ and V.

constraints. Specifically, a large number of nodes (V) in a network may lead to numerous alternative routes that have to be evaluated in terms of their RL. Considering the exponential increase of the number of non-looping routes upon increasing the number of nodes, an algorithm imposing a reduced complexity was required for NL maximization. Therefore, the SOGA of Section 4.3.2.5 was introduced to circumvent the shortcomings of the ESA for larger networks. Our experimental results of Fig. 6.8 and Table 6.3 indicate that using the parameter values of Table 4.14, an approximately 45,000hrs of NL gain was achieved at 2dB SINR by inserting an additional sensor node into the existing WSN. This gain was reduced to about 5,500hrs of NL, when the WSN operates at 10dB SINR. We also observed that for $V \leq 7$, the ESA was a better option due to its lower computational complexity. It is clear from Table 6.4 that the cross-over point was at $V = 7$, where the computational complexity of the ESA and SOGA was similar. The ratio of the NL discrepancy between the SOGA and the optimal NL value of ESA was as low as 3.17%, which corresponds to 1.07×10^4hrs of NL. We assumed that the NL converged to its near-optimal NL value, if the NL gap to the upper bound ratio was less than 3.5%. For example, in the $V = 8$ scenario the NL gap ratio from SOGA to the upper bound ESA was 3.02%. Hence, in the $V = 8$ scenario the NL computed by the SOGA was near-optimal, despite its 2.56 times lower complexity compared

to the ESA. Nonetheless, the SOGA outperformed ESA for any WSN having $V > 7$ due to its lower computational complexity. For convenience, Table 6.4 is provided here in order to present the computational complexity in terms of the number of CFEs required by both the ESA and SOGA for different V values and for the RSS-LTED. The convergence of SOGA to a near-optimal NL value was achieved at a much lower complexity.

Furthermore, we observed in our experimental results of Section 4.4 that both RSS-LTED and RSS-LRBAT provided a better NL owing to their energy-awareness compared to other RSSs. This pattern can be followed in Fig. 4.21 and Fig. 4.22. Additionally, RSS-LNOH typically had a better E2EB performance than the other RSSs due to its delay-awareness, which naturally helped the accumulation of less bit errors, because the scheme selected the specific routes having the least hops, as illustrated in Fig. 4.25(a)–4.25(b) and Fig. 4.26(a)–4.26(b). However, since the objective function maximizes the RL, the RSSs exhibited a similar NL performance. More explicitly, one of our findings is that as long as the RL is maximized, any route associated with the maximum RL amongst the routes having the same maximum RL can be selected for end-to-end transmission. On the other hand, the decision concerning the route selection significantly affects the E2EB performance, since the computation of the E2EB strictly relies both on the number of hops and on the MCSs considered. Nonetheless, 1/2-rate CC soft-decoded QPSK MCS outperformed other MCSs in all scenarios of the ESA and SOGA. For example, in the $V = 4$ scenario of ESA, at the same E2EB of 10^{-3} characterized for the 1/2-rate CC soft-decoded QPSK MCS, approximately 4×10^4hrs of NL gain was achieved over uncoded BPSK and nearly 2.4×10^4hrs of NL gain was attained over 1/2-rate CC hard-decoded QPSK MCS. These gains further increased upon increasing the number of nodes. Moreover, WSNs composed of larger number of nodes resulted in higher E2EB. One of the main reasons for this trend was that the selection strategy of the route associated with the worst-case E2EB requires longer hops, which in turn yields a higher E2EB for larger networks. Another reason for this observation was that WSNs composed of larger number of nodes may result in routes having longer hops that achieve the maximum RL, and since the route associated with maximum RL is selected, in the presence of a longer hop this route will also lead to a higher E2EB.

6.1.4 Chapter 5

The lifetime definitions in previous chapters were based on a single objective, such as the energy dissipation of a particular node lying in the route or in the string topology network. However, several other significant characteristics of WSNs have not been considered in the previous chapters. For example, WSNs suffer from a higher end-to-end delay than their single-hop counterparts and since they rely on batteries minimizing their energy requirements is of prime importance. Therefore, in Chapter 5 we aimed for providing the system designer with a trade-off, hinging on the interplay between the energy dissipation

V	ESA-CFE	SOGA-CFE	Optimal ESA-NL [hrs]	Near-optimal SOGA-NL [hrs]
4	9	362	117,682	117,682
5	35	425	181,886	181,385
6	163	839	256,745	253,381
7	892	1,328	338,474	327,753
8	5,765	2,256	419,264	406,622
10	–	3,453	–	551,086

TABLE 6.4: The number of CFEs required for approaching the convergence of the ESA and SOGA for different V values and for the RSS-LTED only.

and the end-to-end delay in order to obtain the set of Pareto-optimal NL aware routes using multi-objective routing optimization algorithms. Prolonging the NL was dependent on the simultaneous Pareto-optimization of the aggregate energy dissipation and of the end-to-end delay of a route in the WSN considered, as described in Section 5.3. Firstly, we introduced multi-objective optimization and its mathematical definition in Section 5.2. Then, we solved the multi-objective routing optimization problem formulated in (5.5) of Section 5.3 with the aid of novel multi-objective optimization algorithms in a fully-connected WSN in order to identify the set of Pareto-optimal NL-aware routes using the NSGA-II and the MODE algorithms described in Section 5.4, which were appropriately adapted to suit our routing problem.

We then demonstrated in Section 5.5 that both MODE and NSGA-II are indeed applicable to the routing problems considered and that they are capable of finding the Pareto-optimal solutions at a significantly lower complexity than an exhaustive search method, as illustrated in Table 6.5, provided that the number of nodes is higher than or equal to 10. We also proposed a novel multi-objective NL definition, which allows the system designer to strike a trade-off between the energy dissipation and the end-to-end delay. Therefore, depending on the specific application and on the target QoS required, the set of NL aware routes lying on the Pareto front is the set of Pareto-optimal solutions, which characterize the interplay between the energy dissipation and the end-to-end delay. Additionally, we demonstrated that, at the same complexity, the MODE algorithm is capable of finding solutions that are closer to the Pareto front, as shown in Fig 5.9 and in general, MODE converges faster than the NSGA-II, as illustrated in Fig 5.10. The Pareto-optimal solutions we found demonstrated that the conflicting multiple objectives may indeed be reconciled in a solution-set, where the dissipation cannot be reduced without increasing the delay and vice versa.

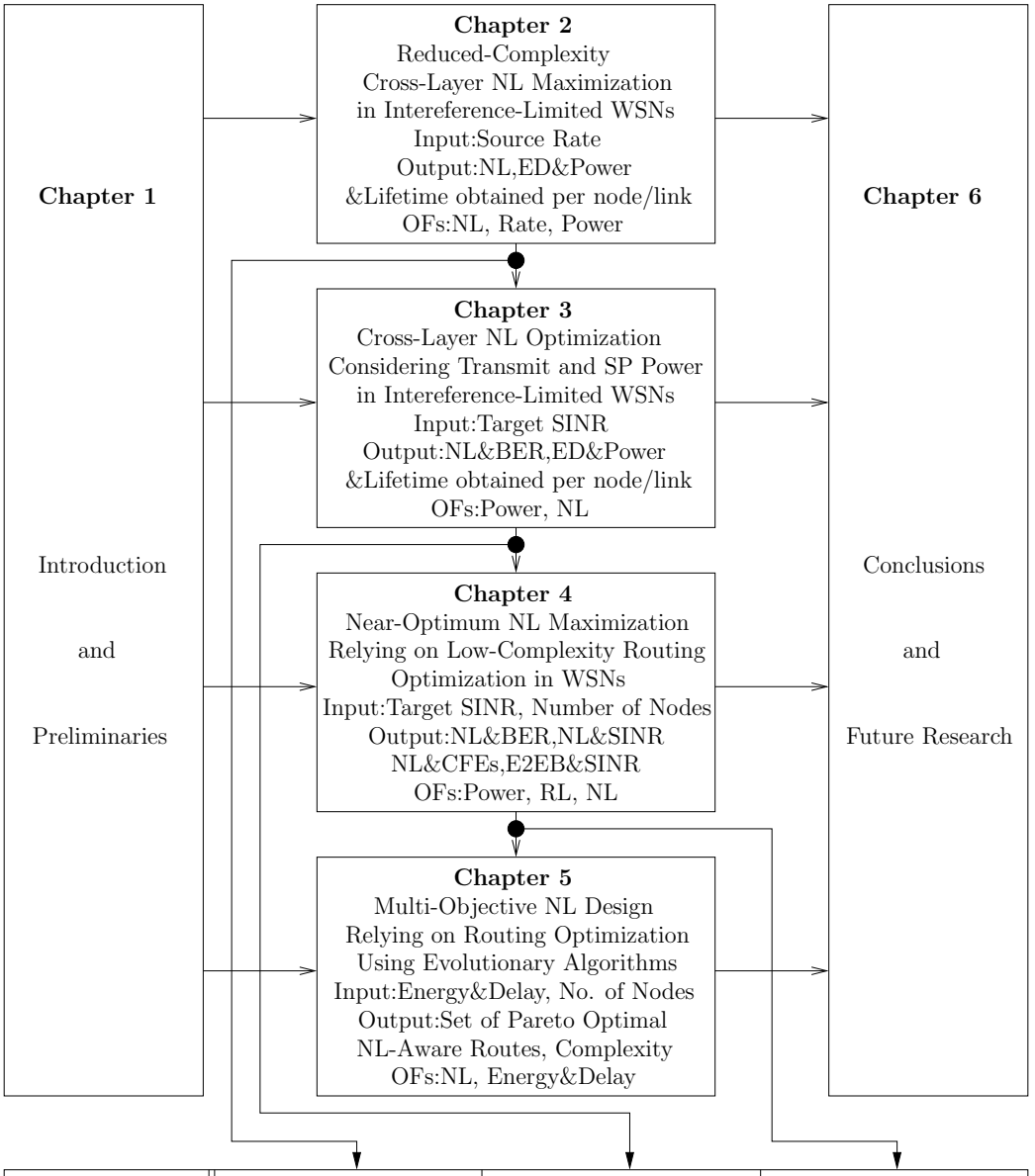

Characteristics	Chapter 2 → Chapter 3	Chapter 3 → Chapter 4	Chapter 4 → Chapter 5
QoS Metrics	Evolved	Unchanged	Evolved
Channel Model	Unchanged	Evolved	Unchanged
Cross-Layer	Unchanged	Evolved	Evolved
Network Topology	Unchanged	Evolved	Unchanged
Objective Model	Unchanged	Unchanged	Evolved
BER Model	Evolved	Unchanged	Evolved
Optim. Variables	Evolved	Evolved	Evolved
NL Model	Unchanged	Evolved	Evolved

FIGURE 6.9: Organization of the thesis, portraying, how the chapters evolve. "Evolved" and "Unchanged" are the terms used for the characteristics of the chapter transitions, which are evolved or remain unaltered. The specific chapter evolutions can be followed in Table 6.6.

Number of nodes, V	NSGA-II	MODE	ESA
6	395	446	65
8	4,557	4,377	1,957
10	1,186	1,112	109,601
12	10,950	10,680	9,864,101

TABLE 6.5: The average number of CFEs required for approaching the Pareto front within 1% averaged over 1000 runs.

6.1.5 Discussions

The characterization of our NL maximization problems is described in Table 6.6, where the evolution of the system model from chapter to chapter can be clearly recognized. Moreover, Fig. 6.9 presents the organization of the thesis, where the evolution and/or the relationship of each chapter is visualized. Explicitly, observe in Table 6.6, whether any of the characteristics of the chapters *evolved* or remained *unchanged*. For example, observe in Fig. 6.9 that the QoS metric is "evolved" during the transition from Chapter 2 to Chapter 3. To understand what has been evolved, the readers are referred to Table 6.6, where in our case the "QoS Metrics" were evolved from "NL, Source Rate" to "NL, SINR, BER". Additionally, one of the distinctive characteristic of our study was the specific choice of QoS requirements.

For example, in Chapter 2 the NL and the source rate were considered as our QoS metrics, since all operations in the network were strictly dependent on the source rate, which determined the transmission rate attained and the power required, which in turn determined the NL. In all of our studies the NL was the most significant QoS metric, since it determined when the operations of the entire network were terminated. For example, the higher the NL, the higher the throughput. Similarly, the higher the NL, the higher the energy efficiency, and so on.

In Chapter 3 and Chapter 4, the NL, the SINR and the BER were considered as the QoS metrics, since the SINR determined the transmit power required, while the transmission quality was constrained by the NL. Then, the system designer was provided with a trade-off between the NL and the BER in order to make an informed decision considering the specific application that may be supported and its QoS.

In Chapter 5, the aggregate energy dissipation per route and end-to-end delay were concurrently optimized as part of a multi-objective optimization problem, where the NL was considered as the QoS requirement based on the Pareto-optimal solutions of the energy-delay trade-off. The rest of the characteristics considered in our studies is provided in Table 6.6.

Nevertheless, here we provide a comparative justification of our various system models in

Characteristics	Chapter 2	Chapter 3	Chapter 4	Chapter 5
QoS Metrics	NL, Source Rate	NL, SINR, BER	NL, SINR, BER	(NL), Energy, Delay
Channel Model	AWGN, Block Fading	AWGN, Block Fading	AWGN	AWGN
Cross-layer Model	Phy, MAC, (Routing)	Phy, MAC	Phy, MAC, Routing	Phy, Routing
Network Topology	String Topology	String Topology	Fully-connected WSN	Fully-connected WSN
Objective Model	Single-objective	Single-objective	Single-objective	Multi-objective
BER Model	Fixed-BER	NL vs BER using MCSs	NL vs BER using MCSs	Error-free
Optimization Variables	NL, Rate, Power	NL, Power	NL, RL, Power	(NL), Energy, Delay
NL Model	Min. Node Lifetime	Min. Node Lifetime	SN Battery Level	Pareto Optimal Energy&Delay

TABLE 6.6: Characteristics of the system models considered.

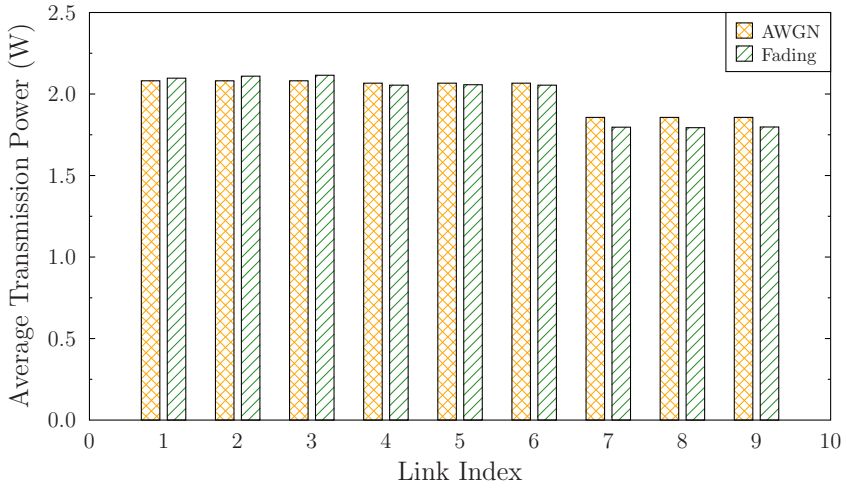

FIGURE 6.10: Average transmit power required for each of the consecutive link indices of Fig. 6.1 using the corresponding parameters of Table 6.8, where the SINR is much lower in this particular system model than that of Chapter 3 and Chapter 4. Note that Table 6.8 indicates the difference of *noise power* between the system models considered.

order to augment, how the NL differs from one scenario to another, depending on the communication parameters and to explicitly identify, which parameters affect the NL most significantly. First of all, observe in Table 6.8 that Chapter 2 does not rely on any *Standard*, where the parameter values are carefully arranged to ensure that the NL optimization framework can produce physically tangible solutions. We would like to emphasize that the study of Chapter 2 provides a simple initial study of NL maximization, where we do not rely on any specific *Standard*. Most importantly, Chapter 2 considers an adaptive model, hence we cannot chose a specific SINR value to directly compare the NL to that of Chapter 3 and Chapter 4. Therefore, the NL value obtained in Chapter 2 cannot be directly compared to that of the other chapters. Broadly speaking, under the same channel conditions, the same transmit rate and the same T SPTS parameter, as portrayed in Table 6.8, the maximum achievable NL in Chapter 2 is around 0.3 hours, while that in Chapter 3 is $43,829$ hours and that in Chapter 4 is $235,526$ hours. Then, the question arises, why the NL of Chapter 2 is enormously different from those in Chapter 3 and Chapter 4? To answer this question, again we have to bear in mind that the parameter values for our initial study of Chapter 2 are arranged so that feasible solutions of the optimization problem can be obtained. In a nutshell, despite the fact that the distance between the consecutive nodes is much smaller and the power amplifier efficiency is considerably higher in Chapter 2, as illustrated in Table 6.8, the noise power is high in Chapter 2 compared to that of Chapter 3 and Chapter 4. For this particular reason, in Chapter 2 the SINR ratio is much lower than in Chapter 3 and Chapter 4. Therefore, we can assume that Chapter 2 is a more noise-contaminated system than the system considered in Chapter 3 and Chapter 4. This is why the effects of the interference are masked by the noise-effects in Chapter 2, which is in contrast to Chapter 3 and Chapter 4.

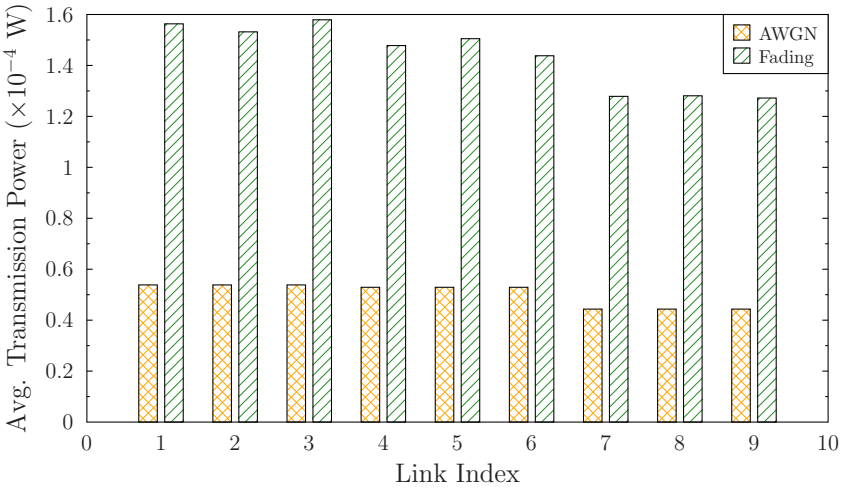

FIGURE 6.11: Average transmit power required for each of the consecutive link indices of Fig. 6.6 using the corresponding parameters of Table 6.8, where the SINR is much higher in this particular system model than that of Chapter 2. Note that Table 6.8 indicates the difference of *noise power* between the system models considered.

Furthermore, we can justify our experimental results in terms of the effects of the specific scheduling scheme characteristics and interference power. Firstly, we recall that in Chapter 2 the distances between the consecutive nodes were set to $d = 1$. Therefore, the power gain G in fact has no effect on the system model, if the distance is fixed to 1. However, the interference imposed by other nodes emerges from various longer distances, which results in a trade-off between the received power and the interference power imposed on the sensor nodes. Here, we investigate the trends observed for the first 6 sensors, which require the highest transmit power, as illustrated in Fig. 6.10. Therefore, we have to study the amount of interference imposed on each sensor node. Hence, we have to identify the potential interferers for each receiving node, as indicated by the arrows in Fig. 6.12, which represents the system model we considered. This portrays the concurrent communications of the nodes and their associated *fixed* distances from their potential interferers encountered in this stationary string topology, as portrayed in Table 6.7. For example, an ongoing communication session over $l_{1,2}$ has a 2 m of distance from its interferer $l_{4,5}$ and a 5 m of distance from its other interferer $l_{7,8}$. Observe in Table 6.7 that the sum of the potential interference powers is nearly the same for the links $l_{1,2}$ and $l_{4,5}$, while the interference power imposed on the eighth node is substantially lower than the other two links. Therefore, in order to satisfy the rate constraint, the transmit power has to be increased for the links $l_{1,2}$ and $l_{4,5}$, where the resultant power versus rate equilibrium corresponds to the true transmit powers, depending on this fixed topology as well as distances. For example, this pattern can be observed for the second, fifth and eighth nodes of Figs. 6.10 and 6.11. Broadly speaking, our optimization problem considered in Chapter 2 requires the scheduled links to satisfy the rate constraints, therefore each of these scheduled links will compete for increasing its transmit power as much as it is necessary. However, the energy dissipation has to be minimized for the sake

Receiving link	(Distance from interferer [m], interferer)
$l_{1,2}$	(2, $l_{4,5}$), (5, $l_{7,8}$)
$l_{4,5}$	(4, $l_{1,2}$), (2, $l_{7,8}$)
$l_{7,8}$	(7, $l_{1,2}$), (4, $l_{4,5}$)

TABLE 6.7: Interference power imposed on receiving nodes relaying on the distances of the potential interferers.

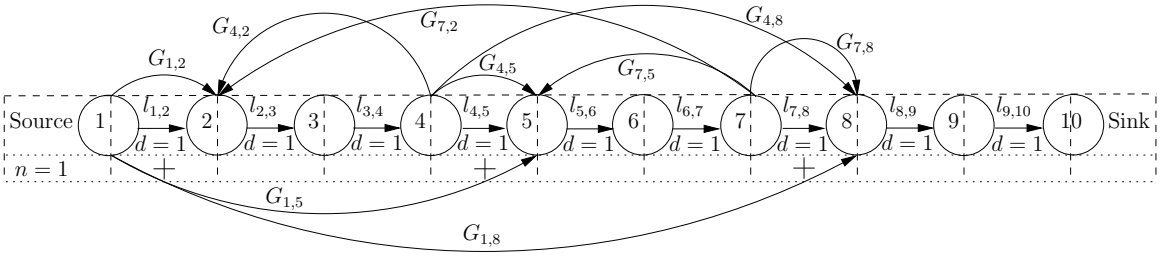

FIGURE 6.12: The illustration presenting the effect of the fixed scheduling scheme and the interference power imposed on sensor nodes. Note that we only exemplify the experimental result for particular SPTS of $T = 3$, as illustrated in $n = 1$ TS and shown with "+" symbol, if activated.

of maximizing the NL, which is the objective function of the optimization problem. Again, both the topology and the potential interferers are fixed at certain locations, and given the source rate we aim for optimizing the transmit rates as well as the powers, which in turn maximizes the NL for a fixed link scheduling. Therefore, depending on the fixed distances and given the path loss, the corresponding power as well as rate variables will be optimized and a beneficial equilibrium will be found for the sake of NL maximization.

To elaborate a little further, the NL difference between Chapter 3 and Chapter 4 is mainly due to the specific NL definition that typically relies on the particular application and on the network topology employed. For example, Chapter 3 considers the NL as the time, when the first node failure is encountered in a string topology, as illustrated in Fig. 6.6, while the NL described in Chapter 4 strictly depends on the SN's battery life. The main reason for the NL being so high in Chapter 4 is mainly because the network exploits alternative routes for the transmission of the source information by aiming to actively rely on the nodes associated with fresh batteries or to route the information over the particular nodes having the highest residual batteries. Hence, the NL becomes high, since the source information is delivered to the sink node by the routes having the best route lifetime after each end-to-end transmission, until the SN completely depletes its battery charge.

In conclusion, in Chapter 2 we commence by building our NL maximization problem as an initial study for this treatise based on a string topology. To solve this optimization problem in a feasible way, the parameters of Chapter 2, as illustrated in Table 6.8, have

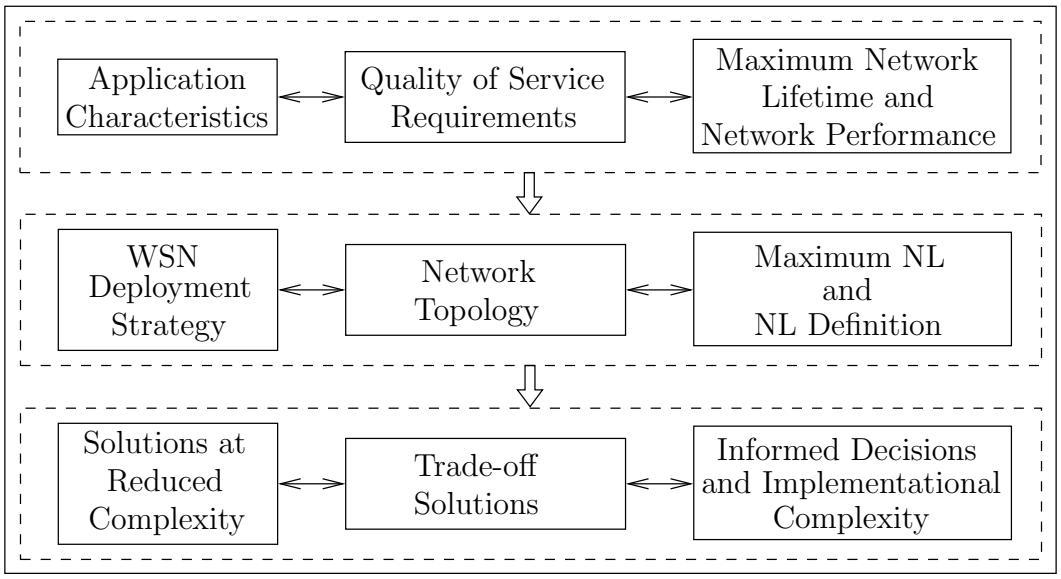

FIGURE 6.13: Design guidelines of energy-constrained WSNs in the interest of maximizing the NL.

to be specifically arranged. Hence, this particular system model does not rely on any *Standards*. As a further advance, in Chapter 3 we extend our NL maximization problem to a realistic scenario, where the communication parameters are specifically selected from the data sheet of a *National Instruments* device, namely from that of the *wireless sensor network programmable analog input measurement nodes* [173], which is based on the *IEEE 802.15.4 Standard*. Note that apart from the transmit power, in Chapter 3 we also consider the impact of the signal processing power on the NL as a further practical improvement. Furthermore, Chapter 4 also relies on the *IEEE 802.15.4 Standard* for the sake of constructing a practical scenario, where the string topology considered in Chapter 2 and Chapter 3 is also evolved to a more complex network, namely the so-called fully connected network. The latter is considered in various scenarios having different number of nodes. Finally, Chapter 5 focuses on a design relying on a multiobjective NL definition, considering the trade-off between the end-to-end delay and energy dissipation. The decision on the selection of a route that provides the best NL is made by the system designer. Therefore, our conclusions in Table 6.8 we do not include emerging from Chapter 5 for the numerical analysis and discussion, since it is mostly based on the design of a NL definition considering multiple conflicting objectives.

6.2 Design Guidelines

We elaborated on the design objectives of WSNs in Section 1.1. Let us now bear in mind the contributions we made towards NL maximization and infer design guidelines for constructing applications of maximum-lifetime WSNs, as portrayed in Fig. 6.13.

Parameters	Chapter 2	Chapter 3	Chapter 4
Channel model	AWGN, Fading	AWGN, Fading	AWGN
Path-loss exponent	4	3	3
Distance between consecutive nodes, d [m]	1	30	$0 < d \lessapprox 56.57$
Noise power, N_0 [dBm]	1	-60	-60
Initial battery charge per node, $\mathcal{E}_i$ [Joule]	5000	5000	5000
Maximum transmit power of a node, $(P_i)_{max}$	50W	10 mW	10 mW
Efficiency of the power amplifier, α	0.99	0.6	0.6
SPTS parameter, T	$\{3, 4, 5, 6, 7, 8, 9\}$	3	3
NL definition based on	First node's failure	First node's failure	SN's failure
Number of slots per link frame, N	18	3	3
Network Topology	String ($V = 10$)	String ($V = 10$)	Complex ($V = \{4, 5, 6, 7, 8, 10, 15, 20\}$)
IEEE Standards	No *Standards*	802.15.4	802.15.4
NL values [AWGN, $T = 3$, 1 (bit/s/Hz)]	Max. 0.3 hours	$43,829$ hours [3.5dB]	$235,526$ hours [3.5dB]

TABLE 6.8: Comparative justification of our system models considering the specific communication parameters in the interest of maximizing the NL.

1. Observe in Fig. 6.13 that determining the characteristics of the application considered and its QoS requirements as well as the network's design objectives play a vital role in terms of maximizing the performance of the WSN. For example, video surveillance applications require higher data rate for maintaining the desired QoE of the user(s). On the other hand, these applications may necessitate a higher transmit power, where the NL may be significantly degraded, since the sensors may be exposed to an increased interference. For such an application, the system designer has to define the lower bounds of the QoS requirements for attaining a longer operational time for the WSN considered. Nonetheless, different design objectives tend to require different strategies for NL maximization. For example, maximizing the NL, while maintaining coverage quality and network connectivity requires different considerations than NL maximization, while maintaining an optimal sleep scheduling scheme and opportunistic routing strategy.
2. Once the application requirements have been determined, the WSN deployment strategy has to be specified, which ultimately determines the network topology that is vitally

important for NL maximization. Explicitly, for example a network having a string topology, where only the adjacent nodes are within each others transmission range, the NL is strictly dependent on that particular node's lifetime, which completely depletes its battery. However, in a network having numerous alternative routes, the NL may be dependent only on the source node's lifetime, since the sensor measurements can be delivered over numerous alternative routes. Therefore, the NL can be defined depending on the application and its network topology deployed.

3. Having described the application characteristics and its QoS requirements along with the NL definition that relies on the network topology constructed, for the sake of NL maximization, finding optimal solutions at a reduced complexity and/or providing trade-off solutions between several important objective functions is vitally important for attaining the optimal communication parameter values at a reduced implementational complexity or for providing the system designer with a well-informed decision for the ensuing hardware implementations using the interplay between several conflicting objectives, while guaranteeing the desired QoS requirements.

6.3 Future Research Ideas

In this section we present a range of future research ideas and discuss several open problems in the context of the NL maximization of WSNs.

6.3.1 Energy Harvesting

Energy harvesting [262–266] is a relatively new concept in wireless sensor networks, where a sensor has the capability to convert various forms of environmental energy into electricity in order to supply the sensor node. Power allocation strategies using energy harvesting sensors can be considered [267–271] in order to extend the NL. Assuming that each sensor has a limited battery capacity, using an external energy source from nature can help in prolonging the NL. However, considering the relatively low efficiency of energy harvesters [262], NL maximization and power allocation mechanisms still play a significant role in keeping the network functional for an extended duration. This contribution of energy harvesters in extending the NL can be formulated as part of the optimization problem, as demonstrated in [145, 272].

6.3.2 Energy Conservation Through Network Coding

In relaying or multi-hop networks, where a receiver is out of the communication range of a transmitter, a signal is forwarded by relaying over many other nodes in order to be delivered to the final destination. In such networks, we forward the signal through intermediate

nodes. However, amplifying or decoding and remodulating the signals before forwarding them is capable of improving the throughput and the energy saving, as discussed in [273–275] or in terms of network coding in [161, 163, 276–279]. However, to exploit network coding several users' signals have to be jointly encoded and diverse network topologies have to be considered. Assuming that the transmission range of all nodes is the same, minimizing the energy consumption is a problem that is equivalent to minimizing the number of transmissions. Thus, we can incorporate this into WSNs by forwarding a signal all the way through to the sink via broadcasting to the neighbor nodes with the aid of relaying. Therefore, we have to introduce the specific number of transmissions into our optimization problem formulation along with network coding in order to guarantee a successful delivery of a certain amount of data to the final destination. This approach can assist us in minimizing the number of transmissions, thus conserving more energy, which translates into extending the NL.

6.3.3 Optimal Scheduling and Signomial Programming Approach

For simplicity, in this treatise we considered a fixed link scheduling approach and thus implemented the SPTS scheduling scheme of Fig. 6.2 for various T values. Even though, we selected one of the best values of T based on the results of [30], an optimal scheduling algorithm is capable of further improving the NL. Additionally, in order to maximize the NL, while optimizing the transmit rate and the power, an SINR-approximation has to be employed by removing the term "1" in

$$r_{l_{i,j},n} \leq \log\left(1 + \frac{G_{i,j}P_{l_{i,j},n}}{\sum_{i' \neq i, l_{i',j'} \in \mathcal{L}_n} G_{i',j}P_{l_{i',j'},n} + N_0}\right), \tag{6.1}$$

as discussed in Section 2.6. However, this approximation must not be invoked in optimal scheduling problems, since the power is not constrained to zero, implying that a node does not have the option of refraining from transmitting if scheduled. For convenience, we provide the relaxed non-convex rate constraint here, which is converted from (6.1) into

$$r_{l_{i,j},n} \leq \log\left(\frac{G_{i,j}P_{l_{i,j},n}}{\sum_{i' \neq i, l_{i',j'} \in \mathcal{L}_n} G_{i',j}P_{l_{i',j'},n} + N_0}\right), \tag{6.2}$$

by employing an approximation of the SINR. This approximation may not cause any problems for high SINR values. However, it has to be reconsidered for the links that are operating at low SINRs. To circumvent this limitation, we may consider using the SP approach of [89, 117] in order to solve optimal scheduling problems. A SP-based power control approach has to be invoked for mediocre SINR, as described in [117], but the approximation invoked for high SINRs is still applicable and requires only a single GP to be solved [129]. However, for the medium to low SINRs, the approximation is not feasible and one has to

solve this non-convex problem as a series of GPs, which are transformed to convex problems. Therefore, invoking a SP-based power control approach is capable of finding the optimal scheduling, so that the NL can be further extended.

6.3.4 Mobility Models

In this treatise, we only considered stationary WSNs. However, it would be interesting to investigate the impact of different mobility models on the NL. We may expect that the NL will be significantly reduced due to the poor link connectivity anticipated. We can utilize the mobility models described in [280] in order to study how the model affects both the convergence of the algorithms as well as the NL. For example, Wang *et al.* [44] demonstrated that the NL may potentially be doubled with the aid of a single mobile relay in WSNs. Therefore, we may consider a network supported by a few mobile sensor nodes that have a high battery charge. The role of the mobile nodes is to assist the nodes that might become a potential bottleneck, since their battery will be depleted much quicker. Therefore, using mobile relay nodes can be exploited for balancing the energy dissipation of the nodes located at the bottleneck, thus this method can help in extending the NL of multi-hop WSNs.

6.3.5 Other Possible Future Research Ideas

Some other possible future research ideas are included in this section.

- Robust Optimization
  Some parameters of the problem formulations are assumed to be constant, whereas in practice these parameters are based on inaccurate estimates with uncertain boundaries. Therefore, we may utilize robust optimization for mitigating the effects of unavoidable errors, such as channel estimation and power control errors [281, 282].
- High Data Rate Applications
  So far, we only considered low data rate applications. However, we may consider wireless video sensor networks (WVSN) [279, 283, 284], which require a high date rate, as in video surveillance networks. In such networks, due to the nature of video transmission, a higher battery capacity per sensor node has to be used. Additionally, we can present the impact of the video encoding power dissipation along with the transmission power on the NL.

6.3.6 Final Remarks

Wireless sensor networks are becoming an essential part of the emerging IoT industry. Therefore, WSNs will continue to be used in many applications ranging from military deployments, industrial deployments, health care to designing intelligent environments, smart

homes and cities, etc. On the other hand, these applications, specifically the applications requiring high data rates, may lead to a high energy consumption. Additionally, energy has always been an issue in the history of battery-operated devices and sensor networks. However, this limitation may potentially be circumvented by energy harvesting devices. At the time of writing, a company called *IDEAL* offers 25+ years of sensor lifetime on battery and no-battery is required at all in their wirelessly powered system. Moreover, researchers from the University of Washington have created a new wireless communication system [285] that maintains interaction between two devices without relying on batteries or mains energy source. However, these devices still have to be improved in terms of their efficiency and cost. The next few decades we will bring about further developments of new communication techniques and energy harvesting devices in order to maximize the energy efficiency and thus to extend the attainable NL. Even though WSNs and the IoT do not have to rely on batteries, energy-efficiency will always be a challenge to be tackled in the future. Therefore, cross-layer optimization, energy-efficient communication techniques, distributed algorithms designed for providing the best available QoS or quality of experience, will have to be intensively studied in the context of these novel devices and communication techniques, which can be utilized by the emerging IoT technology.

Glossary

AF	amplify-and-forward.
AWGN	additive white Gaussian noise.
BER	bit error rate.
BPSK	binary phase-shift keying.
BTS	binary tournament selection.
CC	convolutional code.
CFE	cost function evaluation.
CRN	cognitive radio network.
CSI	channel state information.
DARPA	defense advanced research projects agency.
DCCP	dynamic coverage and connectivity problem.
DCM	distance conversion matrix.
DCMC	discrete-input continuous-output memoryless channel.
DE	differential evolution.
DF	decode-and-forward.
DN	destination node.
DoS	denial of service.
DRN	disaster response network.
DSN	distributed sensor network.
E2EB	end-to-end BER.
EA	evolutionary algorithm.
ED	energy dissipation.
EH	energy harvesting.
EH-WSN	energy harvesting wireless sensor network.
ESA	exhaustive search algorithm.

ETX	expected transmission count.
FF	fitness function.
FH	optimization function handles.
FRMOO	fuzzy-random multi-objective optimization.
GA	genetic algorithm.
GAQR	GA-aided QoS-based routing.
GP	geometric programming.
GPS	global positioning system.
IoT	Internet of things.
IP	Internet protocol.
KKT	Karush-Kuhn-Tucker.
LNOH	least number of hops.
LOS	line-of-sight.
LRBAT	largest remaining SN battery.
LTE	Long Term Evolution.
LTED	least total energy dissipation.
LUT	look-up table.
M-PSK	M-ary phase shift keying.
M2M	machine-to-machine.
MAC	medium access control.
MANET	mobile ad-hoc networks.
MCS	modulation and coding scheme.
MGoDA-LoA	multi-objective global on-demand algorithm with a local on-line algorithm.
MO	multi-objective optimization.
MO-TPSMA	multi-objective territorial predator scent marking algorithm.
MOACO	multi-objective ant colony optimization.
MODA	multi-objective node-deployment optimization algorithm.
MODE	multi-objective differential evolution.
MOEA	multi-objective evolutionary algorithm.
MOEA-D/GSH	multi-objective evolutionary algorithm based on decomposition hybridized with a problem-specific generalized subproblem-dependent heuristic.
MOGA	multi-objective genetic algorithm.
MQRA-NSGA	multi-cast QoS routing algorithm based on the non-dominated sorting based genetic algorithm.

NBI	normal boundary intersection.
NDQO	on-dominated quantum optimization algorithm.
NL	network lifetime.
NLOS	non-line-of-sight.
NSGA	non-dominated sorting based genetic algorithm.
NSGA-II	non-dominated sorting based genetic algorithm-II.
OF	objective function.
OOK	on-off keying.
OSI	open systems interconnection.
PLBR	per-link BER requirement.
PPM	pulse position modulation.
QAM	quadrature amplitude modulation.
QoE	quality of experience.
QoS	quality-of-service.
QPSK	quadrature phase-shift keying.
RANR	random route selection.
RBAT	remaining battery.
REI	residual energy information.
RFID	radio-frequency identification.
RL	route lifetime.
RN	relay node.
RSS	route selection scheme.
SCC	serially concatenated convolutional encoding.
SER	symbol error rate.
SINR	signal-to-interference-plus-noise ratio.
SN	source node.
SNR	signal-to-noise ratio.
SO-TPSMA	single-objective territorial predator scent marking algorithm.
SOGA	single-objective genetic algorithm.
SP	signomial programming.
SPEA	strength Pareto evolutionary algorithm.
SPEA-II	strength Pareto evolutionary algorithm-II.
SPP	signal processing power.
SPTS	spatially periodic time sharing.

TDMA	time-division multiple access.
TS	time slot.
VoIP	voice over IP.
WMN	wireless mesh network.
WSN	wireless sensor network.
WVSN	wireless video sensor networks.

List of Figures

List of Tables

Bibliography

[1] C.-Y. Chong and S. Kumar, "Sensor networks: Evolution, opportunities and challenges," *Proceedings of the IEEE*, vol. 91, no. 8, pp. 1247–1256, August 2003.

[2] I. Akyildiz, W. Su, Y. Sankarasubramaniam, and E. Cayirci, "A survey on sensor networks," *IEEE Communications Magazine*, vol. 40, no. 8, pp. 102–114, August 2002.

[3] ——, "Wireless sensor networks: A survey," *Computer Networks*, vol. 38, no. 4, pp. 393–422, March 2002.

[4] K. Ashton. (2009, June) That 'internet of things' thing: In the real world, things matter more than ideas. Available from: http://www.rfidjournal.com/articles/view?4986.

[5] L. Atzori, A. Iera, and G. Morabito, "The internet of things: A survey," *Computer Networks*, vol. 54, no. 15, pp. 2787–2805, October 2010.

[6] L. Mainetti, L. Patrono, and A. Vilei, "Evolution of wireless sensor networks towards the internet of things: A survey," in *19th International Conference on Software, Telecommunications and Computer Networks (SoftCOM'11)*, Split, Croatia, September 2011.

[7] A. Sehgal, V. Perelman, S. Kuryla, and J. Schonwalder, "Management of resource constrained devices in the Internet of things," *IEEE Communications Magazine*, vol. 50, no. 12, pp. 144–149, December 2012.

[8] S. Tozlu, M. Senel, W. Mao, and A. Keshavarzian, "Wi-Fi enabled sensors for internet of things: A practical approach," *IEEE Communications Magazine*, vol. 50, no. 6, pp. 134–143, June 2012.

[9] D. Christin, A. Reinhardt, P. S. Mogre, and R. Steinmetz, "Wireless sensor networks and the internet of things: Selected challenges," *Proceedings of the 8th GI/ITG KuVS Fachgesprach Drahtlose Sensornetze*, pp. 31–34, 2009.

[10] C. Alcaraz, P. Najera, J. Lopez, and R. Roman, "Wireless sensor networks and the internet of things: Do we need a complete integration?" in *1st International Workshop on the Security of the Internet of Things (SecIoT'10)*, Tokyo, Japan, December 2010.

[11] A. Whitmore, A. Agarwal, and L. Da Xu, "The Internet of things – A survey of topics and trends," *Information Systems Frontiers*, vol. 17, no. 2, pp. 261–274, April 2015.

[12] J. Granjal, E. Monteiro, and J. Sa Silva, "Security for the internet of things: A survey of existing protocols and open research issues," *IEEE Communications Surveys and Tutorials*, vol. 17, no. 3, pp. 1294–1312, August 2015.

[13] K. Romer and F. Mattern, "The design space of wireless sensor networks," *IEEE Wireless Communications*, vol. 11, no. 6, pp. 54–61, December 2004.

[14] D. Puccinelli and M. Haenggi, "Wireless sensor networks: Applications and challenges of ubiquitous sensing," *IEEE Circuits and Systems Magazine*, vol. 5, no. 3, pp. 19–31, September 2005.

[15] V. Gungor and G. Hancke, "Industrial wireless sensor networks: Challenges, design principles, and technical approaches," *IEEE Transactions on Industrial Electronics*, vol. 56, no. 10, pp. 4258–4265, October 2009.

[16] L. Borges, F. Velez, and A. Lebres, "Survey on the characterization and classification of wireless sensor network applications," *IEEE Communications Surveys and Tutorials*, vol. 16, no. 4, pp. 1860–1890, November 2014.

[17] T. Igoe, *Making things talk: Practical methods for connecting physical objects.* O'reilly, 2007.

[18] Y. Chen and Q. Zhao, "An integrated approach to energy-aware medium access for wireless sensor networks," *IEEE Transactions on Signal Processing*, vol. 55, no. 7, pp. 3429–3444, July 2007.

[19] K. Cohen and A. Leshem, "A time-varying opportunistic approach to lifetime maximization of wireless sensor networks," *IEEE Transactions on Signal Processing*, vol. 58, no. 10, pp. 5307–5319, October 2010.

[20] W. Xu, Q. Shi, X. Wei, Z. Ma, X. Zhu, and Y. Wang, "Distributed optimal rate-reliability-lifetime tradeoff in time-varying wireless sensor networks," *IEEE Transactions on Wireless Communications*, vol. 13, no. 9, pp. 4836–4847, September 2014.

[21] K. Phan, R. Fan, H. Jiang, S. Vorobyov, and C. Tellambura, "Network lifetime maximization with node admission in wireless multimedia sensor networks," *IEEE Transactions on Vehicular Technology*, vol. 58, no. 7, pp. 3640–3646, September 2009.

[22] A. Liu, X. Jin, G. Cui, and Z. Chen, "Deployment guidelines for achieving maximum lifetime and avoiding energy holes in sensor network," *Information Sciences*, vol. 230, pp. 197–226, May 2013.

[23] Q. Wang, K. Xu, G. Takahara, and H. Hassanein, "Device placement for heterogeneous wireless sensor networks: Minimum cost with lifetime constraints," *IEEE Transactions on Wireless Communications*, vol. 6, no. 7, pp. 2444–2453, July 2007.

[24] J.-W. Lin and Y.-T. Chen, "Improving the coverage of randomized scheduling in wireless sensor networks," *IEEE Transactions on Wireless Communications*, vol. 7, no. 12, pp. 4807–4812, December 2008.

[25] L. Hanzo, M. El-Hajjar, and O. Alamri, "Near-capacity wireless transceivers and cooperative communications in the MIMO era: Evolution of standards, waveform design, and future perspectives," *Proceedings of the IEEE*, vol. 99, no. 8, pp. 1343–1385, August 2011.

[26] R. Madan and S. Lall, "Distributed algorithms for maximum lifetime routing in wireless sensor networks," *IEEE Transactions on Wireless Communications*, vol. 5, no. 8, pp. 2185–2193, August 2006.

[27] M. Cheng, X. Gong, and L. Cai, "Joint routing and link rate allocation under bandwidth and energy constraints in sensor networks," *IEEE Transactions on Wireless Communications*, vol. 8, no. 7, pp. 3770–3779, July 2009.

[28] H. Wang, N. Agoulmine, M. Ma, and Y. Jin, "Network lifetime optimization in wireless sensor networks," *IEEE Journal on Selected Areas in Communications*, vol. 28, no. 7, pp. 1127–1137, September 2010.

[29] A. Aziz, Y. Sekercioglu, P. Fitzpatrick, and M. Ivanovich, "A survey on distributed topology control techniques for extending the lifetime of battery powered wireless sensor networks," *IEEE Communications Surveys and Tutorials*, vol. 15, no. 1, pp. 121–144, February 2013.

[30] R. Madan, S. Cui, S. Lall, and A. Goldsmith, "Cross-layer design for lifetime maximization in interference-limited wireless sensor networks," *IEEE Transactions on Wireless Communications*, vol. 5, no. 11, pp. 3142–3152, November 2006.

[31] H. Yetgin, K. T. K. Cheung, M. El-Hajjar, and L. Hanzo, "Cross-layer network lifetime maximization in interference-limited WSNs," *IEEE Transactions on Vehicular Technology*, vol. 64, no. 8, pp. 3795–3803, August 2015.

[32] Q. Zhao and M. Gurusamy, "Lifetime maximization for connected target coverage in wireless sensor networks," *IEEE/ACM Transactions on Networking*, vol. 16, no. 6, pp. 1378–1391, December 2008.

[33] H. Kwon, T. H. Kim, S. Choi, and B. G. Lee, "Lifetime maximization under reliability constraint via cross-layer strategy in wireless sensor networks," in *IEEE Wireless Communications and Networking Conference (WCNC'05)*, vol. 3, New Orleans, LA, March 2005, pp. 1891–1896.

[34] ——, "Cross-layer lifetime maximization under reliability and stability constraints in wireless sensor networks," in *IEEE International Conference on Communications (ICC'05)*, vol. 5, Seoul, Korea, May 2005, pp. 3285–3289.

[35] ——, "A cross-layer strategy for energy-efficient reliable delivery in wireless sensor networks," *IEEE Transactions on Wireless Communications*, vol. 5, no. 12, pp. 3689–3699, December 2006.

[36] M. Di Francesco, G. Anastasi, M. Conti, S. Das, and V. Neri, "Reliability and energy-efficiency in IEEE 802.15.4/ZigBee sensor networks: An adaptive and cross-layer approach," *IEEE Journal on Selected Areas in Communications*, vol. 29, no. 8, pp. 1508–1524, September 2011.

[37] S. Raghuwanshi and A. Mishra, "A self-adaptive clustering based algorithm for increased energy-efficiency and scalability in wireless sensor networks," in *IEEE 58th Vehicular Technology Conference (VTC'03-Fall)*, Orlando, Florida, USA, October 2003.

[38] N. Patwari, J. Ash, S. Kyperountas, A. Hero, R. Moses, and N. Correal, "Locating the nodes: Cooperative localization in wireless sensor networks," *IEEE Signal Processing Magazine*, vol. 22, no. 4, pp. 54–69, July 2005.

[39] H. Yetgin, K. T. K. Cheung, M. El-Hajjar, and L. Hanzo, "Cross-layer network lifetime optimisation considering transmit and signal processing power in wireless sensor networks," *IET Wireless Sensor Systems*, vol. 4, no. 4, pp. 176–182, December 2014.

[40] S. He, J. Chen, X. Li, X. Shen, and Y. Sun, "Leveraging prediction to improve the coverage of wireless sensor networks," *IEEE Transactions on Parallel and Distributed Systems*, vol. 23, no. 4, pp. 701–712, April 2012.

[41] D. Wang, E. Liu, Z. Zhang, R. Wang, S. Zhao, X. Huang, and F. Liu, "A flow-weighted scale-free topology for wireless sensor networks," *IEEE Communications Letters*, vol. 19, no. 2, pp. 235–238, February 2015.

[42] K. Phan, H. Jiang, C. Tellambura, S. Vorobyov, and R. Fan, "Joint medium access control, routing and energy distribution in multi-hop wireless networks," *IEEE Transactions on Wireless Communications*, vol. 7, no. 12, pp. 5244–5249, December 2008.

[43] E. B. Hamida and G. Chelius, "Strategies for data dissemination to mobile sinks in wireless sensor networks," *IEEE Wireless Communications*, vol. 15, no. 6, pp. 31–37, December 2008.

[44] W. Wang, V. Srinivasan, and K.-C. Chua, "Extending the lifetime of wireless sensor networks through mobile relays," *IEEE/ACM Transactions on Networking*, vol. 16, no. 5, pp. 1108–1120, October 2008.

[45] J. Luo and J.-P. Hubaux, "Joint sink mobility and routing to maximize the lifetime of wireless sensor networks: The case of constrained mobility," *IEEE/ACM Transactions on Networking*, vol. 18, no. 3, pp. 871–884, June 2010.

[46] Q. Zhang and Y.-Q. Zhang, "Cross-layer design for QoS support in multihop wireless networks," *Proceedings of the IEEE*, vol. 96, no. 1, pp. 64–76, January 2008.

[47] Q. Liu, X. Wang, and G. Giannakis, "A cross-layer scheduling algorithm with QoS support in wireless networks," *IEEE Transactions on Vehicular Technology*, vol. 55, no. 3, pp. 839–847, May 2006.

[48] I. Al-Anbagi, M. Erol Kantarci, and H. Mouftah, "A survey on cross-layer quality of service approaches in WSNs for delay and reliability aware applications," *IEEE Communications Surveys and Tutorials*, no. 99, pp. 1–1, October 2014.

[49] A. Goldsmith and S. Wicker, "Design challenges for energy-constrained ad hoc wireless networks," *IEEE Wireless Communications*, vol. 9, no. 4, pp. 8–27, August 2002.

[50] F. Foukalas, V. Gazis, and N. Alonistioti, "Cross-layer design proposals for wireless mobile networks: A survey and taxonomy," *IEEE Communications Surveys and Tutorials*, vol. 10, no. 1, pp. 70–85, April 2008.

[51] D. Feng, C. Jiang, G. Lim, J. Cimini, L.J., G. Feng, and G. Li, "A survey of energy-efficient wireless communications," *IEEE Communications Surveys and Tutorials*, vol. 15, no. 1, pp. 167–178, February 2013.

[52] B. Fu, Y. Xiao, H. Deng, and H. Zeng, "A survey of cross-layer designs in wireless networks," *IEEE Communications Surveys and Tutorials*, vol. 16, no. 1, pp. 110–126, February 2014.

[53] J. Zuo, C. Dong, S. X. Ng, L.-L. Yang, and L. Hanzo, "Cross-layer aided energy-efficient routing design for ad hoc networks," *IEEE Communications Surveys and Tutorials*, vol. 17, no. 3, pp. 1214–1238, August 2015.

[54] M. Johansson and L. Xiao, "Cross-layer optimization of wireless networks using nonlinear column generation," *IEEE Transactions on Wireless Communications*, vol. 5, no. 2, pp. 435–445, February 2006.

[55] S. Cui, R. Madan, A. Goldsmith, and S. Lall, "Cross-layer energy and delay optimization in small-scale sensor networks," *IEEE Transactions on Wireless Communications*, vol. 6, no. 10, pp. 3688–3699, October 2007.

[56] I. Dietrich and F. Dressler, "On the lifetime of wireless sensor networks," *ACM Transactions on Sensor Networks*, vol. 5, no. 1, pp. 1–39, February 2009.

[57] W. Liu, K. Lu, J. Wang, G. Xing, and L. Huang, "Performance analysis of wireless sensor networks with mobile sinks," *IEEE Transactions on Vehicular Technology*, vol. 61, no. 6, pp. 2777–2788, July 2012.

[58] K. Martinez, J. Hart, and R. Ong, "Environmental sensor networks," *Computer*, vol. 37, no. 8, pp. 50–56, August 2004.

[59] J. Chen, J. Li, and T. Lai, "Trapping mobile targets in wireless sensor networks: An energy-efficient perspective," *IEEE Transactions on Vehicular Technology*, vol. 62, no. 7, pp. 3287–3300, September 2013.

[60] M. Najimi, A. Ebrahimzadeh, S. Andargoli, and A. Fallahi, "Lifetime maximization in cognitive sensor networks based on the node selection," *IEEE Sensors Journal*, vol. 14, no. 7, pp. 2376–2383, July 2014.

[61] J. Du, K. Wang, H. Liu, and D. Guo, "Maximizing the lifetime of k-discrete barrier coverage using mobile sensors," *IEEE Sensors Journal*, vol. 13, no. 12, pp. 4690–4701, December 2013.

[62] H. Salarian, K. Chin, and F. Naghdy, "An energy-efficient mobile-sink path selection strategy for wireless sensor networks," *IEEE Transactions on Vehicular Technology*, vol. 63, no. 5, pp. 2407–2419, June 2014.

[63] J. W. Jung and M. Weitnauer, "On using cooperative routing for lifetime optimization of multi-hop wireless sensor networks: Analysis and guidelines," *IEEE Transactions on Communications*, vol. 61, no. 8, pp. 3413–3423, August 2013.

[64] Y. Chen and Q. Zhao, "On the lifetime of wireless sensor networks," *IEEE Communications Letters*, vol. 9, no. 11, pp. 976–978, November 2005.

[65] C. Cassandras, T. Wang, and S. Pourazarm, "Optimal routing and energy allocation for lifetime maximization of wireless sensor networks with nonideal batteries," *IEEE Transactions on Control of Network Systems*, vol. 1, no. 1, pp. 86–98, March 2014.

[66] J. Li and G. Al-Regib, "Function-based network lifetime for estimation in wireless sensor networks," *IEEE Signal Processing Letters*, vol. 15, pp. 533–536, July 2008.

[67] S. Soro and W. Heinzelman, "Prolonging the lifetime of wireless sensor networks via unequal clustering," in *IEEE International Parallel and Distributed Processing Symposium*, Denver, CO, April 2005.

[68] D. Tian and N. D. Georganas, "A coverage-preserving node scheduling scheme for large wireless sensor networks," in *Proceedings of the 1st ACM international workshop on Wireless sensor networks and applications (WSNA)*, Atlanta, GA, USA, September 2002, pp. 32–41.

[69] W. Mo, D. Qiao, and Z. Wang, "Mostly-sleeping wireless sensor networks: Connectivity, k-coverage, and α-lifetime," in *Proceedings of the 43rd Annual Allerton Conference on Communication, Control and Computing*, Monticello, Illinois, USA, September 2005.

[70] M. Cardei, M. T. Thai, Y. Li, and W. Wu, "Energy-efficient target coverage in wireless sensor networks," in *24th Annual Joint Conference of the IEEE Computer and Communications Societies (INFOCOM'05)*, vol. 3, Miami, FL, USA, March 2005, pp. 1976–1984.

[71] M. Bhardwaj, T. Garnett, and A. P. Chandrakasan, "Upper bounds on the lifetime of sensor networks," in *IEEE International Conference on Communications (ICC'01)*, vol. 3, Helsinki, Finland, June 2001, pp. 785–790.

[72] M. Bhardwaj and A. P. Chandrakasan, "Bounding the lifetime of sensor networks via optimal role assignments," in *IEEE International Conference on Computer Communications (INFOCOM'02)*, vol. 3, NY, USA, June 2002, pp. 1587–1596.

[73] H. Zhang and J. C. Hou, "On the upper bound of α-lifetime for large sensor networks," *ACM Transactions on Sensor Networks*, vol. 1, no. 2, pp. 272–300, November 2005.

[74] K. Wu, Y. Gao, F. Li, and Y. Xiao, "Lightweight deployment-aware scheduling for wireless sensor networks," *Mobile networks and applications*, vol. 10, no. 6, pp. 837–852, December 2005.

[75] B. Cărbunar, A. Grama, J. Vitek, and O. Cărbunar, "Redundancy and coverage detection in sensor networks," *ACM Transactions on Sensor Networks (TOSN)*, vol. 2, no. 1, pp. 94–128, February 2006.

[76] S. Baydere, Y. Safkan, and O. Durmaz, "Lifetime analysis of reliable wireless sensor networks," *IEICE transactions on communications*, vol. 88, no. 6, pp. 2465–2472, June 2005.

[77] J. Li and G. Al-Regib, "Network lifetime maximization for estimation in multihop wireless sensor networks," *IEEE Transactions on Signal Processing*, vol. 57, no. 7, pp. 2456–2466, July 2009.

[78] B. Bejar Haro, S. Zazo, and D. Palomar, "Energy efficient collaborative beamforming in wireless sensor networks," *IEEE Transactions on Signal Processing*, vol. 62, no. 2, pp. 496–510, January 2014.

[79] H. Wang, Y. Yang, M. Ma, J. He, and X. Wang, "Network lifetime maximization with cross-layer design in wireless sensor networks," *IEEE Transactions on Wireless Communications*, vol. 7, no. 10, pp. 3759–3768, October 2008.

[80] L. Van Hoesel, T. Nieberg, J. Wu, and P. J. M. Havinga, "Prolonging the lifetime of wireless sensor networks by cross-layer interaction," *IEEE Wireless Communications*, vol. 11, no. 6, pp. 78–86, December 2004.

[81] H. Nama, M. Chiang, and N. Mandayam, "Utility-lifetime trade-off in self-regulating wireless sensor networks: A cross-layer design approach," in *IEEE International Conference on Communications (ICC'06)*, vol. 8, Istanbul, Turkey, June 2006, pp. 3511–3516.

[82] R. Madan, S. Cui, S. Lall, and A. Goldsmith, "Modeling and optimization of transmission schemes in energy-constrained wireless sensor networks," *IEEE/ACM Transactions on Networking*, vol. 15, no. 6, pp. 1359–1372, December 2007.

[83] J. Zhu, S. Chen, B. Bensaou, and K.-L. Hung, "Tradeoff between lifetime and rate allocation in wireless sensor networks: A cross layer approach," in *26th IEEE International Conference on Computer Communications (INFOCOM'07)*, Anchorage, Alaska, USA, May 2007, pp. 267–275.

[84] J. Li, S. Dey, and J. Evans, "Maximal lifetime power and rate allocation for wireless sensor systems with data distortion constraints," *IEEE Transactions on Signal Processing*, vol. 56, no. 5, pp. 2076–2090, May 2008.

[85] J. Luo, A. Iyer, and C. Rosenberg, "Throughput-lifetime trade-offs in multihop wireless networks under an SINR-based interference model," *IEEE Transactions on Mobile Computing*, vol. 10, no. 3, pp. 419–433, March 2011.

[86] S. Ehsan, B. Hamdaoui, and M. Guizani, "Radio and medium access contention aware routing for lifetime maximization in multichannel sensor networks," *IEEE Transactions on Wireless Communications*, vol. 11, no. 9, pp. 3058–3067, September 2012.

[87] Y. Zhang, J. Wu, and P. J. M. Havinga, "Implementation of an on-demand routing protocol for wireless sensor networks," in *13th International Conference on Telecommunications*, Portugal, May 2006.

[88] D. Palomar and M. Chiang, "A tutorial on decomposition methods for network utility maximization," *IEEE Journal on Selected Areas in Communications*, vol. 24, no. 8, pp. 1439–1451, August 2006.

[89] M. Chiang, C. W. Tan, D. Palomar, D. O'Neill, and D. Julian, "Power control by geometric programming," *IEEE Transactions on Wireless Communications*, vol. 6, no. 7, pp. 2640–2651, July 2007.

[90] IBM's ILOG CPLEX Optimization Studio. http://www-01.ibm.com/support/knowledgecenter/SSSA5P/welcome.

[91] J.-H. Jeon, H.-J. Byun, and J.-T. Lim, "Joint contention and sleep control for lifetime maximization in wireless sensor networks," *IEEE Communications Letters*, vol. 17, no. 2, pp. 269–272, February 2013.

[92] J.-W. Lee, R. Mazumdar, and N. B. Shroff, "Opportunistic power scheduling for dynamic multi-server wireless systems," *IEEE Transactions on Wireless Communications*, vol. 5, no. 6, pp. 1506–1515, June 2006.

[93] A. Ribeiro, "Ergodic stochastic optimization algorithms for wireless communication and networking," *IEEE Transactions on Signal Processing*, vol. 58, no. 12, pp. 6369–6386, December 2010.

[94] S.-J. Kim, X. Wang, and M. Madihian, "Distributed joint routing and medium access control for lifetime maximization of wireless sensor networks," *IEEE Transactions on Wireless Communications*, vol. 6, no. 7, pp. 2669–2677, July 2007.

[95] I. Koutsopoulos and S. Stanczak, "The impact of transmit rate control on energy-efficient estimation in wireless sensor networks," *IEEE Transactions on Wireless Communications*, vol. 11, no. 9, pp. 3261–3271, September 2012.

[96] Y. Chen, Q. Zhao, V. Krishnamurthy, and D. Djonin, "Transmission scheduling for optimizing sensor network lifetime: A stochastic shortest path approach," *IEEE Transactions on Signal Processing*, vol. 55, no. 5, pp. 2294–2309, May 2007.

[97] C. V. Phan, Y. Park, H. Choi, J. Cho, and J. G. Kim, "An energy-efficient transmission strategy for wireless sensor networks," *IEEE Transactions on Consumer Electronics*, vol. 56, no. 2, pp. 597–605, May 2010.

[98] C.-C. Hung, K. C.-J. Lin, C.-C. Hsu, C.-F. Chou, and C.-J. Tu, "On enhancing network-lifetime using opportunistic routing in wireless sensor networks," in *International Conference on Computer Communications and Networks (ICCCN'10)*, Zurich, August 2010, pp. 1–6.

[99] D. Wu, Y. Cai, and J. Wang, "A coalition formation framework for transmission scheme selection in wireless sensor networks," *IEEE Transactions on Vehicular Technology*, vol. 60, no. 6, pp. 2620–2630, July 2011.

[100] P. Wang, H. Jiang, W. Zhuang, and H. Poor, "Redefinition of max-min fairness in multi-hop wireless networks," *IEEE Transactions on Wireless Communications*, vol. 7, no. 12, pp. 4786–4791, December 2008.

[101] G. H. Polychronopoulos and J. N. Tsitsiklis, "Stochastic shortest path problems with recourse," *Networks*, vol. 27, no. 2, pp. 133–143, March 1996.

[102] M. C.-C. Hung, K. C.-J. Lin, C.-F. Chou, and C.-C. Hsu, "EFFORT: Energy-efficient opportunistic routing technology in wireless sensor networks," *Wireless Communications and Mobile Computing*, vol. 13, no. 8, pp. 760–773, June 2013.

[103] W. Saad, Z. Han, M. Debbah, A. Hjorungnes, and T. Basar, "Coalitional game theory for communication networks," *IEEE Signal Processing Magazine*, vol. 26, no. 5, pp. 77–97, September 2009.

[104] J. Matamoros and C. Antòn-Haro, "Opportunistic power allocation and sensor selection schemes for wireless sensor networks," *IEEE Transactions on Wireless Communications*, vol. 9, no. 2, pp. 534–539, February 2010.

[105] J.-H. Chang and L. Tassiulas, "Energy conserving routing in wireless ad-hoc networks," in *IEEE International Conference on Computer Communications (INFOCOM'00)*, vol. 1, Tel Aviv, March 2000, pp. 22–31.

[106] ——, "Maximum lifetime routing in wireless sensor networks," *IEEE/ACM Transactions on Networking*, vol. 12, no. 4, pp. 609–619, August 2004.

[107] C. Hua and T. Yum, "Optimal routing and data aggregation for maximizing lifetime of wireless sensor networks," *IEEE/ACM Transactions on Networking*, vol. 16, no. 4, pp. 892–903, August 2008.

[108] Y. He, I. Lee, and L. Guan, "Distributed algorithms for network lifetime maximization in wireless visual sensor networks," *IEEE Transactions on Circuits and Systems for Video Technology*, vol. 19, no. 5, pp. 704–718, May 2009.

[109] F. Liu, C.-Y. Tsui, and Y. Zhang, "Joint routing and sleep scheduling for lifetime maximization of wireless sensor networks," *IEEE Transactions on Wireless Communications*, vol. 9, no. 7, pp. 2258–2267, July 2010.

[110] S. Amiri, P. Nasiopoulos, and V. Leung, "Collaborative routing and camera selection for visual wireless sensor networks," *IET Communications*, vol. 5, no. 17, pp. 2443–2450, November 2011.

[111] I. Al-Shawi, L. Yan, W. Pan, and B. Luo, "Lifetime enhancement in wireless sensor networks using fuzzy approach and A-star algorithm," *IEEE Sensors Journal*, vol. 12, no. 10, pp. 3010–3018, October 2012.

[112] Y. Peng, Z. Li, D. Qiao, and W. Zhang, "I2C: A holistic approach to prolong the sensor network lifetime," in *IEEE International Conference on Computer Communicatons (INFOCOM'13)*, Turin, Italy, April 2013, pp. 2670–2678.

[113] C.-C. Hsu, M.-S. Kuo, S.-C. Wang, and C.-F. Chou, "Joint design of asynchronous sleep-wake scheduling and opportunistic routing in wireless sensor networks," *IEEE Transactions on Computers*, vol. 63, no. 7, pp. 1840–1846, July 2014.

[114] W. Wallis, *A Beginner's Guide to Graph Theory*. Birkhäuser Boston, 2010.

[115] J.-H. Chang and L. Tassiulas, "Routing for maximum system lifetime in wireless ad-hoc networks," in *Proceedings of the Annual Allerton Conference on Communication, Control and Computing*, vol. 37, IL, USA, September 1999, pp. 1191–1200.

[116] A. Ribeiro, N. Sidiropoulos, and G. Giannakis, "Optimal distributed stochastic routing algorithms for wireless multihop networks," *IEEE Transactions on Wireless Communications*, vol. 7, no. 11, pp. 4261–4272, November 2008.

[117] C. W. Tan, D. Palomar, and M. Chiang, "Solving nonconvex power control problems in wireless networks: Low SIR regime and distributed algorithms," in *IEEE Global Telecommunications Conference (GLOBECOM'05)*, St. Louis, MO, November 2005.

[118] K.-Y. Cai and L. Zhang, "Fuzzy reasoning as a control problem," *IEEE Transactions on Fuzzy Systems*, vol. 16, no. 3, pp. 600–614, June 2008.

[119] J. Yao, C. Lin, X. Xie, A. Wang, and C.-C. Hung, "Path planning for virtual human motion using improved A* star algorithm," in *Seventh International Conference on Information Technology: New Generations (ITNG'10)*, Las Vegas, NV, April 2010, pp. 1154–1158.

[120] V. Rao, G. Singhal, A. Kumar, and N. Navet, "Battery model for embedded systems," in *18th International Conference on VLSI Design*, Kolkata, India, January 2005, pp. 105–110.

[121] Y.-S. Yun, Y. Xia, B. Behdani, and J. Smith, "Distributed algorithm for lifetime maximization in a delay-tolerant wireless sensor network with a mobile sink," *IEEE Transactions on Mobile Computing*, vol. 12, no. 10, pp. 1920–1930, October 2013.

[122] C.-F. Wang, J.-D. Shih, B.-H. Pan, and T.-Y. Wu, "A network lifetime enhancement method for sink relocation and its analysis in wireless sensor networks," *IEEE Sensors Journal*, vol. 14, no. 6, pp. 1932–1943, June 2014.

[123] F. Tashtarian, M. Hossein Yaghmaee Moghaddam, K. Sohraby, and S. Effati, "On maximizing the lifetime of wireless sensor networks in event-driven applications with mobile sinks," *IEEE Transactions on Vehicular Technology*, vol. 64, no. 7, pp. 3177–3189, July 2015.

[124] J. Rao and S. Biswas, "Data harvesting in sensor networks using mobile sinks," *IEEE Wireless Communications*, vol. 15, no. 6, pp. 63–70, December 2008.

[125] J. Luo and J.-P. Hubaux, "Joint mobility and routing for lifetime elongation in wireless sensor networks," in *24th Annual Joint Conference of the IEEE Computer and Communications Societies (INFOCOM'05)*, vol. 3, Miami, FL, USA, March 2005, pp. 1735–1746.

[126] S. Ratnasamy, B. Karp, L. Yin, F. Yu, D. Estrin, R. Govindan, and S. Shenker, "GHT: A geographic hash table for data-centric storage," in *Proceedings of the 1st ACM international workshop on Wireless sensor networks and applications*, Atlanta, Georgia, USA, September 2002, pp. 78–87.

[127] E. B. Hamida and G. Chelius, "A line-based data dissemination protocol for wireless sensor networks with mobile sink," in *IEEE International Conference on Communications (ICC'08)*, Beijing, May 2008, pp. 2201–2205.

[128] S. M. Das, H. Pucha, and Y. C. Hu, "Performance comparison of scalable location services for geographic ad hoc routing," in *24th Annual Joint Conference of the IEEE Computer and Communications Societies (INFOCOM'05)*, vol. 2, Miami, FL, USA, March 2005, pp. 1228–1239.

[129] S. P. Boyd and L. Vandenberghe, *Convex optimization*. Cambridge university press, 2004.

[130] Y.-S. Yun and Y. Xia, "Maximizing the lifetime of wireless sensor networks with mobile sink in delay-tolerant applications," *IEEE Transactions on Mobile Computing*, vol. 9, no. 9, pp. 1308–1318, September 2010.

[131] A. Makhorin, "GNU linear programming kit," *Moscow Aviation Institute, Moscow, Russia*, vol. 38, 2001.

[132] X.-M. Hu, J. Zhang, Y. Yu, H.-H. Chung, Y.-L. Li, Y.-H. Shi, and X.-N. Luo, "Hybrid genetic algorithm using a forward encoding scheme for lifetime maximization of wireless sensor networks," *IEEE Transactions on Evolutionary Computation*, vol. 14, no. 5, pp. 766–781, October 2010.

[133] Y. Lin, J. Zhang, H.-H. Chung, W. H. Ip, Y. Li, and Y.-H. Shi, "An ant colony optimization approach for maximizing the lifetime of heterogeneous wireless sensor networks," *IEEE Transactions on Systems, Man, and Cybernetics, Part C: Applications and Reviews*, vol. 42, no. 3, pp. 408–420, May 2012.

[134] Z. Lu, W. W. Li, and M. Pan, "Maximum lifetime scheduling for target coverage and data collection in wireless sensor networks," *IEEE Transactions on Vehicular Technology*, vol. 64, no. 2, pp. 714–727, February 2015.

[135] X. Deng, B. Wang, W. Liu, and L. Yang, "Sensor scheduling for multi-modal confident information coverage in sensor networks," *IEEE Transactions on Parallel and Distributed Systems*, vol. 26, no. 3, pp. 902–913, March 2015.

[136] C.-P. Chen, S. Mukhopadhyay, C.-L. Chuang, M.-Y. Liu, and J.-A. Jiang, "Efficient coverage and connectivity preservation with load balance for wireless sensor networks," *IEEE Sensors Journal*, vol. 15, no. 1, pp. 48–62, January 2015.

[137] L. Ding, W. Wu, J. Willson, L. Wu, Z. Lu, and W. Lee, "Constant-approximation for target coverage problem in wireless sensor networks," in *IEEE Conference on Computer Communications (INFOCOM'15)*, Orlando, FL, March 2012, pp. 1584–1592.

[138] H. Zhang and J. C. Hou, "Maintaining sensing coverage and connectivity in large sensor networks," *Ad Hoc and Sensor Wireless Networks*, vol. 1, no. 1-2, pp. 89–124, March 2005.

[139] M. Liu, J. Cao, W. Lou, L.-j. Chen, and X. Li, "Coverage analysis for wireless sensor networks," in *Mobile Ad-hoc and Sensor Networks*, ser. Lecture Notes in Computer Science, X. Jia, J. Wu, and Y. He, Eds. Springer Berlin Heidelberg, 2005, vol. 3794, pp. 711–720.

[140] D. Li and H. Liu, "Sensor coverage in wireless sensor networks," *International Journal of Sensor Networks*, vol. 2, 2009.

[141] M. Cardei and J. Wu, "Energy-efficient coverage problems in wireless ad-hoc sensor networks," *Computer Communications*, vol. 29, no. 4, pp. 413–420, February 2006.

[142] R. Cristescu and B. Beferull-Lozano, "Lossy network correlated data gathering with high-resolution coding," *IEEE Transactions on Information Theory*, vol. 52, no. 6, pp. 2817–2824, June 2006.

[143] T. Himsoon, W. Siriwongpairat, Z. Han, and K. Liu, "Lifetime maximization via cooperative nodes and relay deployment in wireless networks," *IEEE Journal on Selected Areas in Communications*, vol. 25, no. 2, pp. 306–317, February 2007.

[144] E. Natalizio, V. Loscri, and E. Viterbo, "Optimal placement of wireless nodes for maximizing path lifetime," *IEEE Communications Letters*, vol. 12, no. 5, pp. 362–364, May 2008.

[145] P. Zhang, G. Xiao, and H. Tan, "A preliminary study on lifetime maximization in clustered wireless sensor networks with energy harvesting nodes," in *8th International Conference on Information, Communications and Signal Processing (ICICS'11)*, Singapore, December 2011.

[146] S. Mini, S. Udgata, and S. Sabat, "Sensor deployment and scheduling for target coverage problem in wireless sensor networks," *IEEE Sensors Journal*, vol. 14, no. 3, pp. 636–644, March 2014.

[147] X. Liu, "A transmission scheme for wireless sensor networks using ant colony optimization with unconventional characteristics," *IEEE Communications Letters*, vol. 18, no. 7, pp. 1214–1217, July 2014.

[148] W. Heinzelman, A. Chandrakasan, and H. Balakrishnan, "Energy-efficient communication protocol for wireless microsensor networks," in *Proceedings of the 33rd Annual Hawaii International Conference on System Sciences*, Maui, HI, USA, January 2000.

[149] M. Magno, D. Boyle, D. Brunelli, E. Popovici, and L. Benini, "Ensuring survivability of resource-intensive sensor networks through ultra-low power overlays," *IEEE Transactions on Industrial Informatics*, vol. 10, no. 2, pp. 946–956, May 2014.

[150] T. Himsoon, W. Siriwongpairat, Z. Han, and K. Liu, "Lifetime maximization by cooperative sensor and relay deployment in wireless sensor networks," in *IEEE Wireless Communications and Networking Conference (WCNC'06)*, Las Vegas, NV, April 2006, pp. 439–444.

[151] S. He, J. Chen, D. Yau, and Y. Sun, "Cross-layer optimization of correlated data gathering in wireless sensor networks," *IEEE Transactions on Mobile Computing*, vol. 11, no. 11, pp. 1678–1691, November 2012.

[152] W. Liang and Y. Liu, "Online data gathering for maximizing network lifetime in sensor networks," *IEEE Transactions on Mobile Computing*, vol. 6, no. 1, pp. 2–11, January 2007.

[153] Y. Wu, Z. Mao, S. Fahmy, and N. B. Shroff, "Constructing maximum-lifetime data gathering forests in sensor networks," *IEEE/ACM Transactions on Networking*, vol. 18, no. 5, pp. 1571–1584, October 2010.

[154] T. Heo, H. Kim, J.-G. Ko, Y. Doh, J.-J. Park, J. Jun, and H. Choi, "Adaptive dual prediction scheme based on sensing context similarity for wireless sensor networks," *IET Electronics Letters*, vol. 50, no. 6, pp. 467–469, March 2014.

[155] J. Kim, X. Lin, N. B. Shroff, and P. Sinha, "Minimizing delay and maximizing lifetime for wireless sensor networks with anycast," *IEEE/ACM Transactions on Networking*, vol. 18, no. 2, pp. 515–528, April 2010.

[156] M. Sichitiu, "Cross-layer scheduling for power efficiency in wireless sensor networks," in *IEEE International Conference on Computer Communications (INFOCOM'04)*, vol. 3, Hong Kong, March 2004, pp. 1740–1750.

[157] A. Chamam and S. Pierre, "On the planning of wireless sensor networks: Energy-efficient clustering under the joint routing and coverage constraint," *IEEE Transactions on Mobile Computing*, vol. 8, no. 8, pp. 1077–1086, August 2009.

[158] Y. Zhao, J. Wu, F. Li, and S. Lu, "On maximizing the lifetime of wireless sensor networks using virtual backbone scheduling," *IEEE Transactions on Parallel and Distributed Systems*, vol. 23, no. 8, pp. 1528–1535, August 2012.

[159] Z. Li, Y. Peng, D. Qiao, and W. Zhang, "Joint aggregation and MAC design to prolong sensor network lifetime," in *21st IEEE International Conference on Network Protocols (ICNP'13)*, Goettingen, Germany, October 2013, pp. 1–10.

[160] E. Rolland, H. Pirkul, and F. Glover, "Tabu search for graph partitioning," *Annals of Operations Research*, vol. 63, no. 2, pp. 209–232, April 1996.

[161] R. Rout and S. Ghosh, "Enhancement of lifetime using duty cycle and network coding in wireless sensor networks," *IEEE Transactions on Wireless Communications*, vol. 12, no. 2, pp. 656–667, February 2013.

[162] Y. Wu, P. Chou, and S.-Y. Kung, "Minimum-energy multicast in mobile ad hoc networks using network coding," *IEEE Transactions on Communications*, vol. 53, no. 11, pp. 1906–1918, November 2005.

[163] L. Ding, P. Wu, Z. Pan, and X. You, "Lifetime optimization for wireless multihop networks with network coding," in *International Conference on Wireless Communications Signal Processing (WCSP'12)*, Huangshan, October 2012, pp. 1–6.

[164] L. Ding, P. Wu, H. Wang, Z. Pan, and X. You, "Lifetime maximization routing with network coding in wireless multihop networks," *Science China Information Sciences*, vol. 56, no. 2, pp. 1–15, February 2013.

[165] V. Shah-Mansouri and V. Wong, "Lifetime-resource tradeoff for multicast traffic in wireless sensor networks," *IEEE Transactions on Wireless Communications*, vol. 9, no. 6, pp. 1924–1934, June 2010.

[166] O. Younis, M. Krunz, and S. Ramasubramanian, "Node clustering in wireless sensor networks: Recent developments and deployment challenges," *IEEE Network*, vol. 20, no. 3, pp. 20–25, May 2006.

[167] G. Gupta and M. Younis, "Fault-tolerant clustering of wireless sensor networks," in *IEEE Wireless Communications and Networking (WCNC'03)*, vol. 3, New Orleans, LA, USA, March 2003, pp. 1579–1584.

[168] ——, "Load-balanced clustering of wireless sensor networks," in *IEEE International Conference on Communications (ICC'03)*, vol. 3, Anchorage, AK, May 2003, pp. 1848–1852.

[169] J. De-Witt and H. Shi, "Maximizing lifetime for k-barrier coverage in energy harvesting wireless sensor networks," in *IEEE Global Communications Conference (GLOBECOM'14)*, Austin, TX, December 2014, pp. 300–304.

[170] G. Martinez, S. Li, and C. Zhou, "Multi-commodity online maximum lifetime utility routing for energy-harvesting wireless sensor networks," in *IEEE Global Communications Conference (GLOBECOM'14)*, Austin, TX, December 2014, pp. 106–111.

[171] J. Feng, Y.-H. Lu, B. Jung, D. Peroulis, and Y. C. Hu, "Energy-efficient data dissemination using beamforming in wireless sensor networks," *ACM Transactions on Sensor Networks*, vol. 9, no. 3, pp. 1–31, May 2013.

[172] Z. Han and H. Poor, "Lifetime improvement of wireless sensor networks by collaborative beamforming and cooperative transmission," in *IEEE International Conference on Communications (ICC'07)*, Glasgow, June 2007, pp. 3954–3958.

[173] Wireless sensor network programmable analog input measurement nodes, NI WSN-3202, NI WSN-3212, NI WSN-3226. http://www.ni.com/datasheet/pdf/en/ds-350.

[174] F. Xue, "Multi-objective differential evolution: Theory and applications," Ph.D. dissertation, Rensselaer Polytechnic Institute, 2004.

[175] F. Xue, A. Sanderson, and R. Graves, "Multi-objective routing in wireless sensor networks with a differential evolution algorithm," in *IEEE International Conference on Networking, Sensing and Control (ICNSC'06)*, Ft. Lauderdale, FL, USA, 2006, pp. 880–885.

[176] E. Zitzler, "Evolutionary algorithms for multiobjective optimization: Methods and applications," Ph.D. dissertation, Doctoral dissertation ETH 13398, Swiss Federal Institute of Technology (ETH), Zurich, Switzerland, 1999.

[177] K. Deb, A. Pratap, S. Agarwal, and T. Meyarivan, "A fast and elitist multiobjective genetic algorithm: NSGA-II," *IEEE Transactions on Evolutionary Computation*, vol. 6, no. 2, pp. 182–197, April 2002.

[178] K. Deb, "Multi-objective optimization," in *Search Methodologies*. Springer US, 2014, pp. 403–449.

[179] D. Yuan, V. Angelakis, L. Chen, E. Karipidis, and E. Larsson, "On optimal link activation with interference cancelation in wireless networking," *IEEE Transactions on Vehicular Technology*, vol. 62, no. 2, pp. 939–945, February 2013.

[180] Z. Yang, Q. Zhang, and Z. Niu, "Throughput improvement by joint relay selection and link scheduling in relay-assisted cellular networks," *IEEE Transactions on Vehicular Technology*, vol. 61, no. 6, pp. 2824–2835, July 2012.

[181] A. Goldsmith, *Wireless communications*. Cambridge University Press, 2005.

[182] H. Yetgin, K. T. K. Cheung, and L. Hanzo, "Multi-objective routing optimization using evolutionary algorithms," in *IEEE Wireless Communications and Networking Conference (WCNC'12)*, Paris, France, April 2012.

[183] P. Li, S. Guo, and V. Leung, "Maximum-lifetime coding tree for multicast in lossy wireless networks," *IEEE Wireless Communications Letters*, vol. 2, no. 3, pp. 295–298, June 2013.

[184] A. Goldsmith and S.-G. Chua, "Variable-rate variable-power MQAM for fading channels," *IEEE Transactions on Communications*, vol. 45, no. 10, pp. 1218–1230, October 1997.

[185] Z. Cheng, M. Perillo, and W. Heinzelman, "General network lifetime and cost models for evaluating sensor network deployment strategies," *IEEE Transactions on Mobile Computing*, vol. 7, no. 4, pp. 484–497, April 2008.

[186] Q. Dong, "Maximizing system lifetime in wireless sensor networks," in *Fourth International Symposium on Information Processing in Sensor Networks (IPSN'05)*, Boise, ID, USA, April 2005, pp. 13–19.

[187] R. Verdone and C. Buratti, "Modelling for wireless sensor network protocol design," in *IEEE International Workshop on Wireless Ad-hoc Networks (IWWAN'05)*, London, United Kingdom, 2005.

[188] R. L. Cruz and A. V. Santhanam, "Optimal routing, link scheduling and power control in multihop wireless networks," in *IEEE Computer and Communications Societies (INFOCOM'03)*, vol. 1, San Francisco, CA, March 2003, pp. 702–711.

[189] U. Kozat, I. Koutsopoulos, and L. Tassiulas, "A framework for cross-layer design of energy-efficient communication with QoS provisioning in multi-hop wireless networks," in *IEEE Computer and Communications Societies (INFOCOM'04)*, vol. 2, Hong Kong, March 2004, pp. 1446–1456.

[190] M. Albulet, *RF power amplifiers*. Raleigh, NC: SciTech, 2001.

[191] R. H. Byrd, M. E. Hribar, and J. Nocedal, "An interior point algorithm for large-scale nonlinear programming," *SIAM Journal on Optimization*, vol. 9, no. 4, pp. 877–900, April 1999.

[192] C.-M. Cheng and H. T. Kung, "Use of relays in extending network lifetime," in *IEEE 60th Vehicular Technology Conference (VTC'04)*, vol. 7, Los Angeles, CA, USA, September 2004, pp. 4655–4659.

[193] D. Duan, F. Qu, L. Yang, A. Swami, and J. Principe, "Modulation selection from a battery power efficiency perspective: A case study of PPM and OOK," in *IEEE Wireless Communications and Networking Conference (WCNC'09)*, 2009, pp. 1–6.

[194] F. Rosas and C. Oberli, "Modulation and SNR optimization for achieving energy-efficient communications over short-range fading channels," *IEEE Transactions on Wireless Communications*, vol. 11, no. 12, pp. 4286–4295, December 2012.

[195] S. Cui, A. Goldsmith, and A. Bahai, "Energy-constrained modulation optimization," *IEEE Transactions on Wireless Communications*, vol. 4, no. 5, pp. 2349–2360, September 2005.

[196] J. Hartwell, G. Messier, and R. Davies, "Optimizing physical layer energy consumption for wireless sensor networks," in *IEEE 65th Vehicular Technology Conference (VTC'07)*, Dublin, April 2007, pp. 76–79.

[197] B. Sklar, *Digital Communications: Fundamentals and Applications*, P. Hall, Ed., 2001.

[198] B. Panigrahi, A. Sharma, and S. De, "Interference aware power controlled forwarding for lifetime maximisation of wireless ad hoc networks," *IET Wireless Sensor Systems*, vol. 2, pp. 22–30, March 2012.

[199] Y. Chen, Y. Yang, and W. Yi, "A cooperative routing algorithm for lifetime maximization in wireless sensor networks," *IET International Conference on Wireless Sensor Network*, pp. 167–172, January 2010.

[200] D. Dahnil, Y. Singh, and C. Ho, "Topology-controlled adaptive clustering for uniformity and increased lifetime in wireless sensor networks," *IET Wireless Sensor Systems*, vol. 2, no. 4, pp. 318–327, December 2012.

[201] D. Agarwal and N. Kishor, "Network lifetime enhanced tri-level clustering and routing protocol for monitoring of offshore wind farms," *IET Wireless Sensor Systems*, vol. 4, no. 2, pp. 69–79, June 2014.

[202] L. Hanzo, T. Liew, and B. Yeap, *Turbo Coding, Turbo Equalisation and Space-Time Coding*. John Wiley & Sons, August 2002. [Online]. Available: http://eprints.soton.ac.uk/258252/

[203] M. El-Hajjar and L. Hanzo, "EXIT charts for system design and analysis," *IEEE Communications Surveys and Tutorials*, vol. 16, no. 1, pp. 127–153, February 2013. [Online]. Available: http://eprints.soton.ac.uk/352320/

[204] K. Al-Agha, M.-H. Bertin, T. Dang, A. Guitton, P. Minet, T. Val, and J.-B. Viollet, "Which wireless technology for industrial wireless sensor networks? the development of OCARI technology," *IEEE Transactions on Industrial Electronics*, vol. 56, no. 10, pp. 4266–4278, September 2009.

[205] V. Raghunathan, C. Schurgers, S. Park, and M. B. Srivastava, "Energy-aware wireless microsensor networks," *IEEE Signal Processing Magazine*, vol. 19, no. 2, pp. 40–50, March 2002.

[206] R. Zhang and J.-M. Gorce, "Optimal transmission range for minimum energy consumption in wireless sensor networks," in *IEEE Wireless Communications and Networking Conference (WCNC'08)*, Las Vegas, NV, March 2008, pp. 757–762.

[207] *IEEE Standard for Information Technology – Local and Metropolitan Area Networks – Specific Requirements – Part 15.4: Wireless Medium Access Control (MAC) and Physical Layer (PHY) Specifications for Low Rate Wireless Personal Area Networks (WPANs)*, Std., September 2006.

[208] L. Lin, X. Lin, and N. B. Shroff, "Low-complexity and distributed energy minimization in multi-hop wireless networks," in *IEEE International Conference on Computer Communications (INFOCOM'07)*, Anchorage, AK, USA, May 2007.

[209] L. Badia, A. Botta, and L. Lenzini, "A genetic approach to joint routing and link scheduling for wireless mesh networks," *Ad Hoc Networks*, vol. 7, no. 4, pp. 654–664, June 2009.

[210] J. Jia, X. Wang, and J. Chen, "A genetic approach on cross-layer optimization for cognitive radio wireless mesh network under SINR model," *Ad Hoc Networks*, vol. 27, no. 0, pp. 57–67, April 2015.

[211] A. Azari and G. Miao, "Lifetime-aware scheduling and power control for M2M communications in LTE networks," in *IEEE Vehicular Technology Conference (VTC'15)*, Glasgow, Scotland, May 2015.

[212] ——, "Lifetime-aware scheduling and power control for cellular-based M2M communications," in *IEEE Wireless Communications and Networking Conference (WCNC'15)*, New Orleans, USA, March 2015.

[213] Y. Cui, Y. Xue, and K. Nahrstedt, "A utility-based distributed maximum lifetime routing algorithm for wireless networks," *IEEE Transactions on Vehicular Technology*, vol. 55, no. 3, pp. 797–805, May 2006.

[214] C. Zhu, S. Wu, G. Han, L. Shu, and H. Wu, "A tree-cluster-based data-gathering algorithm for industrial WSNs with a mobile sink," *IEEE Access*, vol. 3, pp. 381–396, May 2015.

[215] R. Khanna, H. Liu, and H.-H. Chen, "Dynamic optimization of secure mobile sensor networks: A genetic algorithm," in *IEEE International Conference on Communications (ICC'07)*, Glasgow, Scotland, June 2007.

[216] Y. Gu, M. Pan, and W. W. Li, "Prolonging the lifetime of large scale wireless sensor networks via base station placement," in *IEEE Vehicular Technology Conference (VTC'13)*, Las Vegas, USA, September 2013.

[217] H. Chenji and R. Stoleru, "Pareto optimal cross layer lifetime optimization for disaster response networks," in *International Conference on Communication Systems and Networks (COMSNETS'14)*, Bangalore, January 2014, pp. 1–8.

[218] Y. Shi, Y. Sagduyu, and J. Li, "Low complexity multi-layer optimization for multi-hop wireless networks," in *MILITARY COMMUNICATIONS CONFERENCE (MILCOM'12)*, Orlando, FL, October 2012.

[219] A. Behzadan, A. Anpalagan, and B. Ma, "Prolonging network lifetime via nodal energy balancing in heterogeneous wireless sensor networks," in *IEEE International Conference on Communications (ICC'11)*, Kyoto, Japan, June 2011.

[220] O. K. Tonguz and G. Ferrari, *Ad Hoc Wireless Networks: A Communication-Theoretic Perspective*. John Wiley & Sons, Ltd, 2006.

[221] ——, "A communication-theoretic approach to ad hoc wireless networking," in *3rd Annual IEEE Communications Society on Sensor and Ad Hoc Communications and Networks (SECON'06)*, vol. 2, Reston, VA, September 2006, pp. 715–722.

[222] S. Savazzi, L. Goratti, U. Spagnolin, and M. Latva-aho, "Short-range wireless sensor networks for high density seismic monitoring," in *Proceedings of the Wireless World Research Forum*, Paris, May 2009.

[223] J. G. Proakis, *Digital Communications*. McGraw-Hill, 2001.

[224] C. W. Ahn and R. Ramakrishna, "A genetic algorithm for shortest path routing problem and the sizing of populations," *IEEE Transactions on Evolutionary Computation*, vol. 6, no. 6, pp. 566–579, December 2002.

[225] S. Iyengar, H.-C. Wu, N. Balakrishnan, and S. Y. Chang, "Biologically inspired cooperative routing for wireless mobile sensor networks," *IEEE Systems Journal*, vol. 1, no. 1, pp. 29–37, September 2007.

[226] Y. Ye, S. Ci, A. Katsaggelos, Y. Liu, and Y. Qian, "Wireless video surveillance: A survey," *IEEE Access*, vol. 1, pp. 646–660, September 2013.

[227] S. Djahel, R. Doolan, G.-M. Muntean, and J. Murphy, "A communications-oriented perspective on traffic management systems for smart cities: Challenges and innovative approaches," *IEEE Communications Surveys and Tutorials*, vol. 17, no. 1, pp. 125–151, March 2015.

[228] E. Masazade, R. Rajagopalan, P. Varshney, C. Mohan, G. Sendur, and M. Keskinoz, "A multiobjective optimization approach to obtain decision thresholds for distributed detection in wireless sensor networks," *IEEE Transactions on Systems, Man, and Cybernetics, Part B: Cybernetics*, vol. 40, no. 2, pp. 444–457, April 2010.

[229] E. Zitzler and L. Thiele, "Multiobjective evolutionary algorithms: A comparative case study and the strength pareto approach," *IEEE Transactions on Evolutionary Computation*, vol. 3, no. 4, pp. 257–271, November 1999.

[230] M. Camelo, C. Omaña, and H. Castro, "QoS routing algorithm based on multi-objective optimization for wireless mesh networks," in *IEEE Latin-American Conference on Communications (LATINCOM'10)*, Bogota, Colombia, September 2010, pp. 1–6.

[231] K. Deb, *Multi-Objective Optimization Using Evolutionary Algorithms*. New York, NY, USA: John Wiley & Sons, Inc., 2001.

[232] K. Kotecha and S. Popat, "Multi objective genetic algorithm based adaptive QoS routing in MANET," in *IEEE Congress on Evolutionary Computation (CEC'07)*, Vidyanagar, India, September 2007, pp. 1423–1428.

[233] M. Jensen, "Reducing the run-time complexity of multiobjective EAs: The NSGA-II and other algorithms," *IEEE Transactions on Evolutionary Computation*, vol. 7, no. 5, pp. 503–515, October 2003.

[234] A. Zhou, B.-Y. Qu, H. Li, S.-Z. Zhao, P. N. Suganthan, and Q. Zhang, "Multiobjective evolutionary algorithms: A survey of the state of the art," *Swarm and Evolutionary Computation*, vol. 1, no. 1, pp. 32–49, March 2011.

[235] R. Kulkarni, A. Förster, and G. Venayagamoorthy, "Computational intelligence in wireless sensor networks: A survey," *IEEE Communications Surveys and Tutorials*, vol. 13, no. 1, pp. 68–96, February 2011.

[236] N. Sharma and K. R. Anupama, "On the use of NSGA-II for multi-objective resource allocation in MIMO-OFDMA systems," *Wirel. Netw.*, vol. 17, pp. 1191–1201, July 2011.

[237] S. Lalwani, S. Sianhal, R. Kumar, and N. Gupta, "A comprehensive survey: Applications of multi-objective particle swarm optimization (MOPSO) algorithm," *Transactions on Combinatories*, vol. 2, no. 1, pp. 39–101, March 2013.

[238] Z. Zhang, K. Long, J. Wang, and F. Dressler, "On swarm intelligence inspired self-organized networking: Its bionic mechanisms, designing principles and optimization approaches," *IEEE Communications Surveys and Tutorials*, vol. 16, no. 1, pp. 513–537, February 2014.

[239] A. Roy, N. Banerjee, and S. Das, "An efficient multi-objective QoS-routing algorithm for wireless multicasting," in *IEEE 55th Vehicular Technology Conference (VTC'02-Spring)*, vol. 3, Birmingham, Alabama, May 2002, pp. 1160–1164.

[240] X. Cui, C. Lin, and Y. Wei, "A multiobjective model for QoS multicast routing based on genetic algorithm," in *International Conference on Computer Networks and Mobile Computing (ICCNMC'03)*, Beijing, China, October 2003, pp. 49–53.

[241] L. Liu, X. Cao, Y. Cheng, L. Du, W. Song, and Y. Wang, "Energy-efficient capacity optimization in wireless networks," in *IEEE International Conference on Computer Communicatons (INFOCOM'14)*, Toronto, Canada, April 2014, pp. 1384–1392.

[242] D. Alanis, P. Botsinis, S. X. Ng, and L. Hanzo, "Quantum-assisted routing optimization for self-organizing networks," *IEEE Access*, vol. 2, pp. 614–632, 2014.

[243] N. Pantazis and D. Vergados, "A survey on power control issues in wireless sensor networks," *IEEE Communications Surveys and Tutorials*, vol. 9, no. 4, pp. 86–107, February 2007.

[244] D. Jourdan and O. De-Weck, "Layout optimization for a wireless sensor network using a multi-objective genetic algorithm," in *IEEE 59th Vehicular Technology Conference (VTC'04-Spring)*, vol. 5, Milan, Italy, May 2004, pp. 2466–2470.

[245] A. Konstantinidis, K. Yang, Q. Zhang, and D. Zeinalipour-Yazti, "A multi-objective evolutionary algorithm for the deployment and power assignment problem in wireless sensor networks," *Computer Networks*, vol. 54, no. 6, pp. 960–976, 2010, new Network Paradigms.

[246] A. Konstantinidis and K. Yang, "Multi-objective energy-efficient dense deployment in wireless sensor networks using a hybrid problem-specific MOEA/D," *Applied Soft Computing*, vol. 11, no. 6, pp. 4117–4134, 2011.

[247] N. Aitsaadi, N. Achir, K. Boussetta, and G. Pujolle, "Multi-objective WSN deployment: Quality of monitoring, connectivity and lifetime," in *IEEE International Conference on Communications (ICC'10)*, Cape Town, May 2010.

[248] G. Ekbatani-Fard, R. Monsefi, M.-R. Akbarzadeh-T, and M. H. Yaghmaee, "A multi-objective genetic algorithm based approach for energy efficient QoS-routing in two-tiered wireless sensor networks," in *5th IEEE International Symposium on Wireless Pervasive Computing (ISWPC'10)*, Modena, Italy, May 2010, pp. 80–85.

[249] L. Jin, J. Jia, and D. Sun, "Node distribution optimization in mobile sensor network based on multi-objective differential evolution algorithm," in *IEEE International Conference on Genetic and Evolutionary Computing (ICGEC'10)*, Shenyang, China, December 2010, pp. 51–54.

[250] F. Martins, E. Carrano, E. Wanner, R. Takahashi, and G. Mateus, "A hybrid multiobjective evolutionary approach for improving the performance of wireless sensor networks," *IEEE Sensors Journal*, vol. 11, no. 3, pp. 545–554, March 2011.

[251] M. Le Berre, F. Hnaien, and H. Snoussi, "Multi-objective optimization in wireless sensors networks," in *International Conference on Microelectronics (ICM'11)*, Hammamet, Tunisia, December 2011, pp. 1–4.

[252] A. Perez, M. Labrador, and P. Wightman, "A multiobjective approach to the relay placement problem in WSNs," in *IEEE Wireless Communications and Networking Conference (WCNC'11)*, Tampa, FL, USA, March 2011, pp. 475–480.

[253] H. Abidin, N. Din, and Y. Jalil, "Multi-objective optimization (MOO) approach for sensor node placement in WSN," in *7th International Conference on Signal Processing and Communication Systems (ICSPCS'13)*, Australia, December 2013, pp. 1–5.

[254] J. Lu, X. Wang, L. Zhang, and X. Zhao, "Fuzzy random multi-objective optimization based routing for wireless sensor networks," *Soft Computing*, vol. 18, no. 5, pp. 981–994, September 2014.

[255] A. A.-A. M. Rahat, R. M. Everson, and J. E. Fieldsend, "Multi-objective routing optimisation for battery-powered wireless sensor mesh networks," in *Proceedings of the 2014 Conference on Genetic and Evolutionary Computation (GECCO '14)*. New York, NY, USA: ACM, July 2014, pp. 1175–1182.

[256] N. Magaia, N. Horta, R. Neves, P. R. Pereira, and M. Correia, "A multi-objective routing algorithm for wireless multimedia sensor networks," *Applied Soft Computing*, vol. 30, no. 0, pp. 104–112, May 2015.

[257] B. Mahboobi and M. Ardebilipour, "Joint power allocation and routing in full-duplex relay network: An outage probability approach," *IEEE Communications Letters*, vol. 17, no. 8, pp. 1497–1500, August 2013.

[258] H. M. Ammari, "On the energy-delay trade-off in geographic forwarding in always-on wireless sensor networks: A multi-objective optimization problem," *Computer Networks*, vol. 57, no. 9, pp. 1913–1935, 2013.

[259] W. Stadler, "A survey of multicriteria optimization or the vector maximum problem, part I: 1776–1960," *Journal of Optimization Theory and Applications*, vol. 29, no. 1, pp. 1–52, September 1979.

[260] N. Srinivas and K. Deb, "Multiobjective optimization using nondominated sorting in genetic algorithms," *Evolutionary Computation*, vol. 2, no. 3, pp. 221–248, Fall 1994.

[261] S. Das and P. N. Suganthan, "Differential evolution: A survey of the state-of-the-art," *IEEE Transactions on Evolutionary Computation*, vol. 15, no. 1, pp. 4–31, February 2011.

[262] D. Niyato, E. Hossain, M. Rashid, and V. Bhargava, "Wireless sensor networks with energy harvesting technologies: A game-theoretic approach to optimal energy management," *IEEE Wireless Communications*, vol. 14, no. 4, pp. 90–96, August 2007.

[263] P. Mitcheson, E. Yeatman, G. Rao, A. Holmes, and T. Green, "Energy harvesting from human and machine motion for wireless electronic devices," *Proceedings of the IEEE*, vol. 96, no. 9, pp. 1457–1486, September 2008.

[264] A. Harb, "Energy harvesting: State-of-the-art," *Renewable Energy*, vol. 36, no. 10, pp. 2641–2654, October 2011.

[265] S. Sudevalayam and P. Kulkarni, "Energy harvesting sensor nodes: Survey and implications," *IEEE Communications Surveys and Tutorials*, vol. 13, no. 3, pp. 443–461, September 2011.

[266] H. Visser and R. Vullers, "RF energy harvesting and transport for wireless sensor network applications: Principles and requirements," *Proceedings of the IEEE*, vol. 101, no. 6, pp. 1410–1423, June 2013.

[267] A. Kansal, J. Hsu, M. B. Srivastava, and V. Raqhunathan, "Harvesting aware power management for sensor networks," in *43rd ACM/IEEE Design Automation Conference*, San Francisco, CA, July 2006, pp. 651–656.

[268] O. Ozel, K. Tutuncuoglu, J. Yang, S. Ulukus, and A. Yener, "Transmission with energy harvesting nodes in fading wireless channels: Optimal policies," *IEEE Journal on Selected Areas in Communications*, vol. 29, no. 8, pp. 1732–1743, September 2011.

[269] K. Tutuncuoglu and A. Yener, "Optimum transmission policies for battery limited energy harvesting nodes," *IEEE Transactions on Wireless Communications*, vol. 11, no. 3, pp. 1180–1189, March 2012.

[270] S. Mao, M. H. Cheung, and V. Wong, "Joint energy allocation for sensing and transmission in rechargeable wireless sensor networks," *IEEE Transactions on Vehicular Technology*, vol. 63, no. 6, pp. 2862–2875, July 2014.

[271] Z. Ding, S. Perlaza, I. Esnaola, and H. Poor, "Power allocation strategies in energy harvesting wireless cooperative networks," *IEEE Transactions on Wireless Communications*, vol. 13, no. 2, pp. 846–860, February 2014.

[272] S. Yu and C. Lee, "Lifetime maximization in mobile sensor networks with energy harvesting," in *IEEE International Conference on Robotics and Automation (ICRA'11)*, Shanghai, China, May 2011, pp. 5911–5916.

[273] C. Fragouli, J. Widmer, and J.-Y. Le Boudec, "A network coding approach to energy efficient broadcasting: From theory to practice," in *25th IEEE International Conference on Computer Communications (INFOCOM'06)*, Barcelona, Spain, April 2006, pp. 1–11.

[274] J. Goseling, R. Matsumoto, T. Uyematsu, and J. Weber, "On the energy benefit of network coding for wireless multiple unicast," in *IEEE International Symposium on Information Theory (ISIT'09)*, Seoul, Korea, June 2009, pp. 2567–2571.

[275] A. Keshavarz Haddad and R. Riedi, "Bounds on the benefit of network coding for wireless multicast and unicast," *IEEE Transactions on Mobile Computing*, vol. 13, no. 1, pp. 102–115, January 2012.

[276] H. Hosseinmardi and F. Lahouti, "Multicast lifetime maximization using network coding: A cross-layer approach," in *24th Biennial Symposium on Communications*, Kingston, ON, June 2008.

[277] D. Platz, D. Woldegebreal, and H. Karl, "Random network coding in wireless sensor networks: Energy efficiency via cross-layer approach," in *IEEE 10th International Symposium on Spread Spectrum Techniques and Applications (ISSSTA'08)*, Bologna, Italy, August 2008, pp. 654–660.

[278] W. Li, J. Li, and P. Fan, "Network coding for two-way relaying networks over Rayleigh fading channels," *IEEE Transactions on Vehicular Technology*, vol. 59, no. 9, pp. 4476–4488, November 2010.

[279] J. Zou, H. Xiong, C. Li, R. Zhang, and Z. He, "Lifetime and distortion optimization with joint source/channel rate adaptation and network coding-based error control in wireless video sensor networks," *IEEE Transactions on Vehicular Technology*, vol. 60, no. 3, pp. 1182–1194, March 2011.

[280] J. Harri, F. Filali, and C. Bonnet, "Mobility models for vehicular ad hoc networks: A survey and taxonomy," *IEEE Communications Surveys and Tutorials*, vol. 11, no. 4, pp. 19–41, December 2009.

[281] K. Yang, J. Huang, Y. Wu, X. Wang, and M. Chiang, "Distributed robust optimization (DRO), part I: Framework and example," *Optimization and Engineering*, pp. 1–33, 2008.

[282] Y. Wu, K. Yang, J. Huang, X. Wang, and M. Chiang, "Distributed robust optimization (DRO) part II: Wireless power control," *Optimization and Engineering*, 2010.

[283] B. Peng, J. Zou, C. Tan, and M. Wang, "Network lifetime optimization in wireless video sensor networks," in *IET International Communication Conference on Wireless Mobile and Computing (CCWMC'09)*, Shanghai, China, December 2009, pp. 172–175.

[284] J. Zou, C. Tan, R. Zhang, and H. Xiong, "Modeling and optimization of network lifetime in wireless video sensor networks," in *IEEE International Conference on Communications (ICC'10)*, Cape Town, May 2010.

[285] V. Liu, A. Parks, V. Talla, S. Gollakota, D. Wetherall, and J. R. Smith, "Ambient backscatter: Wireless communication out of thin air," in *Proceedings of the ACM Conference on SIGCOMM*, New York, NY, USA, October 2013, pp. 39–50.

Author Index